DEVELOPMENT OF GAN MOSFET GROWTH AND PROCESSING TECHNOLOGY

By

ANDREW M. HERRERO

A DISSERTATION PRESENTED TO THE GRADUATE SCHOOL
OF THE UNIVERSITY OF FLORIDA IN PARTIAL FULFILLMENT
OF THE REQUIREMENTS FOR THE DEGREE OF
DOCTOR OF PHILOSOPHY

UNIVERSITY OF FLORIDA

2008

To my Parents

ACKNOWLEDGMENTS

I want to thank my parents for all the support they have given during my academic carrer. I want to thank Dr. Cammy Abernathy for giving me this opportunity and guiding me to be a successful scientist. I also want to thank Dr. Brent Gila, for teaching me an indescribable amount about specific research processes as well as the general approach towards conducting research. I can easily say that I have learned more from them then anybody else that I have ever met and will probably ever meet.

Appreciation is also given to my fellow group members for their help with growing films or performing characterization that I needed. I would also like to express my appreciation to Dr. Fan Ren for the use of his lab and equipment and to the members of his research group that took the time to explain procedures or answer questions as well as perform some very intergral work required for my project.

TABLE OF CONTENTS

page

LIST OF TABLES

LIST OF FIGURES

Abstract of Dissertation Presented to the Graduate School
of the University of Florida in Partial Fulfillment of the
Requirements for the Degree of Doctor of Philosophy

DEVELOPMENT OF GAN MOSFET GROWTH AND PROCESSING TECHNOLOGY

By

Andrew M. Herrero
December 2008

Chair: Cammy Abernathy
Major: Materials Science and Engineering

In an effort to further the progress of GaN metal oxide semiconductor field effect transistor (MOSFET) technology, some of the major challenges that it faces are addressed. The lack of a capable dielectric is one of the main obstacles to its advancement. One of the potential candidate dielectrics that has been previously looked at is scandium oxide (Sc_2O_3). The epitaxial growth of Sc_2O_3 on GaN is thoroughly examined. Extensive characterization on the structural properties of the Sc_2O_3/GaN material system was performed. Detailed analysis of the characterization results is presented and the thermodynamic and kinetic principles involved are discussed. The characterization analysis was performed in such a manner that makes it applicable to fcc-based cubic oxides, in general. The majority of the candidate dielectrics now being examined for GaN MOS applications are fcc-based cubic oxides, which makes this analysis a valuable tool in assessing the potential of many of these oxide/GaN material systems. The dominant growth technique for GaN production is metal organic chemical vapor deposition (MOCVD). The thermal and chemical stability in a GaN MOCVD environment of some of the potential dielectric oxides is investigated with respect to their structural and electrical properties. The p-n junction is typically the fundamental building block of electronic semiconductor devices. The fabrication of a good p-n junction for p-MOS devices is another obstacle in the development of GaN MOSFET technology. An alternative fabrication technique is explored that

uses the MOCVD regrowth of heavily doped p-type GaN to produce the source and drain regions for a p-MOSFET device. The fundamental principles involved in the regrowth of GaN is considered and discussed. The development of lithography and chemical etching techniques for the fabrication of GaN-based MOS devices is integral to the advancement of GaN MOSFET technology as a whole. The ability of potential dielectric oxides to endure these processing steps is a fundamental requirement for the realization of GaN MOSFET technology. Based on the previous work done in this study, processing sequences for device fabrication are developed and the main issues involved their design are discussed.

CHAPTER 1
INTRODUCTION

A significant amount of research has been performed on the III-nitride semiconductor system due to its numerous potential electronic device applications. GaN, due to its high breakdown field, large thermal conductivity and large bandgap, has been investigated particularly for high power electronic devices. GaN-based field effect transistors (FETs) have produced outstanding results [1-4]. GaN metal semiconductor FET (MESFET) and modulation doped FET (MODFET/HEMT) device structures have shown excellent progress, but a few significant difficulties in device performance still exist. At high temperatures, GaN FETs using Schottky metal gates have had difficulty in achieving stable Schottky contacts, resulting in current leakage. Another difficulty observed is the presence of high parasitic resistances, which degrades the device performance. III-V technology uses a n^+cap layer to reduce parasitic resistance but this approach can not be used to construct a gate recess for GaN-based FETs. GaN chemistry makes wet etching of the recess difficult and dry etching can result in residual lattice damage that will lower the gate breakdown voltage. Besides the previously mentioned problems, the major disadvantage of MESFET and HEMT technology is the lack of being able to produce an enhancement mode device. In order for an enhancement mode device to be produced, an alternative device technology needs to be developed.

Utilizing MOSFET (metal oxide semiconductor FET) technology will allow for the production of an enhancement mode device and can potentially solve the other fabrication problems. Silicon MOSFETs are currently the most widely used transistors. III-nitride based MOSFETs should exhibit, lower leakage currents, lower noise, higher frequency and reduced power consumption. The broader curve of transconductance versus gate voltage shown by MOSFETs results in a higher linearity operation than the other devices. The lower capacitance

between source and gate would result in a larger cut-off frequency (f_T) than GaN MESFETs. At high temperatures, the increased thermal stability of MOSFETs will have an advantage over MESFETs, due to lower leakage currents.

Complementary MOS (CMOS) technology is one of the most popular MOSFET technologies, making use of both *n* and *p* channel transistors in the same substrate. CMOS devices allow for low power, negligible static power dissipation and large noise margins for integrated circuits. The area of transistor technology used to build CMOS circuits is sure to have a significant role in the future of semiconductor technology.

There are several challenges to be overcome in order to develop GaN MOSFET technology successfully. The most important requirement needed is having an appropriate insulating gate material. Since GaN does not have a suitable native oxide to form the barrier between the gate and the channel, an alternative material is needed. Although many dielectric materials have already been investigated for this purpose, the structural and electrical properties of the Oxide/GaN interface are still not well understood. In general, research on the epitaxial growth of oxides on wide bandgap materials has been limited despite the many potential applications for electronic devices. In addition to gate isolation, an important application for any dielectric oxide developed would be for GaN-On-Insulator (GOI) structures. GOI technology has enormous potential for achieving enhanced performance and extended scalability of GaN MOS devices.

There is a large amount of work yet to be done in this field. There are also issues to be addressed with the processing of GaN CMOS devices, particularly the difficulties associated with p-type doping of GaN. The problem of successfully obtaining good p-type GaN has been a major challenge, not only for MOS devices, but for GaN-based electronic technology in general.

The outline and organization of this work is as follows. The literature review in chapter 2 gives an overview of the need and current status of dielectrics for use in GaN MOS technology. The main factors in the MOCVD of GaN and the selective area growth of GaN are discussed as well as the specific application of each towards the production of p-type GaN. Chapter 3 gives the details on the equipment and methods used for this study. Chapter 6 explores the use of MOCVD regrowth as a technique that can be used in the fabrication of GaN MOS devices. Although, the specific aim of this study was towards producing a p-MOS device, most of the steps involved in the fabrication of GaN-based devices in general are studied. Due to the wide application of this technique and the lack of research that has been performed in this area, the fundamental mechanisms involved are considered and possible explanations for observed phenomena are proposed. Chapter 7 addresses the specific issues that are seen in the fabrication of GaN-based MOS devices. The candidate dielectric oxides that were previously examined are investigated with respect to their ability to withstand the different processing steps required for device fabrication, which necessitate the exposure to harmful chemicals and elevated temperatures. The issues that are important factors, based on the limitations of the potential oxides, are discussed as to their effect on designing a processing sequence for device fabrication. Then, all the work that was presented in the previous chapters is used to design the general processing sequences for a GaN p-MOSFET and CMOSFET. Finally, a detailed processing sequence for a GaN p-MOSFET is proposed that uses the specific regrowth technique developed in this study.

CHAPTER 2
LITERATURE REVIEW

Dielectric Materials For GaN-based Devices

Metal Oxide Semiconductor Field Effect Transistor (MOSFET) Devices

A MOSFET device consists of a source and a drain region that has carriers flowing from one to the other. The flow of carriers in the region or channel between the source and the drain is controlled by applying voltage to a gate. The basic structure of a MOSFET is shown in Figure 2-1. There are two fundamental types of MOSFETs based on its operation when a voltage is applied to the gate. If applying voltage to the gate causes an already existing carrier flow in the channel to stop, then the device is a depletion mode type. Essentially, the gate voltage turns a normally on device off. When the device is normally off, where there is no current flow in the channel and applying voltage to the gate induces the flow of carriers in the channel, then the device is an enhancement mode type. A valuable feature of the MOSFET is its ability to be operated in the enhancement mode as well as the depletion mode. Depending on whether electrons or holes produce the channel current, the device is either a n-type or p-type MOSFET, respectively. The gate is separated from the channel by an insulating barrier resistant to the passage of charge carriers. The insulated gate of the MOS structure reduces gate leakage current, which will increase the breakdown voltage [5]. Electrons or holes in the channel are controlled by the gate through capacitive coupling. The ability of the gate to control the channel carriers or transconductance is dependent on the thickness of the gate insulator. By reducing the thickness, a higher drive current can be obtained, which then provides a higher transconductance and more efficient charge control by the gate voltage [6]. The higher drive current is a significant factor in increasing the operational frequency of ICs and achieving higher IC switching speeds. Although decreasing the thickness of the gate insulation gives the gate better control over the channel, this

yields a higher leakage current density between the gate and the channel, driving up power consumption. If the insulation is too thin, a significant amount of current will be allowed to flow from the gate to the channel, mainly due to quantum-mechanical direct tunneling through the gate insulation [6]. Thus a gate insulator is needed that will be able to prevent the leakage of current while allowing good control over the channel as well as being thermally conductive to avoid heat build up. In order to realize GaN-based MOSFET devices, the first prerequisite is the deposition of a suitable material to serve as a gate insulator. Dielectric oxides have significant potential for the application as a gate insulator in GaN-based MOSFET devices.

Application of Dielectrics for GaN-based Devices

Research on epitaxial growth of crystalline oxides on wide bandgap materials has been limited despite the many potential applications for electronic devices. A few of the possible applications for such research are the use of ferroelectric oxides for power switching applications, oxides with anisotropic dielectric constants for high voltage termination, oxides with large electric flux density near breakdown and surface passsivation for the reduction of current collapse [7]. The development of dielectric oxides has enormous potential for GaN-based devices due to the many possible applications. An application that is currently being employed is their use for the passivation of GaN/AlGaN device surfaces [8-10]. The dielectric could also serve as a field oxide allowing an increase in the proximity of neighboring devices without interference.

One of the most promising applications with excellent potential is in GaN-based MOS technology. The development of MOS technology for the production of GaN CMOS devices would be extremely valuable. CMOS devices are comprised of both a *n*-MOS and a *p*-MOS transistor that are connected in series to the power supply and are controlled by the same gate voltage. Since the same signal that turns on a transistor of one type is used to turn off a transistor

of the other type, the design logic devices using only simple switches is made possible [6]. The main advantage of this technology is that it only consumes power when it switches. The difficulty lies in the fabrication of two different types of transistors on the same substrate, which makes this technology inherently more complex than *n*-MOS technology.

Future semiconductor challenges will need advanced isolation techniques and novel transistor architecture. In the silicon industry, a large amount of work has gone towards developing silicon-on-insulator (SOI) structures. SOI wafers have an insulating layer of SiO_2 buried in between a thin device layer and a bulk substrate. The oxide layer is used as an insulating buffer, which results in the elimination of substrate current leakage. Applying this concept to GaN MOSFET technology by using gallium nitride-on-insulator (GOI) substrates has great potential and numerous possible applications.

As the scaling limit of CMOSFETs is approached, other sources of tunneling become significant. Scaling limits depend on the application being considered. For fixed high-performance IC applications, it is more practical to have a large cooling system to remove the heat produced from current leakage, but its affectivity will be limited. The resulting higher power consumption from current leakage can be tolerated by high-performance devices, like microprocessors, but in low-power ICs it interferes with functionality. In mobile and wireless, low-power applications, the removal of the heat produced is a much more difficult problem to deal with. Application of GOI technology for power amplifiers in wireless devices can result in higher output resistance and improvement in the pinchoff characteristics, which equates to high efficiency operation. Since GOI technology can obtain high efficiency with high linearity at low supply voltages, it would be able to satisfy the needed linearity requirements. The excess power

consumption in wireless hand-held devices will become a major driving force for the development of GOI technology.

In a MOSFET, the current leakage into the substrate is the result of direct tunneling between the channel and the substrate, which is similar to that from the gate-dielectric tunneling current. It is a part of the total current that does not get modulated by the gate, which results in lost power that drives up power consumption and reduces efficiency. As down-scaling continues and channel lengths are decreased, extra power consumption due to indirect tunneling between the source and drain and will also become problematic.

The dielectric oxide developed for use as a gate insulator for GaN MOSFETs could be applied as an insulating buffer layer in GOI structures. The advantage gained by the insulating buffer will be reflected in the dc, RF, and power performance of GOI MOSFETs. The reduction of the dynamic switching power of MOSFETs can be achieved by using a GOI wafer that reduces the junction area, which decreases the junction capacitance and thus speed up transistor switching. The dielectric oxide acting as an insulating buffer results in elimination of substrate leakage, better pinchoff characteristics, and improved charge control, which achieves an overall increased performance. A possible application of using an oxide as a buffer layer is that it can serve as a quick release layer through selective etching. This would make it possible to produce free-standing GaN substrates, which has been a difficult challenge in GaN technology from the beginning.

Application of GOI structures for a 3-D integration approach is an effective way to address some of the challenges in GaN MOSFET technology. Using GOI technology allows for novel transistor architecture that can take care of the conflicting demands of performance and power consumption. This approach entails fabricating devices in a 3-D stack together with the

underlying wafer. The 3-D integration of novel devices can provide potential ways to address the dc and ac power consumption issues in advanced ICs. With continual down-scaling, the interconnect spacing will become smaller resulting in coupling loss and cross-talk which will be unacceptable in high density and high frequency ICs. As interconnect distances decrease, the parasitic capacitance effects in the interconnects become more severe. These effects are the limiting factors for dynamic circuit switching speed. The potential high interconnect density of a 3D approach can help address this issue. The increased device density and higher drive currents obtained by using 3-D GOI CMOSFETs may be able to avoid some of the scaling limits of 2-D CMOSFETs. The fundamental challenge of using this 3-D integration approach will be how to fabricate the upper layer of devices without degrading the performance of the multiple lower layers of interconnects and MOSFETs.

Requirements of Potential Dielectrics

One of the main characteristics required of possible gate insulators, besides having a larger bandgap energy, would be having a large dielectric constant (κ). The dielectric constant of a material is a measure of the extent to which it concentrates electric field lines. As the dielectric constant of the insulator increases, the capacitance between the gate and the substrate increases [6]. The drive current is proportional to the gate dielectric capacitance/area [$C_{ox}(\varepsilon_o\kappa/t_{ox})$]. Essentially, the gate capacitance is the dielectric constant divided by thickness. A higher drive current provides a higher transconductance and thus using a thick high-κ dielectric allows the gate to control the channel just as well as thinner lower-κ dielectric. The thicker the insulator, the less current leakage there is between the gate and the substrate. Therefore, having a large dielectric constant loosens thickness constraints and allows for the gate leakage to be minimized.

Another main factor that will determine a dielectric's applicability is its thermal stability, required for both the processing and operation of the devices. Thermal decomposition of the oxide's structure would result in a decrease in the performance of MOS devices. The oxide/GaN interface quality is a critical issue for GaN-based MOS devices. Increasing the smoothness of the Oxide/GaN interface will prevent localized high breakdown fields, minimize the interface state density (D_{it}) and provide a high carrier mobility [11]. The thermal stability of the oxide/GaN interface must be excellent due to the high temperatures it will experience during processing. A factor reflecting the transistors performance would be the bias-temperature instability (BTI). BTI is the undesirable increase of the threshold voltage (V_T) of a MOSFET during continuous operation at a temperature elevated by the thermal dissipation in the IC. The improvement of a transistor's BTI may be achieved through the use of strongly bonded oxides [6, 12].

The degree of lattice mismatch between GaN and the oxide plays a significant role in the structural quality of the grown oxide. If there is a large lattice mismatch between the oxide film and the GaN substrate, dislocations are produced at the interface and throughout the oxide film during growth. These dislocations act as leakage paths and cause the breakdown voltage to be rather low [13]. The interfacial density of states (D_{it}) is also directly affected by the mismatch at the interface. Thus it is essential that the growth of the dielectric oxide on nitrides is epitaxial with minimal defects in order to maximize the dielectric breakdown strength and minimize the D_{it}.

Current Status of Candidate Dielectrics

The standard gate insulation, used in Si-MOSFET technology is silicon dioxide (SiO_2). The continuing down-scaling of MOSFET device dimensions has motivated the replacement SiO_2 as the standard gate insulation with a material having a larger dielectric constant (κ). The need for better gate dielectrics is important to MOSFET technology in general.

A number of rare earth oxides have been shown to grow epitaxially on GaAs and Si. Several dielectrics, such as AlN [14, 15], Ga_2O_3 (Gd_2O_3) [14, 16, 17], SiO_2 [18, 19], Si_3N_4 [20] and MgO [21, 22] have been investigated for use in GaN MOS devices and have mainly produced mediocre results. Thin films of Gd_2O_3 deposited on GaAs have produced a low interfacial density of states (D_{it}). Although the results thus far for Gd_2O_3 have been promising, its small bandgap of 5.3 eV and large ~20% lattice mismatch with GaN makes its successful application as a dielectric for GaN very difficult.

An oxide that has shown significant potential as both a MOS gate and for surface passivation on GaN is Sc_2O_3 [5, 23-28]. Sc_2O_3 has a bandgap of 6.3 eV and dielectric constant of 14. Sc_2O_3 exists in the same cubic bixbyite crystal structure as Gd_2O_3 and should grow in a (111)-orientation parallel to the GaN (0001) basal plane. Although the ~9.2% mismatch between Sc_2O_3 (111) and GaN (0001) is much smaller than that of Gd_2O_3 and GaN, it is still quite large and poses a potential problem in maintaining the structural quality of the oxide. Excellent quality films of Sc_2O_3 have been epitaxially grown on GaN. These films were extensively characterized before and after high temperature annealing, and showed that the oxide film was thermally stable and that the quality of the interface was unaffected.

Another oxide with good potential that is currently being explored is MgCaO. The promising characteristic of MgCaO is that if the concentrations of Mg and Ca are equal, the ternary oxide has a perfect lattice match to GaN on its (111) plane. A problem with using Mg and Ca is the large difference in their ionic radius, which results in immiscibilty. This was evident from AES depth profiling of the MgCaO samples where the Ca had segregated to the surface [29]. Despite the Ca segregation in the MgCaO samples, HRXRD of the films have not shown any the presence of phase separation into MgO or CaO. A small shoulder off of the (004)

GaN peak is the only peak attributable to MgCaO, which indicates its excellent lattice match with GaN. Using a digital growth approach of alternating MgO and CaO layers has produced films with minimal Ca segregation. Recent growth of AlN on MgCaO has shown that the MgCaO was thermally stable up to 800^{o}C in an oxygen free UHV environment. One advantage of using MgCaO is its easy etchibility, which would allow it to be used as a release layer for the growth of free-standing GaN films. These initial results are promising for the use of MgCaO as a dielectric oxide in GaN-based devices.

One of the initial steps towards the integration of dielectric oxides into GaN MOSFET technology has been demonstrated with the use a stacked gate dielectric of SiO_2/Gd_2O_3 [30, 31]. The successful fabrication of an *n*-channel depletion mode GaN MOSFET with SiO2/Gd2O3 was performed. The Gd_2O_3 was epitaxially grown on the GaN and had a smooth interface. The large lattice mismatch between Gd_2O_3 and GaN produced a large dislocation density in the oxide causing the breakdown voltage to be low. Amorphous SiO_2 was deposited onto the Gd_2O_3 in an attempt to improve the breakdown voltage. The SiO_2/Gd_2O_3 stacked gate dielectric resulted in a reduction in the gate leakage and had no detrimental effects to the Gd_2O_3/GaN interface. The SiO_2 reduced the leakage by terminating the dislocations in the Gd_2O_3 film.

The fabrication of an enhancement mode MOS diodes has also been demonstrated using MgO as the gate dielectric [32]. With MgO as the gate insulator the gate contact demonstrated good rectification and a much larger breakdown voltage than if no insulator had been used. C-V measurements showed clear modulation from accumulation to depletion. Self-heating did not seem to be a problem from the I-V measurements that showed no sign of negative resistance effects. These initial results show that there is great potential for GaN-based MOS devices but also that there is still a lot more work to be done.

Growth of Oxide and GaN Heterostructures

Research on the heteroepitaxy of oxides on GaN is limited and relatively new. Thus knowledge of the field is inadequate and its understanding is far from complete. The critical section of the Oxide/GaN heterostructure that will have an integral part in device performance is the interface. Roughening of the interface negatively affects the carrier mobility and can increase the D_{it}. The production of defects at the interface during growth will contribute to an increase of the interface roughness. To minimize the interface roughness before any growth it is essential that the GaN substrate have a very smooth surface and that an *in-situ* cleaning of GaN of the surface is performed. The lattice mismatch between the oxide and GaN has a large effect on the bulk crystal quality of the oxide. The stress produced from the lattice mismatch usually results in the production of dislocations in order to minimize it. The lattice mismatch between the Sc_2O_3 (111) and GaN (0001) planes is approximately 9.2%. Although this mismatch is large, epitaxial Sc_2O_3 has been grown on GaN with a threading dislocation (TD) density calculated to be on the order of $10^9 cm^{-2}$ for the Sc_2O_3 film, which is the typical TD density for MOCVD GaN on sapphire. The TDs originate from the underlying GaN substrate. The interaction of the step flow growth of the Sc_2O_3 film with the surface termination of TDs of screw character, results in spiral growth due to pinning of the surface steps. Typical GaN will usually display this morphology when grown on (0001) sapphire.

Growth of epitaxial films on substrates with a large lattice mismatch forms a mosaic structure of misoriented grains. The mosaic structure is characterized by the tilt and twist of the misoriented grains, which corresponds to the out-of-plane and in-plane misorientations respectively. The in-plane orientation relationship of the film and substrate as well as the degree of in-plane misorientation can be determined from XRD pole figure measurements. Since most of the candidate dielectric oxides that are being investigated have a cubic lattice structure, the in-

plane crystal orientation of the oxide deposited on the hexagonal structure of GaN will play an important role in the oxides quality. The cubic oxides will grow in a (111)-orientation parallel to the GaN (0001) basal plane. One of the promising dielectric oxides, Sc_2O_3 with a cubic bixbyite crystal structure has been deposited epitaxially on GaN.

The subsequent growth of GaN on top of the Oxide/GaN structure will have many of the same growth issues as that for the oxide growth. The oxide surface will also need to be very smooth to minimize defects in the GaN and at the interface. To achieve a smooth oxide surface the growth conditions need to be optimized for 2-D step-flow growth, which can be done using *in-situ* RHEED. GaN growth on Gd_2O_3/GaN has been demonstrated [33]. From cross-section TEM, it was seen that the Gd_2O_3 layer terminated the threading dislocations in the bottom GaN layer. This prevented the propagation of these TDs into the upper GaN layer.

Metal Organic Chemical Vapor Deposition (MOCVD) of GaN

Thermodynamic and Kinetic Factors of MOCVD Growth

The metal-organic chemical vapor depostion (MOCVD) of GaN is a nonequilibrium growth technique that transports trimethylgallium (TMG) and ammonia (NH_3), diluted in hydrogen gas over a heated substrate and susceptor, where they react to form GaN. The basic reaction for the MOVPE growth of GaN is given by Equation 2-1.

$$Ga(CH_3)_3(g) + NH_3(g) \Rightarrow GaN(s) + 3CH_4(g) \quad (2\text{-}1)$$

This is a simplified expression of the actual reaction that ignores the specific reaction path and all the intermediates that are produced. The MOCVD process for GaN is composed of numerous possible reaction pathways, for which a complete understanding of the reaction mechanisms is not known in detail [34]. The main reaction pathways in the MOCVD of GaN involve the kinetics of adduct formation, decomposition, oligimerization and dissociation [34]. From all the experimental data and modeling the main rate-limiting reaction pathways are identified and

shown in Table 2-1. The specific rate-limiting pathway is dependent on the reactor geometry and the growth conditions used.

The decomposition rate of TMG is considered to be predominantly homogeneous [35]. The resulting gaseous precursor species are assumed to have unit sticking coefficient and immediately decompose upon contact with the hot surface incorporating Ga and N into the film [36]. This assumption is reasonable at high temperatures and agrees well with observed results of the methyl group dissociation from adsorbed TMG and MMG species until Ga is deposited [35].

From the experimental evidence, it is well established that most of the TMG forms an adduct with NH_3 as soon as it enters the chamber [37]. The two form the gas-phase adduct, trimethylgalliummonamine ($TMG:NH_3$) at low temperatures. This strong adduct reaction between NH_3 and TMG is believed to be a primary gas phase reaction [37]. The adduct formation has been assumed to be collision rate-limited by the interaction between the two molecules [36]. From the FTIR and TPD experiments it was observed that the adduct instantly eliminates a methane molecule after forming and produces $[(CH)_2Ga:NH_2]_x$ [38, 39, 35]. This adduct-derived species is therefore the dominant Ga species in the boundary layer. Since the MOCVD growth of GaN is diffusion-limited, it is the transport and decomposition of this species $[(CH)_2Ga:NH_2]_x$ through the boundary layer that is the main rate-limiting step.

The MOCVD of p-type GaN

To obtain p-type GaN (p-GaN) during MOCVD growth, a metalorganic gas with Mg is used as the dopant source. The predominant p-type dopant source used in GaN MOCVD is Bis-cyclopentadienyl magnesium (CP_2Mg). The main issue with Mg-doping during MOCVD growth is the formation of Mg-H complexes [40]. The H is a byproduct of the ammonia (NH_3) decomposition that passivates the Mg acceptors by forming Mg-H complexes and thus limiting

the electrical activity of the Mg atoms. In order to produce p-type carriers, activation of the Mg atoms is needed. The activation process is usually performed by thermal annealing. The activation of p-type carriers in GaN is dependent on the annealing temperature and atmosphere. The hydrogen-passivated Mg acceptors are thermally stable up to 7000^{o}C. Annealing treatment for hole activation should occur under nitrogen at temperatures of between 700 and 750^{o}C [40]. The annealing step under these conditions is critical for the activation of Mg acceptors in GaN.

Another issue with the Mg-doping of GaN during MOCVD growth is the formation of defects induced by the Mg atoms. Due to its poor hole activation efficiency, a very large concentration of Mg needs to be incorporated into the growing films in order to obtain a significant level of doping. The excessive amount of Mg often leads to the production of structural defects. Under certain growth conditions, Mg segregates and causes formation of several different types of defects. The types of defects are dependent on the growth conditions and polarity. The defects that differed with polarity are most likely due to the different surface reconstructions and positions that the Mg atoms are incorporated within the unit cell. For Ga-polarity, the dominant defects were hollow triangular features oriented with a base on the (0001) c-planes and six $\{11\bar{2}2\}$ side facets [41]. This shows that Mg segregated on particular planes tends to prevent further growth. This corresponds well with the model of growth rate dependence on the growth facet. Growth of the $\{11\bar{2}2\}$ plane was overtaken by the dominant (0001) growth plane and Mg was incorporated in different positions from the rest of the bulk growth.

Selective Area Growth (SAG) of GaN

Selective area growth has been used to produce several different types of GaN-based microstructures and devices. One selective area growth technique that was developed in order to minimize the dislocation density of GaN layers grown on sapphire is epitaxial lateral overgrowth

(ELO) [42]. Since there are no bulk GaN substrates available thin films of GaN must be heteroepitaxial grown on foreign substrates in order for it to be used to fabricate a device. Heteroepitaxial growth on dissimilar substrates produces defects within the growing layers. These defects can propagate into the epilayers that are later grown on top to form device structures, which can be detrimental to device performance. The subsequent growth of thin epitaxial layers forms the basis of GaN-based electronic devices. This is a significant issue in GaN epitaxy due to the standard substrate used for growth is sapphire, which has a particularly large lattice mismatch with GaN of 16%.

The standard ELO method uses previously grown GaN/sapphire substrates with a silicon dioxide (SiO_2) film deposited on it that has stripes patterned into it. The stripes or trenches in the SiO_2 run across the whole wafer surface and expose some of the underlying GaN. An illustration of a typical ELO substrate is shown in Figure 2-2. The main principle behind this technique is that only the exposed GaN will serve as areas for new growth and that once the growth has reached the trench edge it will begin to grow laterally over the SiO_2. The laterally growing faces will eventually meet forming a layer of GaN with a largely reduced dislocation density. The reduction in dislocation density is because dislocations only propagate vertically and thus will not spread into the laterally grown material.

One of the main goals in ELO is to maximize the lateral growth rate. From numerous ELO experiments it is known that the lateral growth rate from different facets varies depending on the orientation. Thus, the orientation of the stripes of open windows is an important factor when trying to optimize the lateral growth rate. Stripes that are oriented in directions perpendicular to the (0001) plane will have a lateral growth maxima and minima every 30^o [43]. As shown in Figure 2-3, the maxima and minima correspond to the $<1\bar{1}00>$ directions $<11\bar{2}0>$

within the GaN unit cell. Growth from the stripes that are oriented along the $<1\bar{1}00>$ directions will be lateral growth dominant producing a rectangular growth from the open windows whereas growth from $<11\bar{2}0>$ oriented stripes will be vertical growth dominant which results in a more triangular growth. Figure 2-4 shows what the resulting growth on an ELO substrate would look like for each orientation.

It has been shown that ELO growth is influenced by several factors that include temperature, V/III ratio, and the mask fill factor [44-47]. The V/III ratio is optimized by increasing it through the decrease in the TMG flow. By decreasing the amount of available Ga species to react, the incorporation of Ga into the lattice will be limited to the most energetically favorable growth facets. The dominant lateral growth plane is the $(11\bar{2}0)$, where vertical growth occurs from the (0001). The $(11\bar{2}0)$ plane has a larger dangling bond density than the (0001). Therefore, the $(11\bar{2}0)$ has a larger number of free surface bonds which equates to a larger number of sites for *Ga* and *N* incorporation, which makes the $(11\bar{2}0)$ more favorable for the adsorption of reactant species. Thus, the limited availability of *Ga* species enhances the lateral growth rate through the preferential growth on the $(11\bar{2}0)$ over the (0001). It has been shown that the growth regime in which the growth is taking place influences the growth rate of specific planes differently [42]. This is illustrated in Figure 2-5, where the dependence of the facet growth rate on the temperature and pressure is shown.

Another SAG technique that involves the regrowth from etched regions is pendeo-epitaxy (PE) [48-50]. The typical substrates used in PE (Figure 2-6) are similar to those used in ELO except that the trenches on the substrate extend down through the GaN and into the SiC substrate. The main objective is the same as that for ELO, which is obtained through the exclusive lateral growth from the sidewalls of the etched trenches and then vertically up to the

surface of the mask. The growth then proceeds just as in ELO, where it grows up and over the mask to coalesce with another growth front. The influence of the temperature on the lateral growth rate using the PE technique has been studied and it was shown using a growth temperature above the optimal temperature for standard growth, significantly increases the lateral growth rate while the vertical growth rate is decreased [48]. The reasoning for the increase in lateral growth with temperature is due to the decrease in the adatom diffusion length on the surface before it desorbs. This follows along with the previous approach of decreasing the TMG flow. By decreasing the amount of time the reactant species are on the surface essential limits the number of available species to react with and thus favors growth of the $(11\bar{2}0)$ plane.

A simple model was developed by Coltrin and Mitchell for the qualitative analysis of SAG growth of GaN in rotating disk reactor (RDR) [59]. This model uses three main parameters, *Da*, θ, and ε to determine and control the growth regime of the system. The Damkohler number (*Da*) is a measure of the relative speed of the main growth reaction compared to the transport of the reactant species through the boundary layer. It is used to determine whether growth is reaction rate limited or transport limited. *Da* is a dimensionless number defined by Equation 2-2,

$$Da = \frac{k\delta}{D} \tag{2-2}$$

where δ is the boundary layer thickness, *k* is the reaction rate constant and *D* is the gas phase diffusion coefficient. The fill factor (θ) is the fraction of exposed area available for growth to occur. This parameter is commonly used in the ELO of GaN and is defined by Equation 2-3.

$$\theta = \frac{w}{p}\ , \quad p = m + w \tag{2-3}$$

where *m* is the width of the mask, *w* is the width of the window and *p* is the pitch. These parameters are illustrated in Figure 2-C. The product of θ and *Da* (Equation 2-4) can then be

used to control the growth conditions of the specific growth system to ensure it is in the proper growth regime.

$$\theta Da \gg 1 \text{ (transposrt-limited)}, \quad \theta Da \leq 1 \text{ (reaction-limited)} \tag{2-4}$$

The SAG efficiency (ε) is the measure of the amount deposited on the exposed regions compared to a standard maskless deposition. Thus for a standard growth of a GaN film on a sapphire substrate with no mask, ε would be 1. Equation 2-5 defines ε and shows how the efficiency is directly dependent on θ and Da.

$$\varepsilon = \frac{\theta Da}{1 + \theta Da} \tag{2-5}$$

Selective Regrowth of p-GaN

It was shown that the efficiency of incorporation of Mg into the GaN lattice was dependent on the growth plane [51]. The selective regrowth of p-GaN by MOCVD has been performed on III-nitride- based devices [51, 52]. The sidewalls of the device structure, after dry etching, were inclined and rough. The regrowth of Mg-doped GaN over the device structure resulted in the formation of three distinct facets. Together with the (0001) surface, the sidewalls were very smooth vertical $\{11\bar{2}0\}$ facets and a small $\{11\bar{2}2\}$ inclined facet at the shoulder was observed. Characterization of the structure after regrowth showed that the Mg concentration on the three faces was different. The variation in the incorporation of Mg atoms into the different growth planes is due to the deviation in the probability of the Mg sticking to the surfaces. The most probable reason for the difference in the Mg sticking probability is the dissimilarity in the surface structures of the three facet surfaces. The growth rates of the (0001), $\{11\bar{2}2\}$ and $\{11\bar{2}0\}$ facets significantly differ. The growth rates of these facet surfaces are a function of the growth temperature and pressure. The changes in the growth rates of each facet are due to the relative surface stability which is dependent on surface energy [42]. At lower temperatures, the growth

rate of the $\{11\bar{2}2\}$ surface is dominant and poor surface migration of the Ga atoms causes the (0001) surface to roughen. As the temperature is increased the (0001) surface becomes smooth and the (0001) and $\{11\bar{2}0\}$ planes become the dominant growth facets. At low P or high T the $\{11\bar{2}2\}$ facet becomes unstable because the surface nitrogen atoms are not stabilized. Then the $\{11\bar{2}0\}$ and (0001) surfaces become energetically favorable due to their smaller density of dangling bonds and will dominate the growth. If the pressure becomes too low or the temperature becomes too high, the (0001) surface becomes rough again due to the increasing rate of evaporation of absorbed Ga species on the surface. The differences in the dangling bond densities and the growth rates of the facet surfaces must affect the sticking and incorporation probability of Mg atoms. The relationship between the dominant growth facets with respect to temperature and pressure is illustrated in Figure 2-6. The figure also shows the dependence of the Mg incorporation on the dangling bond densities of the different growth surfaces.

To further complicate the matter, it has been shown that the growth rate of the different facets is affected by introducing Mg into the growth environment [53]. Having Mg present decreases the vertical growth rate and increases the lateral growth rate. The decrease of the (0001) growth rate with the addition of Mg suggests that Mg incorporates at the surface on group III sites and that this results in competition for occupancy of group III sites between Ga and Mg species [54].

Issues With the Development of GaN-based p-MOS Devices

The reliable production of p-type GaN has been an impediment to the development of GaN-based device technology. The n-type doping of GaN is well established but p-type doping still has many issues associated with it. Efficient p-type doping of GaN has been an incessant challenge due to the difficulty in achieving high hole concentrations. Mg is the most commonly

used p-type dopant due to its successful application in optoelectronic devices. Despite this success, Mg doping in GaN has many inherent difficulties. The difficulties of Mg as a p-type dopant are due to its large hole mass and its high ionization energy (E_v>170 meV) [55]. The deep nature of the Mg-acceptor results in a poor hole activation of only a few percent at room temperature. To overcome this it becomes necessary to heavily dope the GaN with excessively high Mg concentrations. The heavy Mg doping often results in the creation of structural and electrically-compensating defects, which significantly degrade the hole mobility and result in resistive p-GaN films [56].

It has been shown that ion implantation is not an effective method for p-type doping of GaN [55]. The concentration of p-type carriers is usually significantly less than what it was predicted to be. This is most likely due to the fact that unintentionally doped GaN is inherently n-type. The lattice damage produced during the implantation process probably also contributes to the n-type lattice defects created. Annealing after the implant process in order to correct the lattice damage has been shown to not increase the hole density [57]. The doping of GaN with Mg during MOCVD growth has shown better success than with ion implantation. However, as was previously mentioned, there are still several issues that make it difficult for the production of high quality p-GaN.

For wide-bandgap semiconductors in general, it is difficult to fabricate low resistance ohmic contacts. Ohmic contacts for *n*-GaN have been well developed mainly due to GaN being intrinsically *n*-type. The difficulties with *p*-type doping of GaN have made the development of ohmic contacts to *p*-GaN very challenging. In order to produce low resistance ohmic contacts, a highly doped surface layer and/or a low Schottky barrier height is needed. The poor hole mobility and low hole concentration that exist for Mg-doped *p*-GaN results in large sheet

resistance, which prevents the fabrication of reliable ohmic contacts with low contact resistivities [56]. The lack of ohmic contacts for *p*-GaN makes electrical characterization measurements of *p*-GaN using conventional I-V and C-V techniques very difficult. It has been observed that increasing the work function of the metal contact decreases the resistance at the *p*-GaN/metal interface exponentially [58]. In general for a p-type semiconductor, the metal work function needs to be equal to or larger than that for the seiconductor. Thus for *p*-GaN this would require a metal with a work function of approx. 8 eV, which does not exist [55]. An alternative process is needed to increase the surface doping or decrease the barrier height as well as an accurate method to measure the barrier height in *p*-GaN.

Another problem that is associated with the processing p-MOS devices is the plasma damage created from the dry etching of p-GaN. After a plasma dry etch, an increase in the reverse breakdown voltage has been observed that is attributed to a reduction in acceptor concentration in the surface of p-GaN. At high flux plasma conditions conversion to an n-type surface has been observed. The exposure of the p-GaN surface to the plasma produces shallow donor states, which decreases the hole concentration near the surface [57]. The creation of shallow donor states has been attributed to nitrogen vacancies. A method that is commonly used for removing plasma-induced damage is high temperature annealing. Annealing at temperatures >900^{o}C can also significantly decrease p-type conduction due to nitrogen loss from the p-GaN surface.

Table 2-1. Rate-limiting kinetic Scheme for the MOCVD of GaN from TMG and NH_3.

Main Reactions		k_o	E_a (kcal/mol)	Ref
Adduct formation	$(CH_3)_3Ga + NH_3 \Rightarrow (CH_3)_3Ga{:}NH_3$	coll.	0.0	[8]
Methane elimination	$(CH_3)_3Ga{:}NH_3 \Rightarrow (CH_3)_2Ga{:}NH_2 + CH_4$	$(4.3\pm.41)\times10^{13}s^{-1}$	48.7 ±5.3	[4]
Oligimerization	$3[(CH_3)_2Ga{:}NH_2] \Rightarrow [(CH_3)_2Ga{:}NH_2]_3$	coll.	0.0	[8]
Dissociation	$(CH_3)_2Ga{:}NH_2$ / $[(CH_3)_2Ga{:}NH_2]_3 \Rightarrow$ Products	$4.0\times10^{13}s^{-1}$	50.5	[4]

Activation energies are in (kcal/mol) and pre-exponentials are in s^{-1}. Rate constants are given by $k=k_0 \exp(-E_a/RT)$. coll. = collision rate-limited

Table 2-2. Dependence of Mg concentration on the dangling bond densities of the different growth surfaces.

Plane	Dangling bond density	Mg concentratiom
(0001)	11.4 nm^{-2}	Maximum
$\{11\bar{2}0\}$	14.0 nm^{-2}	-
$\{11\bar{2}2\}$	17.8 nm^{-2}	Minimum

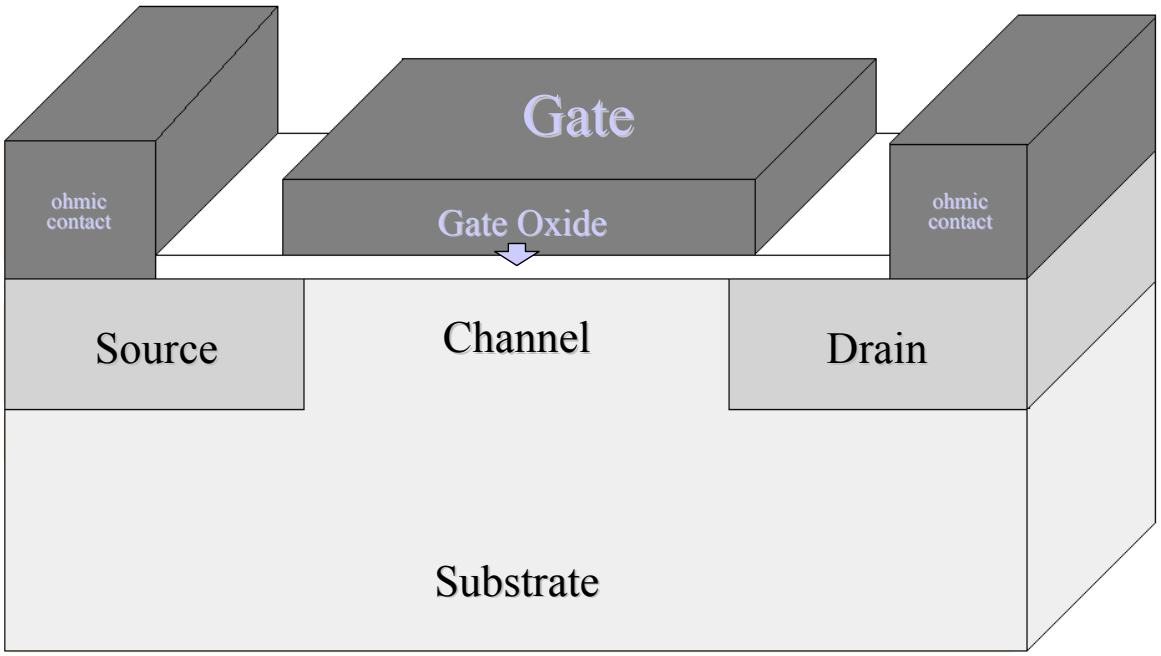

Figure 2-1. Basic structure of a MOSFET device.

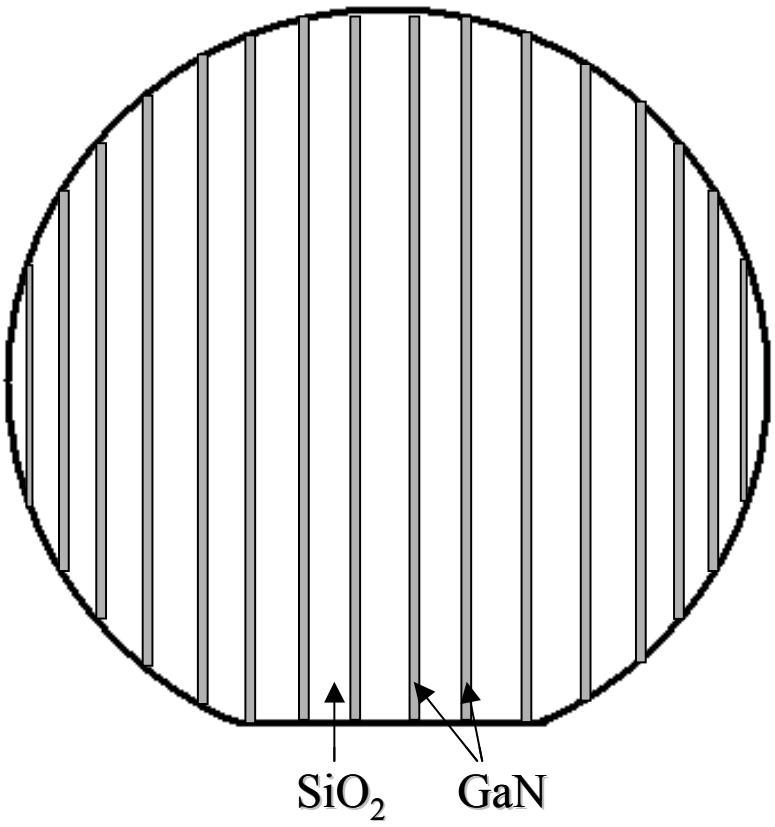

A

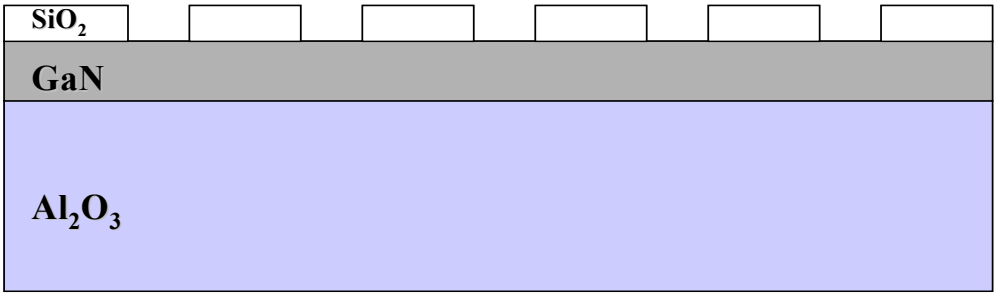

B

Figure 2-2. Typical structure of an ELO substrate. A) Plan View B) Cross section View.

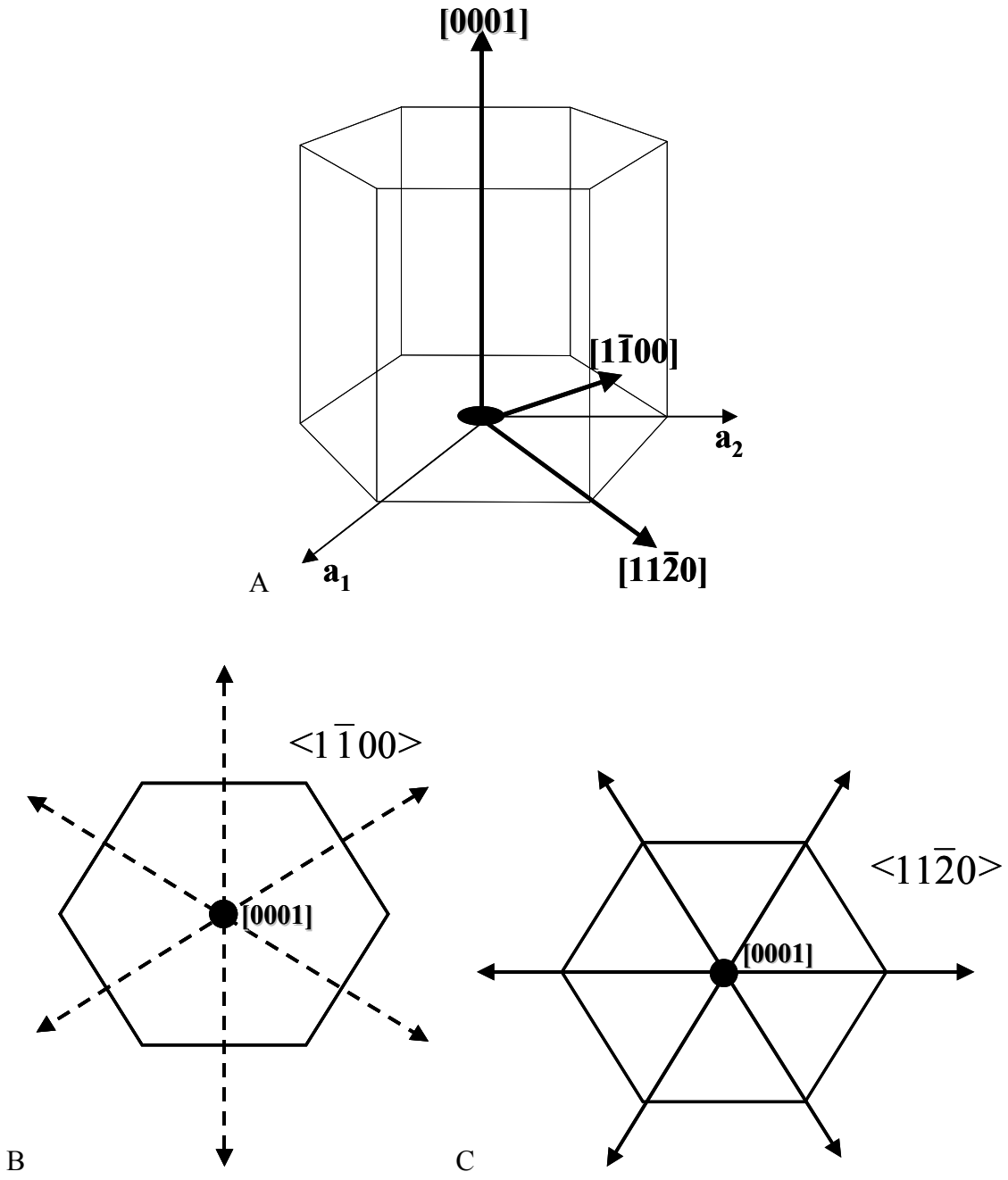

Figure 2-3. Orientation and directions defined. A) GaN unit cell. B) The <1$\bar{1}$00> directions. C) The <1120> directions

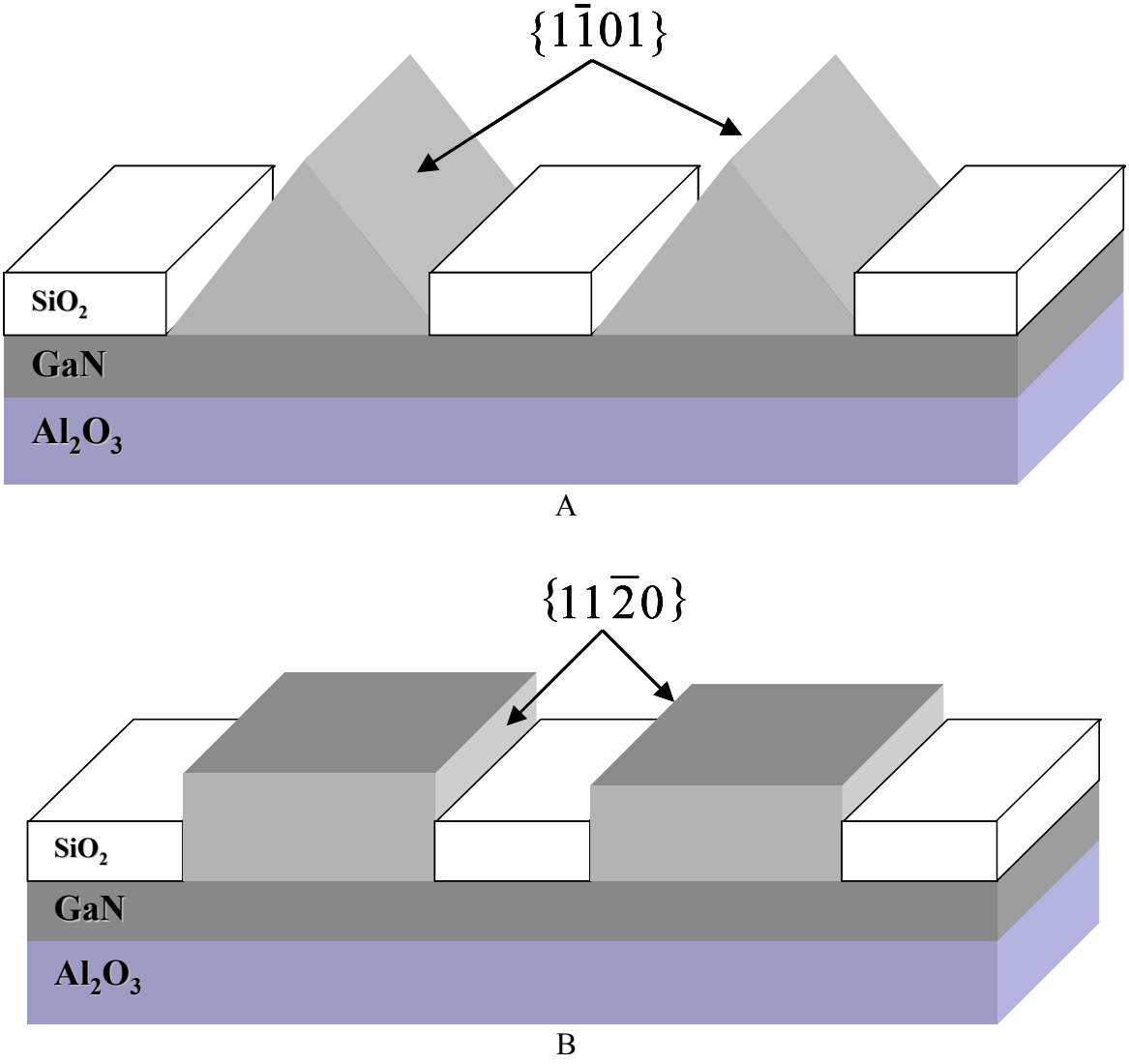

Figure 2-4. Illustrations of the Growth mechanisms from an ELO substrate. A) For <1120> oriented stripes. B) For <1101> oriented stripes.

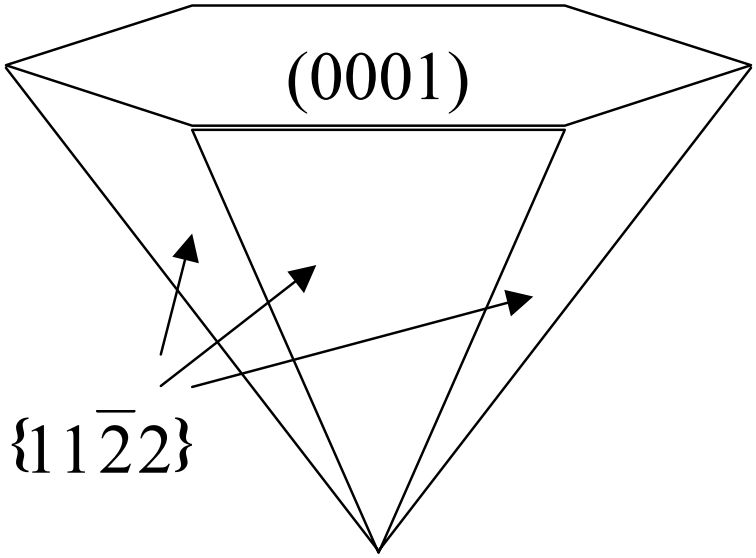

Figure 2-5. Mg-induced defect formed during growth.

Figure 2-6. Relationship between the facet growth rate and the reactor pressure and temperature.

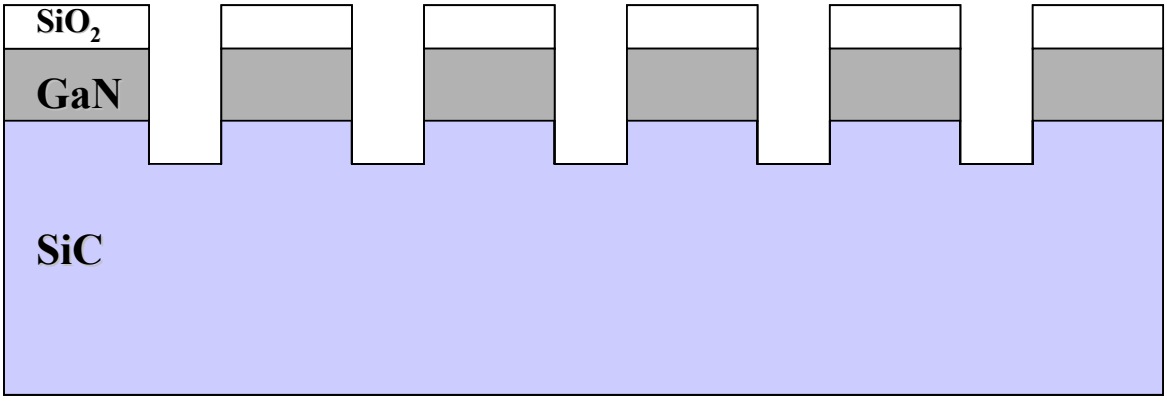

A

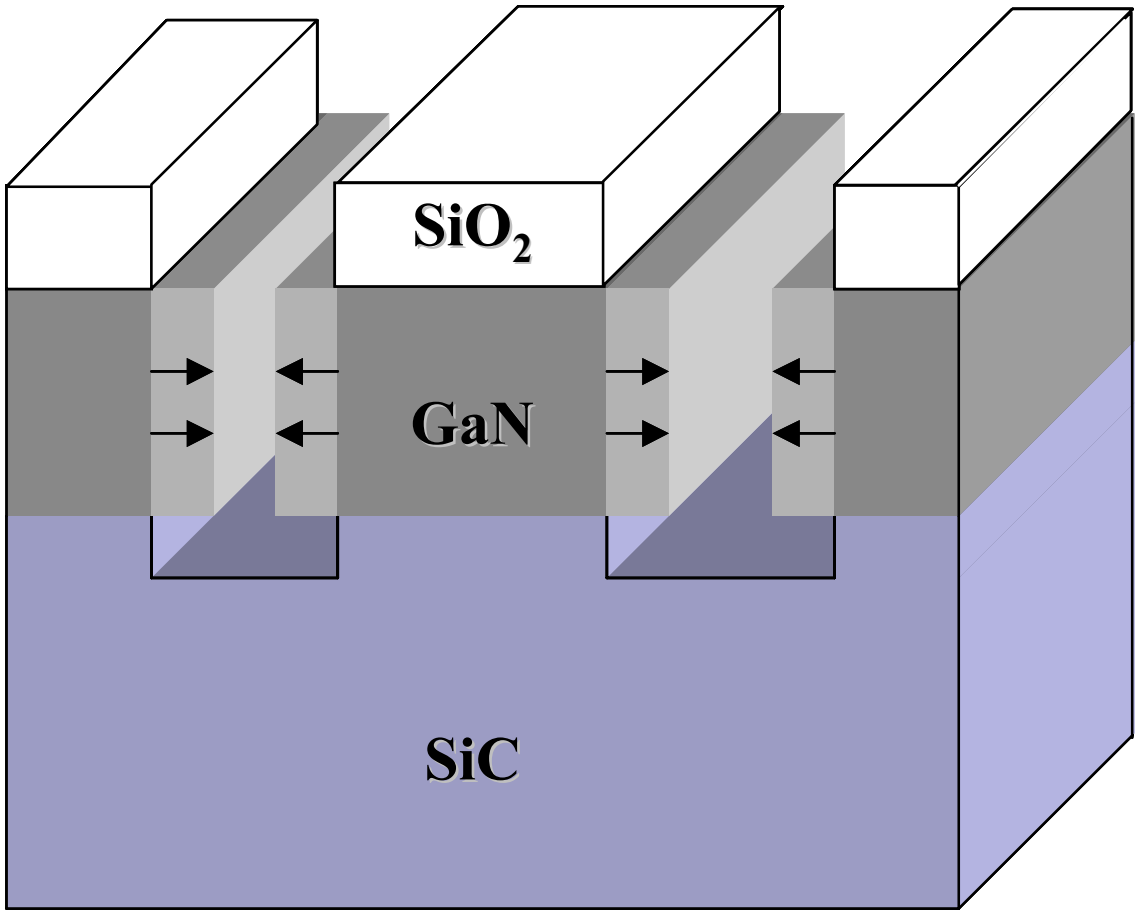

B

Figure 2-7. Structure of a substrate used for pendeo-epitaxy. A) Cross section view. B) Illustration showing how growth occurs from the sidewalls.

CHAPTER 3
EXPERIMENTAL APPROACH

Growth of Oxide and GaN Heterostructures

The MOCVD of GaN Substrates

The GaN substrates and device structures were grown in a Veeco/Emcore P75 MOCVD vertical rotating disk reactor. In figure 3-1, the basic layout of the reactor is shown, where it can be seen how the reactant gases are delivered to the surface of the substrate that is being rotated up to 1500 rpm and that can be heated to over 1100^{o}C. The reactor has Ga, Al, and In metalorganic sources available, thus allowing the growth of any group III nitride film. Which of the two group III metalorganic Ga sources on the system, trimethylgallium (TMG) and triethylgallium (TEG) that will be used for the GaN growth is dependent on the application of the film. TEG is known to produce less carbon contamination but TMG is less expensive and is the predominant source used for MOCVD growth of GaN. The *n* and *p*-type dopant sources will respectively be silane (SiH_4) and bis-cyclopentadienyl magnesium (Cp_2Mg). All the metalorganic sources are delivered to the reaction chamber using nitrogen as the carrier gas. The group V source will be ammonia (NH_3) using nitrogen as the carrier gas. The substrates used for growth will predominantly be (0001) oriented sapphire (Al_2O_3).

The rate-limiting step of MOCVD processes is generally determined by surface kinetics or by mass transport. For the MOCVD of GaN the temperatures and pressures are high making the boundary layer thicker and more difficult for reactants to reach the growth surface. The high temperatures also allow the decomposition of the reactants to occur more rapidly and thus any molecule that reaches the surface reacts instantly [36]. Therefore it is usually assumed that the MOCVD of GaN is performed in the diffusion-limited regime, over a temperature range of 600-1100^{0}C. The growth rate is proportional to the flux of the atoms being transported through the

gas-phase to the interface. Since ammonia is in large excess compared to TMG, it is the pyrolysis and diffusion of the Ga species through the boundary layer that is the main pathway controlling the growth rate. Parasitic side reactions can decrease the growth rate by limiting the flux of the Ga species to the growing interface.

For the flow over the substrate, the concentration gradient in the Ga species is established over a boundary layer of thickness (δ). The flux of the Ga species through the boundary layer (J_{Ga}) is given by Fick's first law of diffusion in Equation 3-1. Since the growth rate is proportional to the this flux, the growth rate (R) can be calculated from the flux by using Equation 3-2.

$$J_{Ga} = \frac{D_{Ga}\left(P^{*}_{Ga} - P^{i}_{Ga}\right)}{\delta RT} \tag{3-1}$$

$$R = \frac{J_{Ga} MW_{Ga}}{\rho_{Ga}} \tag{3-2}$$

In Equation 3-1, D_{Ga} is the diffusion coefficient of the Ga species, P^{*}_{Ga} is the input partial pressure of the Ga species, P^{i}_{Ga} is the partial pressure of the Ga species at the solid/vapor interface. In Equation 3-2, MW_{Ga} is the molar weight of Ga and ρ_{Ga} is the GaN density.

To observe and analyze the growth *in-situ*, an emissivity compensated pyrometer was used. Emissivity compensated pyrometry is an extremely important tool for *in-situ* analysis of MOCVD growth. The greatest advantage of this technique is the complete lack of intereference between the process being measured and the instrument. For the MOCVD growth of thin films emissivity-compensated pyrometry is used to measure the wafer's thermal emission using a pyrometer, measure its surface reflectivity using a reflectometer, calculate its emissivity and then calculate the wafer's temperature.

All surfaces absorb different amounts of electromagnetic energy from radiation. The fraction of energy absorbed by a material is defined as its spectral absorptivity (α). Emissivity (ε) is defined as the fraction of the thermal emission emitted by a surface compared to that of a perfect absorber of radiation. Both the absorptivity and the emissivity are dependent on the wavelength, exit angle and polarization of the radiation as well as the ambient temperature. Using Kirchhoff's radiation law (Equation 3-3) and the law of energy conservation for the relationship between the total reflectivity (R) and absorptivity (Equation 3-4), the key relationship for emissivity compensated pyrometry (Equation 3-5) is derived.

$$\varepsilon = \alpha \tag{3-3}$$

$$R + \alpha = 1 \tag{3-4}$$

$$\varepsilon = 1 - R \tag{3-5}$$

The emissivity compensated pyrometer is a device that combines a reflectometer and a pyrometer to provide real-time accurate measurements of the reflectivity and temperature of the wafer surface during the growth. The equipment for emissivity compensated pyrometry consists of an optical head and a computer with a data acquisition board. The configuration of the equipment with respect to the wafer is illustrated in Figure 3-2. The optical head has an LED that is thermostabilized and emits light at a wavelength of 930 nm and is modulated at a rate of 5.2 kHz. The main photodiode of the optical head measures the thermal emission from the wafer and the LED light that is reflected by wafer. Using special digital processing algorithms, the reflectivity and emission data from the raw signal is extracted with low noise and high time resolution. The emissivity compensated pyrometer that was used was designed to measure the temperature of both transparent and opaque substrates as well as the wafer carrier. Each surface will have different reflectivity and emissivity variations. Emissivity is dependent on the

properties of the material and the surface, which can significantly change during MOCVD growth, making it difficult to perform accurate temperature measurements. A typical plot of the temperature and reflectivity for the MOCVD growth of GaN substrates is shown in Figure 3-3 and is used to monitor the growth *in-situ* and in real time. It is an extremely valuable tool for understanding and controlling how each growth occurs.

Molecular-Beam Epitaxy Of Oxide Dielectrics

The oxide dielectrics that were studied were grown using molecular-beam epitaxy (MBE). MBE is a highly controlled growth process in which beams of precursor atoms are aimed towards a heated substrate where growth of a thin film takes place. The precursor source materials are contained in heated effusion cells that have a small orifice in the wall of the cell that is directed toward the substrate. A shutter is used to separate sources from the growth chamber. When growth is desired using a particular source, the shutter is opened producing an atomic beam of the source, whose flux is controlled by the temperature of the cell. This allows for very precise control of the film thickness and composition as well as the dopant incorporation. The substrate is also rotated during growth to produce excellent uniformity.

One of the main advantages of MBE is its ability for *in-situ* measurement due to the use of an ultrahigh vacuum (UHV) environment. This allows for real-time control of the growth and makes MBE a valuable research tool for studying the growth processes involved. Two techniques that were used in the growth of the oxide thin films is mass spectrometry and reflection high-energy electron diffraction (RHEED). Mass spectrometry was used for measuring the source fluxes and for residual gas analysis. RHEED reflects high-energy electron beams at very small angles from the growth surface to monitor the film structure.

Many of the same processes that occur in MOCVD are involved in MBE growth. These include the transport and adsorption of the precursor species onto the substrate, then the

nucleation and growth of the film, and finally the desorption of unreacted species from the surface. Control of these processes is essential for the growth of high quality films and was accomplished by optimizing the growth conditions such as the substrate temperature and flux.

The MBE of scandium oxide (Sc_2O_3)

The Sc_2O_3 films were grown on the MOCVD GaN/Al_2O_3 (0001) substrates. The substrates were cleaned prior to growth using subsequent *ex-situ* and in-*situ* treatments [6]. They were grown using molecular beam epitaxy (MBE) of an elemental solid source and oxygen plasma in a modified RIBER 2300 MBE reactor to thicknesses of 80 to 400 Å at a substrate temperature of 575^0C. The sources used were elemental Sc (99.999%) at a cell temperature of 1190^0C and oxygen (99.9995%) plasma. The oxygen plasma was created using an Oxford Scientific RF plasma source operating at 300 W forward power. During growth, the samples were rotated at 15 rpm. The substrate temperature, oxygen flow rate, and solid source fluxes were varied in order to obtain the optimal growth of the oxide films. Growth quality was examined *in-situ* through RHEED analysis of the oxide surface.

The MBE of magnesium oxide (MgO)

The MgO films were grown on the MOCVD GaN/Al_2O_3 (0001) substrates that were cleaned prior to growth using both *ex-situ* and in-*situ* treatments. The MgO films were deposited using molecular beam epitaxy (MBE) in a modified RIBER 2300 at a substrate temperature of 100^0C. The sources used were elemental Mg (99.999%) at a cell temperature ranging from 340^0C to 360^0C and oxygen (99.9995%) plasma created using an Oxford Scientific RF plasma source operating at 300 W forward power. The oxygen pressure was kept below $5x10^{-6}$ Torr to ensure a low growth rate. For the growth of MgO, a low growth rate ranging from 8.0–14.0 Å

/min was used. When the MgO films that are grown at a lower growth rate are less vulnerable to the chemical and thermal treatments involved in device processing.

Deposition of Silicon Dioxide (SiO_2)

Plasma-enhanced chemical vapor deposition (PECVD) was used to deposit silicon dioxide (SiO_2) on the MOCVD GaN/Al_2O_3 substrates . PECVD uses radio-frequency (RF) and microwave plasmas that contain highly-reactive species to deposit thin films onto a substrate at relatively low temperatures between 25 to 500^0C. Two important advantages of PECVD are the large deposition area and the deposition of high-temperature materials at low temperatures. The value of low temperature deposition is in its application in electronic device fabrication. High temperatures can degrade the structure and properties of materials that are used in device processing. Another important advantage of PECVD is the wide range of film properties possible due to the large amount of deposition parameters that can be varied. These include the substrate temperature and bias potential as well as the discharge pressure and power of the plasma.

Like MOCVD, PECVD is a particularly complex technique due to all the possible species involved and processes occurring on the surface of the growing film as well as in the plasma. Since the SiO_2 films are only being used as a mask for selective growth in MOCVD, the film properties are not that important other than it must be thermally stable due to the high growth temperatures used in MOCVD. Thus, the optimization of deposition conditions was minimal. Since growth occurs through the competition between deposition and etching, the conditions must at least be optimized such that deposition is ensured so that substrate is not damaged.

A Plasma-Therm SLR series PECVD reactor was for the deposition of 1000 Å of silicon dioxide (SiO_2) at a temperature of 255^0C. The plasma used was produced at a pressure of 900 mTorr using 30 watts of power. Silane (SiH_4) and nitrous oxide (N_2O) were used as the reactant gases, each at a flow rate of 200 sccm.

Substrate Preparation for Selective Area Regrowth by MOCVD

Titanium (Ti) and tungsten (W) coating of substrates

For substrates that had the oxide deposited using MBE, an extra step was involved to make samples compatible to both the MBE and MOCVD reactors. The normal method of mounting the substrate to a molybdenum block with indium metal was not used in the fear that any indium remaining on the substrate will contaminate the MOCVD reactor. To avoid using indium metal to mount the substrates in MBE, a layered structure of titanium and tungsten was sputtered on the backside of the substrates. The layered metal film on the substrate's backside was needed because sapphire and GaN both don't absorb the radiation and thus will not be heated to the temperature necessary for deposition. The metal film will absorb the radiation and uniformly heat the substrate. The introduction of Ti layers within the W was done in order to keep the W from popping off the backside due to stress. To deposit the Ti/W metal layers, a Kurt Lesker CMS-18 sputter deposition tool was used. Deposition via sputtering occurs when ions from an Ar plasma strike a solid metal target, which eject metal atoms that are then deposited onto a sample.

Photolithography of the regrowth pattern

Photolithography involves the patterning of two-dimensional designs onto a sample using the selective passage of light through a mask of the desired pattern. The sample is covered by a uniform layer of photoresist, which is a polymeric material that is sensitive to light. When the photoresist exposed to light, photodissociation occurs, where the bonds in the long polymeric chains are broken making it soluble in a suitable chemical solvent.

Two types of photoresist were used depending on the application. For the dry etching of the oxide and GaN, Shipley 1045 was used because it was thicker and gave more protection to the substrate from the harsh dry etching environment. For all other processes that required

photoresist, Shipley 1818 was used. The general application procedure for both types of photoresist was the same except for the chemical solvent used.

The photoresist was applied through a spin-on procedure using a Laurell WS-400A 6NPP/Lite that uses a vacuum to secure the sample to a mount as it rotates. The photoresist was dispensed using a dropper onto the sample and then immediately started rotating at a speed of 4000 rpm for 30 seconds. When finished, the samples were heated to 115^0C for 5 minutes in order for the photoresist to partially dry so that it will not adhere to the mask during exposure.

The sample was then loaded into a Karl Suss MA6 mask aligner, which has the proper mask secured in place. The sample was then properly oriented and aligned with respect to the mask. Depending on the specific application, this step could require a few seconds up to an hour and may require several iterations of photoresist application and removal. Once the sample is properly aligned, it was exposed to a UV lamp for a specific amount of time. The minimum feature size attainable is controlled by diffraction effects, which limit the feature definition to about one-half of the wavelength of the light used. To maximize the feature definition the sample was placed directly in contact with the mask. The exposure time would vary from 30-45 seconds depending on the status of the lamp.

After exposing the samples to the UV light they are gently stirred around in either Rohm and Haas MF-321 or MF-322 developer for Shipley 1818 and 1045 respectfully for approximately 30 seconds. Sometimes a few more seconds in the developer is needed to fully remove the photoresist within all the features. After rinsing off the developer, the samples are heated on a hot plate to 115^0C for 5-20 minutes, depending on the application.

Etching of the oxide and GaN heterostructures

Wet etching of the SiO_2 films was done using a diluted (25-50%) buffered oxide etch (BOE). To wet etch MgO films a very dilute (.25%-1%) solution of phosphoric acid (H_3PO_4) was used. Sc_2O_3 films were wet etched using a sulfuric acid solution (H_2SO_4:H_2O (1:1)). No wet etchants are available for GaN.

Dry etching of SiO_2 was performed using a Technics Micro-RIE series 800-II reactive ion etcher (RIE). RIE is a plasma etching process that contains both a chemical and physical etching component. In RIE the sample is exposed to a chemical etchant in a plasma that reacts with surface. The physical component is from the ions in the plasma that transfer kinetic energy to the sample, which removes material by sputtering. The ion beam also enhances the chemical reaction rate by exciting reactants and creating steps on the surface. The steps have dangling bonds that are readily available for reaction. The process gas was CF_4. The plasma was produced using a flow rate of 30 sccm and 50 W of power. To dry etch the features into the MgO and Sc_2O_3 thin films as well as the GaN substrate, an Unaxis Shuttlelock reactive ion etcher (RIE) with inductively coupled plasma (ICP) module was used. This system utilizes the advantages of both the RIE and ICP etching methods by combining them. The system is equipped with a 2 KW inductively coupled power supply and a 600 W RIE power supply, along with two 13.56 MHz RF power supplies. The process gases used were chlorine (Cl_2) and argon (Ar).

Pretreatment

After etching, the etch depth is verified using a profilimeter. Then the photoresist is removed in subsequent treatments of acetone, isopropanol and methanol. The sample will now be examined for quality using SEM and an optical microscope. For samples that used a SiO_2 regrowth mask, within an hour before loading the sample in the reactor for the regrowth, it is exposed to 30 sec. of O_2 plasma in the Micro RIE. The sample is then submerged in (1:10)

$HCl:H_2O$ solution for 1 minute and rinsed and blown dried with N_2 gas immediately before loading into the reactor. This is to remove any possible residue remaining from the photoresist and any other contaminants that might have been acquired during post processing characterization.

Fabrication of GaN-Based Diodes

The main equipment and materials that were used and the description of the steps taken for photolithography were described previously. The photolithography processes used in diode fabrication are mostly the same. Only the particular materials used and any different procedures that are specific to the fabrication of the diodes are described.

Fabrication of MOS Diodes

Photolithography of the diode pattern

When metal gates were being deposited for the fabrication of oxide diodes LOR 3B was used with a layer of Shipley 1818 on top. The LOR 3B is used because it develops quicker than the 1818 and thus produces an undercut under the top layer of 1818. This allows for an easier removal of the deposited metal on the masked regions and produces uniformly shaped metal gates on the oxide. The rest of the procedure is the same as mentioned above except for the use a different mask. Also, since the structure will not be exposed to any dry etching conditions, a bake of the photoresist after developing is not used.

Deposition of the metal gate contacts

The metal gate contacts for the oxide diodes were deposited using the same Kurt Lesker CMS-18 sputter deposition tool that was used to deposit titanium and tungsten on the substrate backsides. The metal gate structures consisted of 120 nm of gold (Au) on top of 30 nm of platinum (Pt) circular contacts with a diameter of 100 μm. No pretreatment of the oxides was performed prior to the metal deposition.

Fabrication of p-n Junction Diodes

Photolithography of p-type ohmic contact pattern

After the p-GaN regrowth, the samples were processed in order to make p-n junction diodes for electrical characterization. The first step was to deposit a mask for the deposition of the ohmic metal contacts. For some samples the same mask that was used as the regrowth pattern was used for the ohmic metal deposition. This was very difficult, since the regrowth areas were not always uniform and were extremely difficult to distinguish from the substrate. An alternative mask was used that consisted of smaller features consistently repeated. The features were small enough so that a significant amount of regrown areas had a contact but not too small such that it would be very difficult to place a probe on one during electrical characterization.

Deposition of p-type ohmic metal contacts

For the deposition of the p-type ohmic contacts for the p-n junctions, electron beam evaporation was used instead of sputtering, which was used to deposit the metal gates for the oxide diodes. It has been shown that sputtering the ohmic contacts can damage the p-GaN surface, which leads to a very resistive contact. Electron beam evaporation was performed using a CHA-Industries Mark-40 to deposit a layer of nickel (Ni) followed by a layer of Au. The thickness of each layer was varied in order to determine the optimal contact structure. Reference pieces of both n-type and p-type GaN were also patterned and place next to the p-n junction samples during the metal deposition. The reference samples will make it possible to distinguish between having a poor contact and having a poor p-n junction.

Annealing of p-type ohmic contacts

After deposition of the ohmic contacts, current-voltage (I-V) measurements were performed on the samples. Specific contacts were measured and their location was marked with optical photographs. In order to achieve good ohmic contacts to p-GaN, they must be annealed.

All contact annealing was performed in AG Associates HeatPulse 610 RTA system. After all I-V measurements were made, a piece of each sample was cleaved off and annealed in the RTA under ultra high purity O_2 at a temperature of 500^0C for 10 minutes. Pieces of the n and p-type GaN reference samples were also annealed at the same time.

Material and Device Characterization

Characterization of Oxide/GaN and Regrown Structures and Interfaces

The characterization on the Oxide/GaN heterostructures was focused on the chemical, structural and electrical properties of the Oxide/GaN interface. This is due to its large influence on device performance and the lack of knowledge concerning the dynamics of this interface. The following sections will describe the techniques that were used to characterize the Oxide/GaN heterostructures and regrown p-n junctions.

X-Ray Diffraction (XRD)

X-ray diffraction (XRD) is an extremely valuable technique for the structural characterization of materials due to the nondestructive sample preparation and the relatively large measurement volume. X-ray diffraction (XRD) is caused by the constructive interference of x-rays scattered from lattice planes in a crystalline solid. In XRD a collimated beam of x-rays penetrates a crystal and the intensity of the reflected beam is measured. The x-rays will interfere constructively when Bragg's law is satisfied. Bragg's law is stated as Equation 3-1.

$$n\lambda = 2d\sin\theta \tag{3-1}$$

Where n is an integer number of wavelengths, λ is the x-ray wavelength, d is the separation between neighboring planes and θ is the Bragg angle. If the angle that the x-rays scatter and the lattice plane spacing are such that Bragg's law is fulfilled, then the reflected beams will be in phase and interfere constructively. At scattering angles other than the Bragg angle, the reflected beams will be out of phase and destructive interference will occur. Thus, for a given crystal

structure, its diffraction pattern is uniquely produced only at a specific angle. This allows for the determination of the specific phases present in the solid as well as the crystal quality of each.

The measurements were performed using a Philips X'Pert materials research diffractometer (MRD) system in thin film configuration with mirror and monochromator using CuK radiation (1.54 Å). Using x-ray reflectivity (XRR) the interface roughness and film thickness for a sample was determined. XRR uses a low angle of incidence near the critical angle for the total reflection of x-rays. The low angle used only enhances the diffracted intensity from thin surface layers. This makes the technique particularly valuable for the characterization of thin film growth. The in-plane orientation of the films was determined from numerous pole figure measurements.

Transmission Electron Microscopy (TEM)

Transmission-electron microscopy (TEM) was used for analysis of oxide/GaN heterostructures and the MOCVD regrown films. For TEM analysis, a very thin slice of a material is prepared and mounted, usually from 500 nm to less than 100 nm depending on the material. In the microscope, an electron beam with an energy ranging from 20 keV to 100 keV is transmitted through the specimen to produce an image or a diffraction pattern of the specimen. The electrons that emerge from the other side of the sample create diffraction spots on the backfocal plane of the object lens and produce a real image on the image plane of the object lens. The diffraction pattern and image can then be viewed using the magnifying lenses to magnify and project them onto a fluorescent screen.

Both the directly transmitted beam and diffracted beams of electrons are used for observation in TEM. The different techniques used in TEM are based on which beams are being used. Apetures on the microscope allow for one or more of the beams to be selectively chosen to form the image or pattern that is seen on the screen. To form a diffraction pattern using this

method it is called selective-area diffraction (SAD). In a diffraction pattern the large central diffraction spot corresponds to the directly transmitted beam, while all the other spots correspond to the numerous diffracted beams. There are two main techniques used for producing a real image. Bright-field (BF) imaging uses the directly transmitted beam and dark-field (DF) imaging uses a diffracted beam to produce an image. In general, the more beams that are used to form the image, the higher the resolution will be. For lower resolution imaging of the bulk oxide/GaN heterostructures and MOCVD regrown films, a JEOL 200CX analytical electron microscope was used.

Beams with different proximities to the optical axis will not focus at the same point. Thus in conventional TEM, it is usually not possible to focus the directly transmitted beam together with the diffracted beams, which puts a fundamental limitation on the resolution that can be achieved. In high resolution TEM (HRTEM), the diffracted beams are coming off at very small angles and thus remain close to the optical axis. The various diffracted beams combine with the directly transmitted beam in the image plane to cause a sharply defined focal spot. The origin of the sharp definition of the focal spot is that outside the focal spot the beams begin to destructively interfere. This causes the intensity to quickly decay as the distance from the spot increases. The sharpness of the image increases with the amount of diffracted beams that can be focused. With the ability for lattice imaging, HRTEM is an excellent tool for analyzing interfaces. To study the Oxide/GaN interface in more detail, cross sections of the samples were made for HRTEM analysis. HRTEM imaging was performed using a JEOL 2010F Field Emission Scanning Transmission Electron Microscope

Focused Ion Beam (FIB)

The cross-sectional TEM samples were prepared using a Dual-Beam Focused Ion-Beam FEI Strata DB235 FIB/SEM and then viewed using the JEOL 2010 microscope. Focused ion

beam processing uses a 30 kV Ga^+ ion source that is capable of forming a very small probe with a high current density to remove material by physical sputtering. The ion beam can be rastered in defined patterns, which allows for very selective etching. The FIB technique has several advantages over the conventional method of TEM sample preparation, which involves mechanical polishing and Ar ion milling of the sample. The FIB process is very rapid, simple to perform and damage caused by mechanical polishing can be avoided completely. Perhaps the most valuable aspect of FIB is its ability to make TEM samples at very specific, minute locations. This makes it an indispensable tool in the microelectronics industry for analyzing semiconductor devices. One problem that can be encountered when using the FIB process is the formation of amorphous layers containing implanted gallium atoms. This damage can be particularly detrimental to HRTEM imaging. Specimen retrieval was made *in-situ* using a Omniprobe Autoprobe 200, were the specimen is removed from the bulk sample by welding it to the probe using platinum and lift it out (Figure 3-5). The specimen is then welded onto a copper mount where the final thinning is done. This method has several advantages over the *ex-situ* glass rod and micromanipulator technique that uses a fragile copper grid. In addition to a much lower occurrence of specimen loss, it has the ability to be put back into the FIB and thinned some more if it was too thick for high resolution imaging.

Scanning Electron Microscopy (SEM)

Scanning-electron microscopy (SEM) was used to study the substrates in each stage of processing before any growth and the films that were regrown after the experiment. In SEM, an electron beam with an energy ranging from 1 keV to 30 keV is rastered over the surface of the material being analyzed. Using a scintillation counter and photomultiplier tube, the backscattered and secondary electrons that are emitted from the surface of the material are collected and

processed to form a visual image of the surface. Control of the magnification and depth of field is achieved through varying the focal lengths.

Due to the penetration of the electrons into the material, charging of the sample can occur and the image will be distorted. Since oxide films are not conductive and oxides were used as a mask for the regrowth, some distortion in the SEM images can be seen at high magnifications. To minimize the effect of charging, the samples could have been carbon coated or the oxide removed. For imaging of the substrates before regrowth, this was obviously not a viable option. For the analysis of samples after the regrowth had taken place, oxide removal and carbon coating were not used due to the need to further process the samples for electrical characterization.

The SEM column of a FEI DB125 dual beam FIB/SEM and a JEOL 6400 were used to characterize the samples. Both SEMs operate using thermionic emission to produce the electron beam. This occurs through the heating of a tungsten filament to the point where the electrons have enough energy to escape and are emitted from the filament as a beam. The majority of the images were taken using a 5 keV electron beam at magnifications from 100x to 50,000x.

Atomic Force Microscopy (AFM)

Atomic-force microscopy (AFM) was used to determine the surface morphology and roughness of the GaN and oxide thin films that were grown. In AFM a probe is rastered over the surface of a sample and the interaction of the probe with the surface produces a voltage signal that is sent to a computer, which constructs an image of the surface from the signals. The signals from the probe are proportional to the interatomic force between the probe and the surface of the sample. Unlike a traditional microscope, atomic force microscopes have two measures of resolution. One is the plane of the measurement and the other is perpendicular to the surface. The in-plane resolution is dependent on the geometry of the probe, which is given by how sharp it is. A sharper probe will produce a higher resolution in the image. The vertical resolution is

dependent on the vibrations of the probe over the surface. That is why it is important that the microscope have adequate vibration isolation from the surrounding environment. By minimizing the vibrations of the instrument, the vertical resolution can be maximized

There are two methods to measure the force with the probe, contact and tapping mode. In contact mode a constant force is applied to the surface and the probe directly follows the topography of the surface. The image is formed by direct measurement of the motion of the probe. In tapping mode, the probe is sent a signal to keep the height of above the surface constant. The voltage across the probe that is needed to maintain the constant height becomes the signal. Tapping mode is usually used on relatively smooth films when the surface roughness is not too large and produces higher resolution images than contact mode. The surface morphology and roughness of the GaN and oxide films was studied with a Digital Instruments Nanoscope III AFM operating under tapping mode.

X-Ray Photoelectron Spectroscopy (XPS)

X-ray photoelectron spectroscopy (XPS) was used to analyze the chemical structure of the samples. XPS uses photoemission to provide information concerning the surface region of the solid. The process of photoemission involves the absorption of a photon and the subsequent emission of an electron by the photoelectric effect.

When photoemission is carried out with x-rays, it is called XPS. In XPS, monoenergetic X-rays using either an Al (1486.6 eV) or Mg (1256.6 eV) source irradiate a sample causing electrons to be emitted and the resulting energy spectrum and photoelectron yield are measured as a function of photon energy using a hemispherical analyzer. The electron mean free path in solids is limited and for the kinetic energy range of electrons in XPS, the electron escape depth ranges from .2 to 2 nm. Thus only the atoms on the surface that interact with the x-rays will emit electrons that are able to be measured. The binding energy of the core electrons is determined

from the difference in energy of the incident photon and the emitted electrons that are measured. The binding energy of core electrons is unique for each element, allowing for identification of which atoms are present. For each electron to be emitted from the atom's core, it must pass through the valence shells. Thus, the exact value of the electron's energy is sensitive to the distribution of valence electrons surrounding the atom's core. When atoms form chemical bonds, their valence electron distribution becomes distorted and the emitted electron's energy will change. The resulting shifts in energy are characteristic of particular bonds. Thus, in addition to identifying which elements are present, it is possible to determine exactly how each is bonded to each other. This information is extremely valuable for analyzing interfaces when there exists the possibility of an interfacial reaction taking place.

Depth profile XPS was used to determine the chemical bonding scheme at the interface. Performing these measurements before and after annealing will show if any secondary reactions occurred as a result of annealing as well as show if any species have diffused into any of the films. A shift in the binding energy peak of an element and the magnitude of that shift can show if any of the elements have reacted to form new species at the interface. The XPS measurements were performed using a Perkin-Elmer PHI 5100 ESCA system.

Auger Electron Spectroscopy (AES)

Auger emission spectroscopy (AES) is an important tool for determining the chemical composition of the surface of a solid. AES is similar to XPS, but instead of using x-rays to eject electrons from an atom, it uses other electrons. In AES, a beam of high energy electrons impinges on the surface of a solid, which causes some core-level electrons to be ejected. When a high energy electron knocks out a core-level electron, it leaves a vacancy in that electron shell. A higher energy core electron can fill the lower energy vacancy if it releases some energy. One way this is accomplished is by colliding with another electron in its shell and transferring the

excess energy to it. If the excess energy is great enough, a fraction of the electrons receiving the excess energy will be ejected from the solid. This mechanism is called the Auger process and the electrons emitted are called Auger electrons. Since the energies of the inner core electrons are unique to each element, the atoms that are present can be identified. Auger electrons do not have that much energy, so their escape depth is limited to the vicinity of the first few surface layers, making AES a surface technique. The energy of the Auger electrons is measured and the energy distribution is plotted. Each peak in the plot corresponds to a specific element and the intensity of the peak provides quantitative information about that element's relative quantity.

The stoichiometry and chemical uniformity of the bulk films were determined by depth profile AES. This technique is also able to show if diffusion of any species into any of the layers has occurred. The AES measurements will be performed using a Perkin-Elmer PHI 660 Scanning Auger Multiprobe system.

Current-Voltage (I-V) Measurements

All the current-voltage (I-V) measurements were made using a Hewlett Packard Model 4145. For testing of the oxide diodes, compliance was set at 100 nA, and the voltage was swept in the positive direction until the forward breakdown was reached. The forward breakdown voltage for 100 μm gate contacts was chosen at a current of 80 nA, which produces a current density of 1 mA/cm^2. To determine the breakdown field, the breakdown voltages were divided by the thickness of oxide dielectric.

I-V measurements made on the p-n junction diodes were performed using a compliance of 1 μA. The voltage was swept in the negative and positive directions until the reverse and forward breakdown voltages respectfully, were determined.

Capacitance-Voltage (C-V) Measurements

C-V measurements were made with a Hewlett Packard Model 4284 LCR that was connected to a computer using Lab View software. A voltage signal of superimposed AC and DC current was supplied by the LCR meter. The oxide diodes were measured using hysteresis starting from positive voltages and sweeping to negative voltages. The frequency was varied in the range of 100 kHz to 1 MHz in Cp-Rp mode at varying oscillation voltages.

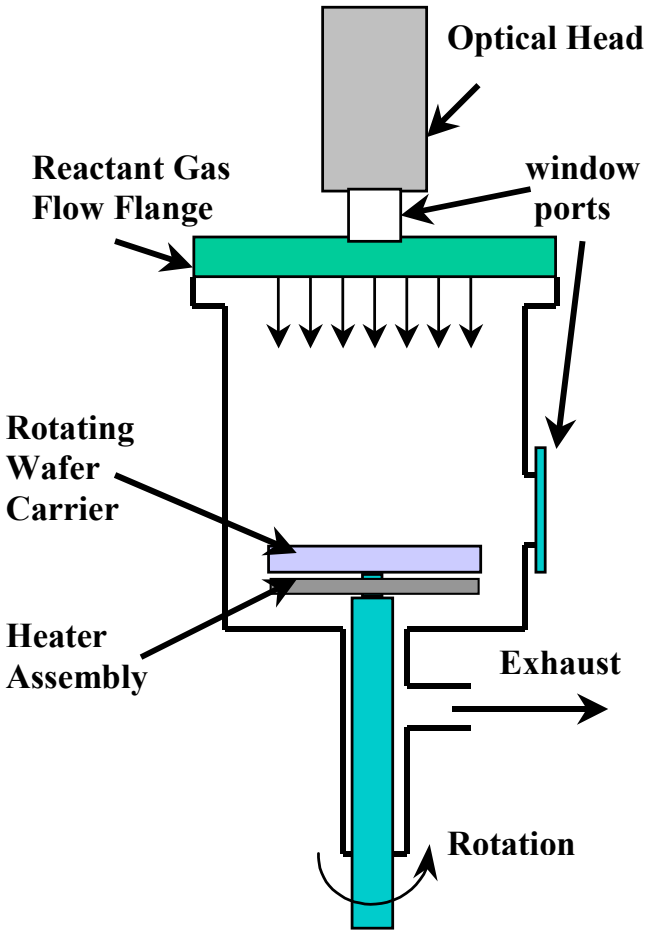

Figure 3-1. Illustrtation of the basic layout of the Veeco/Emcore P75 MOCVD vertical rotating disk reactor.

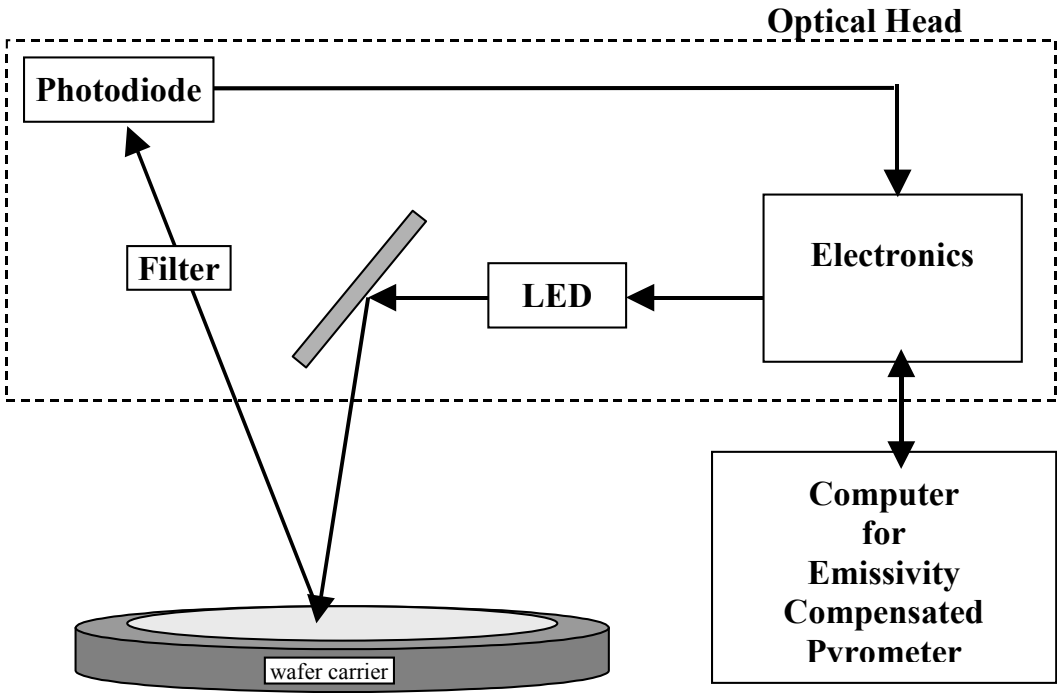

Figure 3-2. Configuration used for emissivity compensated pyrometry during MOCVD growth.

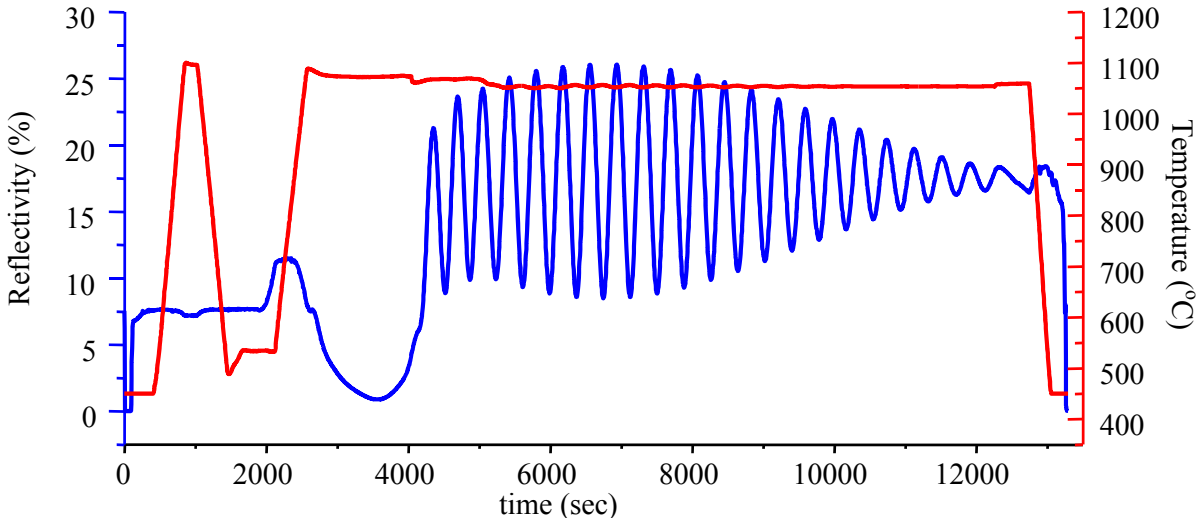

Figure 3-3. Example of the reflectivity and temperature profile for the growth of GaN substrates by MOCVD.

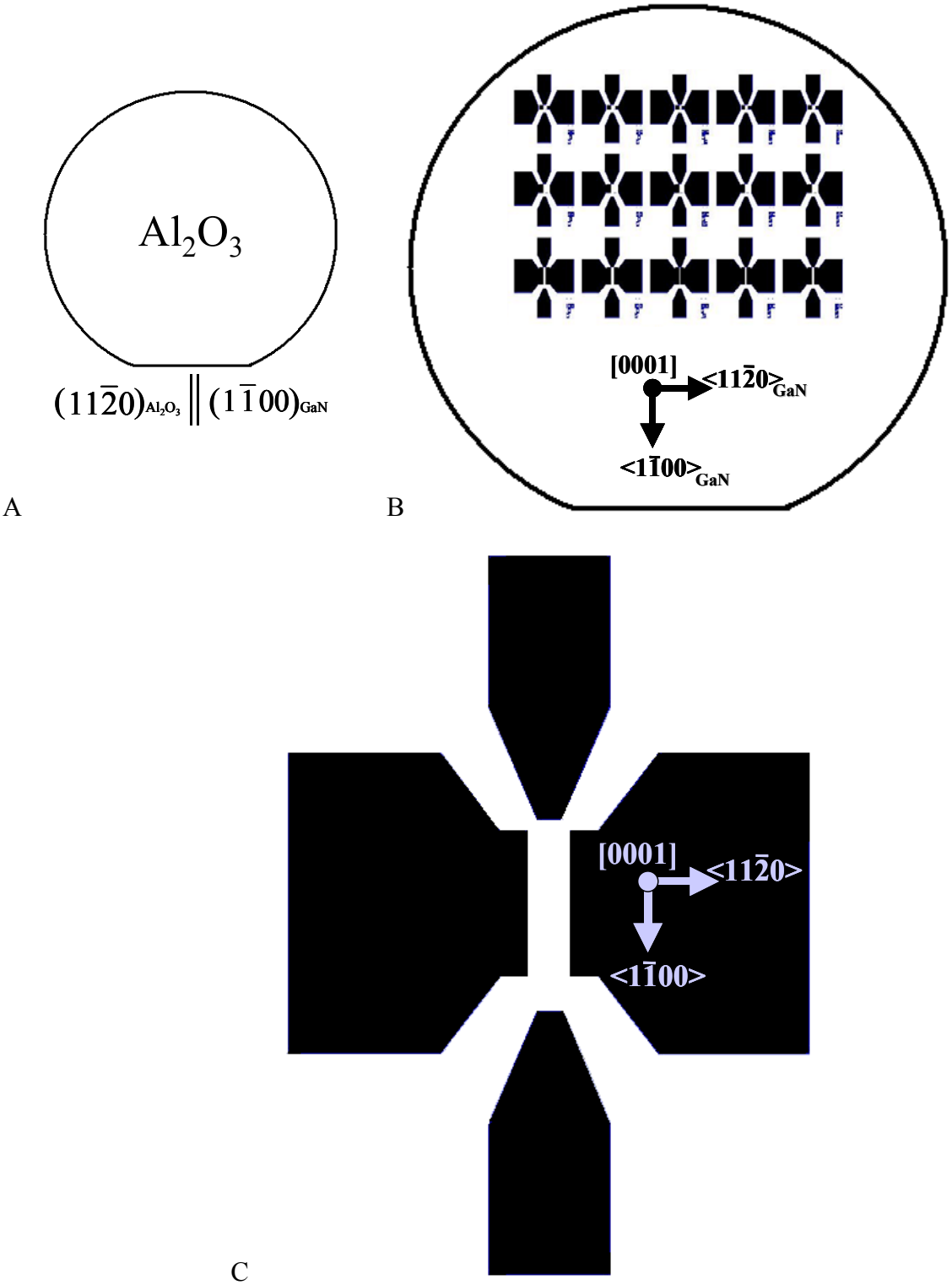

A B C

Figure 3-4. Orientation of substrate and regrowth pattern. A) Orientation of sapphire substrate and its relation to GaN. B) Orientation of the regrowth pattern with respect to the substrate. C) Orientation of a single unit of the regrowth pattern.

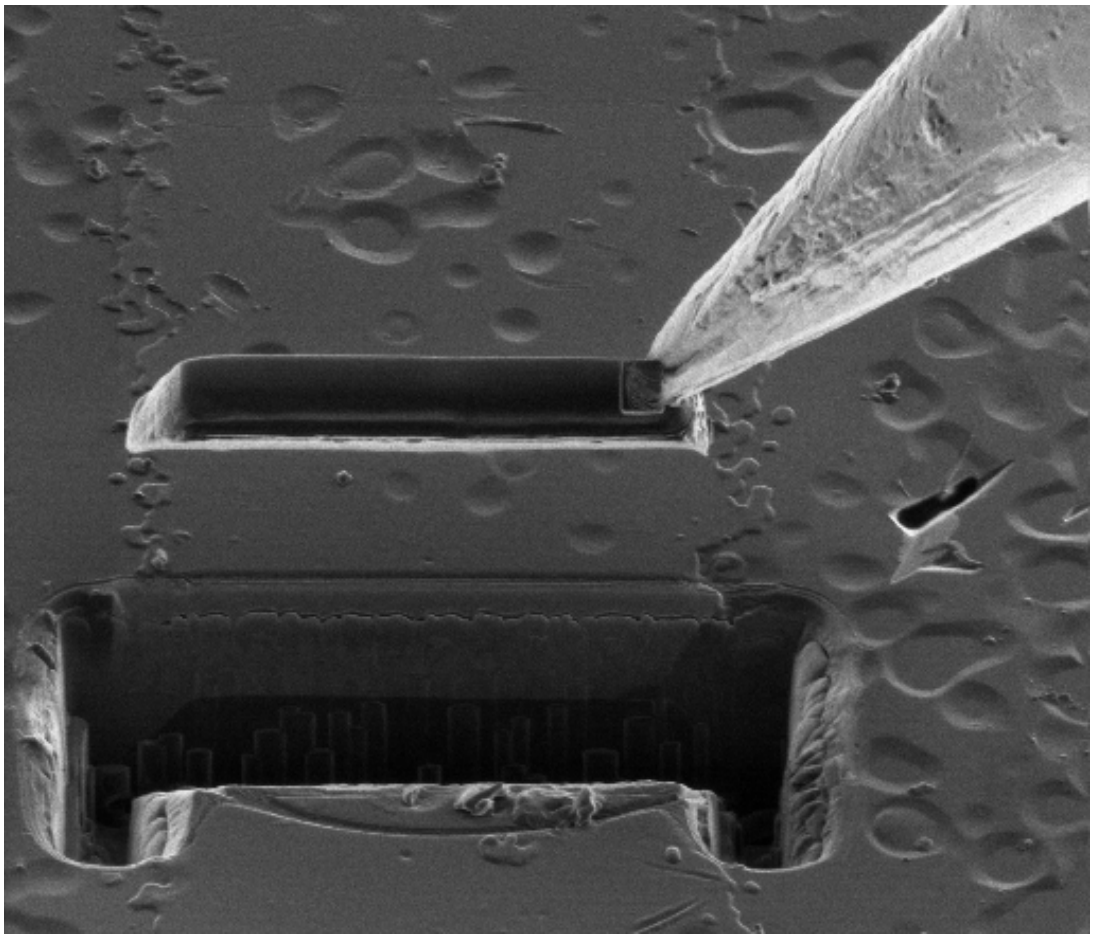

Figure 3-5. Image of a sample during the FIB process for TEM preparation.

CHAPTER 4
EPITAXIAL GROWTH OF SC_2O_3 FILMS ON GAN: RESULTS AND DISCUSSION

Characterization of Sc_2O_3 Films on GaN

Thin films of scandium oxide (Sc_2O_3) were epitaxially deposited on GaN via molecular beam epitaxy using elemental Sc and an oxygen plasma. After growth, some of the Sc_2O_3 films were annealed in the MBE chamber at a temperature of 800^0C and a pressure of 10^{-7} Torr for 5min without the use of oxygen plasma overpressure. The structural quality of Sc_2O_3 films, before and after annealing, was characterized using high-resolution x-ray diffraction, atomic force microscopy (AFM) and high-resolution transmission electron microscopy (HRTEM). Electrical characterization was performed through the fabrication and testing of Sc_2O_3 diodes. Although the focus of this chapter is on Sc_2O_3, the following analysis is applicable, in general, to the growth of face centered cubic (fcc) based oxide thin films on GaN substrates. This makes this investigation particularly significant since the potential dielectrics for GaN-based devices that are currently being proposed within the field are nearly all fcc-based cubic oxides. Thus the detailed analysis of the characterization results can serve as an outline for the general examination of other potential oxide dielectrics for GaN-based devices.

Sc_2O_3 has the cubic bixbyite structure (space group $Ia\bar{3}$). Under suitable conditions, all rare earth metals form a sesquioxide RE_2O_3, and all rare earth metal oxides can obtain the bixbyite structure. The cubic bixbyite structure is a vacancy-ordered derivative of the fluorite structure, where only six of the eight tetrahedral positions are occupied. In the bixbyite structure of sesquioxides, the metal atoms are arranged in an fcc lattice with the oxygen atoms occupying the tetrahedral positions. A unit cell of crystalline Sc_2O_3 (bixbyite) has 80 atoms, where the 32 Sc atoms are in two crystallographically non-equivalent six-fold coordinated sites, *b* and *d*. The two Sc sites can be viewed as being positioned in the middle of a cube with oxygen atoms

occupying six of the eight corners of the cube with the only difference between them being which two corners are left empty. One fourth of the Sc atoms occupy the *b* site, which has six equidistant oxygen atoms and the two oxygen vacancies are along one diagonal of the cube. The other three fourths of the Sc atoms occupy the *d* site, which is coordinated to six oxygen atoms at three different distances, and the two oxygen vacancies are on one face of the cube diagonal from each other [59]. All of the oxygen atoms occupy the same general position. It is the ordering of the oxygen vacancies that makes the unit cell of the bixbyite structure so large. Figure 4-1 shows exactly how the two Sc sites, *b* and *d* are positioned.

As mention before, the oxide/GaN interface for any potential dielectric is critical to device performance. Interfacial reactions at this interface can be quite detrimental. In order to determine the possibility of an interfacial reaction occurring at the Sc_2O_3/GaN interface, thermodynamic calculations were performed for all possible reactions at the interface. The possible reactions and their Gibbs free energy are listed in Table 4-1 at elevated temperatures that could be experienced during the processing and fabrication of a GaN-based device.

The surface morphology of the Sc_2O_3 films using AFM is shown in Figure 4-2. The root mean square roughness of the films is 0.38 nm and 0.35 nm for before and after annealing, respectively. The atomically smooth surface was also observed *in-situ* via reflection high energy electron diffraction during the growth and annealing of the oxide films. The well-defined terraces in the image are characteristic of two-dimensional step-flow growth. The dark spots are depressions that are due to the surface termination of pure screw or mixed threading dislocations (TD). The TDs originate from the underlying GaN substrate. The interaction of the step flow growth of the Sc_2O_3 film with the surface termination of TDs of screw character, results in spiral growth due to pinning of the surface steps. Typical GaN will usually display this morphology

when grown on (0001) sapphire. The TD density was calculated to be on the order of 10^9 cm^{-2} for the Sc_2O_3 film, which is the typical density for MOCVD GaN on sapphire.

The crystalline structure of the Sc_2O_3 films, before and after annealing, was analyzed using high-resolution x-ray diffraction (HRXRD). The volume of the sample that is being measured for X-ray diffraction is much larger than that for TEM. Thus, X-ray pole figure analysis offers more reliable data on the overall epitaxial orientation relationship between the film and substrate.

Using x-ray reflectivity (XRR) the interface roughness for a sample before and after annealing was determined. The XRR scans in Figure 4-3 show that the difference between the two is very small. After fitting the data to a model, the interface roughness was determined to be 0.414 nm and 0.451 nm for before and after annealing, respectively. The model that fit the data did not contain an interfacial layer, implying that no interfacial reaction occurred at the Sc_2O_3/GaN interface. Thus annealing the oxide film roughens the Sc_2O_3/GaN interface by only a small amount. The smoothness of the Sc_2O_3 surface and Sc_2O_3/GaN interface should prevent localized high breakdown fields as well as the smoothness of the interface should provide a high carrier mobility and a low D_{it} [60].

The out-of-plane crystalline quality of the annealed films was determined from ω and ω-2θ rocking curves. The full width at half maximum for the Sc_2O_3 (222) peak was 408.6 arcsec. From this measurement a lattice constant of 0.9875 nm was calculated, showing that the strain in the film is ~.3% indicating that as expected the film is relaxed. The ω-2θ rocking curve of the Sc_2O_3 (222) peak is shown in Figure 4-4. From the figure, the Laue oscillations around the Sc_2O_3 (222) Bragg reflection are clearly visible, which reveals the lateral homogeneity of the film as well as confirms the XRR results of a smooth well-defined interface between the Sc_2O_3 film and

GaN substrate. The film thickness calculated from the period of the Laue oscillations agrees with the value determined from the XRR data to within 2%. Grazing incidence *θ-2θ* (GIXRD) measurements, which are particularly sensitive to the top 100 nm of the sample, also confirmed the lack of misoriented Sc_2O_3 grains.

The in-plane orientation of the annealed films was determined from numerous pole figure measurements. The pole figure measurements were made by tilting the sample normal out of the X-ray plane defined by the source and detector to an angle Ψ, which was varied from 0° to 75° in 1° increments. Then the diffracted intensities were measured for the Sc_2O_3 planes as the sample was rotated about the normal through an angle φ from 0° to 360°.

In Figure 4-5, the $Sc_2O_3\{222\}$pole figure shows the in-plane orientation of the Sc_2O_3 films. The {222} pole figure was taken at a 2θ of 31.40°. The sharp peaks around the center at a Ψ of 70.5° are from the {222} planes. The well defined, narrow {222} peaks and the lack of any other reflections shows that the Sc_2O_3 films are very textured with respect to the *c*-axis. Normally the pole figure for a (111)-oriented cubic film at this angle would produce only three reflections around the center. The pole figure in Figure 4-5 shows six reflections at a Ψ of 70.5°. It is not possible for a cubic material to exhibit sixfold symmetry. Since GaN possesses a hexagonal structure it was initially assumed that the reflections belonged to the GaN $(10\bar{1}0)$ plane that has a 2θ value of 32.41°, is close to that of the $Sc_2O_3\{222\}$, which is 31.40°. The problem with assigning the reflections to the GaN $(10\bar{1}0)$ plane is that the $(10\bar{1}0)$ has an interplanar angle of 90° to the (0001) and thus would not produce any polar reflections. In view of the fact that the measurement was made at the correct 2θ for $Sc_2O_3\{222\}$ and the reflections appear at the correct Ψ for the cubic $Sc_2O_3\{222\}$planes, they had to be attributed to the $Sc_2O_3\{222\}$planes. Therefore, instead of viewing the reflections as a single set of six, they were seen as two sets of three. It is

suspected that the existence of the extra three reflections is due to 180° rotational twinning of the {111} planes. In Figure 4-5, the two twin orientations are labeled as *I* and *II*. From the twin's {222} peak intensity it is possible to determine their respective volumes, since the peak intensity is proportional to the volume of the twins. The relative intensity of the reflections show that there is about an equal amount of both twin orientations. Care should be taken in making any conclusions from a pole figure in this situation. If there exists an equal amount of twin domains, such that the intensity of the two twin variants are approximately the same, then one could erroneously assume a pattern of higher symmetry. Then the existence of an additional symmetry element could lead to the selection of an incorrect higher symmetry space group, which results in assigning the wrong lattice structure to the material. The observation of sixfold symmetry in the RHEED patterns of bixbyite oxides growing on GaN has mistakenly been attributed to the oxides growing with an hexagonal close packed (hcp) lattice structure [33]. This is not very likely since these oxides only exist in an hcp structure at temperatures greater than 2000^0C and the observations were made during their growth at significantly lower temperatures. Further investigation is necessary to prove that the film has grown epitaxially in two twin orientations.

In order to help determine that the extra peaks in the {222} pole figure are really due to twinning, a pole figure of the Sc_2O_3(440) was performed at a 2θ of 52.54°. The {440} peaks are the second most intense diffraction peaks of Sc_2O_3, which will produce significant diffraction in order to characterize the epilayer. The inter-planar angle between (440) and (111) plane is 35.26°. Thus the pole figure should give three strong peaks at a Ψ of 35.26° separated by 120°. If twins are present, diffraction from them should produce an additional three peaks midway between the normal (matrix) {440} peaks thus producing a total of six peaks at a Ψ of 35.26° separated from each other by 60°. As can be seen in the {440} pole figure in Figure 4-6, there are

six reflections at a Ψ of 35.26° separated by 60°. This strongly suggests that the Sc_2O_3 film is twinned and from their relative intensity that there is an equal amount of both twin orientations. The three large reflections at a Ψ of 58° are from the sapphire (Al_2O_3) substrate $(02\bar{2}4)$ plane. Although Sc_2O_3 does also exist in a hexagonal close-packed structure that would exhibit this sixfold symmetry, it is very unlikely that the same reflections could be acquired at the 2θ and Ψ values that correspond to two different diffraction planes of the cubic structure.

The pole figures in Figures 4-5 and 4-6 were performed on annealed samples. To see if the possible twinning was due to the annealing treatment, the same pole figure scans were performed on Sc_2O_3 films that received no anneal. The same twin reflections with the same relative intensity were seen in the {222} pole figures for both the annealed and unannealed Sc_2O_3 films. This suggests that the twinning was not the product of annealing, but that it was caused during the growth of the films.

The XRR and ω-2θ rocking curve measurements show that the Sc_2O_3/GaN interface was smooth and abrupt and was not damaged from the anneal. Although this data does give a good indication of the quality of the interface, it is not definitive and does not completely rule out the existence of an interfacial layer. To study the Sc_2O_3/GaN interface in more detail, cross sections were prepared for high resolution (HR) viewing in the TEM. Figure 4-7 shows HR-TEM images taken at the Sc_2O_3/GaN interface. Figure 4-7B is a HR-TEM lattice image showing a close-up view of the Sc_2O_3/GaN interface. From the image the single crystal nature of the interface is apparent. There is also no evidence of any interfacial layer between the Sc_2O_3 and GaN as was predicted from the thermodynamic calculations.

Additional evidence of the existence of twinning is seen in Figure 4-7A. The images in Figure 4-7 are multibeam phase contrast images where, along with the transmitted spot, the

twinning {111} spots also contribute to the image. In Figure 4-7A, the Sc_2O_3 film shows an enhancement of {111} lattice fringes. The enhanced lattice fringes are moire fringes due to the overlapping of the twin variants. For TEM images where the overlap between two crystals with almost exactly equal lattice parameters occurs, a moiré pattern is produced. A moire pattern will form if a beam diffracted by both crystals is allowed to recombine with the transmitted beam to form the final image. This double diffraction effect is responsible for the formation of moire patterns. In this situation, the moire pattern in the image was formed by setting the objective aperture so that it would admit the transmitted and {111} beams in both crystals. The transmitted and double diffracted beams recombine and the resulting interference between them produces the fringe pattern. The intensity, contrast and position of the moiré fringes change continuously when the specimen is tilted or bent. As a result, some variation in the intensity and contrast of moiré fringes can be observed. The variation in the intensity of the moiré fringes is related to $\sin(\pi t_1 s)$. Where t_1 is the distance between the top surface and the interface and s is the displacement parameter. s is the local divergence of the Bragg spot in the reciprocal spacing due the strain in lattice. Any change of t_1 or s can affect the contrast of the moiré fringes. The value of s is more changeable due to the variation of strain at the interface. The intensity of moiré fringes is also related to the thickness along e^- beam (t). Due to the method of sample preparation using the FIB technique, the thickness is not constant through the length of the specimen. Moiré pattern analysis can be valuable given that they can provide information about the crystal structure of the sample even if the lattice planes cannot be resolved.

The corresponding selected area diffraction pattern taken for the lattice image in Figure 4-7 was taken and is shown in Figure 4-8A. By measuring the distances of the reflections and the angles between them, the diffraction pattern consists of the GaN $(11\bar{2}0)$ and Sc_2O_3 (110) zone

axis. When taking the reflection measurements it is discovered that the diffraction pattern actually consists of two sets of spots corresponding to the Sc_2O_3 (110) zone axis. The two sets are determined to be those of the two twin variants as was seen in the pole figure scans. The twinning occur on {111} planes and the twin axis is determined to be the $\left[\bar{1}11\right]$ because a mirror reflection of one set of reflections about this axis uniquely determines the extra set that is observed. It can be seen that the diffraction pattern for each twin variant can be obtained through rotating the other 180^o about the twin axis. This same situation was discussed in [61] for the case of a (110) diffraction pattern of {111} twins in the fcc system, where the twin axis is parallel to the reciprocal lattice plane corresponding to the diffraction pattern. This electron diffraction pattern consists of three sets of diffraction patterns, one belongs to the $\left(11\bar{2}0\right)$ zone axis of GaN and the other two belong to the (110) zone axis of the Sc_2O_3 twin variants. In Figure 4-8B, the diffraction pattern reflections for both Sc_2O_3 twin variants and GaN are indexed. The twin reflections were indexed using the equations that were derived in [61].

In the diffraction pattern many extra spots are also visible. These extra spots are due to double diffraction caused by the dynamic nature of diffraction from single crystals. Double diffraction is commonly seen when twinning occurs. Anytime diffracted beams from one domain of the specimen passes into another, additional scattering of the beams occurs. The double diffraction effect that was seen in the diffraction pattern is due to the geometry in which the diffraction pattern was taken, which is shown in Figure 4-9. Thus given the specimen orientation and the fact that double diffraction is a necessary requirement for the formation of the moiré fringes that were seen in Figure 4-7, double diffraction is expected to occur.

Another consequence of double diffraction is that forbidden reflections which have zero structure factors can have finite, strong intensities when the electron beams are properly oriented.

This explains the appearance of the forbidden reflections in the GaN diffraction pattern. In a diffraction pattern for the GaN $(11\bar{2}0)$ zone axis all reflections of the type (000*l*) with *l* odd are forbidden.

From both the TEM and pole figure analysis the orientation relationship between the Sc_2O_3 film and the GaN substrate is determined to be:

$$Sc_2O_3(111) \parallel GaN(0001)$$

$$Sc_2O_3[110] \parallel GaN[11\bar{2}0]$$

$$Sc_2O_3[1\bar{1}2] \parallel GaN[1\bar{1}00]$$

The Sc_2O_3/GaN orientation relationship is illustrated in Figure 4-10, where the orientation of each twin variant to the GaN substrate is shown.

Thermodynamic and Kinetic Analysis of Twin Growth

The origin of the twinning is believed to be due to a variation in the stacking sequence of the oxide films. The epitaxial growth of cubic Sc_2O_3 on a hexagonal GaN (0001) substrate will occur through the stacking of {111} atomic planes in the <111> direction. The stacking sequence in the oxide film is equivalent to the stacking sequence of the close packed planes in an fcc structure *(ABCABC…)*. If you view the bixbyite cubic structure of Sc_2O_3 as an fcc array of Sc atoms, it can be seen in Figure 4-11 that there is only one possible position for the Sc atoms of the first monolayer at the interface, which is shown as *A*. For the second layer, the normal stacking sequence would have Sc atoms in the *B* position. But in this situation there are two different sites, *B* and *C*, which are equally favorable for the Sc atoms. Thus, the closed-packed stacking arrangement on the GaN (0001) surface is equally probable in two different sequences (...*ABCABCABC*… and …*ACBACBACB*...). The two stacking sequences would then represent two twin variants, each of which resulting in a different in-plane orientation. Twinning is

realized by a mirror operation at the basal plane. This can be seen in Figure 4-12 where, a 180° rotation of one orientation around the twinning axis will produce the other. Thus, a mirror operation at the basal plane will transform both the structure as well as the diffraction patterns of the two twin variants into each other.

In general, for the epitaxy of fcc {111} films on a hexagonal (0001) substrate, growth will occur through the nucleation of islands that continue to grow until they coalesce together into a single film. During the initial stage of Sc_2O_3 growth, there are many nucleation sites on the surface of the substrate. The nuclei will randomly adopt one of the two twin orientations. Some nuclei grow in the *ABCABC*... sequence, while others will grow in *ACBACB*... sequence. After nucleation, lateral growth of the islands takes place by incorporating atoms that reach the island by diffusing across the surface. When two islands with different orientations come together, a twin boundary will form perpendicular to the surface. This boundary will usually be noncoherent or semicoherent and possess a relatively large energy. Since the nuclei of both twin variants should be produced in equal amounts, Twin growth will occur universally over the surface, since step-flow growth is not possible due to the absence of steps on the growth surface.
Thus the resulting microstructure of the film will uniformly consist of twinned domains containing equal amounts of both variants and possess a large number of twinning boundaries.

The amount of twinning and the formation of twin boundaries can be controlled to some degree through the optimization of the nucleation and growth conditions. The size of the twin domains depends on the rate of nucleation and the growth rate. Both the nucleation rate and the size of the nuclei are strong functions of temperature. Although many nuclei may form on the substrate surface, only the nuclei that are at least a specific critical size will become established and grow. Smaller nuclei will shrink and supply atoms to the larger ones. As the critical size

increases, the density of the nuclei will decrease due to fewer stable nuclei forming. The critical size for nuclei growth increases with the temperature due to the reduction in the driving force for nucleation. At low deposition temperatures, the rate of nucleation will be very high due to a small diffusion length of the nucleating species. If the atoms cannot diffuse to an island before the average time for nucleation, the atom will form a nuclei. If the nucleation rate is high, many nuclei of both twin variants are formed resulting in a heavily twinned film. At higher temperatures, nuclei growth will be more energetically favorable then nucleation. Thermodynamically, it is more favorable for atoms to be incorporated at the growth front of an island than to nucleate on the substrate surface. The high temperature is needed to provide enough energy for sufficient surface mobility. If the atoms can diffuse to an island before the average time for nucleation, then island growth will be dominant and the nucleation rate will be low. When the nucleation rate is low, fewer nuclei will be produced and each nucleus will gradually grow to one large twin orientation, which will lead to an increase of the twin domain sizes. This will result in a large decrease in the amount domains and grain boundaries in general. More importantly, it will decrease the number of twinned boundaries as well as antiphase boundaries, where the oxygen sublattices are shifted with respect to each other. Just like the stacking sequence of the Sc atoms, there is no energetically favored arrangement of the ordered oxygen vacancies. Thus, antiphase boundaries are expected to form between the domains with varying oxygen vacancy sublattices.

Another parameter that needs to be carefully controlled and optimized, is the degree of supersaturation, which is dependent on the flux of the reactants towards the surface. The amount of available adatoms on the surface that can contribute to growth is the difference between the flux of atoms arriving to and desorbing away from the surface. The flux of atoms evaporating off

the surface is strongly dependent on the growth temperature. At higher growth temperatures, the desorption flux will be very large and a significant amount of atoms will be desorbed from the surface before they are incorporated into the growing monolayer. If the desorption flux is greater than the incident flux of atoms arriving, decomposition will occur. Thus, at high temperatures the incident flux must be sufficiently large to ensure an adequate degree of supersaturation. Since nucleation will also be enhanced at high supersaturations, the incident flux should not be too high. If the incident flux is too large and the supersaturation is exceedingly high, self agglomeration of reactant species occurs which will result in an increase of islands nucleating. This mechanism limits the maximum growth rate possible in MBE growth.

It should be kept in mind that another mechanism for twin formation is also possible. The other mechanism is analogous to the one previously discussed but it will produce a different type of twin boundary. In the previous discussion, the difference in the (111) stacking sequences was between to two separate domains. But within a single domain, if an error in the stacking of the (111) planes occurs during growth, the stacking sequence of the (111) planes could be lost by accident. The subsequent layers can then grow in a twin orientation to the previous layers, resulting in a twin boundary that runs parallel to the growth surface. The free energy of the {111} plane is lower than that of all other planes in the fcc lattice and the twin boundary formed will be a coherent twin plane with a relatively small energy. This makes it easy for the {111} plane to lose its normal stacking sequence. In the fcc structure, the <111> directions are the most likely axis for twinning due to the *ease* that mistakes in the stacking sequence can be made on the {111} surface.

The formation of this type of twin boundary can also be controlled through optimization of the growth conditions. In order to preserve the stacking sequence, that originated at the

substrate interface, throughout the growth of the film, the growth rate needs to be finely tuned. Due the increased temperature and large flux, the growth rate will be high, which will lead to a much higher frequency of errors occurring in the stacking sequence and to a larger concentration of point defects and impurities being incorporated into the growing film. If the growth rate is too fast, there will not be sufficient time for defects to be eliminated from the growing layers.

One way to completely inhibit the nucleation of two different twin orientations is to remove the perfect symmetry of the substrate surface that makes both orientations equally possible by using a vicinal substrate. Epitaxial growth is frequently performed on vicinal surfaces that are slightly misoriented a few degrees off axis in order to produce an arrangement of surface steps for growth to take place. For the growth of fcc {111} films on a hexagonal substrate, a miscut off of the (0001) will expose steps on the surface. The surface steps contain sites that are more favorable for bonding than the flat surface of the substrate. This is analogous to the previous situation of island growth, where it is thermodynamically, more favorable for atoms to be incorporated at the step sites than to nucleate on the substrate surface. Thus, the nucleation of islands on the flat terraces can be avoided. The growth of the film will proceed through the lateral propagation of the steps producing a single continuous layer. This is commonly referred to as step-flow growth. By providing a favorable spot for atom attachment, the steps remove the sixfold symmetry of the GaN(0001) surface that led to the two degenerate threefold orientations of the Sc atom sublattice. The surface steps will now favor the growth of only one of the twin variant orientations. This approach was used for the growth of bixbyite oxides to be used as high κ dielectrics in Si-based devices [62-68]. It was observed that the growth of the oxide films on Si(100) substrates also produced twin oriented domains in equal amounts [62-64]. It was shown that the use of vicinal substrates essentially eliminated the

twinning and produced films with a single orientation. An example of the preferential growth of a single orientation at a step of is shown in Figure 4-13. The figure is a HR-TEM image taken at the Sc_2O_3 /GaN interface. The image shows a step on the surface of the GaN substrate, where the Sc_2O_3 film has gone from two twin orientations to only one at the step.

A competition between attachment at steps and nucleation on a terrace will still exist and thus the growth conditions must still be optimized so that step flow growth is realized. The same analysis in the island growth model is still mostly applicable for this situation. At higher temperatures, growth from steps will be more favorable then nucleation due to the energy provided for adequate surface diffusion to the steps. Another factor to be considered, is determining the exact amount of miscut that should be used. The degree at which the substrate is misoriented will determine the distance that the steps are separated. Increasing the angle of miscut will result in a smaller separation between the steps. This will decrease the average diffusion length before an atom reaches a step, making it more probable for step-flow growth to occur. In general, to ensure that 2D growth will be dominant, the mean diffusion distance should be much larger than the step separation. If the steps are too close together, step bunching can occur, which will be detrimental to the film quality.

It has been shown that Sc_2O_3 can be grown epitaxially on GaN by MBE. Characterization of the Sc_2O_3 films was performed on the films as grown and after annealing at 800°C for 5 min. AFM and XRR were used to study the oxide surface and Sc_2O_3/GaN interface. Results showed that both the surface and interface were atomically smooth and remained so after annealing. The in-plane and out-of-plane orientation of the oxide films was examined using HRXRD. The ω and ω-2θ rocking curves and GIXRD scans showed that the out-of-plane orientation was excellent. They showed that after annealing, the film had a laterally homogenous coherent thickness, as

well as a smooth Sc_2O_3/GaN interface. From the pole figure measurements the oxide films showed that they were highly textured along the c-axis and that the film grew in twin in-plane orientations with respect to the GaN substrate. Using HRTEM, the single crystal nature of the Sc_2O_3/GaN interface was seen and twin orientation of the films was further confirmed through lattice imaging and analysis of the diffraction pattern. Growth can be optimized to minimize the extent of twinning and possibly be eliminated all together through the use of miscut substrates. This shows that Sc_2O_3 films grown on GaN substrates can have excellent structural quality and thus has enormous potential for use as a dielectric in GaN-based MOS devices.

Table 4-1. Gibbs free energy values for all possible reactions at the Sc_2O_3/GaN interface.

Possible Reactions at Oxide/GaN Interface	ΔG_{Rxn} (kJ/mol) T=900K (627°C)	T=1100K (827°C)	T=1400K (1127°C)
$Sc_2O_3 + GaN \Rightarrow ScN + Ga_2O_3$	+625.8	+628.9	+633.0
$(2)Sc + (3)O + GaN \Rightarrow Sc_2O_3 + GaN$	-1642.4	-1584.9	-1499.3
$(2)Sc + (3)O + Ga + N \Rightarrow Sc_2O_3 + GaN$	-1644.8	-1562.6	-1440.2
$(2)Sc + (3)O + (2)GaN \Rightarrow (2)ScN + Ga_2O_3$	-1237.8	-1182.4	-1101.0
$Sc + (3)O + (2)Ga + N \Rightarrow ScN + Ga_2O_3$	-1019.0	-933.7	-807.7

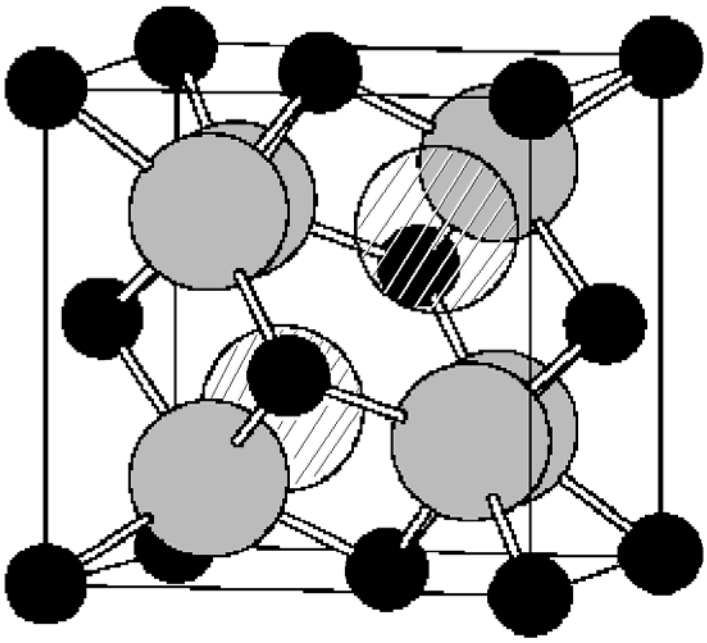

A

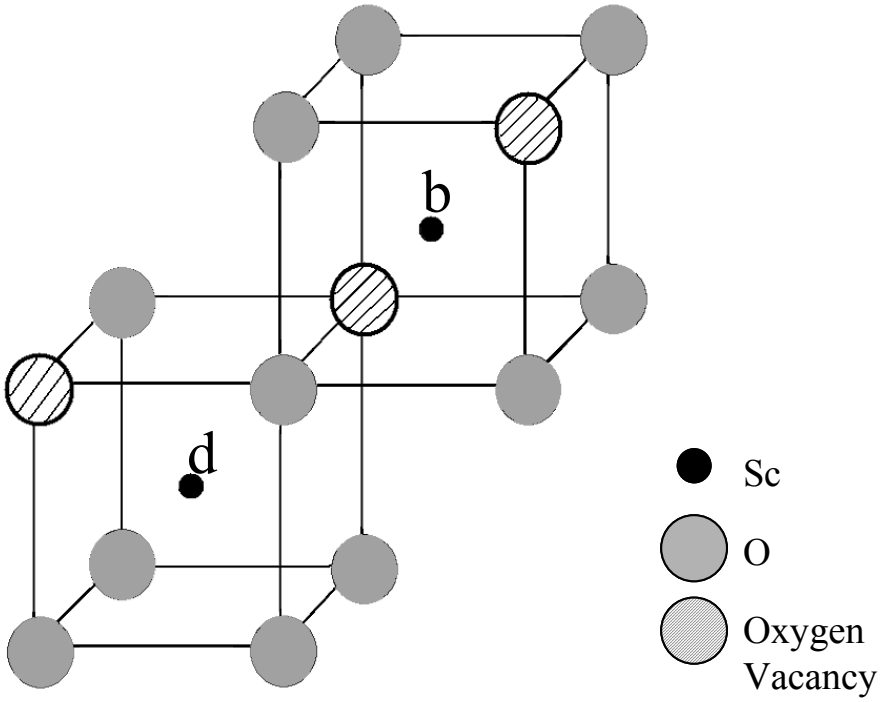

B

Figure 4-1. Bixbyite structure of Sc_2O_3 A) One eighth of the bixbyite structure unit cell. B) Position of the two non-equivalent Sc sites, b and d in the bixbyite structure of Sc_2O_3. The Sc ions are indicated by the small dark circles. The oxygen sites are the large filled circles and the vacant oxygen sites are the large striped circles.

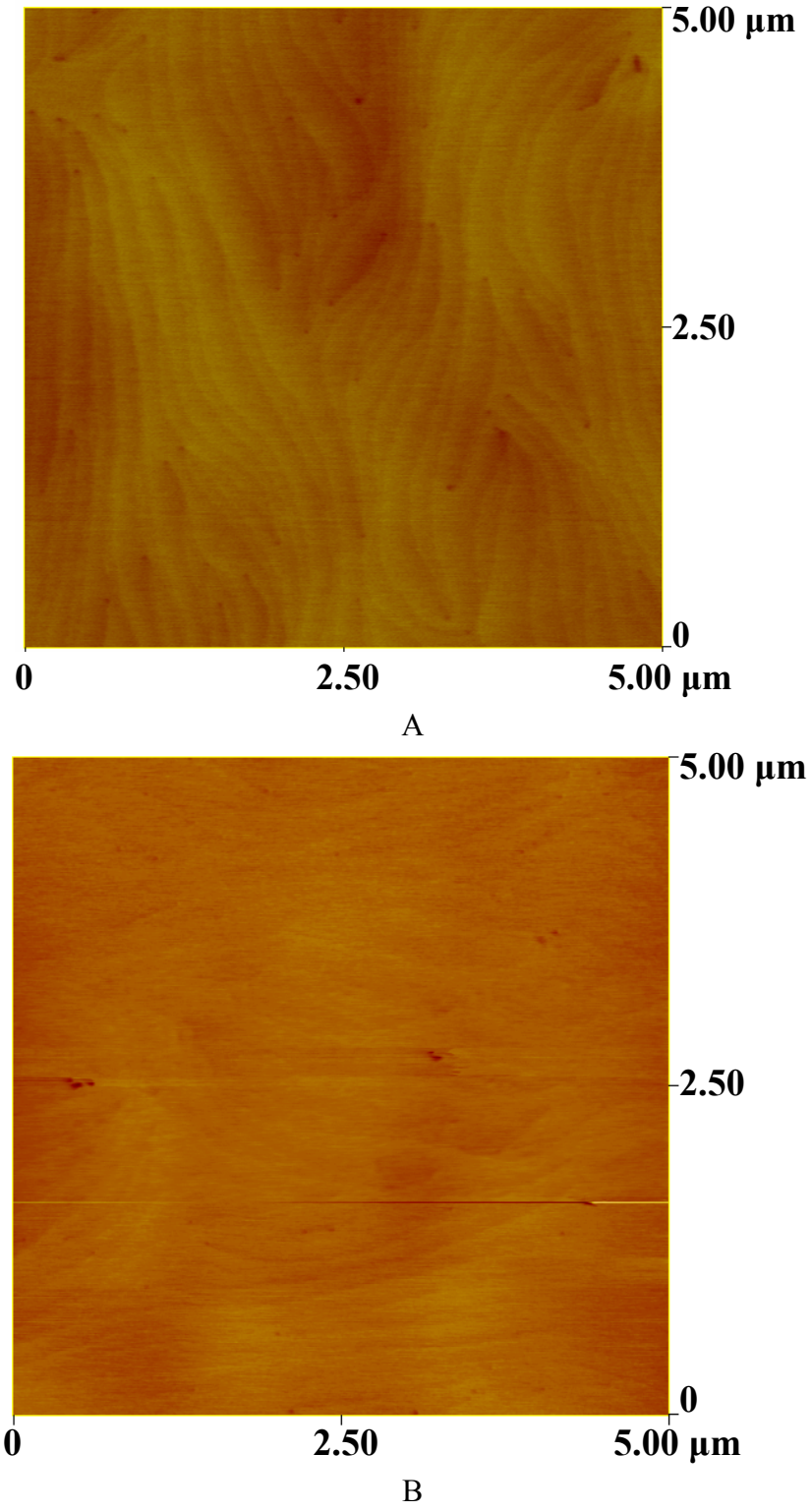

Figure 4-2. AFM of the Sc_2O_3 films A) before and B) after annealing at 800°C.

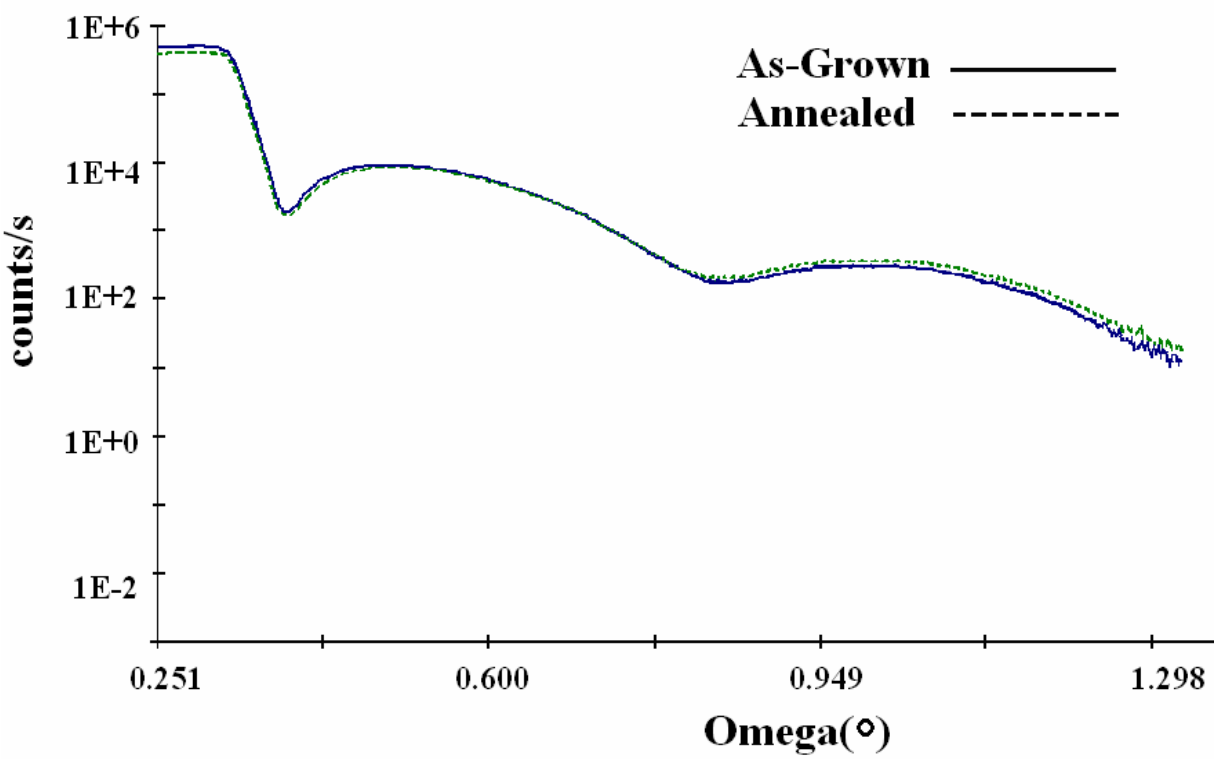

Figure 4-3. XRR of the Sc_2O_3 films before and after annealing at 800°C.

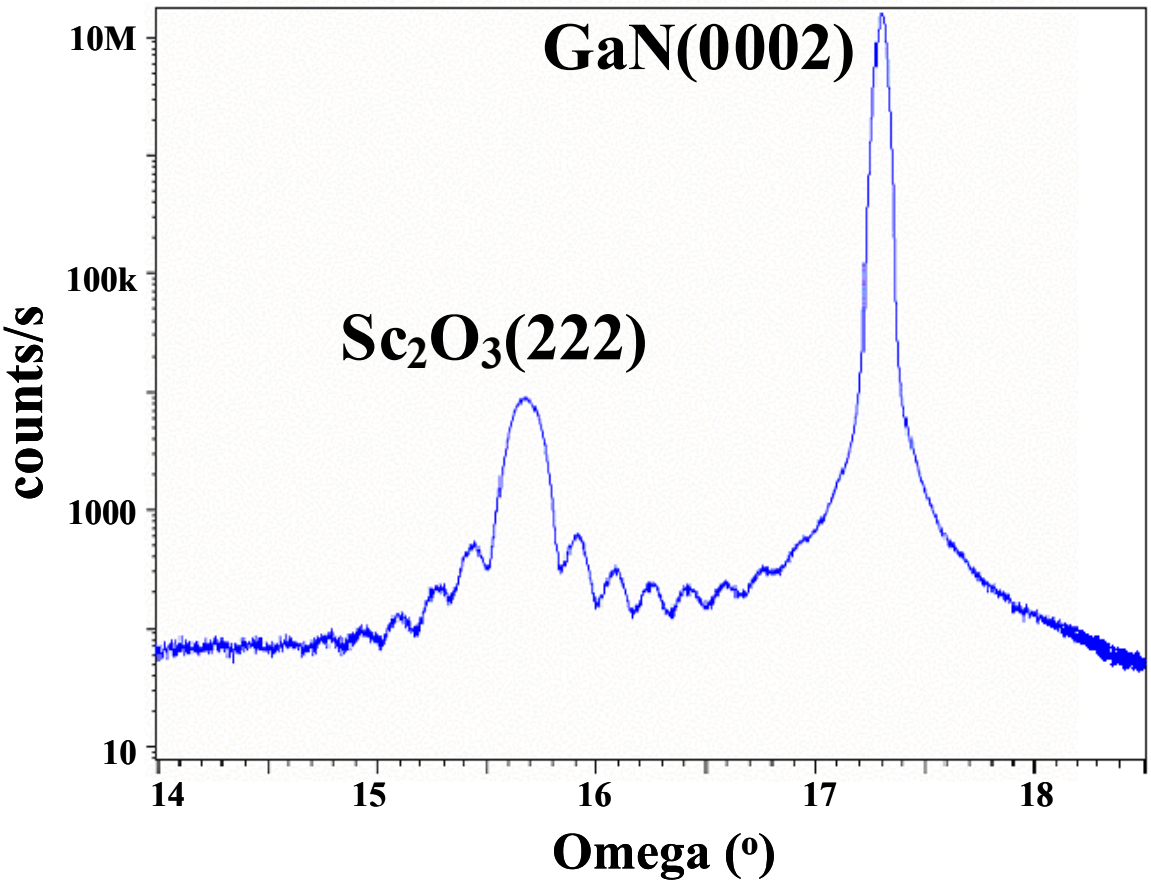

Figure 4-4. The ω-2θ rocking curve of the Sc_2O_3 (222) peak of the annealed Sc_2O_3 film.

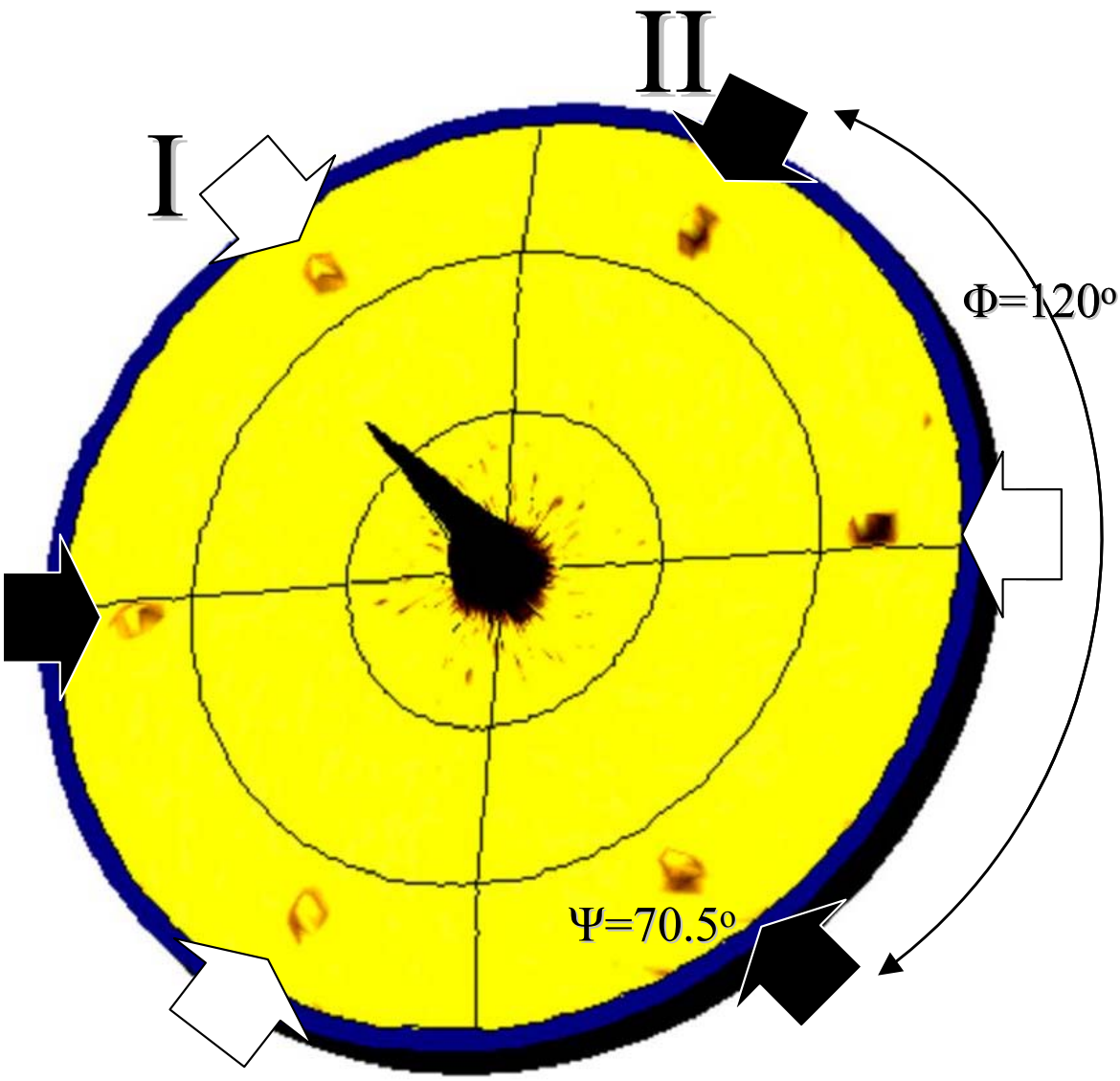

Figure 4-5. Pole figure measurement of the Sc_2O_3 {222} reflection. The white arrows designate the reflection peaks from one twin orientation and the black arrows designate the other's reflections

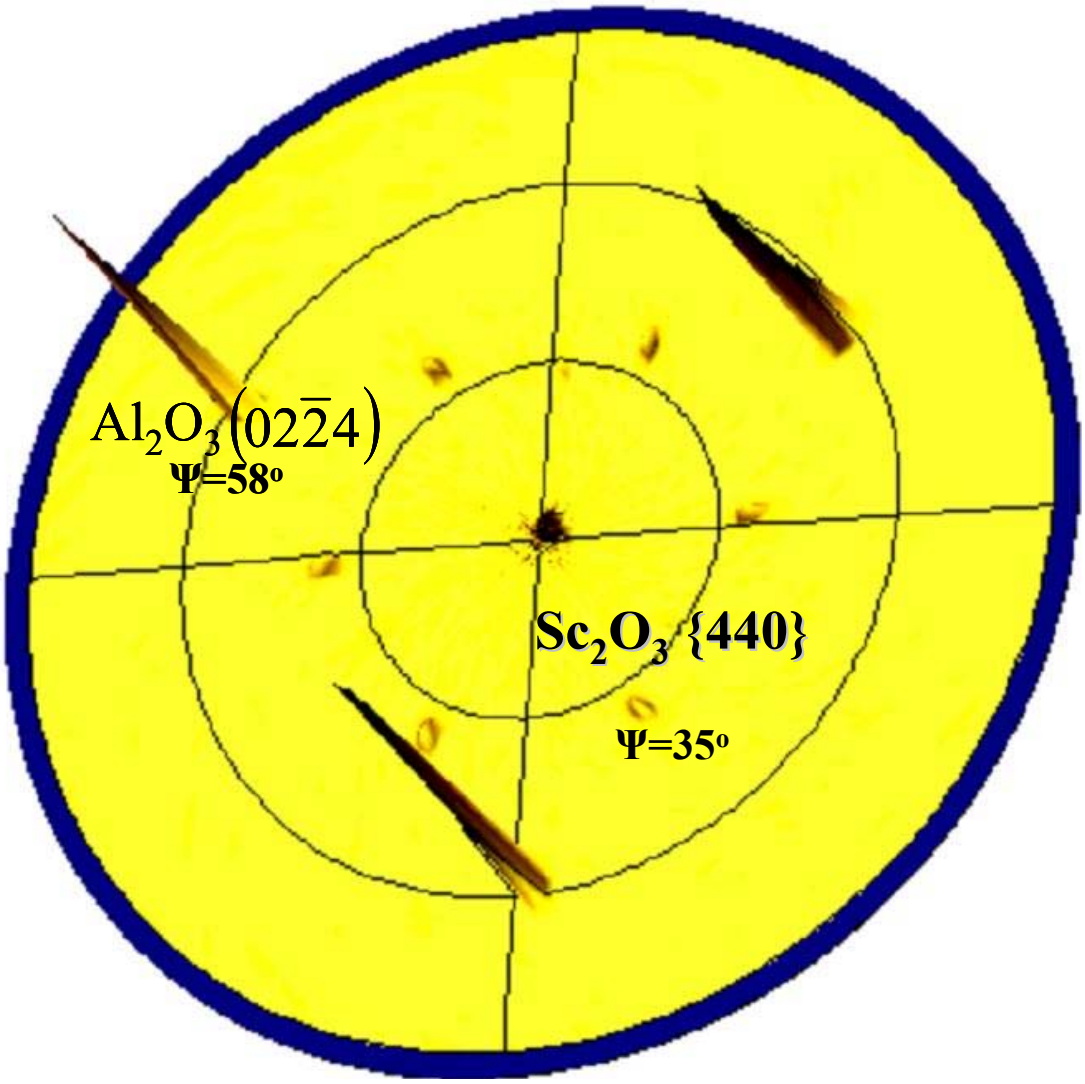

Figure 4-6. Pole figure measurement of the Sc_2O_3 {440}. The six reflections around the center at a Ψ of 35° are the two sets of twin orientations. The sapphire substrate is responsible for the three large reflections at a Ψ of 58°.

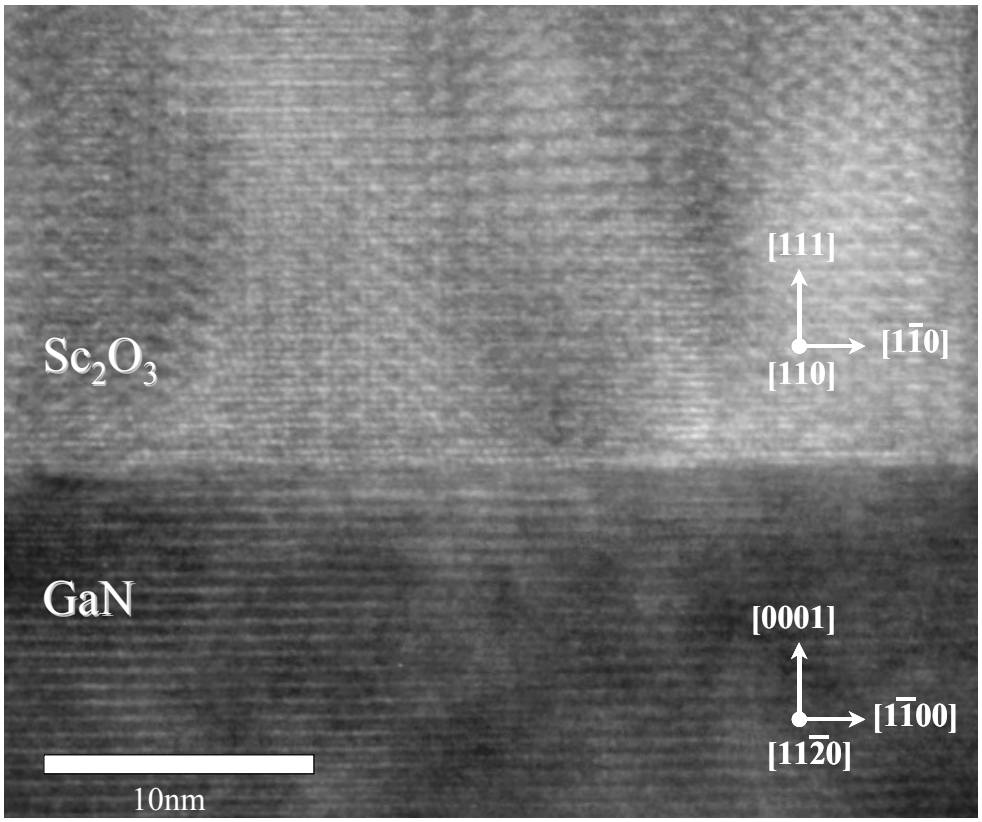

A

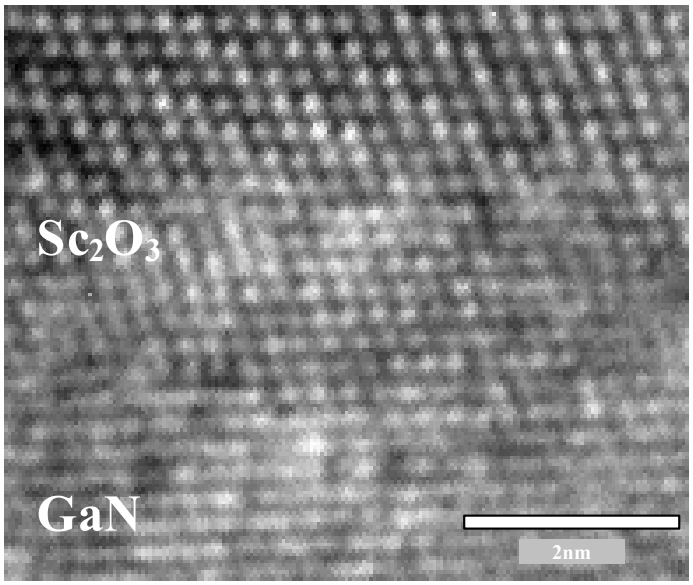

B

Figure 4-7. Cross-sectional HRTEM images of the Sc_2O_3/GaN interface after annealing. A) Large scale view showing the abrupt interface and the moiré fringes caused by the twinning of the (111) planes. B) Lattice image of the interface showing its single crystal nature.

A

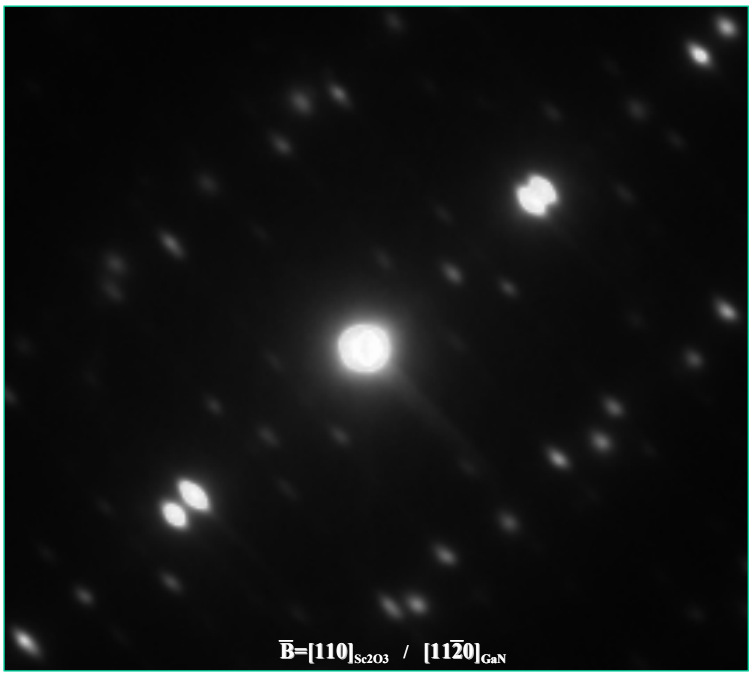

B

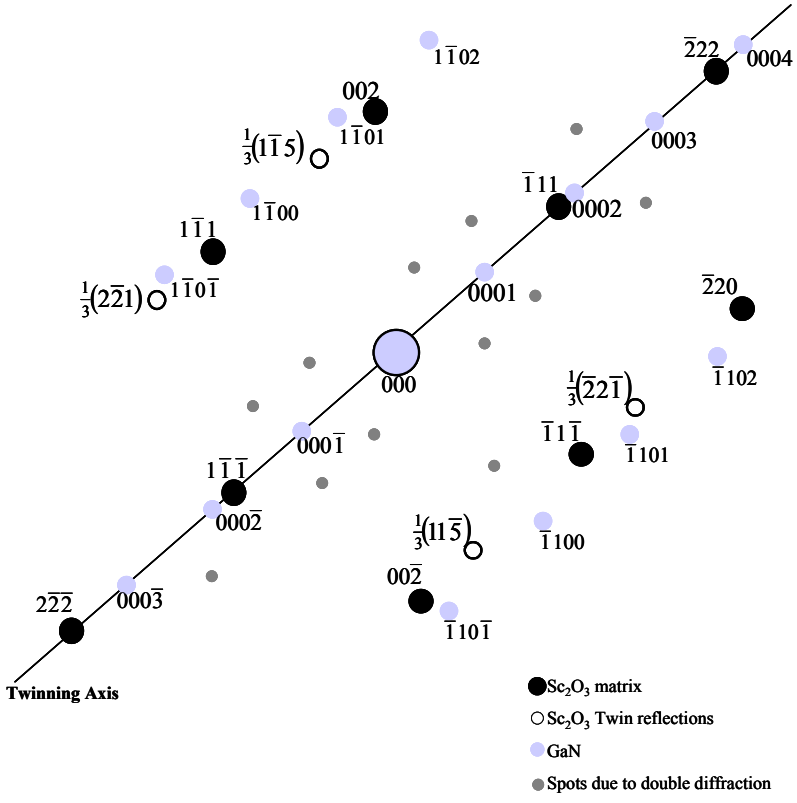

Figure 4-8. TEM of Sc_2O_3/GaN interface. A) Selected area electron diffraction pattern was taken from the vicinity of the Sc_2O_3/GaN interface. B) Indices for the reflections in the diffraction pattern for A).

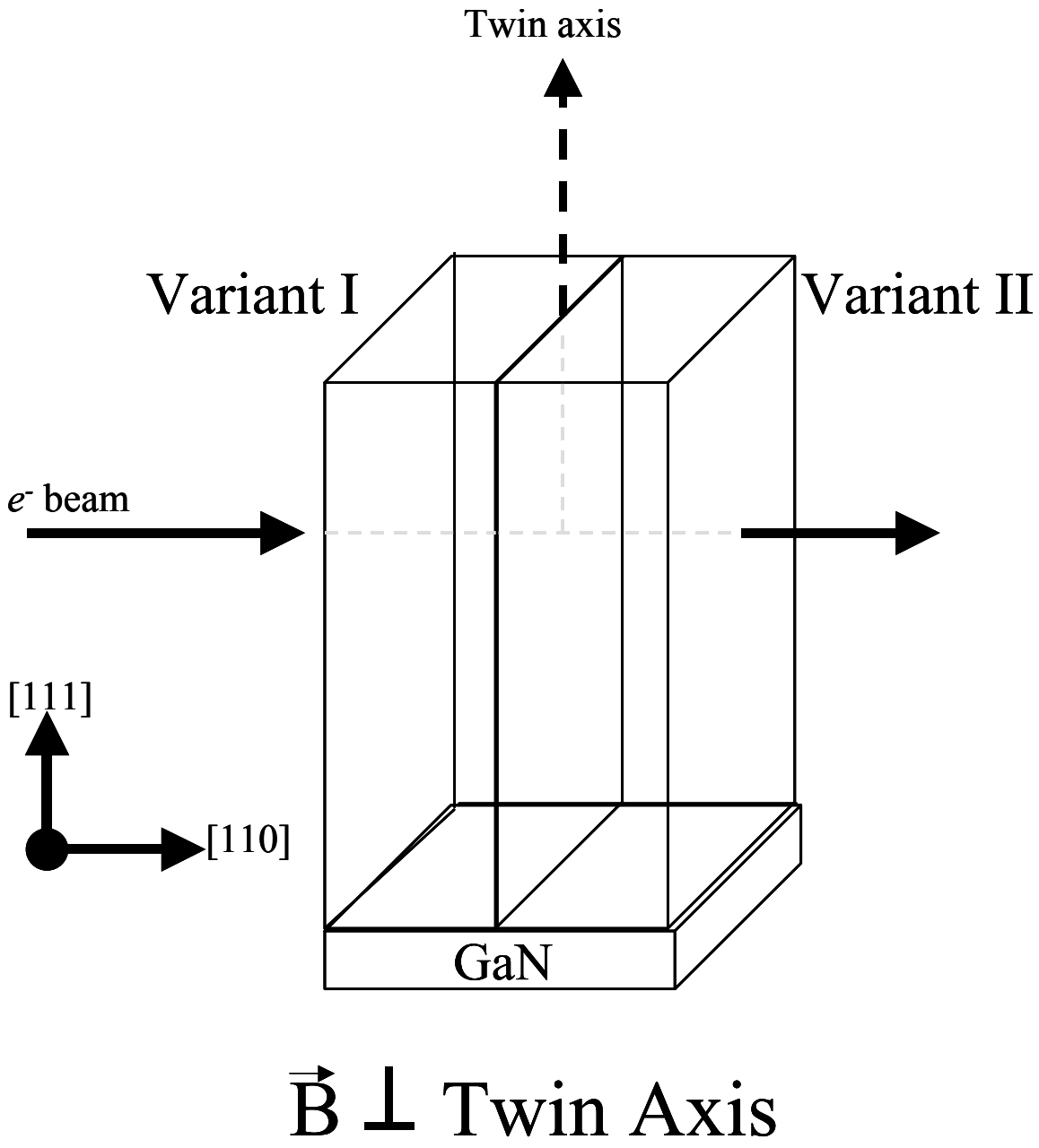

Figure 4-9. Geometry of the electron beam with respect to the sample for the diffraction pattern in figure 4-8.

$$Sc_2O_3(111) \parallel GaN(0001)$$

$$Sc_2O_3[110] \parallel GaN[11\bar{2}0]$$

$$Sc_2O_3[1\bar{1}2] \parallel GaN[1\bar{1}00]$$

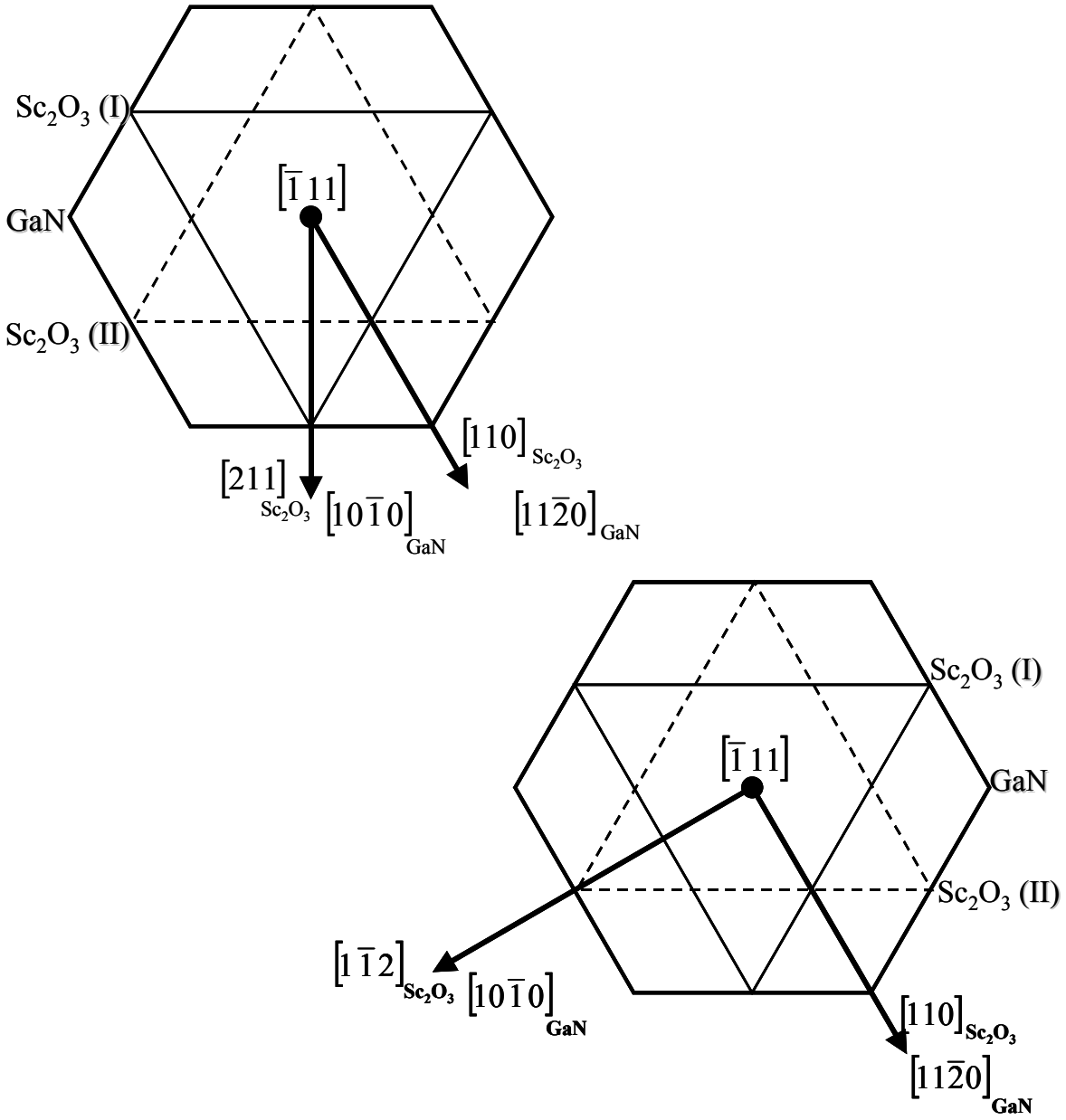

Figure 4-10. Epitaxial orientation relationship between the two twin orientations of Sc_2O_3 and the GaN substrate.

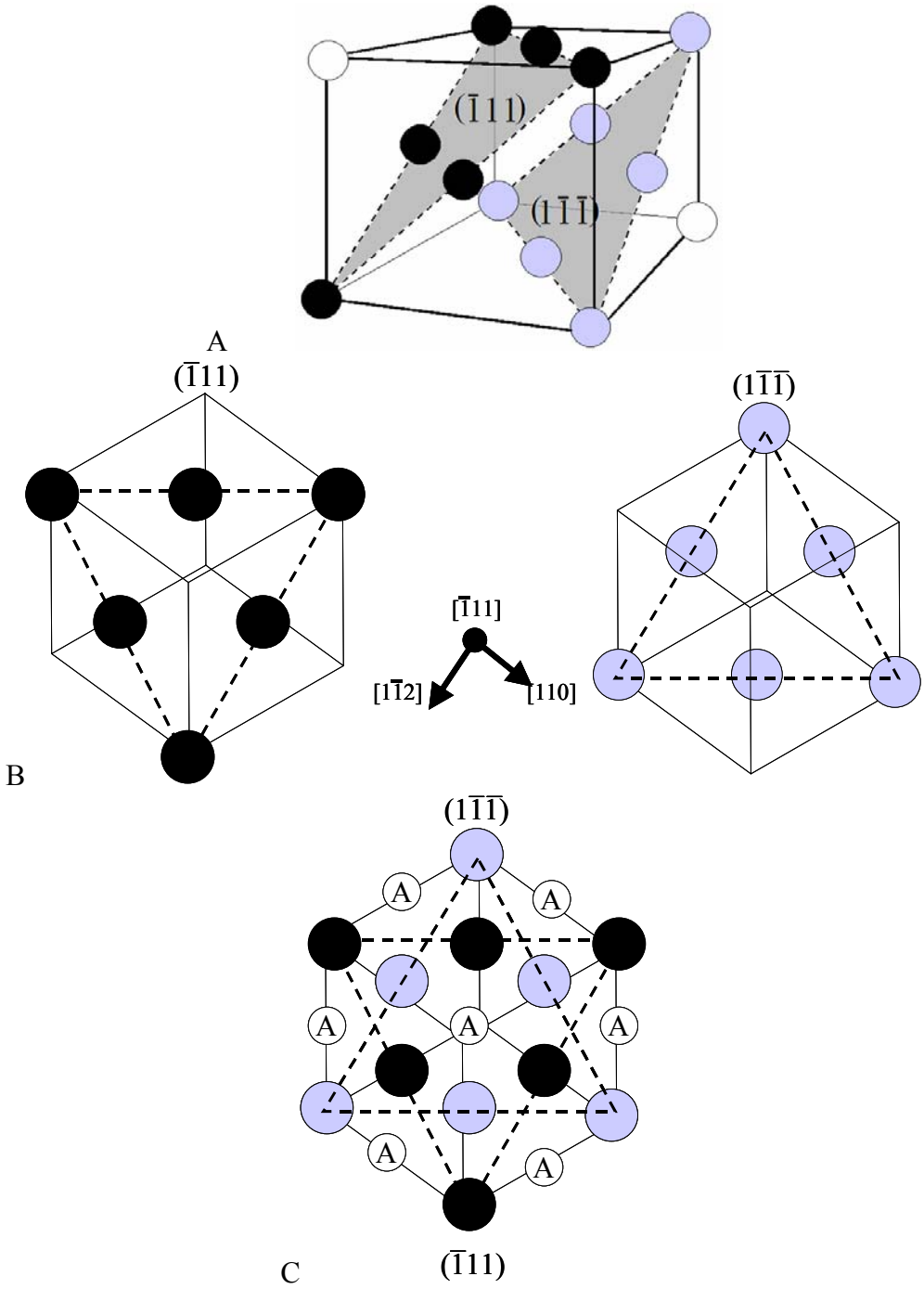

Figure 4-11. Atomic positioning of the $(\bar{1}11)$ and $(1\bar{1}\bar{1})$ planes within the face-centered cubic unit cell. A) The positioning of each plane with respesct to the other situated within the same unit cell. B) The $[\bar{1}11]$ view of each plane within the unit cell. C) The $[\bar{1}11]$ view of both planes situated within the same unit cell showing all atomic positions with the first layer in the stacking sequence labeled A.

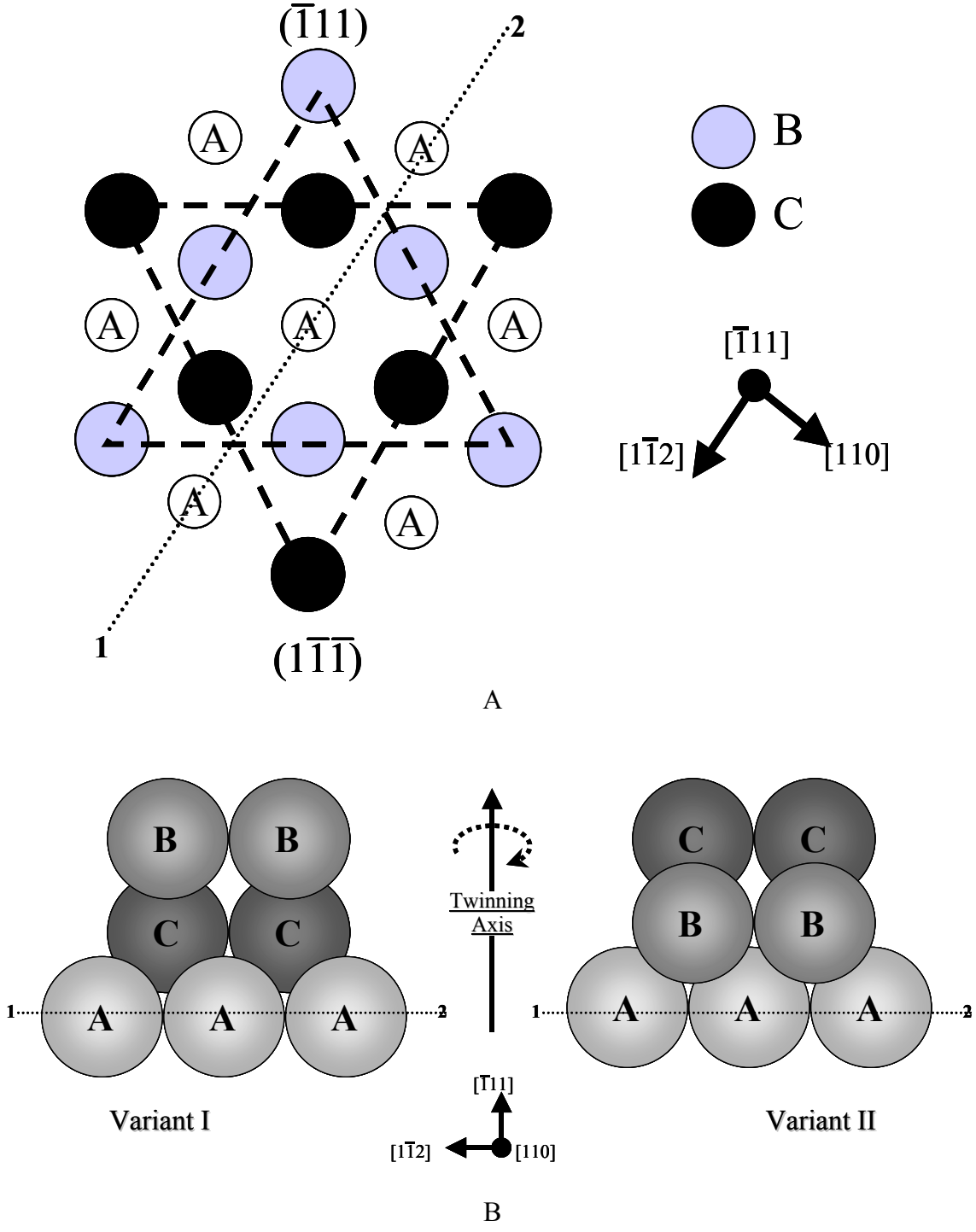

Figure 4-12. Orientation of the two twin variants. A) Atomic positions of each twin orientation for the {111} stacking sequence. B) The [110] view of the {111} stacking sequence showing how a 180^{o} rotation around the twin axis transposes one variant into the other.

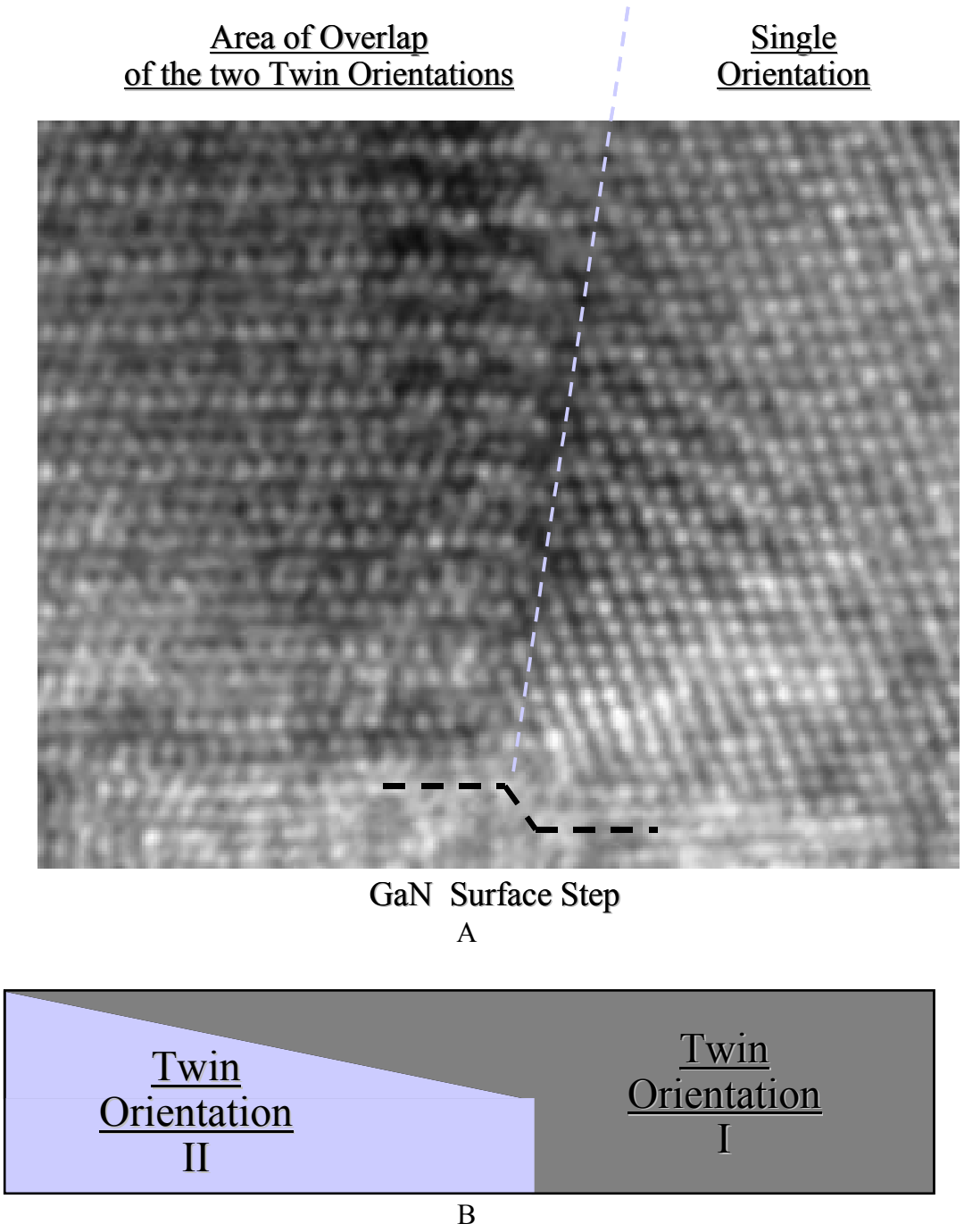

Figure 4-13. HRTEM of the Sc_2O_3/GaN interface. A) HRTEM lattice image of the GaN / Sc_2O_3 interface where two twin orientated grains terminate at a step on the GaN surface where only a singleorientation has preferentially nucleated. B) Illustration of TEM sample structure shown in (A) from an overhead view.

CHAPTER 5
STABILITY OF DIELECTRICS FOR GAN-BASED ELECTRONIC DEVICES: RESULTS AND DISCUSSION

For a potential dielectric oxide to be suitable for use in GaN-based MOS devices, its thermal and environmental stability needs to be thoroughly examined. Although some studies have been performed on these oxides [69], little to no work has been done with respect to their stability in the GaN MOCVD environment. Since MOCVD is the dominant technique for the commercial production of GaN-based devices, the ability of a potential dielectric to withstand the MOCVD environment is a critical factor in determining its suitability for such devices. The previous chapter showed that one potential dielectric, Sc_2O_3 was thermally stable up to 800^0C in an oxygen deficient environment. To further examine the thermal and environmental stability of Sc_2O_3 and other potential dielectrics, they were subjected to high temperature anneals in an MOCVD environment. The annealing conditions used are the growth conditions used in the regrowth of GaN because these set of conditions are relatively harsh compared to those used for the standard MOCVD GaN growth.

The annealing conditions used are those used for the regrowth of p-type GaN except for the lack of TMG and Cp_2Mg flow. The rate of temperature increase is the same and the time spent at the growth temperature of 1085^0C will be 30 minutes, which is the average time for used for the p-GaN regrowth experiments. The pressure is 45 Torr and the H_2 and NH_3 flows are 2 and 1.5 standard liters per minute (slm), respectively. Since the regrowth conditions are comparatively harsher than standard MOCVD growth conditions, these experiments should provide an excellent indication of the oxide's stability in most GaN MOCVD applications.

In order to determine the likeliness that any undesired side reactions with the oxides will occur in the GaN MOCVD environment, thermodynamic calculations were performed for all possible reactions of each oxide with any of the species that will be present. Since their specific

application in this study is for the use as a mask during the regrowth of p-type GaN, any possible reactions with Mg have also been calculated. The possible reactions and their Gibbs free energy were calculated at an elevated temperature that would be the maximum temperature that could be experienced in the MOCVD environment. Since good quality p-type GaN is difficult to attain, partially due to the problems associated with the doping during growth, calculations were made for possible reactions that included Mg, which would be present during the growth of p-type GaN. The GaN MOS diodes used for this study were fabricated on n-type GaN substrates with a carrier concentration of approximately $5x10^{16}$ cm^{-3}. The gate metal consisted of a Pt and Au layered structure with a thickness of 30 nm and 120 nm respectively.

The MOCVD Anneal of SiO_2 Thin Films

SiO_2 is the standard dielectric used in silicon device technology. It is also the standard mask used for GaN ELO and other SAG techniques. Since SiO_2 has been studied extensively in the GaN MOCVD environment, it is an excellent standard to compare the other prospective dielectric oxides with. Although SiO_2 has largely been proven to withstand the MOCVD GaN environment, with respect to its structural properties, very little work has actually been performed that specifically looks at the effect on the SiO_2 film itself from the MOCVD environment.

The possible reactions for SiO_2 in the GaN MOCVD environment and their Gibbs free energy are listed in Table 5-1. From the list of reactions in Table 5-1, the one that could be most problematic is number 5. Although reactions 7 and 8 have a larger free energy value and thus a greater probability for a spontaneous reaction to occur, the likeliness of excess oxygen being present in any significant amount is remote. Reaction 5 on the other hand is troublesome for two reasons. The first is the consumption of available Mg that is needed in significant amounts to achieve p-type GaN. The other is the production of excess Si, which is an n-type dopant. The

presence of excess Si would cancel out the effects of Mg on the growth properties. This consumption of Mg and production of excess Si would make it extremely difficult to control and predict the level of p-type doping during growth. The effect on the surface morphology of the SiO_2 films from the MOCVD anneal is seen in Figure 5-1. The morphology appears to be largely the same after annealing. The difference seen in the images is mainly due to a change in the scale that the measurement was taken with, which results in a change in the contrast of the image. The roughness calculations for the film, before and after annealing, were 2.1 nm and 2.4 nm, respectively. Thus, a small amount of roughening of the surface does appear to occur during the MOCVD anneal. The XRR of the SiO_2 film before and after annealing is shown in Figure 5-2. The slight decrease in the peak amplitude is indicative of a small increase in roughening, which agrees well with the AFM results.

The MOCVD Anneal of MgO Thin Films

Magnesium oxide has a cubic rocksalt crystal structure that grows with a {111} orientation on the GaN (0001) surface, which results in a 6.5% lattice mismatch. The initial growth of the film on GaN at 100^0C is single crystal but then develops a polycrystalline structure after about 40 Å of growth [69]. MgO has been studied for passivation and use as a gate dielectric for GaN-based devices [70-73]. It has proven very effective in mitigating surface carrier traps of GaN-based HEMT devices [36]. The possible reactions with MgO in the MOCVD GaN environment and their thermodynamic values are listed in Table 5-2. From a thermodynamic viewpoint, MgO should be stable during GaN MOCVD growth. If the MgO surface is hydroxylated, which commonly occurs, it should still be quite stable considering the large free energy of reaction values that are listed in Table 5.2. What could be problematic is the likelihood of Mg and NH_3 reacting to form magnesium nitride (Mg_3N_2). From the reaction values shown in the table, atomic magnesium will easily react with NH_3 as well as all its

dissociated forms including atomic nitrogen. The reactivity of Mg species with NH_3 is a common problem in the MOCVD of p-GaN. If the MgO film is Mg-rich and has an excess of Mg metal that could participate in reactions with NH_3, the formation of a Mg_3N_2 layer on the surface could degrade it's dielectric properties. If the film is being used as a regrowth mask, the Mg_3N_2 layer could be favorable for the nucleation of GaN islands. Diffusion of excess Mg from the bulk to the surface could be a catalyst towards decomposition of the whole MgO film.

Using the optimal growth conditions for diode performance thin films of MgO with a thickness of 300 Å were grown and annealed in the MOCVD reactor under GaN growth conditions. The AFM scans of the MgO films before and after annealing are shown in Figure 5-3. Significant roughening of the MgO surface is seen in the annealed sample. The surface roughness of the as grown sample was 1.89 nm. After annealing the sample, the roughness increased significantly to 18.1 nm. It is unclear if the roughening is from the formation of Mg_3N_2 or decomposition from the loss of Mg or O. The XRR measurements of the as grown and annealed MgO films are shown in Figure 5-4. The large decrease in the peak amplitudes of the annealed sample is due to the roughening of the surface. To obtain a more quantitative description of the effect of annealing on the MgO film, the two XRR scans were also modeled using the Wingixa program. A thorough qualitative analysis of the measurement should always be performed before trying to model it using software. Otherwise, it could be very time consuming trying to get the model to fit the measurement and an incorrect model could easily be produced. The models produced from the scans indicate that only a minimal decrease in thickness occurs after annealing and that no film was formed on the surface. The models do show a very large increase in the surface roughness, which was seen with the AFM. One good result was that the models show that the MgO /GaN interface had very minimal roughening.

Although the increased roughness of the MgO film after annealing reduces the accuracy of the model's predictions, a general range for a particular parameter can be obtained. Thus, the exact value of the interface roughness after annealing is not reliable, but the lack of a significant change in the roughness is. In Figure 5-5, the high frequency C-V measurement for the MgO film before and after annealing is shown. The absence of a hysteresis window is indicative of a low interface trap density (D_{it}). Considering the large amount of roughening of the surface that was seen after annealing, it is surprising that the MgO/GaN interface did not roughen enough to produce a D_{it} that would be observed in the C-V measurement. Thus, the C-V measurement for the annealed MgO film agrees with the XRR model that shows that no significant roughening of the MgO/GaN interface occurred during the MOCVD anneal. The increase in the capacitance after annealing is evidence of additional charge in the oxide or at the oxide/GaN interface. The shift of the flatband voltage (V_{FB}) towards negative voltages indicates the addition of positive charges. The excess positive charge could be due to Ga^{3+} diffusing from the GaN into the MgO during the anneal.

The MOCVD Anneal of Sc_2O_3 Thin Films

The possible reactions with Sc_2O_3 in the MOCVD GaN environment and their thermodynamic values are listed in Table 5-3. From looking at the values for the possible Sc_2O_3 reactions in the table, it appears that Sc_2O_3 should be quite stable in the MOCVD environment except if there is excess Sc present. Although Sc_2O_3 is especially strong, being that its dissociation value is 1499.3 kJ/mol, it is very possible that the Sc_2O_3 film will have excess Sc metal within it from the growth. If the Sc metal diffuses to the surface and reacts with an NH_x species to form ScN, this could be very detrimental to the film's properties. Since ScN is a semiconductor, the formation of a very thin film of ScN on the surface of the Sc_2O_3 could act as

a conduction path and would therefore render the insulating properties of the Sc_2O_3 film ineffective.

Two types of Sc_2O_3 films were annealed. One was grown at a high temperature (HT) of approximately 600^0C and the other at a low temperature (LT) of around 100^0C. The Sc_2O_3 films that were annealed had a thickness of approximately 200 Å. In Figure 5-6A, the AFM image shows that the surface of the HT-Sc_2O_3 before the MOCVD anneal is very smooth. The terraces in the image are characteristic of two-dimensional step-flow growth. The AFM roughness measurement gave an R_{ms} value of .28 nm. In Figure 5-6B, the AFM image of the same Sc_2O_3 film after it has been annealed shows that the surface had roughened significantly. The roughness measurement gave an R_{ms} value of 3.68 nm, which is an order of magnitude greater then before it was annealed. In other annealing studies, Sc_2O_3 has shown good thermal stability up to temperatures near those used in this study and never produced such a large change in surface morphology. The scenario that was discussed before, in which excess Sc metal in the oxide film reacts with NH_x species at the surface to form ScN could possibly explain the dramatic roughening of the surface.

The XRR plots for the HT-Sc_2O_3 film before and after annealing are plotted together in Figure 5-7 in order to gain a qualitative evaluation of the effect of the MOCVD anneal. From qualitative analysis of the two XRR scans, a comparison of the two shows that the scan of the annealed film has a decrease in the overall intensity. This is indicative of the surface becoming rougher, which was shown to be true from the AFM. Although the overall intensity of the scan has decreased, the amplitude of the individual fringes has not. This shows that the film's interface, which is the Sc_2O_3/GaN interface, has not roughened at all. As mentioned before, the oxide/GaN interface is critical for device performance, thus maintaining a stable interface with

the GaN substrate during the MOCVD anneal shows promise for the use of HT-Sc_2O_3 as a dielectric in GaN-based MOS devices.

Upon closer inspection it is observed that the fringe spacing or period of the annealed film has slightly decreased. A decrease in the fringe spacing is caused by an increase in the film thickness. It can also be seen that the area around the critical angle has changed noticeably. Figure 5-7B is a close-up of the area around the critical angle, which shows how the two scans differ from each other. The position of the critical angle is dependent on the density of the surface film or films. Thus, if a thin film of ScN formed during the anneal, the change in density could produce the observed change in the scan.

Since the thermal stability of the Sc_2O_3 grown at a high temperature was so stable in the GaN MOCVD environment, Sc_2O_3 films grown at a low temperature (LT) were annealed in the same environment. In Figure 5-8, the AFM scans show that the change in the surface roughness after annealing was minimal. The sample before annealing had a roughness of .852 nm and after it was 1.25 nm. This result is confirmed from the XRR measurement of the sample before and after. The XRR scans of the LT-Sc_2O_3 film before and after annealing are shown in Figure 5-9. The LT-Sc_2O_3 films appear to remain quite stable after annealing with only a minor degree of roughening indicated by the minimal decrease in the amplitude of the peaks.

The high frequency C-V measurements of the HT and LT-Sc_2O_3 films, before annealing, is shown in Figure 5-10. Both films have a small hysteresis window, which shows the existence of interface traps. The LT-Sc_2O_3 film does appear to have a superior capacitance response then the HT-Sc_2O_3 film. When both the annealed HT and LT-Sc_2O_3 films were tested using the probe station, every diode on both films shorted. It was thought that a conductive layer of ScN could have formed on the surface during the anneal, which causes the current to circumvent the oxide

to reach the indium contact. To determine if ScN was formed, XPS of the annealed Sc_2O_3 surface was performed. In Figure 5-11, the XPS scan of the Sc2P peaks shows a significant peak corresponding to Sc-N bonding was seen on the surface. After sputtering down to the bulk film, the Sc-N peak is gone. This confirms that a ScN layer forms on the Sc_2O_3 surface when exposed to the GaN MOCVD environment. The shorting seen in the diodes must be due to the ScN layer acting as a direct path for the current. In Figure 5-11 there is also an illustration of the mechanism causing the diodes to short.

The MOCVD Anneal of Sc_2O_3/MgO Thin Films

A major drawback of MgO is its lack of environmental stability. Thin films of MgO have been shown to degrade in atmosphere due to its reaction with water vapor at room temperature to form magnesium hydroxide, $Mg(OH)_2$ [74,75]. Its exposure to ambient air results in the formation and bonding of several different species on the MgO surface, mainly from reactions with H_2O and CO_2 [76]. Other studies have shown that MgO surfaces tend to absorb water, which leads to hydroxylation and the formation of $Mg(OH)_2$ [77-79]. As long as the MgO's exposure to atmosphere is minimized, it has proven to be a good candidate for use as a dielectric in GaN MOS devices. To protect the MgO surface, a thin capping layer of Sc_2O_3 of approximately 50 Å has been deposited on the MgO film. This has shown to be very effective in preventing the degradation of the MgO film in atmosphere [69].

The AFM images of the Sc_2O_3/MgO film in Figure 5-12, show that like the bulk Sc_2O_3 film the as grown material is particularly smooth, with an R_{ms} value of .367 nm and exhibits step flow growth characteristics. Unfortunately, it also roughened considerably after being annealed, producing an R_{ms} value of 3.50 nm. This amount of roughening is about the same as that was seen with the annealing of Sc_2O_3 alone.

XRR measurements were made of the Sc_2O_3/MgO film before and after the MOCVD anneal and are plotted together for comparison in Figure 5-13. A qualitative analysis of the two scans when compared to one another shows that there is a large change in the film after being annealed. The most distinguishing feature between the two is the large decrease in the fringe amplitude. As previously mentioned, a decrease in the fringe amplitude signifies an increase in the interface roughness. The situation is more complicated now, due to the existence of two interfaces, the Sc_2O_3/MgO and the MgO/GaN interface. Also, the AFM measurements showed that there was an appreciable amount of roughening of the surface after the MOCVD anneal. However, the overall intensity seems to not have decreased at all after annealing. These results were perplexing. After thorough evaluation of the scans and consideration of the material system, a consistent assessment of the situation was achieved that corroborates all the characterization results. In order to perform a good analysis of the measurement, one must understand how it was produced. In general, the origin of the fringes in an XRR scan is the product of the reflections from the different interfaces combining to produce interference fringes. The difference in the reflectivity of different interfaces is not only due to the roughness of that interface but to the difference in the density of the two materials that make up the interface. Thus, what is believed to have occurred is that the Sc_2O_3 film was completely dissolved into the MgO film. This explains the decrease in the fringe amplitude from the interdiffusion that occurred at the Sc_2O_3/MgO interface. The conflict with the AFM results, with respect to the surface roughening, can be explained by looking at a close-up of the critical angle area shown in Figure 5-14. In the image, it can be seen that after annealing there is shift of the critical angle, which makes it appear that the overall intensity has not changed, but in actuality, the whole curve is shifted up. The critical angle is a function of the density and so the shift of the critical angle

represents a change in the density of the material. The change in the critical angle and the shift up of the whole curve can be explained through the dissolution of the Sc_2O_3 film into the MgO. If Sc_2O_3 dissolves into the MgO, the density of the film would change. The incorporation of nitrogen from NH_x species in the MOCVD environment most likely also contributed to the change in density. The increase in the overall intensity of the curve is due to the increase in the thickness of the film from the dissolution of the Sc_2O_3 into the MgO. The dissolution is further supported by the disappearance of the isolated fringe, which was most likely from the thin Sc_2O_3 film. The large decrease in the fringe amplitude compared to the scan of the film before annealing, doesn't necessarily signify that the oxide/GaN interface has roughened. Due to changes in the material system, the decrease in amplitude could be from only having one oxide film instead of two now. Thus, it is unclear if the oxide/GaN interface has roughened during the MOCVD anneal. To determine if the Sc_2O_3 film had dissolved into the MgO film, XPS was going to be performed on the annealed surface, but the film had severely degraded from exposure to air before it could be done

In Figure 5-15, the high frequency C-V measurement for the Sc_2O_3/MgO (50/250 Å) film is shown. The C_{ox} for the stacked structure was calculated using Equation 5-1.

$$C_{Total} = \frac{1}{C_{MgO}} + \frac{1}{C_{Sc_2O_3}} \tag{5-1}$$

The shift of the C-V curve towards positive voltages usually indicates the addition of negative charge in the oxide. The newly formed negative charge could be due to the substitution of Sc^{3+} for Mg^{2+} in the MgO lattice. The introduction of this defect ($Sc_{Mg}^{\bullet}$) with a positive charge would require the formation of a negative charge in order to maintain neutrality. The negative charge would be magnesium vacancies (V_{Mg}'') that would be more likely to respond to the ac frequency

than the positively charged $Sc_{Mg}^{\bullet}$. The production of negative charge from Sc_2O_3 dissolving into the MgO film is described by the reaction

$$Sc_2O_3 \rightarrow 2\,Sc_{Mg}^{\bullet} + 3\,O_O^x + V_{Mg}'' \qquad (5\text{-}2)$$

The effect of the thickness of the Sc_2O_3 cap for MgO films was investigated. The thickness of the Sc_2O_3 cap was increased to 100 Å, while the thickness of the MgO film was decreased to 200 Å so that the gate oxide would remain a total of 300 Å. From the AFM scans shown in Figure 5-16, the surface shows only a minimal amount of roughening after the MOCVD anneal. From the XRR scans of the Sc_2O_3/MgO (100/200 Å) films before and after being annealing shown in Figure 5-17, the increase in the Sc_2O_3 thickness to 100 Å did not protect the stacked structure from roughening. Since the AFM shows only minimal roughening of the surface, the decrease in the peak amplitude could be due to the dissolution of the Sc_2O_3 into the MgO film. The annealed Sc_2O_3/MgO (100/200 Å) film was kept under vacuum if it wasn't being characterized in order to prevent any degradation from exposure to air. The annealed sample was analyzed using XPS. A scan of the surface showed the presence of Mg, which can be seen in Figure 5-18.

The high frequency C-V measurement of the Sc_2O_3/MgO (100/200 Å) film displayed an extremely large difference after annealing. There is a significant increase in the capacitance after the film was annealed. Unlike the Sc_2O_3/MgO (50/250 Å), the shift in the C-V curve was towards negative voltages indicating the inclusion of positive charge. The MgO film alone also showed a negative shift and it was suggested that Ga diffusion from the substrate could be responsible.

The thermal and environmental stability of potential dielectrics for use in GaN-based devices was examined. The effects of a high temperature anneal in an MOCVD environment

using the growth conditions that were used in the experiments for the regrowth of GaN were looked at. The conditions used are those used for the regrowth of p-type GaN except for the lack of TMG and Cp_2Mg flow. It appears all the dielectric oxides that were examined were degraded in some way from the GaN MOCVD anneal. This is not too surprising since it's a very harsh and reactive environment. Table 5-4 lists the roughness and breakdown values before and after annealing in the MOCVD environment. For the application of a gate dielectric, the Sc_2O_3/MgO stacked structure appears to be the most promising. Particularly the (50/250 Å) structure showed only a small decrease in the breakdown field after being annealed.

Table 5-1. Possible reactions and their Gibbs free energy for SiO_2 in the p-type GaN MOCVD environment.

	Reaction	ΔG_{Rxn} (kJ/mol)	Conditions and processes
1	$SiO_2 \Rightarrow Si + O_2$	+661.5	Decomposition of SiO_2
2	$4NH_3 + 3SiO_2 \Rightarrow Si_3N_4 + 3°_2 + 6H_2$	+1267.5	Si_3N_4 formation
3	$4NH_3 + 3SiO_2 \Rightarrow Si_3N_4 + 6H_2O$	-47.1	
4	$4NH_2 + 3SiO_2 \Rightarrow Si_3N_4 + 4H_2O + O_2$	+49.1	
5	$2Mg + 2SiO_2 \Rightarrow Mg_2SiO_4(s) + Si$	-285.2	Consumption of Mg Production of n-type dopant
6	$Mg + 2SiO_2 \Rightarrow MgSiO_3(s) + SiO$	-33.6	
7	$Mg + 2SiO_2 + O \Rightarrow MgSiO_3(s)$	-475.4	If excess Oxygen is present
8	$Mg + SiO_2 + O \Rightarrow Mg_2SiO_4(s)$	-946.7	If excess Oxygen is present
9	$6Mg + Si_3N_4 \Rightarrow 2Mg_3N_2 + 3Si$	-33.6	Reaction with Si_3N_4

Table 5-2. The possible reactions and their Gibbs free energy for MgO in the p-type GaN MOCVD environment.

Reaction		ΔG_{Rxn}(kJ/mol)	Conditions and processes
1	$MgO \Rightarrow Mg + O$	+442.9	Decomposition of MgO
2	$MgO + NH_3 \Rightarrow MgOH(g) + NH_2$	+550.0	Magnesium hydroxide formation
3	$½MgO + NH_3 \Rightarrow ½MgOH_2(g) + NH_2 + ½Mg$	+78.8	
4	$3MgO + 2NH_3 \Rightarrow Mg_3N_2 + 3° + 6H$	+953.4	Magnesium nitride formation
5	$3MgO + 2NH_3 \Rightarrow Mg_3N_2 + 3H_2O$	+442.5	
6	$3MgO + 2NH_2 \Rightarrow Mg_3N_2 + 3° + 2H_2$	+684.8	
7	$3MgO + 2NH \Rightarrow Mg_3N_2 + 3° + H_2$	+474.2	
8	$3MgO + 2N \Rightarrow Mg_3N_2 + 3O$	+1171.2	
9	$3Mg + 2NH_3 \Rightarrow Mg_3N_2 + 3H$	-375.3	
10	$3Mg + 2NH_2 \Rightarrow Mg_3N_2 + 2H_2$	-643.9	
11	$3Mg + 2NH \Rightarrow Mg_3N_2 + H_2$	-854.5	
12	$3Mg + 2N \Rightarrow Mg_3N_2$	-157.5	
13	$3Mg(OH)_2(s) + 2NH_3 \Rightarrow Mg_3N_2 + 6H_2O(g)$	+692.1	Magnesium hydroxide reactions
14	$4Mg(OH)_2(s) + 2NH_3 \Rightarrow Mg_3N_2 + MgOH(g) + 6H_2O(g)$	+1287.0	
15	$Mg(OH)_2(s) + NH_3 \Rightarrow MgOH(g) + H_2O(g) + NH_2$	+577.8	

Table 5-3. Possible reactions and their Gibbs free energy for Sc_2O_3 in the p-type GaN MOCVD environment.

	Reaction	ΔG_{Rxn} (kJ/mol)	Conditions and processes
1	$Sc_2O_3 \Rightarrow 2Sc + 3O$	+1499.3	Decomposition of Sc_2O_3
2	$Sc_2O_3 + 2NH_3 \Rightarrow 2ScN + 3° + 6H$	+931.5	ScN formation
3	$Sc_2O_3 + 2NH_3 \Rightarrow 2ScN + 3H_2O$	+421.5	
4	$Sc_2O_3 + 2NH_2 \Rightarrow 2ScN + 3° + 2H_2$	+662.9	
5	$Sc_2O_3 + 2NH \Rightarrow 2ScN + 3° + H_2$	+452.3	
6	$Sc + NH_3 \Rightarrow ScN + 3H$	-283.9	If elemental Sc is present
7	$Sc + NH_2 \Rightarrow ScN + H_2$	-418.2	
8	$Sc + NH \Rightarrow ScN + ½H_2$	-523.5	

Table 5-4. Comparison of dielectric oxides before and after MOCVD anneal.

Dielectric	Thickness		Surface roughness (nm)	Average forward breakdown voltage (V)	Forward breakdown field at 1mA/cm^2 (MV/cm)
MgO	300Å	As Grown	1.89	1.13	0.38
		Annealed	18.1	0.225	0.08
Sc_2O_3/MgO	50/250Å	As Grown	.367	2.25	0.75
		Annealed	3.50	2.08	0.70
Sc_2O_3/MgO	100/200Å	As Grown	.231	2.12	0.71
		Annealed	1.29	0.936	0.31
HT-Sc_2O_3	200Å	As Grown	.226	1.82	0.91
		Annealed	3.68	*	*
LT-Sc_2O_3	200Å	As Grown	.852	4.94	2.47
		Annealed	1.25	*	*

*= electrical short was measured.

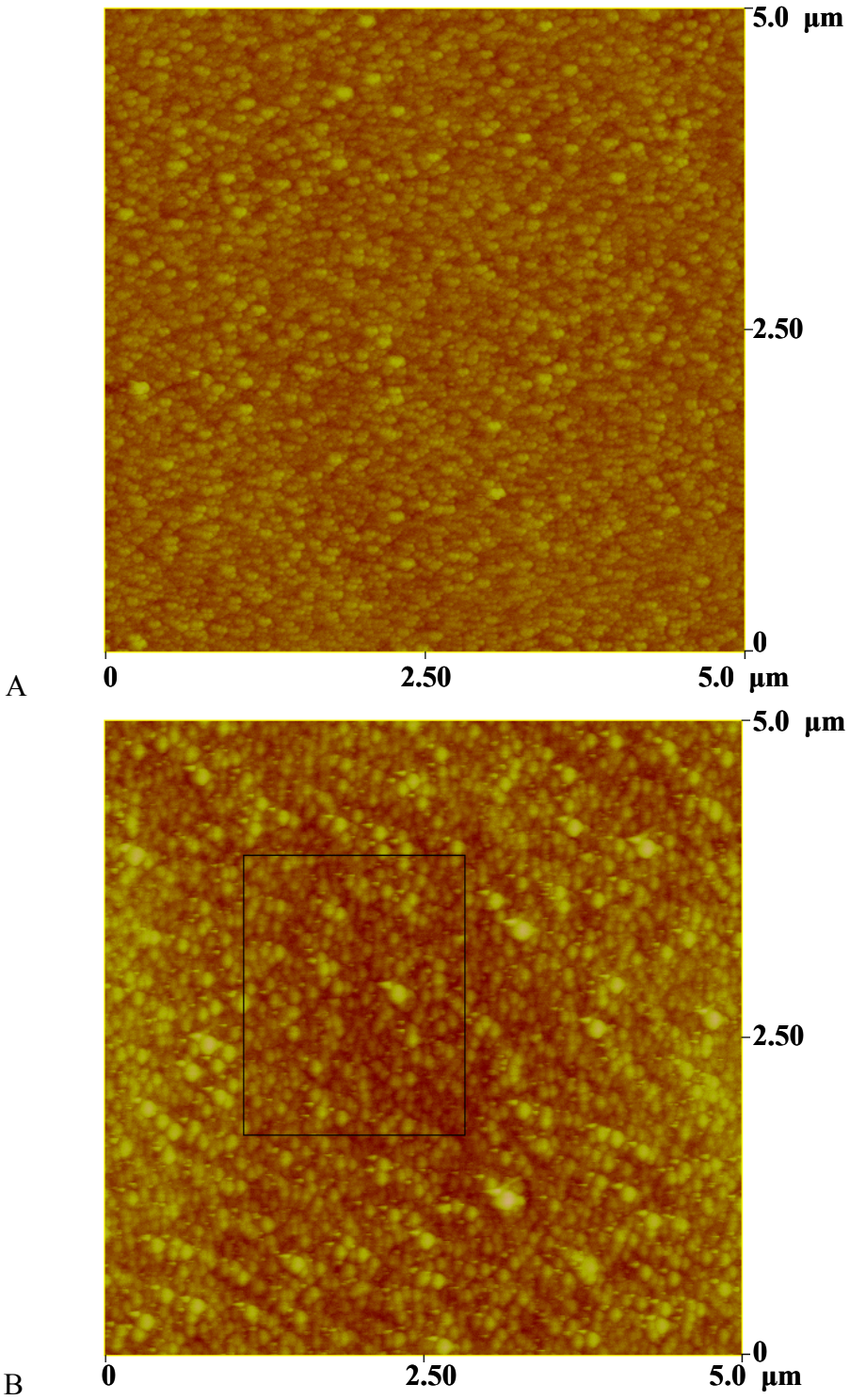

Figure 5-1. AFM measurements of the SiO_2 films. A) As grown. B) After being annealed in a p-type GaN MOCVD environment.

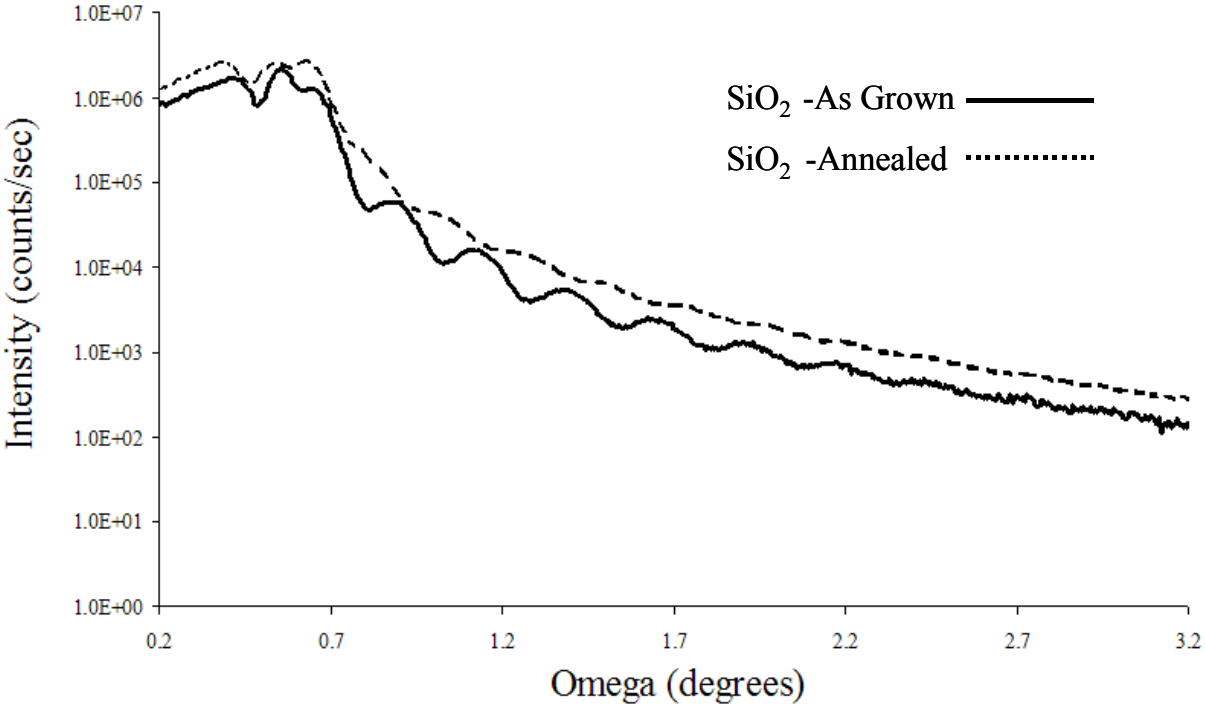

Figure 5-2. XRR measurements of SiO_2 films before and after being annealed in a p-type GaN MOCVD environment.

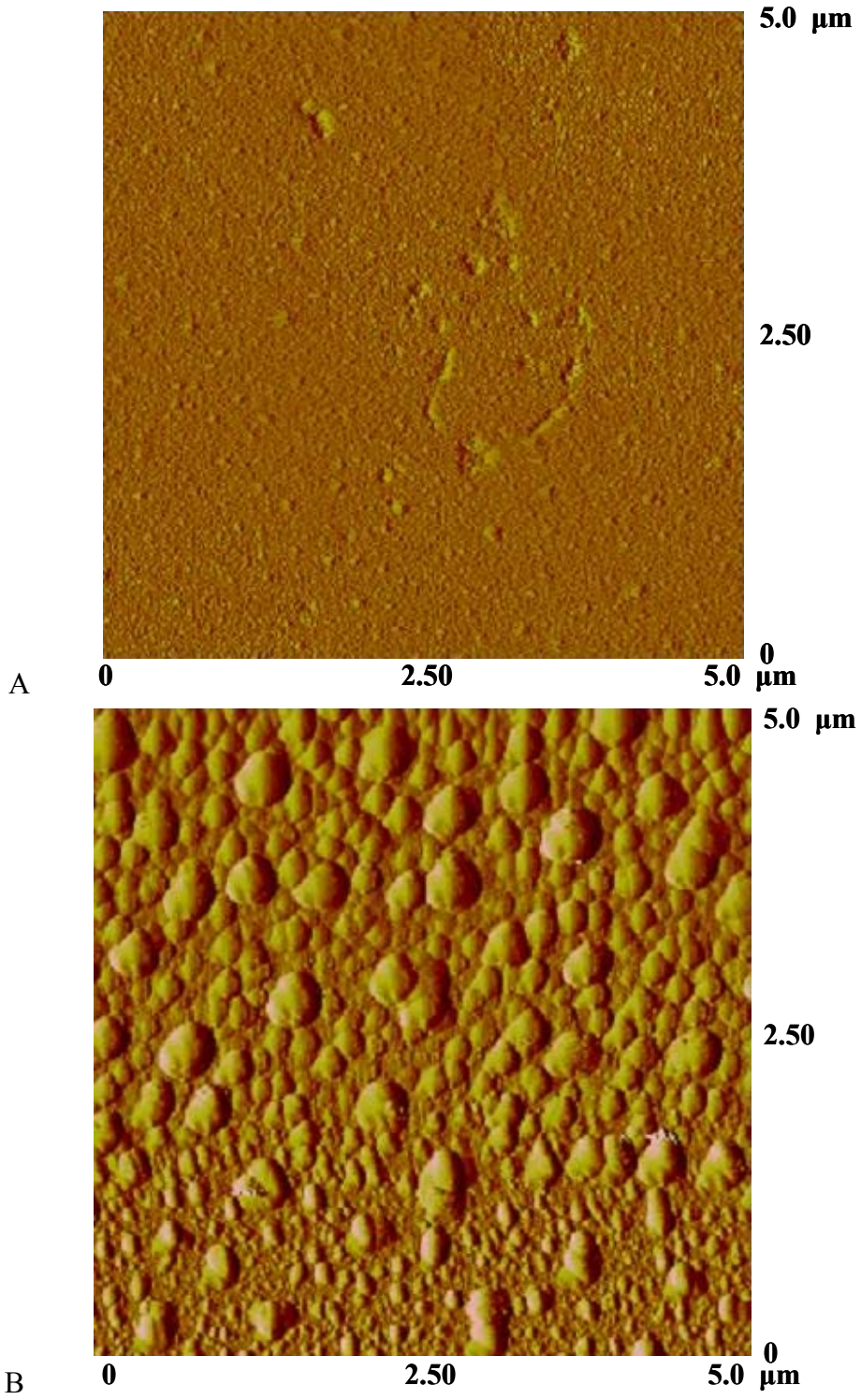

Figure 5-3. AFM measurements of MgO films. A) As grown. B) After being annealed in a p-type GaN MOCVD environment.

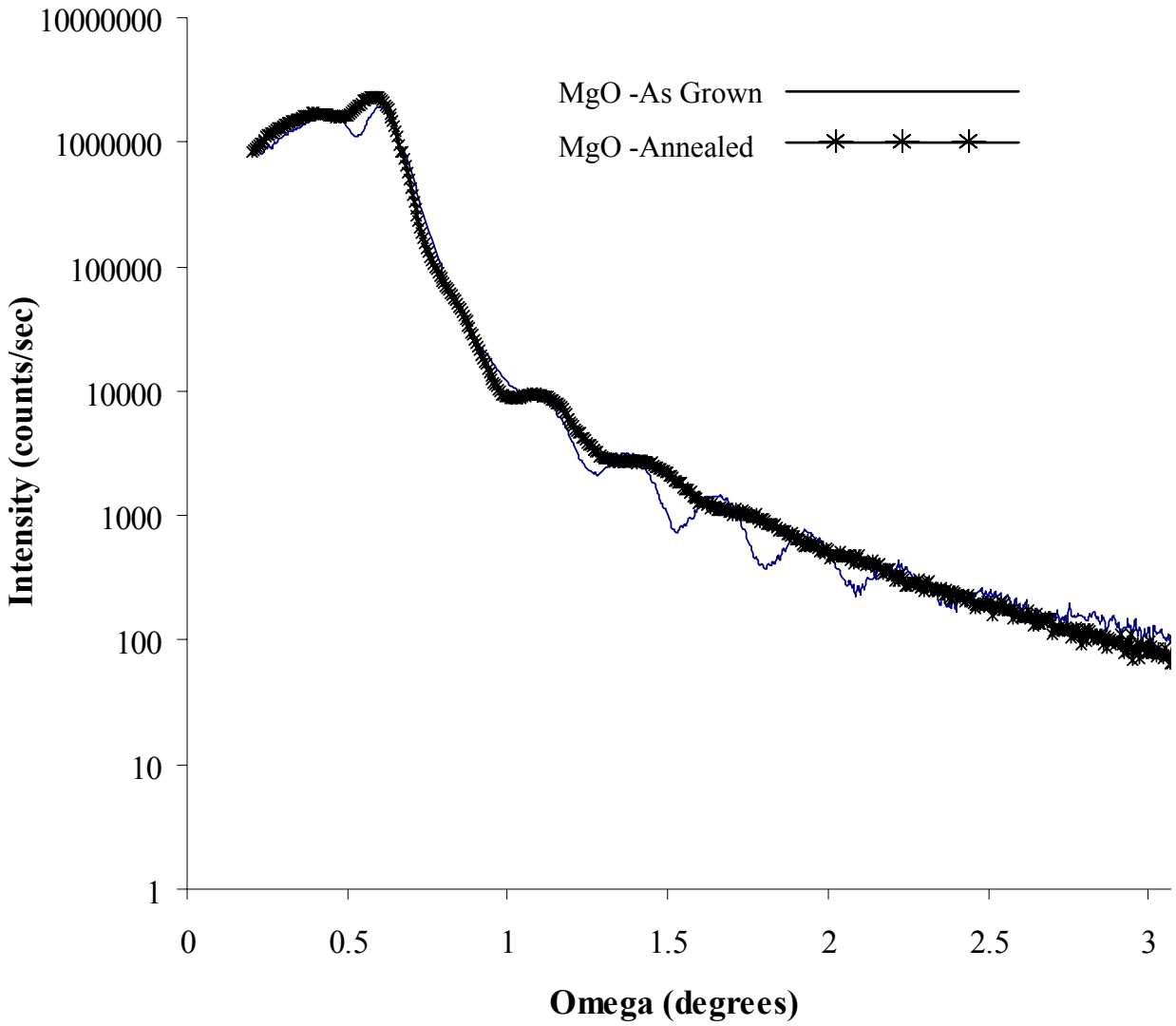

Figure 5-4. XRR measurements of MgO films before and after being annealed in a p-type GaN MOCVD environment.

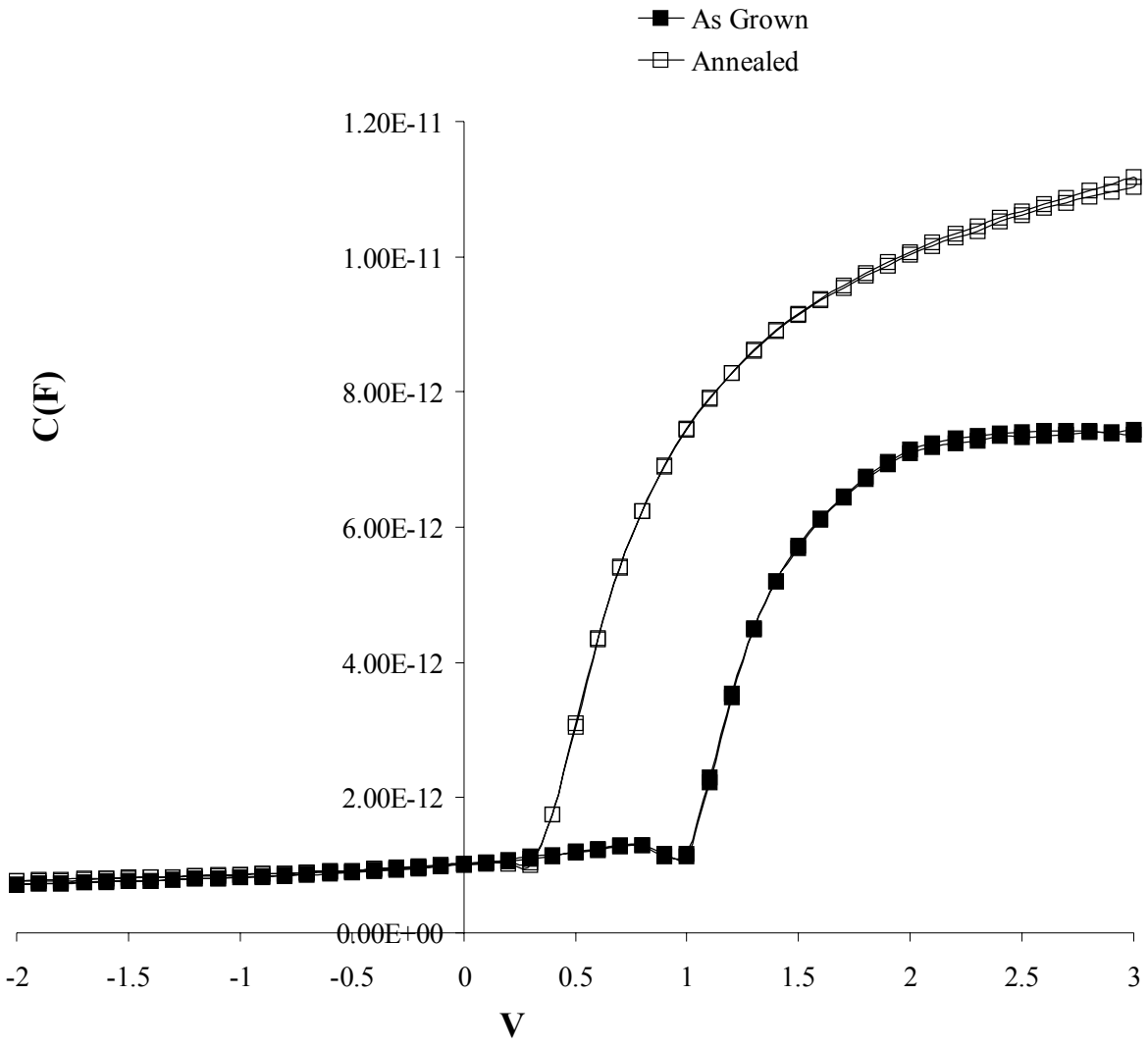

Figure 5-5. C-V measurements of MgO diodes taken before and after being annealed in a p-type GaN MOCVD environment.

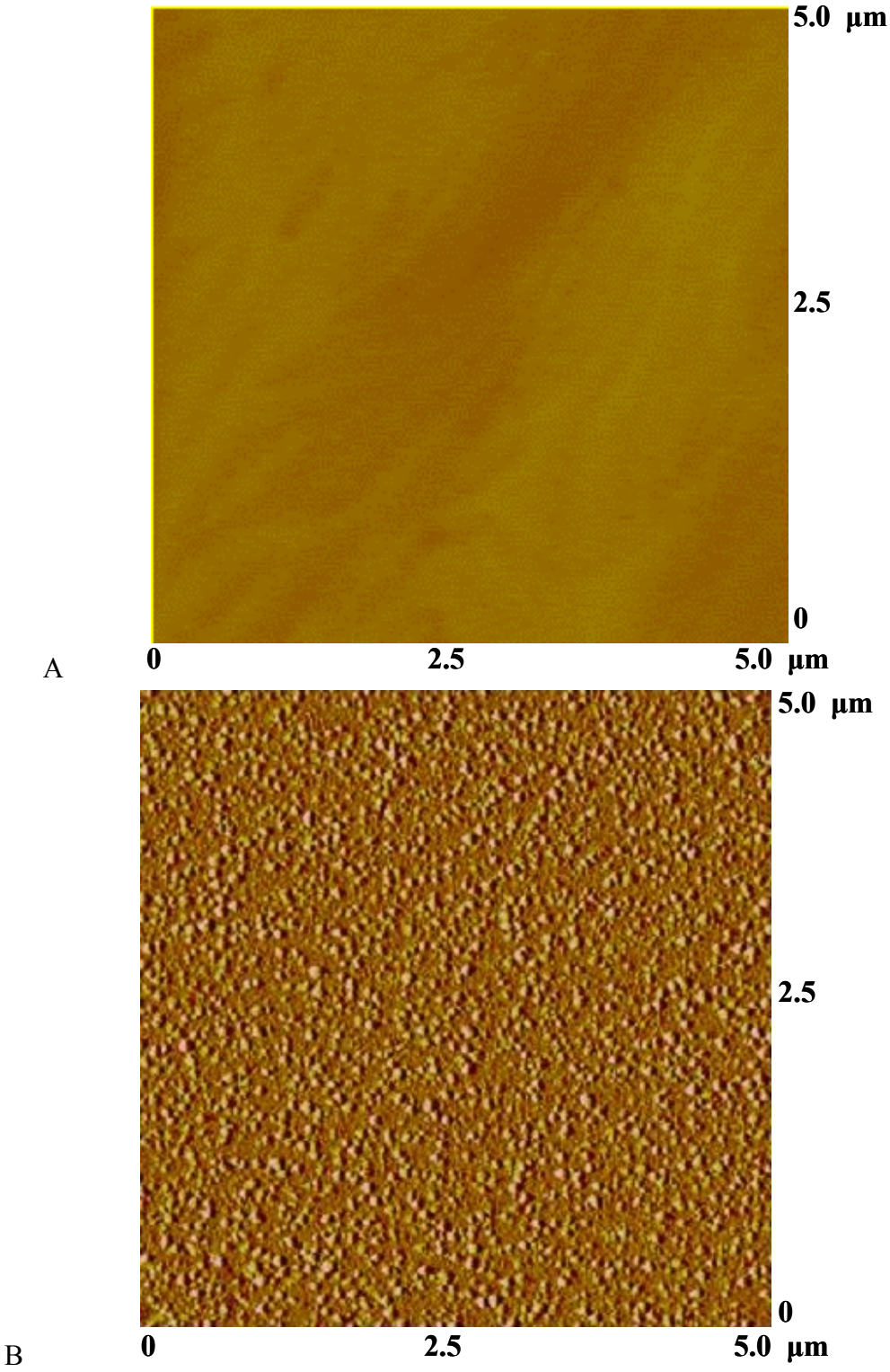

Figure 5-6. AFM measurements of the HT-Sc_2O_3 film. A) As grown. B) After being annealed in a p-type GaN MOCVD environment.

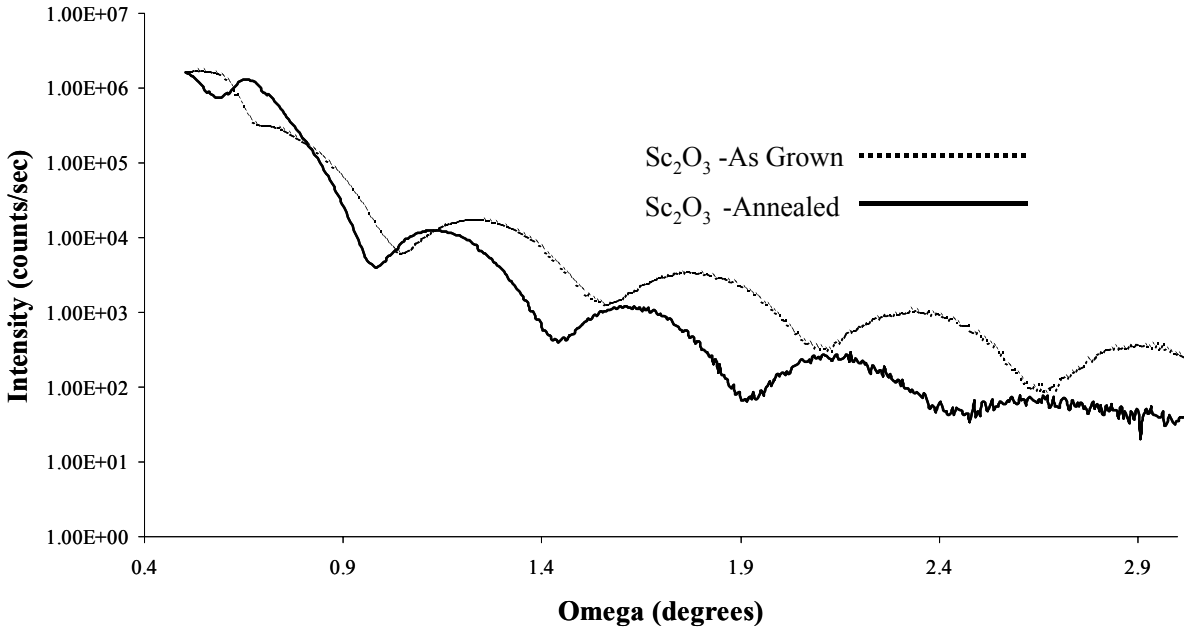

A

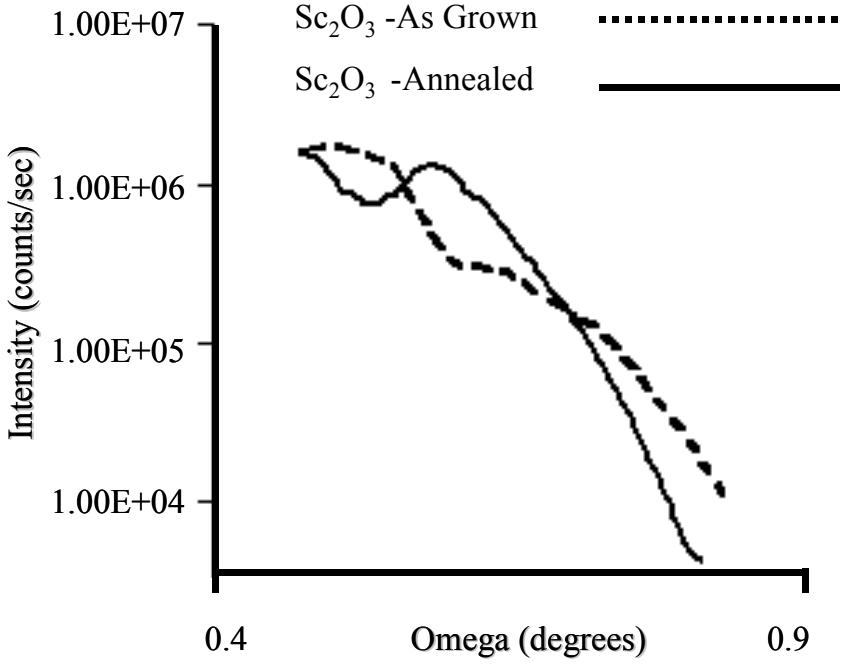

B

Figure 5-7. XRR measurements of the Sc_2O_3 film before and after being annealed in a p-type GaN MOCVD environment. A) Complete plots of both scans. B) Close up of the critical angle region.

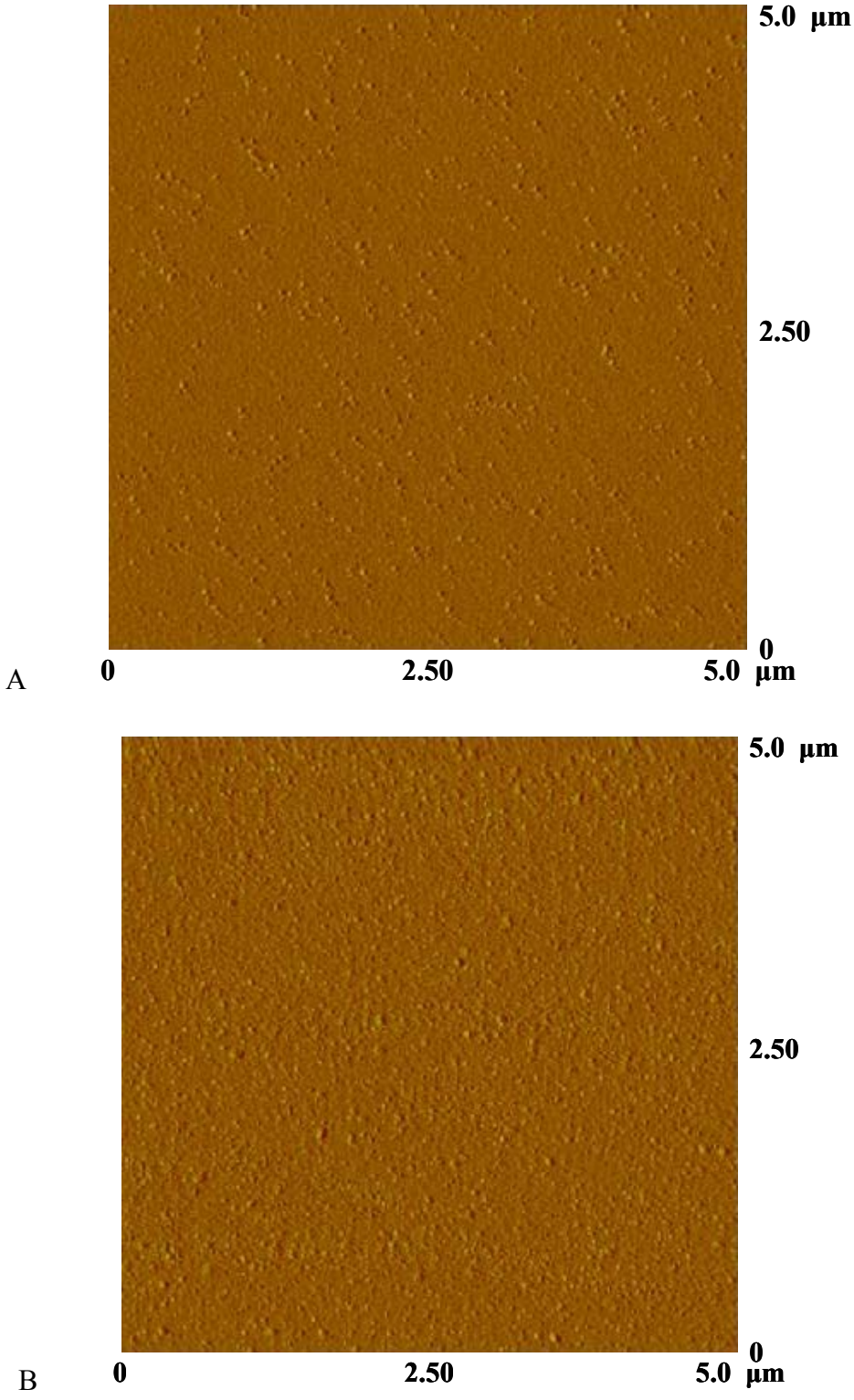

Figure 5-8. AFM measurements of the LT-Sc_2O_3 film. A) As grown. B) After being annealed in a p-type GaN MOCVD environment.

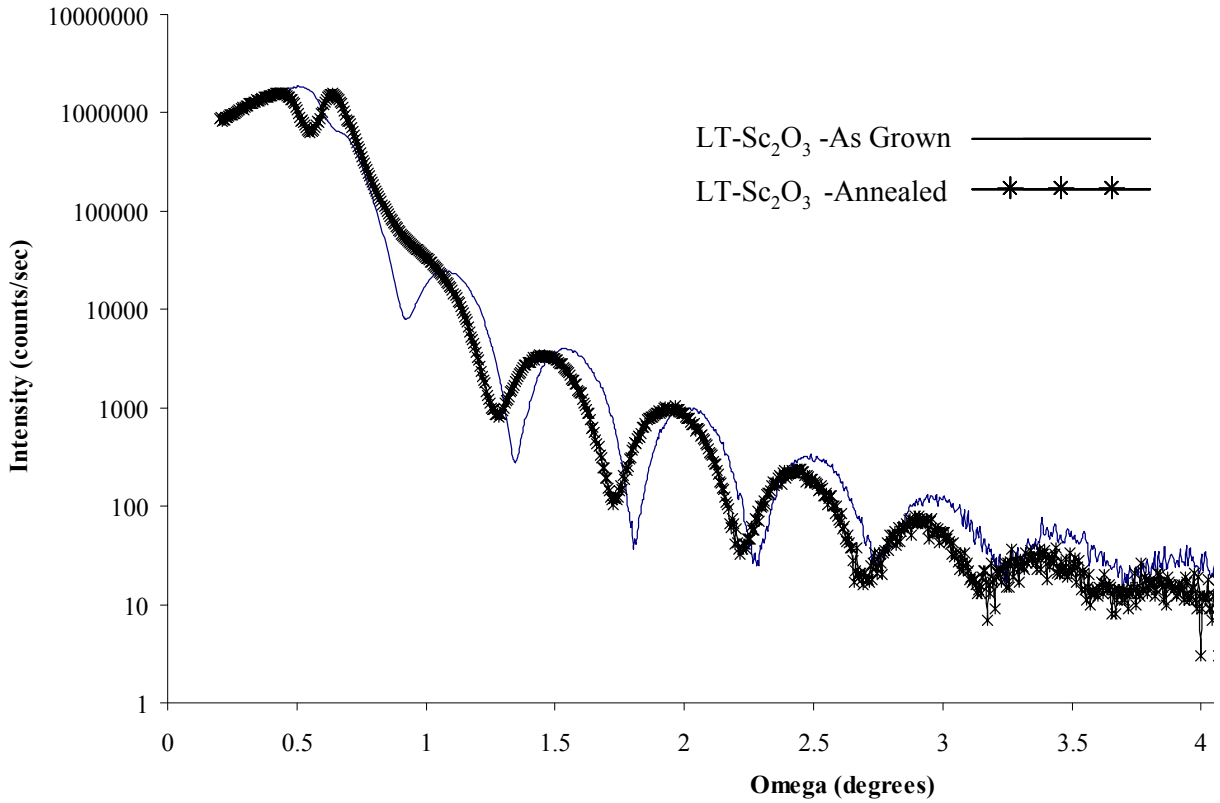

Figure 5-9. XRR measurements of LT-Sc_2O_3 films before and after being annealed in a p-type GaN MOCVD environment.

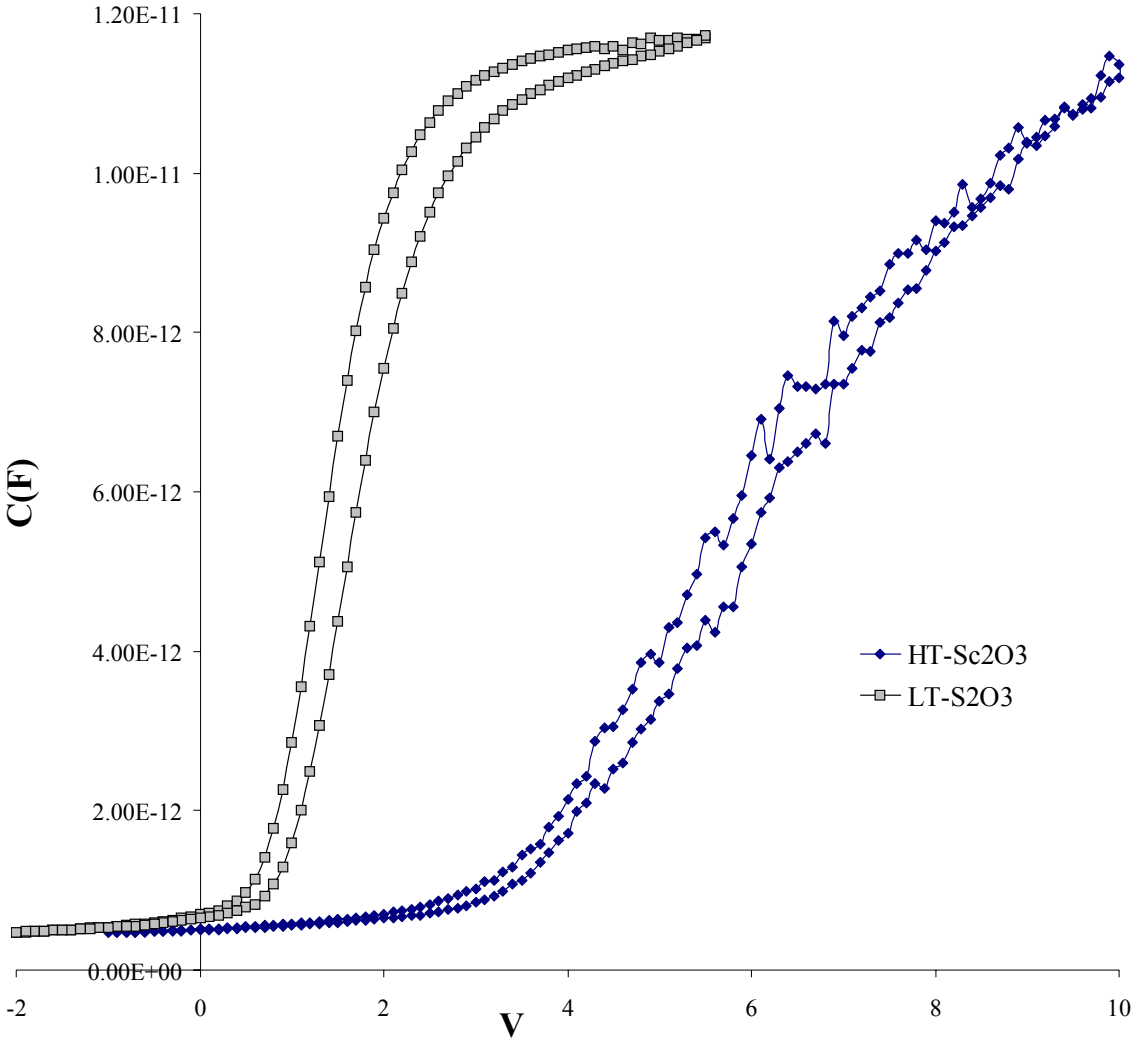

Figure 5-10. High frequency (1MHz) C-V measurements of the HT and LT-Sc_2O_3 films before being annealed in a p-type GaN MOCVD environment.

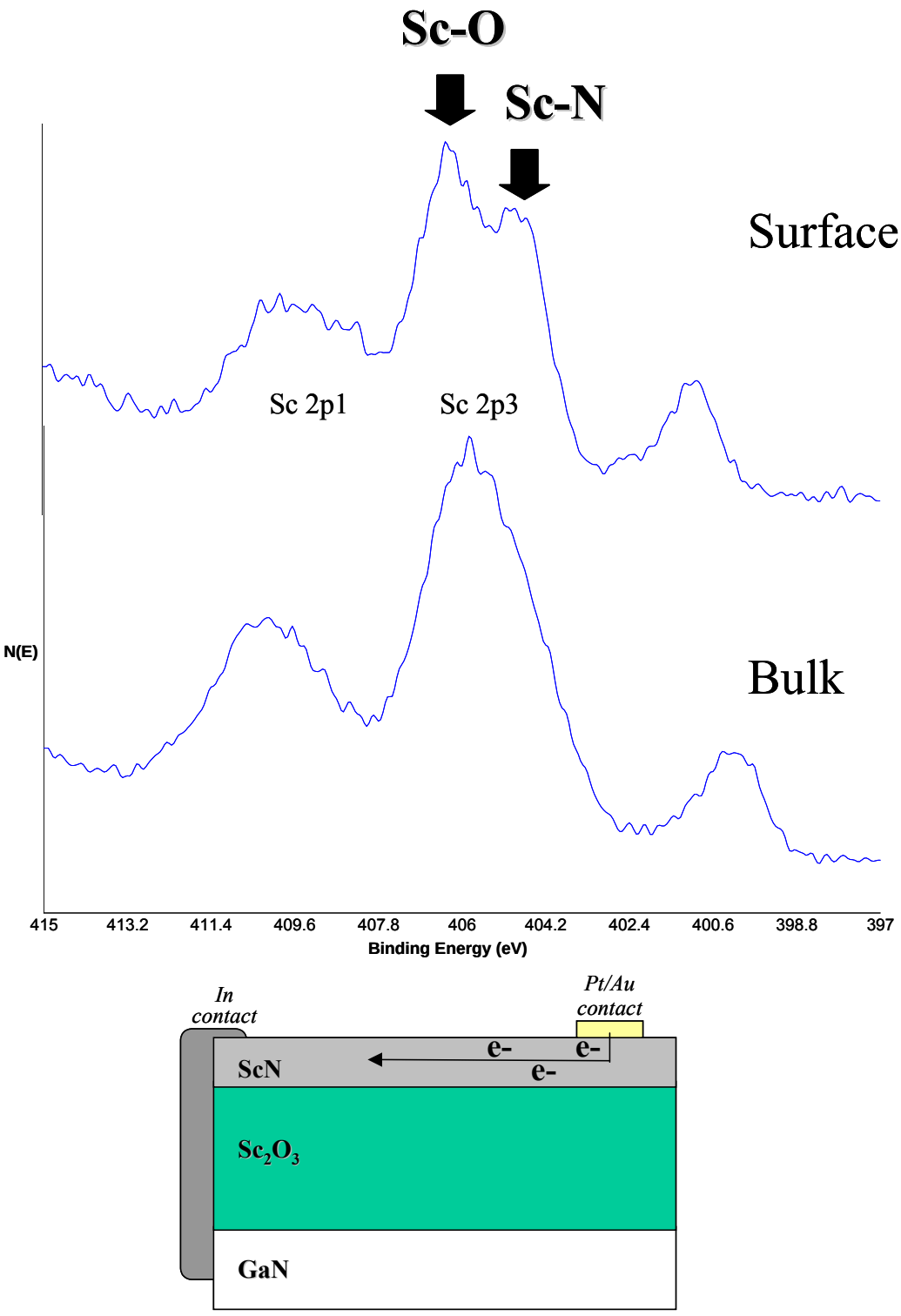

Figure 5-11. XPS Measurements of the Sc 2p peaks of the Sc_2O_3 film after the MOCVD anneal and an illustration of the shorting mechanism due to the ScN layer.

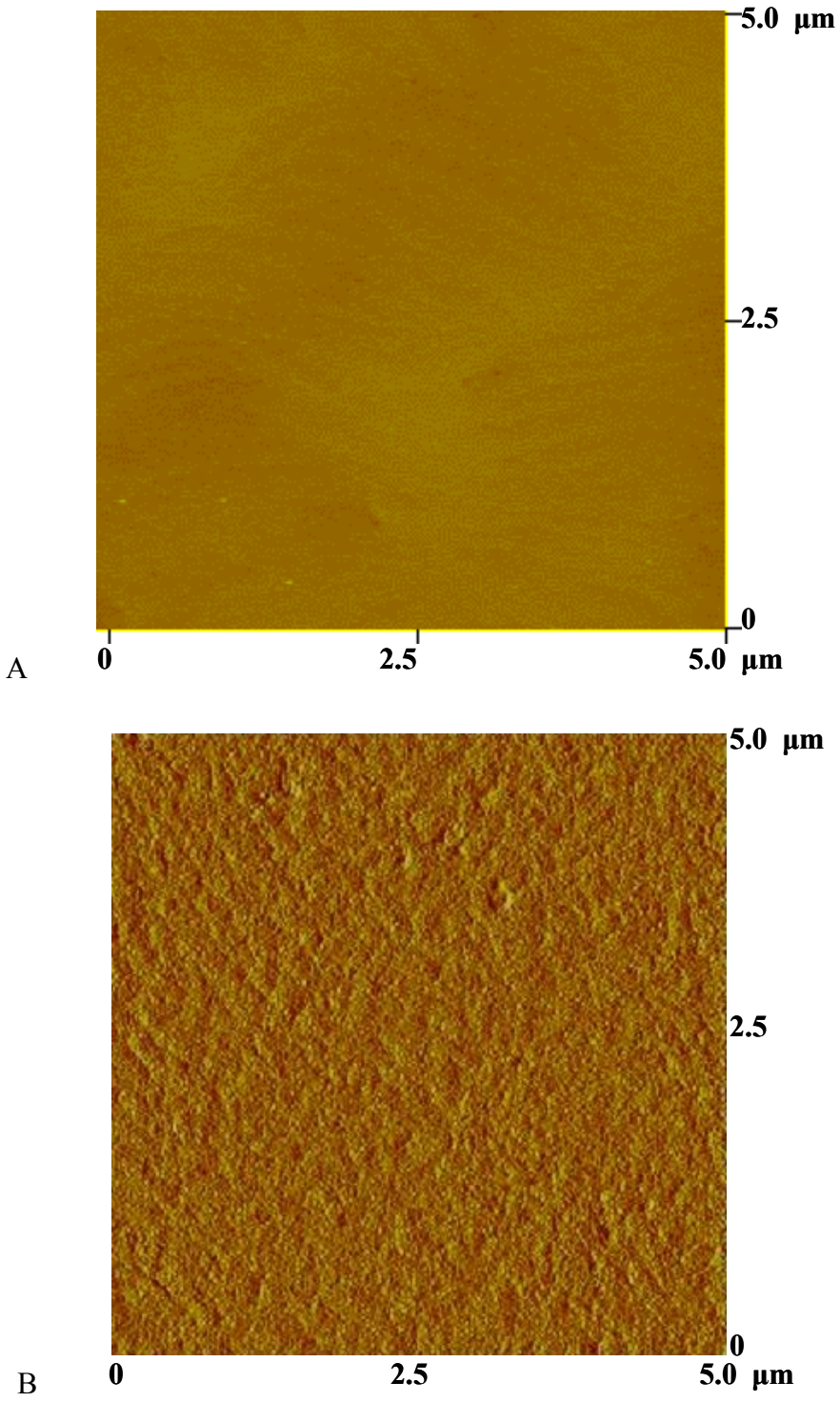

Figure 5-12. AFM measurements of the Sc_2O_3/MgO (50/250 Å) film. A) As grown. B) After being annealed in a p-type GaN MOCVD environment.

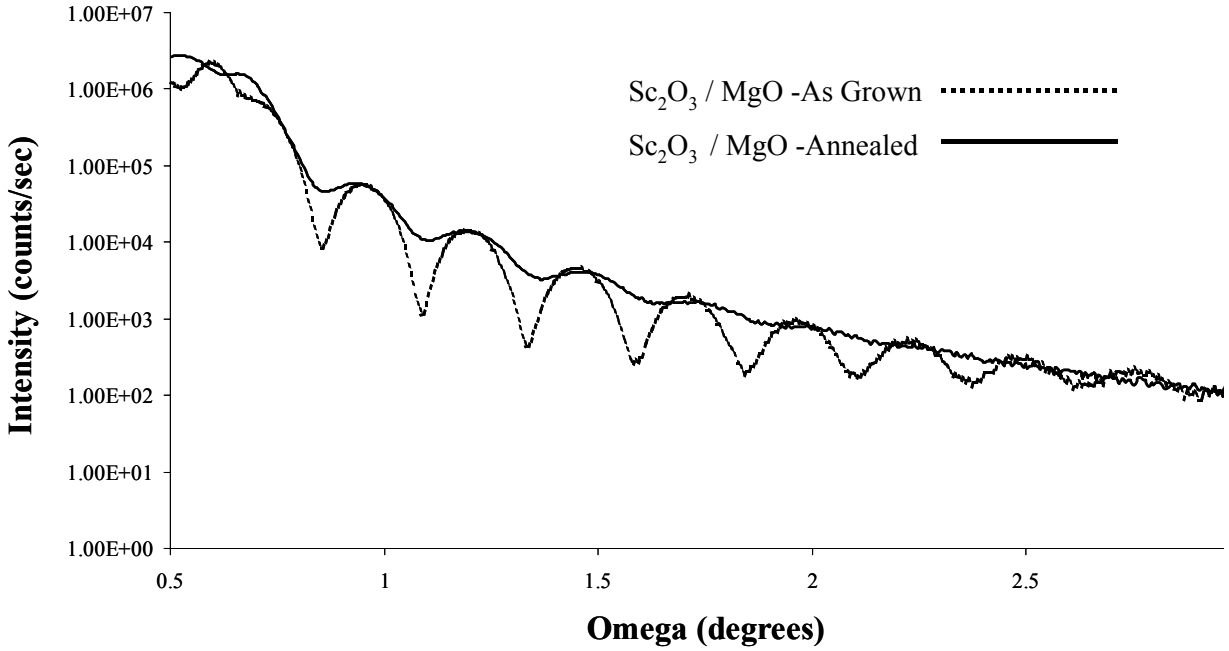

Figure 5-13. XRR measurements of Sc_2O_3/MgO (50/250 Å) films before and after being annealed in a p-type GaN MOCVD environment.

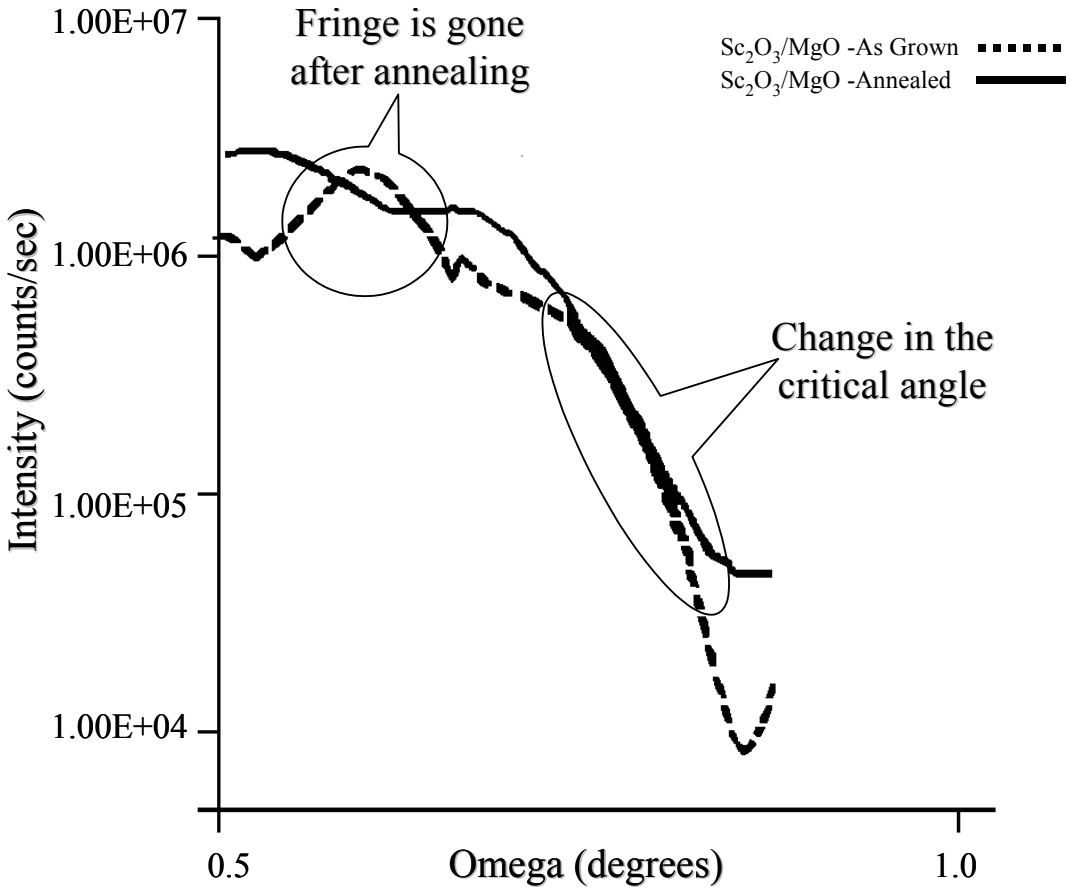

Figure 5-14. Close-up of the critical angle area of the XRR scans for the Sc_2O_3/MgO (50/250 Å) film.

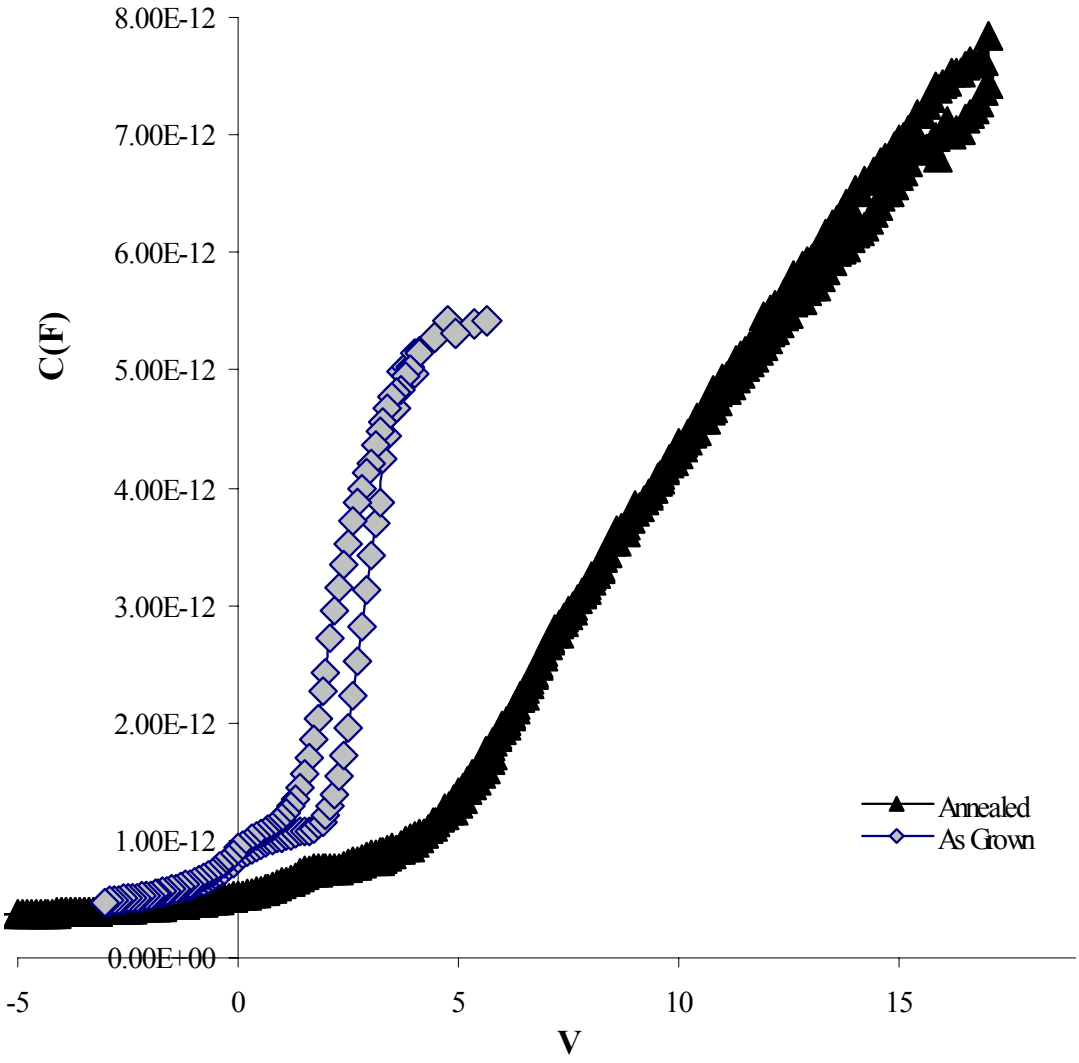

Figure 5-15. High frequency (1MHz) C-V measurement for the Sc_2O_3/MgO (50/250 Å) film before and after the MOCVD anneal.

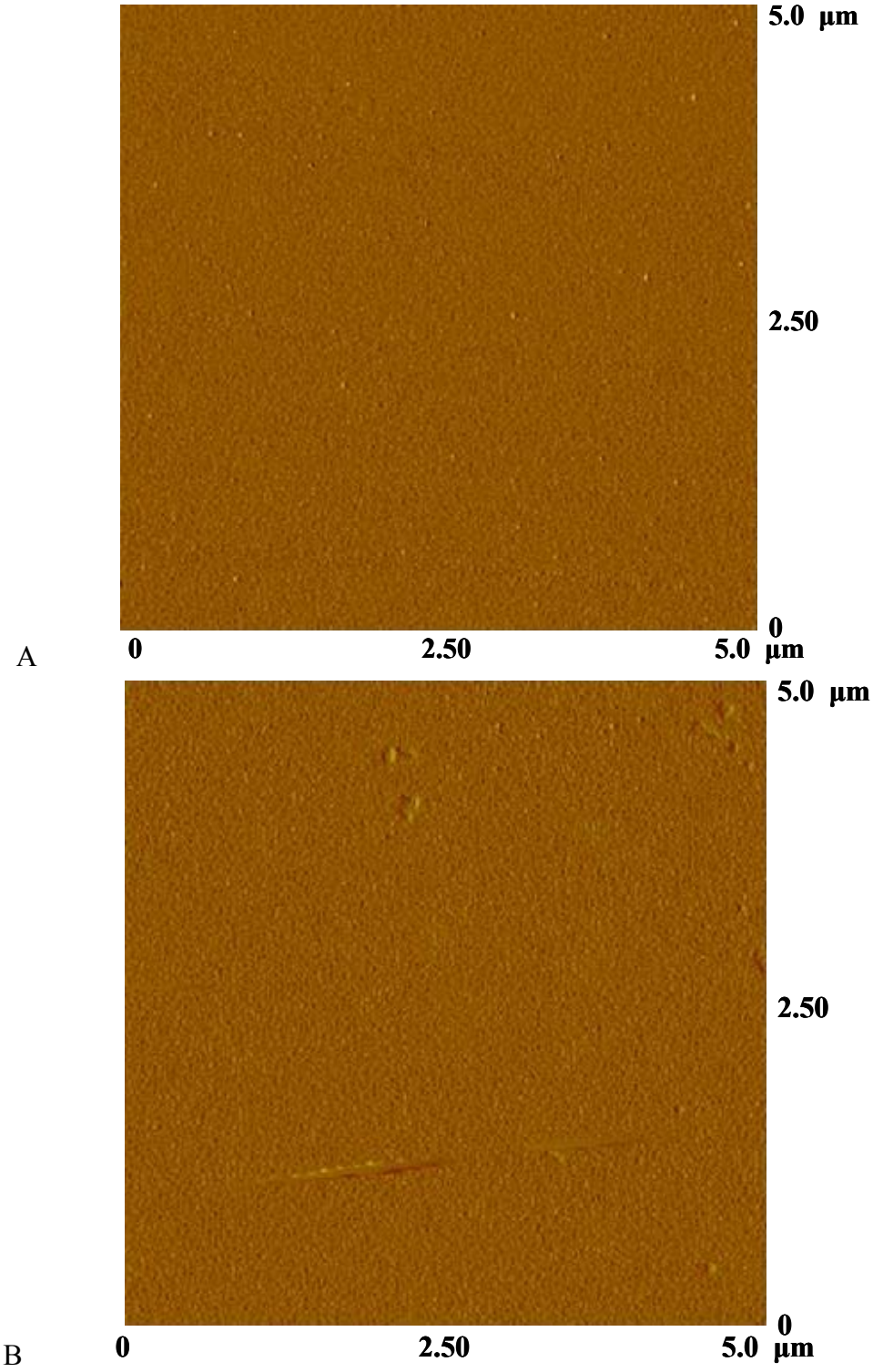

Figure 5-16. AFM measurements of the Sc_2O_3/MgO (100/200 Å) film. A) As grown. B) After being annealed in a p-type GaN MOCVD environment.

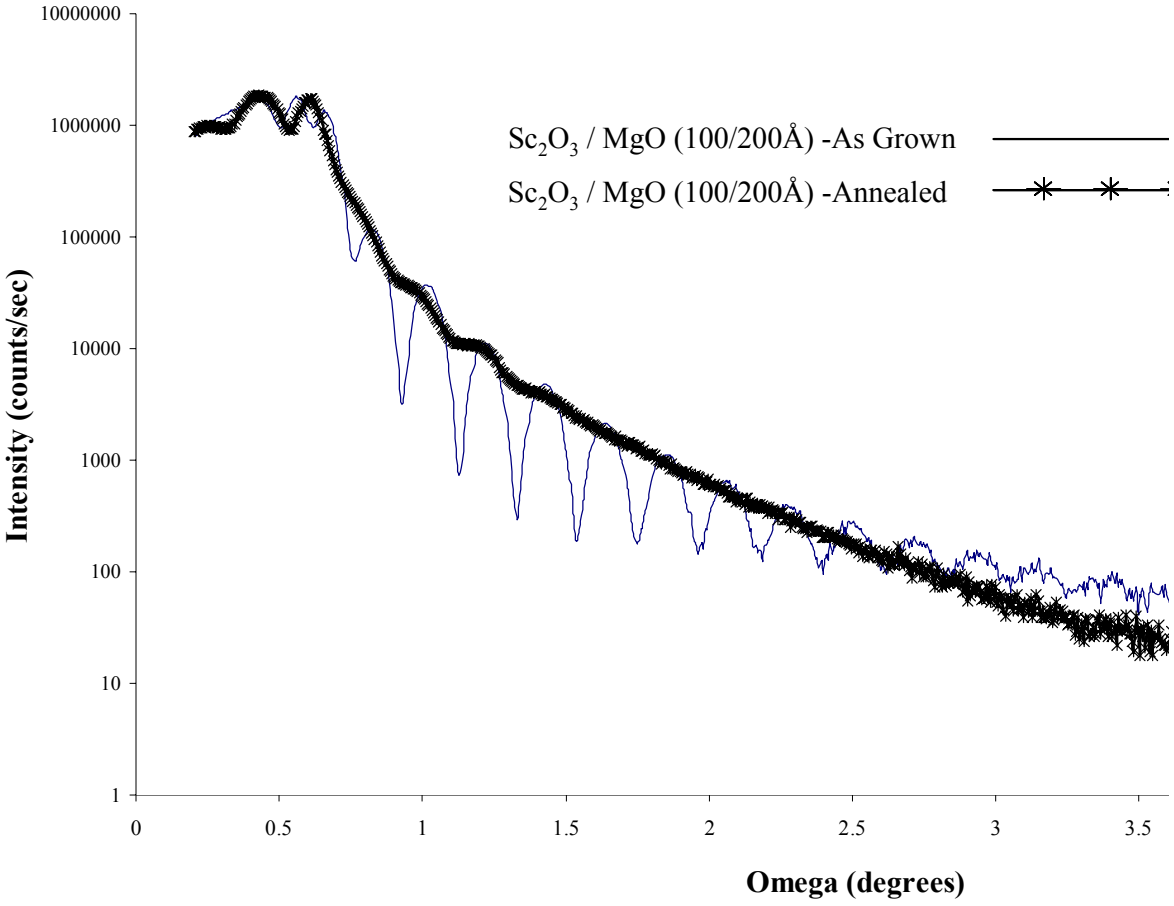

Figure 5-17. XRR measurements of Sc_2O_3/MgO (100/200 Å) films before and after being annealed in a p-type GaN MOCVD environment.

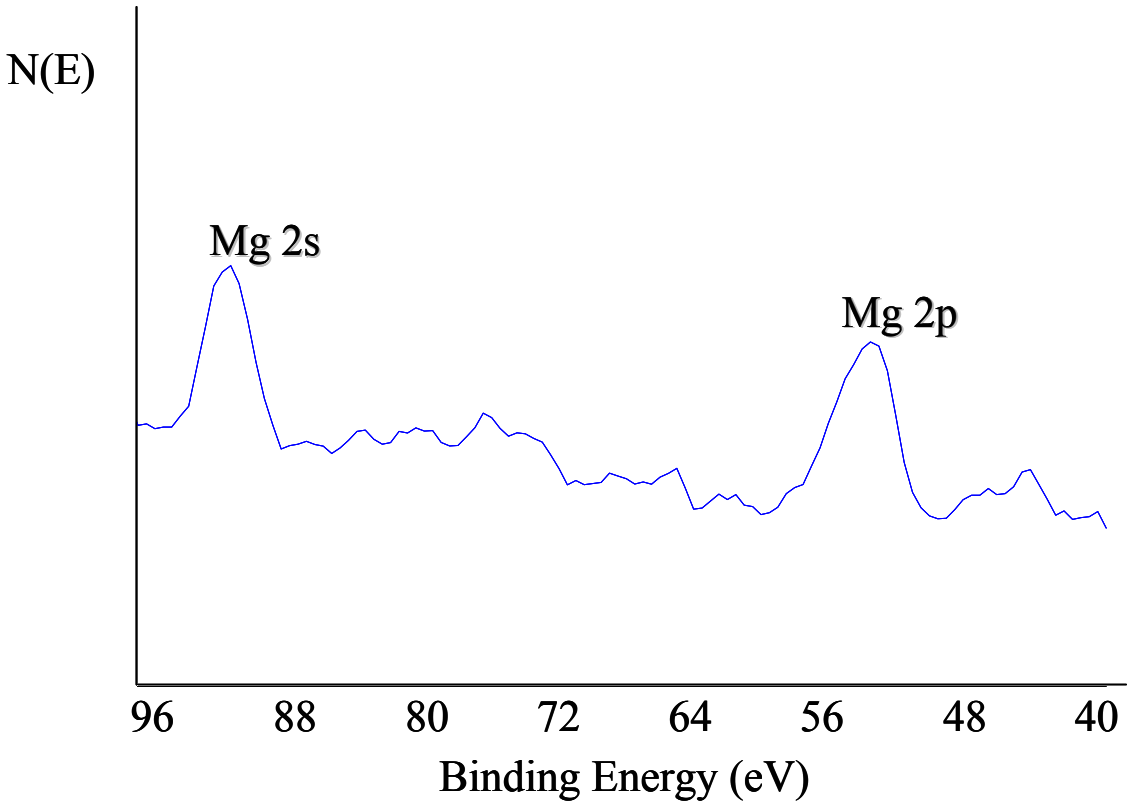

Figure 5-18. XPS of the Sc_2O_3/MgO (100/200 Å) film after being annealed in a p-type GaN MOCVD environment.

CHAPTER 6
SELECTIVE AREA REGROWTH OF P-TYPE GAN: RESULTS AND DISCUSSION

The technology of III-Nitride semiconductor regrowth for device fabrication has the potential to produce novel and innovative designs of electronic devices. It can also provide alternative fabrication methods of conventional device structures that are otherwise ineffective or inefficient. This is particularly true for advanced GaN-based devices, which has several material and device issues to overcome in order to make them feasible. Very little work has been done in this area despite its varied applications and great potential. Some work that has been performed was the regrowth of n^+ GaN as ohmic contacts for AlGaN/GaN HEMT devices [80-83]. That work was very focused on that specific application with little examination of the general regrowth mechanisms. The regrowth of GaN into the etched features of a GaN substrate is extremely complex, due to the numerous variables that are involved. The first area of difficulty is the substrate preparation, which requires photolithography, etching and other processing steps that are still not fully developed for GaN device fabrication, let alone for regrowth applications. Another difficulty is due to the MOCVD growth technique, which by itself is very complex and difficult to model, despite the advancements made in the understanding of the fundamental mechanisms in the last decade. The progress made was mainly achieved through experiment and required an enormous amount of work on the subject. The same situation is applicable to GaN regrowth due to the large number of steps involved and the variables that each step possesses. This area of research is still just beginning and lacks empirical evidence needed to form a better understanding of the technique. Development of this technology is quite worthwhile and has great value in advancing the understanding of both the MOCVD growth and device processing of GaN.

The difficulty in producing high quality and heavily doped p-type GaN was discussed earlier. A novel application of MOCVD regrowth is to regrow the p^+ source and drain regions of a GaN p-MOSFET. This alternative approach to creating the p^+ regions would avoid the problems associated with *p*-type doping via ion implantation by doping the material during the MOCVD regrowth. The regrowth of the p^+ GaN source and drain regions of a p-MOS device was explored. The regions for the p^+ source and drain were etched out of the substrate and then GaN, heavily doped with Mg was selectively regrown into the etched trenches.

The approach used for the selective regrowth of the p^+ regions is based on the method of pendeo-epitaxy, which is a variation of epitaxial lateral overgrowth (ELO) [84]. Unlike conventional ELO techniques, the focus in pendeo-epitaxy is on growth laterally from the trench walls rather than the normal growth direction of [0001]. Using this approach for the regrowth of p-type GaN has a number of advantages. First, the lateral growth from the trench walls will result in a large decrease in threading dislocations in the regrown material compared to that which is in the bulk. This is the basis of all lateral overgrowth techniques because the threading dislocations in bulk GaN, which run perpendicular to the surface, do not propagate into the laterally regrown material. Secondly, the lateral growth from the trench walls will more likely create a good interface at the p-n junctions, which is critical to device performance. Usually in epitaxial lateral overgrowth, the interface where two growth fronts meet is highly defective. Having the two growth fronts meet in the middle ensures that this defective interface is not at a p-n junction. This is illustrated in Figure 6-1. Another advantage is the large growth rate anisotropy that is inherent in the growth system, where the lateral growth rate is much faster than the vertical growth rate. As previously mentioned, the introduction of Mg into the MOCVD growth environment causes an increase in lateral growth rate, while at the same time, inhibiting vertical growth in the [0001]

direction. This effect becomes larger as the Mg concentration increases, which is fortuitous, since a particularly large Mg concentration is needed in order to achieve an adequate hole activation. Thus increasing the ratio [Mg]/[Ga] will increase the lateral growth rate. The [Mg]/[Ga] ratio will be a critical growth parameter to be optimized by the adjustment of the Cp_2Mg and TMG flow rates. Using this approach, the growth conditions during regrowth of the Mg-doped GaN layers need to be optimized for lateral growth and so that the $\{11\bar{2}0\}$ facet will have the highest hole concentration. The selective area regrowth brought up several issues that would not otherwise exist for conventional epitaxy. The real difficulty was not in trying to achieve heavily doped p-type material but was in obtaining p^+ GaN by selectively regrowing it in the etched features of a processed substrate.

Substrate Preparation

The preparation of the substrates for MOCVD regrowth involves many different steps, each of which requires optimization. The optimized procedure for the regrowth substrate preparation will be briefly described in this section. The optimization process and the issues involved will be discussed in more detail in the next chapter. The first step was the growth of the main GaN substrate layer whose doping was dependent on the specific application needed. For samples that were to be regrown in order to determine the level of p-type doping of the regrowth, substrates were grown with a larger n-type carrier concentration. Substrates to be used to fabricate a MOSFET were grown lightly n-type doped. The next step was the deposition of the regrowth mask. The parameters for the SiO_2 deposition were given in chapter 3. Due to its thermal and environmental stability, very little work was needed in optimizing the SiO_2 deposition conditions. After about a 1000 Å of SiO_2 was deposited, the mask pattern used for the regrowth was put down using photoresist and standard photolithography techniques. As

previously mentioned, the growth rate of different planes in GaN varies. Due to this, the regrowth pattern needs to be specifically oriented so that the critical interfaces correspond to the growth planes with maximum lateral growth rate. For the samples that used SiO_2 as the regrowth mask, the difficulty in processing the substrate arrived when the oxide needed to be etched. After exploring both wet and dry etch recipes and then optimizing the conditions, a good reproducible procedure was developed. The development of a good SiO_2 etch process did not require excessive iterations due to highly developed knowledge base that exists from its use in Si-based technology. A larger amount of work was needed to develop a good GaN etch recipe. The main problem that was encountered during the dry etching of GaN using Cl_2/Ar plasma was the appearance of unetched pillars. Figure 6-2 shows an example of a substrate that formed pillars from the dry etch. To improve the etched surface morphology, the RF and ICP powers were varied in several different fashions. Although the morphology improved somewhat, complete removal of the pillars did not occur. By adjustment of the Cl_2/Ar ratio, a smooth surface free from pillars was finally obtained. An increase in the chemical component was needed, which was achieved through increasing the Cl_2 flow rate. An image of a substrate that was etched using the optimized conditions is shown in Figure 6-2C.

Structural Characterization: Optimization of p^+ GaN Regrowth Conditions

Thermal Stability of Processed Substrates for Regrowth

At temperatures above 700^0C, thermal decomposition of GaN begins to occur. Heating the sample to the growth temperature is not instantaneous and requires several minutes. Therefore the substrate will experience temperatures greater than 700^0C for a large time before any growth is initiated. The impact on growth could be significant if extensive decomposition of the substrate or regrowth mask occurs before any growth has begun. The extent of decomposition is dependent on the environmental conditions. Studies conducted on the thermal

decomposition of GaN in MOCVD applications have shown that the gas composition and flow rates have a large affect on the GaN decomposition rate [85-92]. In order to help optimize the growth conditions and determine the effects of the high temperatures upon the initial heating up to the growth temperature several annealing experiments were performed using patterned substrates. The substrates were etched and processed exactly as those being used for the regrowth.

The first conditions used for annealing were the exact same conditions used for heating the substrate up to the growth temperature during regrowth. The pressure was 45 Torr and the NH_3, H_2 and N_2 flows were 1.5, .5 and .5 slm, respectively. Once at the growth temperature of 1090^0C, the substrate remained at that temperature for 5 minutes and then the exact same regrowth conditions for ramping down the temperature were used. The only difference between this annealing experiment and an actual regrowth run was the absence of TMG and Cp_2Mg flow. In Figure 6-3, the SEM images of the substrate before and after annealing show that heavy decomposition of the etched GaN surface occurs during the initial heating of the substrate to the growth temperature. In order to see the effects of the anneal on an unetched GaN surface, a small area of the substrate did not receive the GaN dry etch. The area was covered with photoresist after etching the SiO_2 to protect the surface from the dry etch environment. The role of the mask and the relative amount of exposed GaN present during annealing was also examined by annealing a patterned and etched substrate without any type of regrowth mask. It was etched in the exact same way, only the etch mask was removed prior to annealing. The effect of the anneal on each of these three substrate variations can be seen in Figure 6-4, which shows the SEM images of each after annealing. Figure 6-4B is an image of the unetched GaN surface after annealing and shows that under these annealing conditions roughening and decomposition of the

GaN surface occurs regardless of being etched or not. From the figures it is apparent that there is a considerably larger amount of decomposition of the etched than the unetched surface. The image in Figure 6-4C shows a substrate that was annealed under the same conditions but without a regrowth mask. From the image, it is quite obvious that the regrowth mask and the amount of exposed GaN surface play a significant role in the decomposition mechanism. The most intriguing observation in Figure 6-4C is that growth has taken place from the sidewalls even though no TMG has been introduced into the reactor chamber. This phenomenon is known as mass transport regrowth and has been seen in similar situations where substrates having etched features were placed in an MOCVD environment [93]. Besides the mass transport regrowth, the image shows that decomposition of the etched GaN surface has occurred as in the previous case, but to a lesser extent and the surface roughening has dramatically decreased. The decomposition and roughening of the unetched GaN surface was expected from the scenario in Figure 6-4B, but like the etched surface there was a large decrease in the degree of roughening. Another observation that can be made is that the SiO_2 film shows no signs of degradation and appears to be chemically and thermally stable under these conditions.

Once it became apparent that decomposition of the substrate upon heating to the growth temperature does occur, several more substrate annealing experiments were performed in order to determine to optimum conditions for heating the substrate before growth that will minimize the amount of decomposition. Ga desorption has shown to be a minimal contribution to the decomposition of GaN at elevated temperatures. The main mechanism by which GaN decomposition occurs is through the loss of nitrogen, which occurs through the formation and evaporation of N_2. At the high temperatures required for growth, the mobility of N adatoms is increased resulting in a larger amount of N atoms meeting to form N_2 and desorbing. Increasing

the flow of NH_3 has been shown to decrease the rate of decomposition of GaN at elevated temperatures [86]. The proposed mechanism for the reduction in decomposition with increasing NH_3 flows is related to the adsorption of NH_3 on the GaN surface and blocking the surface sites needed for the diffusion of N adatoms [85]. Thus, the diminished N mobility results in a decrease in the loss of N through N_2 desorption and consequentially reduces the rate of decomposition. Therefore the first variable that was adjusted was the NH_3 flow rate. To increase the NH_3, the pressure was increased in order to maintain the proper flow dynamics. The NH_3 flow was doubled from 1.5 to 3.0 slm. After annealing with the increased NH_3 flow, the substrate was still particularly rough and so the NH_3 was doubled again to 6.0 slm. The images for both substrates annealed under the increased NH_3 flows are shown in Figure 6-5. It is easily seen that despite the large NH_3 flow, the surface still roughened. From the images, the morphology appears to become smoother towards the edges of the features. It is believed that this is possibly due to a relative increase in the NH_3 concentration at the edges of the feature due to a lack of reaction and dissociation on the SiO_2 mask. This is analogous to the growth rate enhancement seen with increased TMG concentrations at the mask edges, which will be discussed later. Although these surfaces are a marked improvement over the previous samples, they are still too rough and not optimal for regrowth.

H_2 has been shown to increase the decomposition rate of GaN in MOCVD environments [85]. Therefore, the next set of experiments was annealing the regrowth substrates without any H_2 flow and only using nitrogen. When the substrates were annealed without any H_2 flow, significant mass transport was observed. As seen in Figure 6-6, regrowth occurred from the sidewalls of the etched features. Figure 6-6A and B were annealed at different pressures but maintained the same ratio of NH_3 to N_2. It appears that the conditions for Figure 6-6B enhanced

the mass transport regrowth but the excess regrowth seen is due to the increased exposed area from the larger SiO_2 undercut. This effect is illustrated in Figures 6-6C and D, where two features from the same annealed sample show different degrees of mass transport regrowth due to the amount of exposed GaN surface adjacent to the sidewalls. In Figure 6-6D, the exposed GaN has roughened due to the loss of material, which was transported to the sidewalls. The NH_3 flow was further increased in an attempt to maintain a smooth surface. When the ratio of NH_3 to N_2 was doubled there was a large decrease in mass transport regrowth and an increase in decomposition. This is seen in Figure 6-7, where the SEM images of a specific etched feature of a regrowth substrate are shown before and after annealing. The artifact from etching that is circled in Figure 6-7A is shows no change after annealing except at the bottom edge, where regrowth has taken place. The large decomposition and minimal mass transport regrowth were seen when H_2 flow was used during annealing.

To explain the observations produced from the previous annealing experiments, both the thermodynamic and kinetic factors need to be considered. When etched features with different surface energies are heated, thermodynamics dictates that there will be a drive towards minimizing the total surface energy. The previous samples that were annealed using H_2 flow, showed minimal regrowth only at the edges along the bottom of the sidewalls. These corners have a large surface energy and thus it was energetically favorable for regrowth to occur there. The difference in the surface energies of the sidewalls ($\{1\bar{1}00\}$ and $\{11\bar{2}0\}$) from the bottom (0001) surface should have also been a driving force for regrowth to occur. Yet, further regrowth from the rest of the sidewall did not occur. In contrast, the samples that were annealed without H_2 showed regrowth occurring to a much greater extent from the whole sidewall, except at particularly high NH_3 flows. To explain this behavior, kinetic factors and the role of H_2 need to

be factored in. When annealing with H_2 present, surface H could be blocking surface sites necessary for Ga adatoms to diffuse across the surface. Surface H could also be responsible for blocking sites needed for N adatoms to diffuse. A decrease in N adatom mobility would result in a decrease of N_2 desorption and thus an increase in the amount of N adatoms on the surface. Either mechanism or both together would lead to an increase in the Ga adatom diffusion barrier. The diminished mobility of the Ga adatoms made it energetically unfavorable for regrowth to occur on the rest of the sidewalls. Essentially, the surface energy difference in the corners was greater than this energy barrier but the difference in surface energy between the planes was not, which resulted in selective mass transport regrowth that was observed. For the regrowth substrates annealed without H_2, the absence of surface H and/or the reduction in surface N resulted in the decrease of the Ga adatom diffusion barrier, which increased the Ga adatom mobility and thus a larger amount of regrowth was now energetically favorable.

The last observation of increasing decomposition and decreasing mass transport regrowth at very high NH_3 flows could be explained through surface H despite the lack of H_2 flow. If excess NH_3 flow is used this could have resulted in a large amount of surface H from the dissociation of NH_3. Therefore, the same site-blocking mechanism could explain the lack of Ga diffusion to the sidewalls for regrowth to occur. The site blocking should also decrease the N adatom diffusion, resulting in a reduction in the loss of N through N_2 desorption, but the greater decomposition seen contradicts this. The excess decomposition could be explained through the loss of N through the reforming of NH_3 by bonding with available surface H and then desorbing as NH_3 instead of N_2. The formation of NH_3 has been seen when annealing GaN in an H_2 environment [91]. It has also been suggested that the presence of a large H population could favor NH_3 reformation through bonding with adsorbed NH_x species [85]. The complete

mechanism for the decomposition of GaN through the loss of N through NH_3 formation is shown in Equation 6-1

$$N_{(adsorbed)} + H_{(adsorbed)} \rightarrow NH_{x(adsorded)} + H_{(adsorbed)} \rightarrow NH_{3(desorbed)} \quad (6\text{-}1)$$

Realizing that decomposition was unavoidable, the next set of experiments consisted of introducing a small amount of TMG during the heat up in order to balance out the decomposition. In addition to needing to determine the amount of TMG to use, the rate at which to introduce the TMG and the temperature to initiate flow was also established. The temperature when TMG flow was started was around 700^0C, which is around the point at which decomposition begins to occur for GaN. The rate at which the TMG flow was ramped up was made to be in sync with the rate of temperature increase. The same temperature and ramp rate were also used during the cooling down of the substrate. The amount of TMG desired was such that excess decomposition could be prevented, while not producing any premature growth. After multiple iterations of varying the amount and introduction rate of TMG during the temperature increase, a set of satisfactory conditions that were achieved. Since decomposition is inevitable, it becomes necessary to balance out the rate of decomposition with the rate of growth. It is impossible to get the perfect balance between growth and decomposition. Thus, conditions must be set that they either lean towards a little decomposition or a little growth. The optimized flow conditions were chosen to favor minor growth over decomposition. Figure 6-8A shows the result of excess TMG being introduced during the heat up to the growth temperature, while Figure 6-8B shows the regrowth substrate after being annealed under optimized TMG flow conditions. The surface morphology and roughness were determined using AFM. Figure 6-9 shows the surface morphology of the regrowth substrate surface after annealing. Roughness measurements

produced an R_{ms} value of 2.64 nm, which is rougher than the surface after etching, but is a large improvement over the roughening seen under all previous annealing conditions.

Growth Evolution

The selective area growth of GaN had never been attempted in our reactor before, thus the creation of a good growth recipe required starting from a previously developed recipe for conventional bulk growth. Using the work that has been performed for the SAG and ELO of GaN in the literature, the growth conditions were varied in order to achieve the maximum lateral growth rate while minimizing the vertical growth rate. The initial regrowth experiments were performed using a line mask pattern etched into the SiO_2 without etching the GaN substrate underneath. The growth conditions used were the exact same as those used for the bulk growth of some heavily doped p-type GaN. Although all the growth conditions were the same, there is always a growth rate enhancement factor that needs to be accounted for in SAG growth. Since no growth is suppose to take place on the mask, the reactant species that approach the surface of the mask all diffuse until they reach an exposed area to adsorb. This produces a large excess of reactants reaching the exposed area at the same time, which is equivalent to a large increase in the TMG flow rate. To account for the large increase in the growth rate, the time of the growth was substantially decreased. As can be seen in Figure 6-10, after only 15 minutes of growth, the growth rate varied from .17 μm/min in Figure 6-10A to .61 μm/min in Figure 6-10D. The change in the growth rate was dependent on the proximity to an exposed area of the GaN surface, where the SiO_2 had been removed prior to the regrowth. In Figure 6-11, a plot of the growth rate as a function of the distance from the exposed area shows how the growth rate increases with the distance. Figure 6-11 shows how the large increase of the growth rate with the distance until about 300 μm. After 300 μm, the rate of increase changes signifying a different growth regime. In this regime, the growth rate is nearly constant with an increase in distance and thus showing

the accurate growth rate enhancement effect, since the exposed area is far enough away so as to not significantly consume any of the active growth species. Figure 6-10C and D demonstrate how the greatly accelerated growth rate decreases the quality of the growth. In Figure 6-10C, distinctive faceted pits can be seen on the (0001) plane of the regrown feature. These are most likely attributable to the Mg-induced defects that were discussed earlier. The excessively large Cp_2Mg flow rate coupled with the extremely fast growth rate will produce such defects during the growth of p-type GaN.

An unexpected result that was observed was the nucleation of GaN islands on the SiO_2. As shown in Figure 6-12, there had been a considerable amount of nucleation on the SiO_2, which is not suppose to occur in MOCVD. The islands were identified as GaN using EDX as shown in Figure 6-12B and C. This is a good indication that the TMG flow rate was too high and after a large reduction in the TMG flow, the nucleation of GaN islands on the SiO_2 mask was never seen for any other regrowth experiments.

The regrowth mechanism was studied by stopping the regrowth at different times to see how the growth evolves. All of these samples used for this study were grown at the exact same conditions except for the length of time of the main growth layer. Figure 6-13 shows the images of a sample that was grown for only 10 minutes and then was unloaded. It can be seen in each feature that islands have nucleated uniformly and have begun to expand laterally. The average diameter of the islands is approxiamately 8.0 μm. This corresponds to a lateral growth rate of .4 μm/min. By using a profilimeter the average height of the islands was determined to be approxiamately 2 μm, which gives a vertical growth rate of .025 μm/min. Thus, the ratio of the lateral growth rate to the vertical growth rate (G_L/G_V) is 16.

The next sample was stopped after 20 minutes of regrowth and then was taken out and viewed with the SEM. Figure 6-14B shows the growth within a single feature. After 20 minutes the sidewalls have grown out about 5μm and the islands have coalesced so that none of the original etched surface is exposed. In Figure 6-14B, the arrows are pointing out that growth from the sidewalls has occurred equally in both the $<1\bar{1}00>$ and $<11\bar{2}0>$ directions. In traditional ELO growth, when the mask pattern is properly oriented with respect to the substrate, growth in the $<11\bar{2}0>$ direction is dominant. The lack of a dominant growth direction could be due to the misalignment of the mask pattern. A close up of a corner of one of the features, seen in Figure 6-14C, shows that the growth hasn't extended vertically to the SiO_2 surface. This growth height would be ideal for device applications, but this is only the height around the edges. The height towards the middle is still too thin.

The last sample was stopped after 30 minutes and then looked at. In Figure 6-15, images of a regrown feature after 30 minutes are shown. It can be seen that growth has continued through the expansion of the islands. By looking at Figure 6-15A, it may seem that growth is very 3-dimensional and that a large height difference exists between the edges and the middle. The view shown in Figure 6-15B shows that the morphology is fairly 2-dimensional and that the lateral growth has remained dominant. The enhanced lateral growth rate is demonstrated by the growth in the middle and between the islands that has planarized. A close up view of the same feature at an angle is shown in Figure 6-15C. It is apparent that vertical growth has not occurred uniformly around the edges. In some places growth is above the SiO_2 surface and has begun to proceed laterally over it. At the edge furthest away in the image, some growth is still below the height of the SiO_2 surface. The growth that occurs up and over the SiO_2 shows the expected behavior normally seen for ELO growth. When the regrowth begins to grow above the original

GaN surface height and over the SiO_2, growth occurs in the $<11\bar{2}0>$ direction with little to no growth in the $<1\bar{1}00>$ direction. This can be seen in Figure 6-16, which is a close up of the corner of a feature that has begun to grow over the SiO_2 mask. It appears that the mask pattern was correctly oriented with respect to the substrate and that unlike standard ELO growth, the regrowth within the etched features shows no preferential growth direction. The difference in the growth behavior can be explained by thermodynamics considerations. At the beginning of the growth the dominant driving force for growth is the minimization of the surface energy. The high surface energy of the corners and etched surfaces causes nucleation to occur uniformly within the etched feature in order to minimize the surface energy. Once growth begins to proceed laterally out of the etched feature, the dominant driving force is now the difference in the growth rates of the specific planes.

Role of Mg in SAG Regrowth

The incorporation of Mg has been seen to increase when growth was only on a quarter of a wafer compared to growth on a full wafer using the same growth recipe. This indicates that even on a larger scale, selective growth increases the percentage of Mg being incorporated into the growing film. This may appear to be a benefit at first, but this increased incorporation can be problematic if the Mg/Ga ratio is too high. As was mentioned earlier, at high Mg concentrations, hollow pyramidal defects will form during MOCVD growth of p-GaN. The formation of this type of defect is commonly seen at grain boundaries due to Mg segregation. It is believed that the cause of these defects is due to the clustering of Mg, which leads to a variation in the unit cell positions of the Mg atoms being incorporated [41, 94, 95]. The accumulation of Mg onto specific planes prevents subsequent GaN growth, which results in the formation of the faceted defects [41, 96]. It has been suggested that their origin is the result of the local agglomeration of Mg around some impurities [94]. Other work has shown that these defects will form even at very low

concentrations of carbon and oxygen and thus their formation is only due to the excessively high Mg concentration [41]. Therefore, it is not possible to completely avoid these defects when a high p-type doping level is desired and a large Mg concentration is needed. Although, the formation of these defects is unavoidable, optimizing the growth conditions can minimize their occurrence. As illustrated in Figure 6-17, smaller clusters will produce pyramidal defects that come to a point, where as larger clusters will form truncated pyramids. The extent of defect formation and their shape can provide a good guide in optimizing the growth conditions.

An image of an optimized regrowth is shown in Figure 6-18A. The arrow is pointing to a Mg-induced defect of the kind that was described before. Figure 6-18B is a very highly magnified view of that same defect at an angle. The faceted sides can be discerned in the image. A screw dislocation is also identified in the image for comparison. The large overview image in Figure 6-18A was shown to emphasize how isolated this defect was. When the ratio of Mg to Ga is too great, the appearance of these defects can be significant and occur uniformly throughout the regrown material. An example of regrowth where the Mg/Ga ratio was too high is shown in Figure 6-19. The images show the faceted pinholes running all along the boundaries between the islands. It was not realized at first that these were Mg-induced defects. The sample had only been grown for 10 minutes and so it was believed that the gaps between the islands would merge and close up as the islands coalesce. Thus this same recipe was used again but the growth time was now 60 minutes. This experiment was also performed in order to determine the growth behavior after an extended amount of time. The images of the sample grown for 60 minutes are shown in Figure 6-20. From the images, it can be assessed that the growth did not turn out as was predicted. It appears that the faceted gaps between the islands continued their growth through the perpetuation of the faceted sides.

Alternative Approaches for GaN Regrowth

Effect of Regrowth Mask on Doping

As mentioned in the literature review, achieving a high level of p-type doping for GaN is very difficult. The first step in trying to obtain a high hole concentration was to first develop a recipe for growth of conventional non-SAG p^+GaN. A recipe was created that produced a hole carrier concentration of about $5x10^{17}$ cm^{-3}, which was determined from Hall measurements. This p^+ GaN recipe was then used for SAG growth on an SiO_2 patterned substrate. Only 2/3 of the substrate was patterned with a line mask that was only etched into the SiO_2. The other third of the substrate had no SiO_2 or pattern on it. An illustration of the substrate can be seen in Figure 6-21, where the orientation and location of the area without any SiO_2 or pattern can be seen as well as the dimensions of the mask. The bulk GaN area was used to do Hall measurements. The Hall data showed an n-type carrier concentration of approximately $2x10^{17}$ cm^{-3}. Additional Hall measurements were done and this experiment was repeated in order to confirm this result. Every measurement produced an n-type carrier concentration in the range of 1 to $3x10^{17}$ cm^{-3}. It appeared that there was a strong autodoping effect occurring from the SiO_2. In all other p-type growths where SiO_2 was used as a regrowth mask, a detectable p-type doping level was never achieved. This autodoping effect was also seen by another group that showed using SIMS that there was a significant amount of Si being incorporated into the regrown material [97]. They showed that approximately four times as much Si then oxygen was incorporated into the regrown material despite there being twice as much oxygen present in the SiO_2 film. The autodoping from the SiO_2 prevents any p-type GaN from being regrown. For ELO or other regrowth applications, where n-type doping is not a problem or even desired, the use of SiO_2 has never been an issue. If p-type GaN was needed to be regrown for any number of potential applications in GaN device technology it would not be possible using SiO_2. Moreover, this autodoping effect prevents the

regrowth of semi-insulating (SI) u-GaN as well, which is of enormous importance for GaN devices. Therefore a significant need exists for an alternative mask material for MOCVD GaN regrowth applications.

Regrowth Using Alternative Masks

In order to avoid autodoping of the p^+ GaN regrowth of the p-MOSFET source and drain but also to further develop GaN regrowth technology, other thin films were examined and tested for use as a regrowth mask. The best candidates were the dielectric oxides that had already proven to be structurally stable in the MOCVD GaN environment. The processing of MgO and Sc_2O_3 for use as a regrowth mask introduces some issues that didn't exist with SiO_2. The difficulty is in the dry etch process because both MgO and Sc_2O_3 use the same Cl_2 plasma chemistry that is used for GaN. The problems encountered during processing and process optimization is discussed later. This section focuses on the properties of the regrown material when using an alternative mask material.

MgO

The first oxide that was examined was MgO. The use of MgO as a regrowth mask had the added benefit that if any autodoping was to occur, the incorporation of Mg would be heavily favored over oxygen similar to the autodoping seen with SiO_2. Based on the MOCVD annealing experiments MgO should be good to use as a regrowth mask, since it did not completely fall apart and Mg_3N_2 did not form. Despite its stability during annealing, the use of MgO as a regrowth mask was unsuccessful. MgO has been successful as a regrowth mask for short growth times, but for longer times nucleation and growth of GaN occurs on the MgO surface. The hydroxylated surface of MgO which takes the form of $Mg(OH)_2$ requires very high temperatures for an extended amount of time in order to remove the hydroxyl groups [98-99]. Ammonia (NH_3) has been shown to adsorb on the surface of dehydroxylated MgO and undergo heterolytic

dissociation to form NH_2 [100]. It could be that when given enough time, the dissociation of NH_3 on the MgO surface could act as a favorable nucleation site for GaN.

Sc_2O_3

The poor results obtained from using MgO, led to investigating the use of Sc_2O_3 as a regrowth mask. The stability of the Sc_2O_3 during the MOCVD annealing experiments makes it a good candidate for use as a regrowth mask. The only issue that could be problematic is the formation of ScN on the mask surface. The presence of ScN could cause nucleation and growth to occur between the features on the mask surface. The optimized growth conditions determined for regrowth using SiO_2 were used for regrowth with a Sc_2O_3 mask. Assuming that there isn't any nucleation occurring on the Sc_2O_3 surface, diffusion of the active growth species across the surface of SiO_2 and Sc_2O_3 should be similar. An SEM image after regrowth with a Sc_2O_3 mask is shown in Figure 6-22. This image shows the large-scale uniformity in growth and the absence of any nucleation on the Sc_2O_3 mask. The regrowth within every feature was smooth and uniform. Figure 6-23 are magnified images of a typical feature after regrowth.

In addition to the uniformity exhibited in the x and y dimensions, the thickness of the regrowth was very uniform despite the difference in feature size. This can be seen in Figure 6-24, where the thickness was constant for different feature sizes. These images also exhibit the ability for well-controlled growth at small dimensions when using Sc_2O_3 as a regrowth mask. This allows for regrowth of device components on a practical scale with dimensions that are normally employed. The nonuniformity seen along the growth edges in Figure 6-25 is due to the shape of the etched feature. This issue was mentioned earlier, where the decomposition of photoresist etch mask causes a ragged edge along the etched features. The use of a Ni mask for etching may be needed if a solution to enhance the etch stability of PR is not discovered.

When compared with growth using SiO_2 as a regrowth mask, the regrown material appears to look the same. Upon closer inspection though, a striking difference was noticed. Shown in Figure 6-26, along the edges of the features at the interface of the larger growth plateau and the thinner growth that continues towards the middle, dislocations can be seen all along both edges shown in the image. These defects could be due to the poor incorporation of Si into the lattice during growth. These dislocations should prove to be quite detrimental to device performance. Another difference that was observed between regrowth using Sc_2O_3 instead of SiO_2, was the effect of increased Mg flow on the growth morphology. The role of Mg and the formation of Mg-induced defects were discussed earlier with respect to using an SiO_2 regrowth mask. Unlike the growth performed using SiO_2, a large increase was seen to improve the surface morphology and no Mg-induced defects were observed. Figure 6-27 gives a comparison of the growth morphology for an increase in Mg flow when Sc_2O_3 is used as the regrowth mask. The Mg flow was doubled, while all other conditions were kept constant. After increasing the standard Mg flow of 11 sccm to 22 sccm, the morphology has become significantly smoother. The improved morphology and absence of Mg-induced defects could be related to the dislocation formation that was shown in Figure 6-26. Mg is known to react with SiO_2 and perhaps the excessive defect formation was the result of the agglomeration of a reaction by-product between Mg and SiO_2 that inhibited growth. This could be an additional barrier to achieving p-type GaN when SiO_2 is used as a regrowth mask.

Electrical Characterization

Fabrication of Device Test Structure for Electrical Characterization

One difficulty that was encountered was in the mask realignment for depositing the ohmic metal p-type contacts. Since the regrowth mask was initially intended to be used as the final metal layer for a MOSFET, it was logical to use the same mask to deposit the metal

contacts. This mask was attractive as a contact mask due to the large size of the features, which makes it easier to test using the probes. When the SiO_2 was removed prior to depositing the contact mask, realignment was not possible. The regrown material was too similar to the substrate in order to discern the edges of the features. Thus, for all regrowth samples, it was necessary to leave the oxide regrowth mask on before the deposition of the metal contacts. This issue is now a fundamental parameter in the device processing sequence that needs to be factored in when designing the processing sequence. This issue will be examined further in another section. Even with the regrowth mask, there was still a problem in aligning the mask. The difficulty in realigning the mask was the change in the shape of the features from their original shape on the mask. The development and exposure conditions of the photoresist (PR) were not to blame, because even if the features in the PR had perfectly matched the mask, the regrown material wouldn't. The non-uniform growth over the SiO_2 made it extremely difficult to realign the mask in order to have the metal deposited exactly over the regrown material.

This problem was resolved by using a different mask that was not part of the MOSFET set, which consisted of numerous arrays of large features that were uniformly shaped and spaced. Enough of the features on the mask lined up with regrown areas to allow for a significant portion of the sample to be tested. This solution was not ideal and required the measuring and comparing of several different masks before a suitable one was found. Nevertheless, it did prove to be effective if not efficient.

Electrical Characterization of Regrown p-n Junction Diodes

Several regrowth samples that showed good, uniform growth and surface morphology were processed into device structures in order to determine their electrical properties. Before any processing steps were performed, it was necessary to anneal the samples in order to activate the holes. This activation anneal is standard procedure for p-type GaN because of the hydrogen

compensation of the Mg that occurred from the MOCVD growth. All p-type GaN samples were annealed in the RTA under nitrogen gas at a temperature of 750^{o}C for 5 minutes.

The regrown area was much too small to directly determine the p-type carrier concentration or holes (h^{+}) using Hall measurements. In order to test the properties of the regrown material, it was examined on the basis of how it behaved as a pn-junction. The fundamental property of a p-n junction is its ability to only allow current to flow in one direction. This rectifying behavior is controlled through the polarity of the voltage being applied. Figure 6-28 shows the typical I-V curve for a p-n junction, as well as the configuration and polarity for the cases of forward and reverse bias. Under forward bias conditions, the forward voltage drop that is actually measured will be greater than that predicted from theory due to resistance of the metal contacts and measurement probes. The current measured when the p-n junction is reverse biased will be greater than the predicted value due to current leakage and eventually achieve a significantly large value when it reaches it's breakdown point. Current voltage (I-V) measurements were performed on the devices that were fabricated. Due to autodoping from the SiO_2 mask, a successful p-n junction could not be measured.

The samples regrown using a Sc_2O_3 mask were processed into device test structures and examined. After deposition and annealing of the Ni/Au contacts on the samples grown with the Sc_2O_3 mask, I-V measurements were performed. As was previously mentioned, a conductive ScN layer forms on the surface of Sc_2O_3 when it is exposed to the GaN MOCVD environment. This ScN layer produced electrical short measurements for the MOCVD annealed Sc_2O_3 films that were tested before. The same difficulty in performing the I-V measurements also occurred for the regrowth samples. In order to determine if the regrown material was p-type, an indirect method using the measurement between two regrown features was used. This arrangement is a

pnp junction. In order to rule out any possible contribution of the contact resistance, a measurement was made between two contacts that were both on the same regrown feature. The configuration of both the measurements is shown in Figure 6-29. The I-V curve from the two contacts on the same regrown feature was almost ohmic, showing that there is very little contact resistance. When two contacts were measured on different regrown features using the configuration shown in Figure 6-29B, the I-V curve in Figure 6-30 shows a large energy barrier for both positive and negative voltages. Since the barrier at the semiconductor/metal interface was shown to be minimal, the increased energy barrier must be due to the regrowth/substrate junction. This barrier could be attributed to the regrowth of very resistive undoped material. Although it is highly unlikely that perfectly undoped material was regrown, this possibility should be ruled out. In order to determine for sure, additional measurements were made of samples regrown with varying Mg flows. The I-V curves for three samples that were regrown using a Sc_2O_3 mask at different Mg flows is shown in Figure 6-31. At first, the reduction of the energy barrier with increasing Mg flow seems to be the opposite of what one would expect. From previous experiments, its known that the incorporation rate of Mg is enhanced for selective area growth and that increasing the Mg concentration past an optimal point starts to reduce the active hole concentration. Thus, since the Mg flow at 11 sccm should already result in a large Mg concentration compared to bulk growth, a large increase in Mg should produce a decrease in the h^+ population. Further increasing the Mg would lead to a further reduction in h^+ until the material would eventually be n-type. This is what is believed to be occurring and exhibited in the I-V measurements. In order to perform more accurate measurements of the regrown samples, further processing of the samples will be performed so as to confirm the results shown here. After further verification, this will be the first demonstration of selectively regrown p-type GaN

in the literature. This opens up the possibility of numerous applications for use in GaN-based devices.

Selective area regrowth for the fabrication of GaN-based devices was investigated. An examination of the general mechanisms involved in the selective area regrowth of GaN was performed. The effects of the reactor conditions on the processed regrowth substrate prior to growth were studied. The optimal conditions to avoid excessive decomposition were determined. The growth the conditions that influence the regrowth from etched features and the growth evolution were examined and discussed. The regrowth of the p^+ GaN source and drain regions of a p-MOS device was explored as an alternative approach to creating the p^+ regions. This would avoid the problems associated with *p*-type doping via ion implantation by doping the material during the MOCVD regrowth. The regions for the p^+ source and drain were etched out of the substrate and then GaN, heavily doped with Mg was selectively regrown into the etched trenches. The extent of autodoping from the use of SiO_2 as the regrowth mask was significant and completely prevented the regrowth of p-type GaN. Alternative oxides were examined for use a regrowth mask. The use of MgO and Sc_2O_3 as a regrowth mask was explored. The use of MgO as a regrowth mask was shown to be unsuccessful and the probable mechanism of failure is discussed. The use of Sc_2O_3 as a regrowth mask was demonstrated and successful regrowth was accomplished. All etched features were completely regrown without any nucleation occurring on the Sc_2O_3 mask or any significant degradation of the Sc_2O_3 surface. The quality of the regrown material was compared when SiO_2 versus Sc_2O_3 was used as the regrowth mask. Unlike regrowth with SiO_2, the morphology appears to improve with increasing Mg and defects associated with Mg, that were seen with the use of SiO_2, were absent. A reaction product between SiO_2 and Mg was proposed as a possible cause of these defects. The very uniform and

smooth morphology that was achieved using Sc_2O_3 as a regrowth mask and its improved growth capability when compared to SiO_2, show that has enormous potential for this application. Device test structures were made from the regrown samples using a Sc_2O_3 mask. Due to the formation of a conductive ScN layer on the surface, proper I-V measurements of a p-n junction were not possible. Measurements determining the contact resistance as well as a pnp configuration, indirectly showed the existence of a p-n junction. Assuming further testing confirms these results, this will be the first successful demonstration of selectively grown p-type GaN to date. This possibility creates the potential for developing many new and enhanced methods of fabricating GaN-based devices.

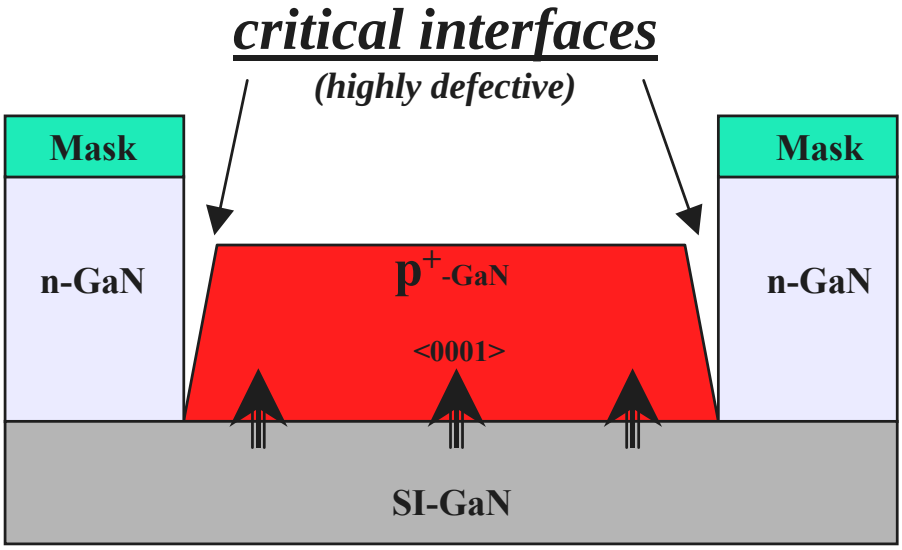

A

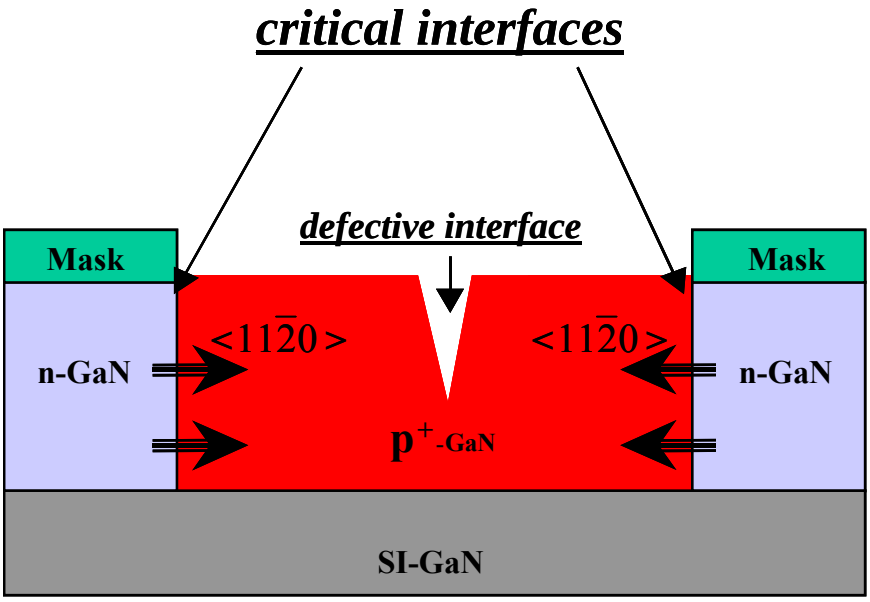

B

Figure 6-1. Illustration of two possible regrowth techniques showing the location of the resulting defective interfaces. A) Vertical growth <0001> is dominant B) Lateral growth <11$\bar{2}$0> is dominant.

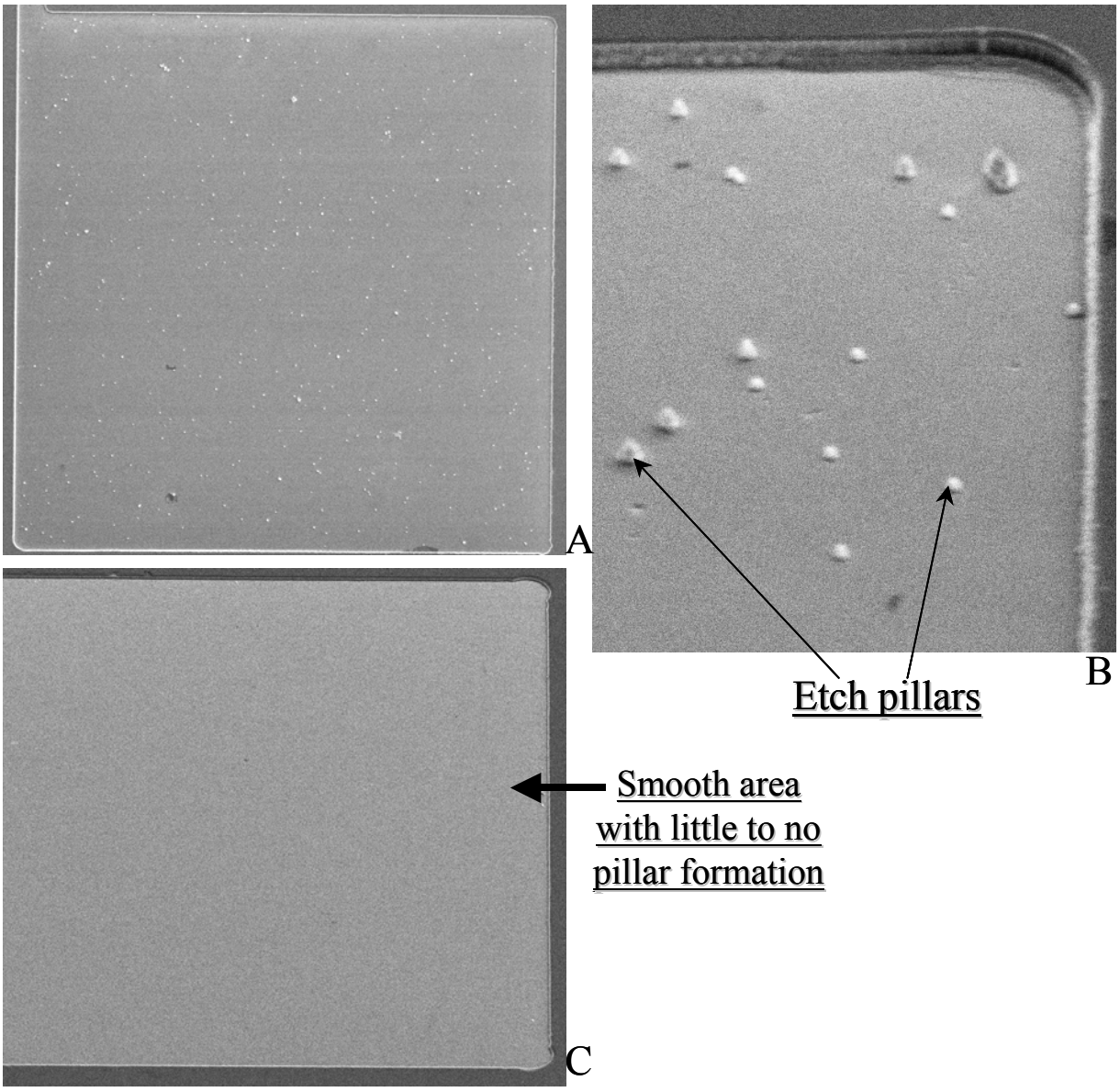

Figure 6-2. SEM images of regrowth substrates after processing. A) Substrate showing pillars produced from the GaN dry etch. B) Close-up of the etch pillars. C) Substrate processed using the optimized conditions

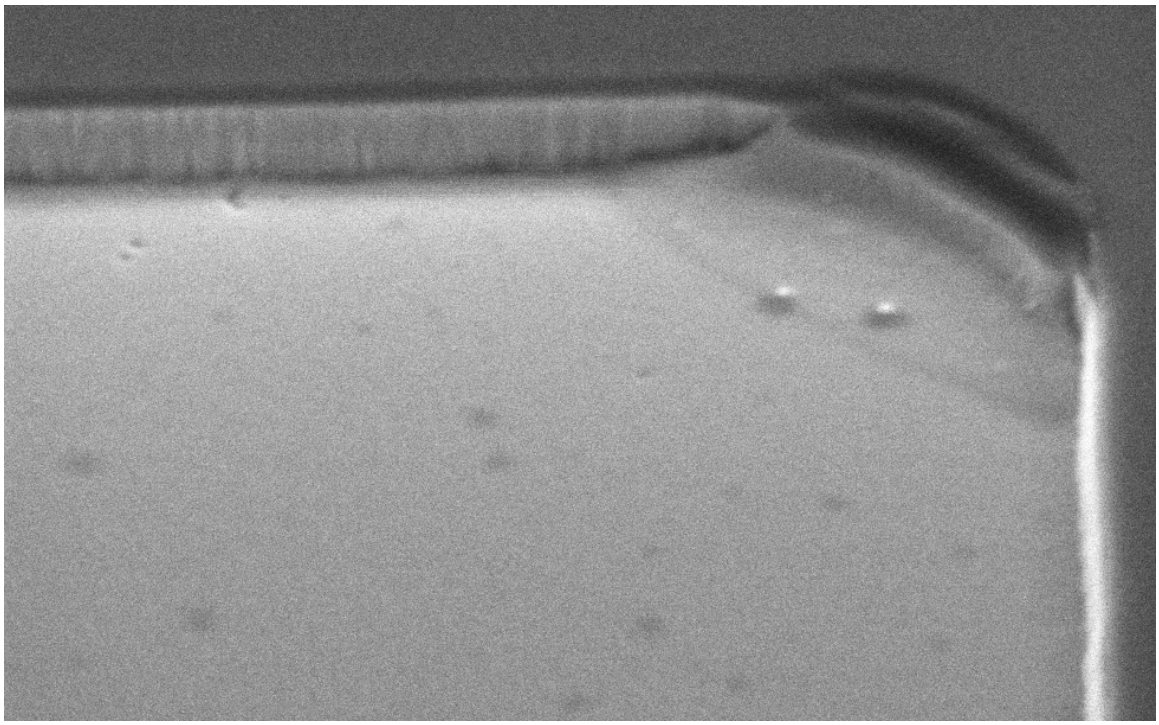

A

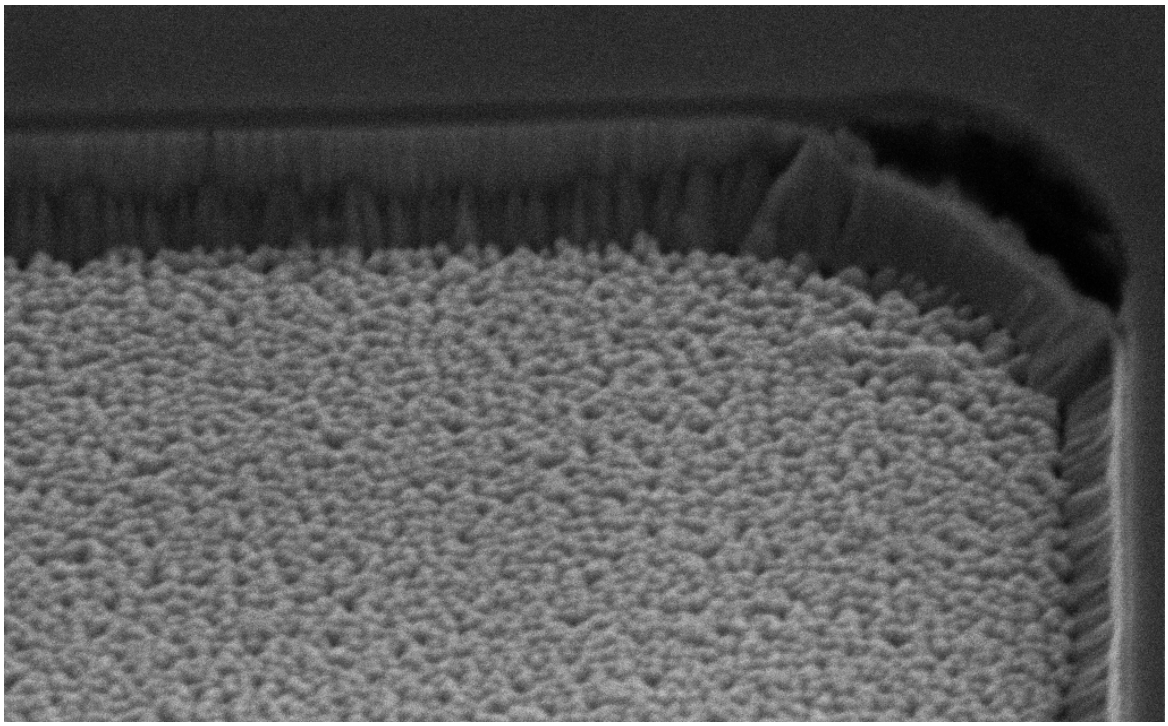

B

Figure 6-3. SEM images of an etched and patterned substrate for regrowth. A) Before annealing at the regrowth temperature. B) After annealing.

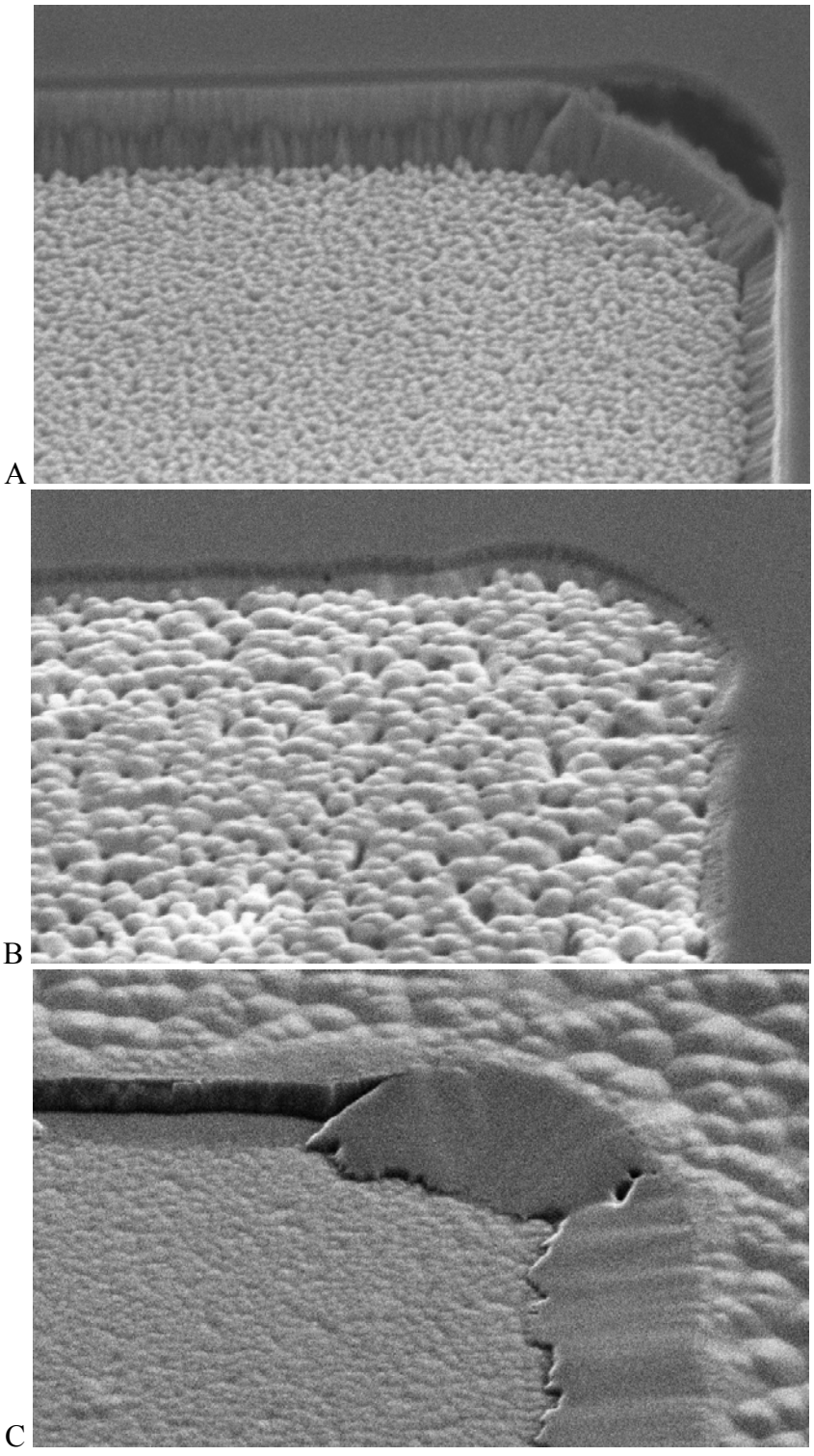

Figure 6-4. SEM images of processed regrowth substrates after annealing. A) Standard etched and patterned substrate used for regrowth. B) SiO_2 Etched and patterned area of the same substrate in (A) that was not GaN etched. C) Etched and patterned substrate that was annealed without a regrowth mask.

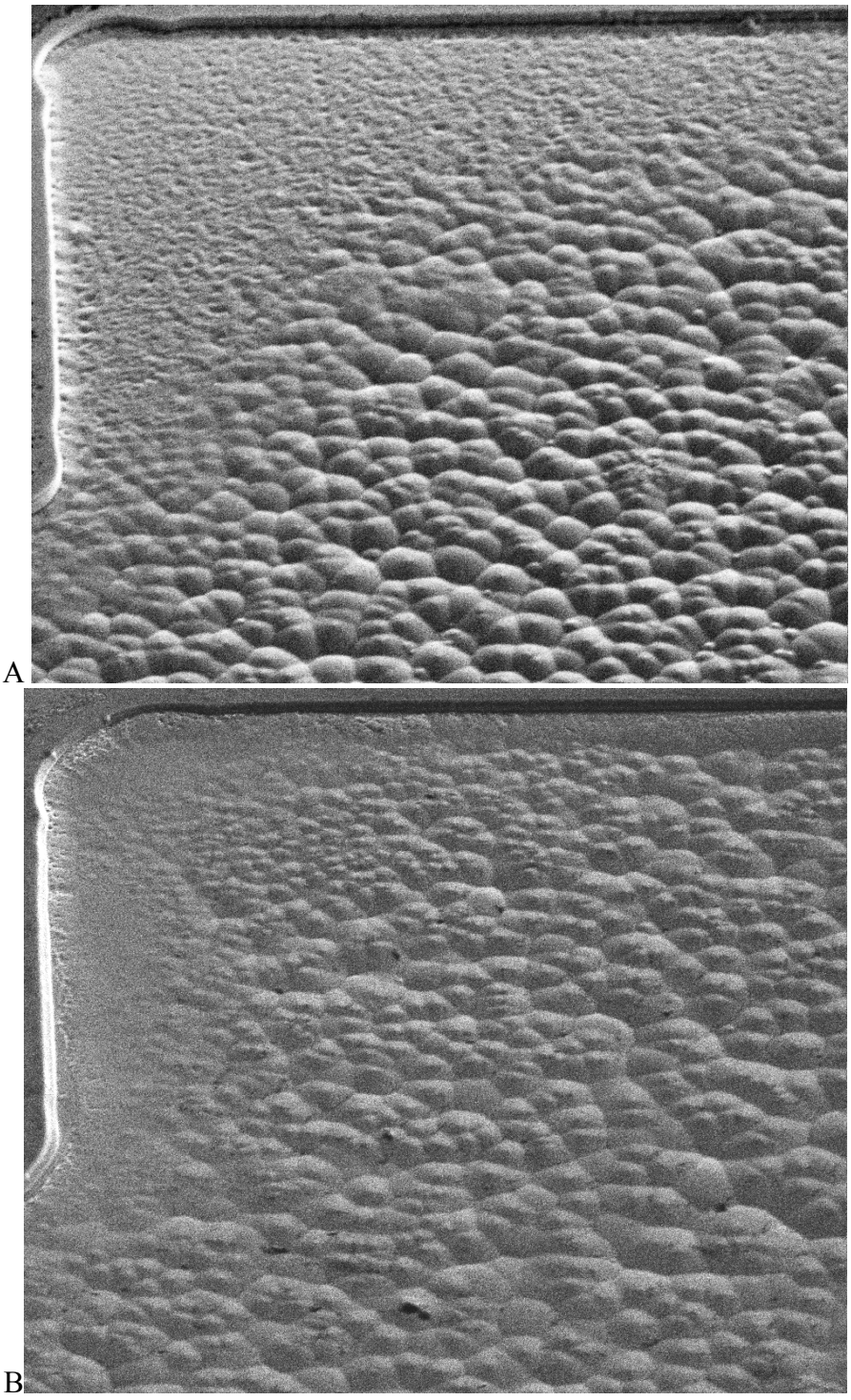

Figure 6-5. Effect of NH_3 flow during high temperature annealing. A) Sample annealed with an NH_3 flow of 3 slm. B) Sample annealed with an NH_3 flow of 6 slm.

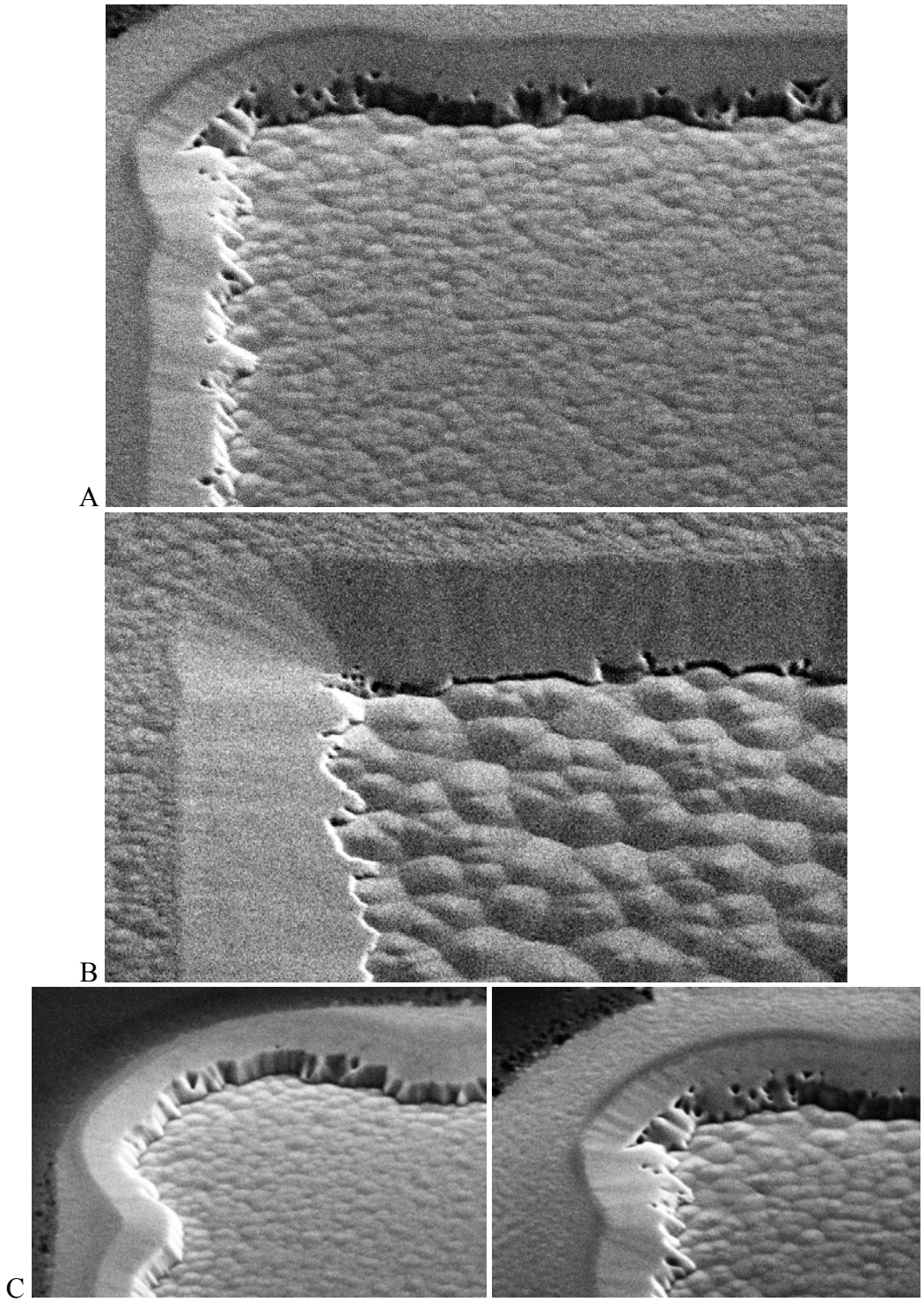

Figure 6-6. SEM images of annealed substrates without H_2 flow . A) At a pressure of 45 Torr. B) At a pressure of 300 Torr. C) Effect of amount of exposed GaN surface on mass transport growth during high temperature annealing.

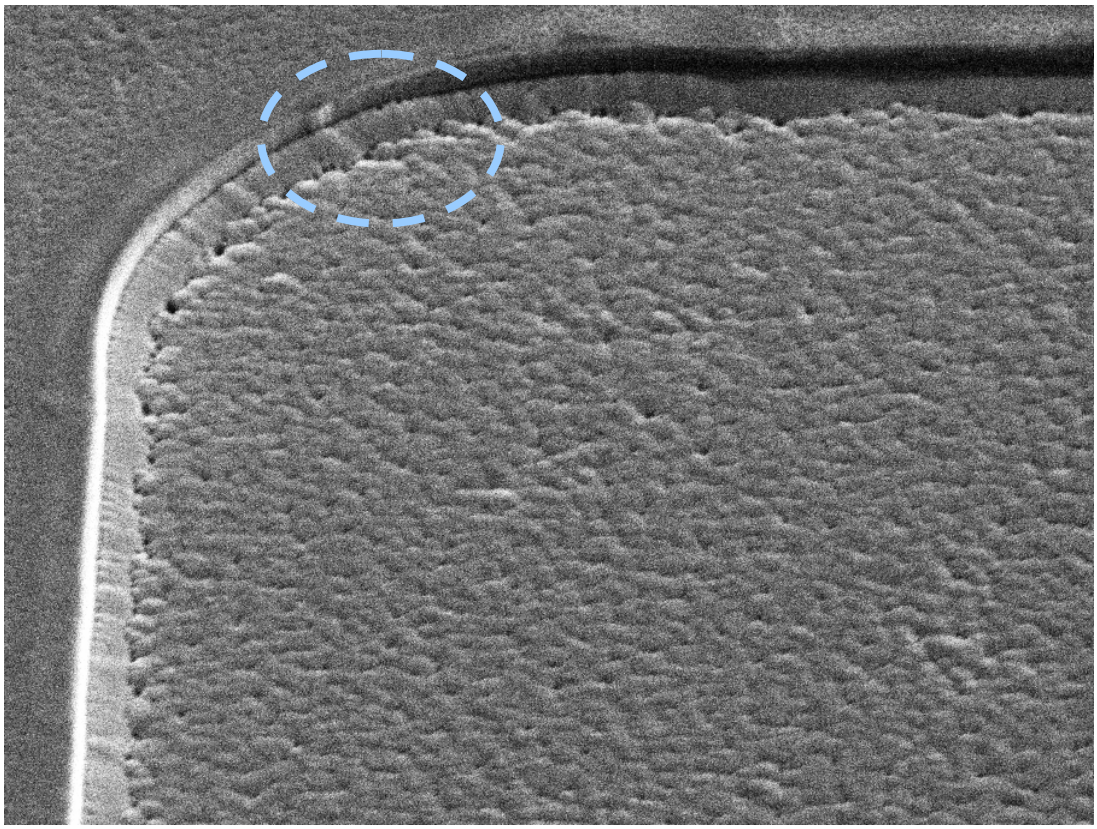

A

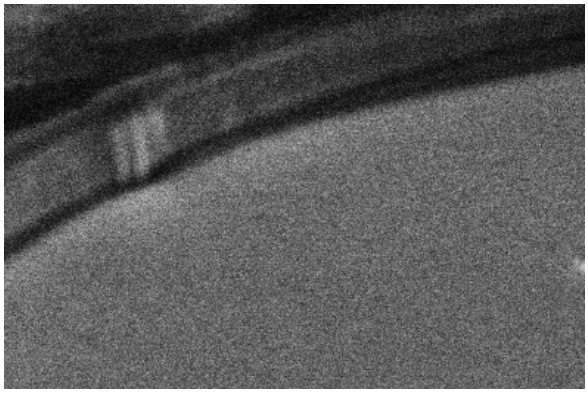

B

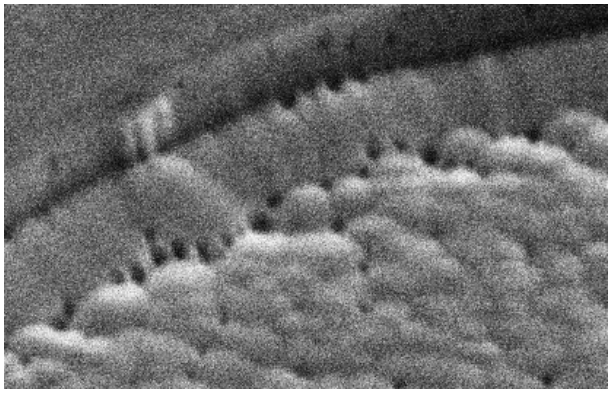

C

Figure 6-7. Effect of increasing the NH_3 partial pressure during high temperature annealing. A) Sample annealed with an NH_3 pressure ratio of 8. B) Area circled in (A) before annealing. C) Same area circled in (A) after annealing.

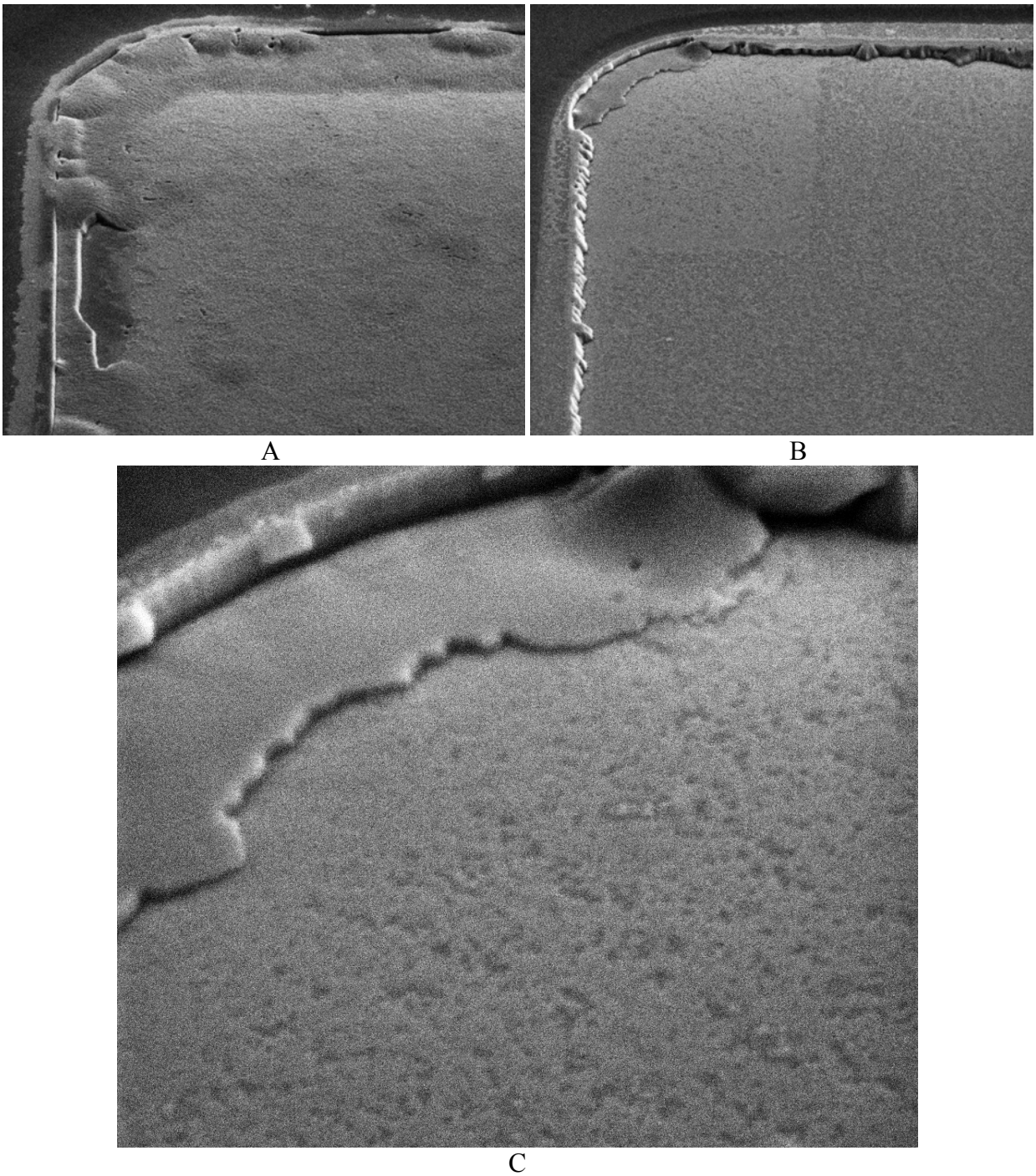

Figure 6-8. SEM of regrowth substrates after annealing using TMG. A) Excess TMG flow conditions. B) Optimized TMG flow conditions. C) High magnification of the substrate surface in (B).

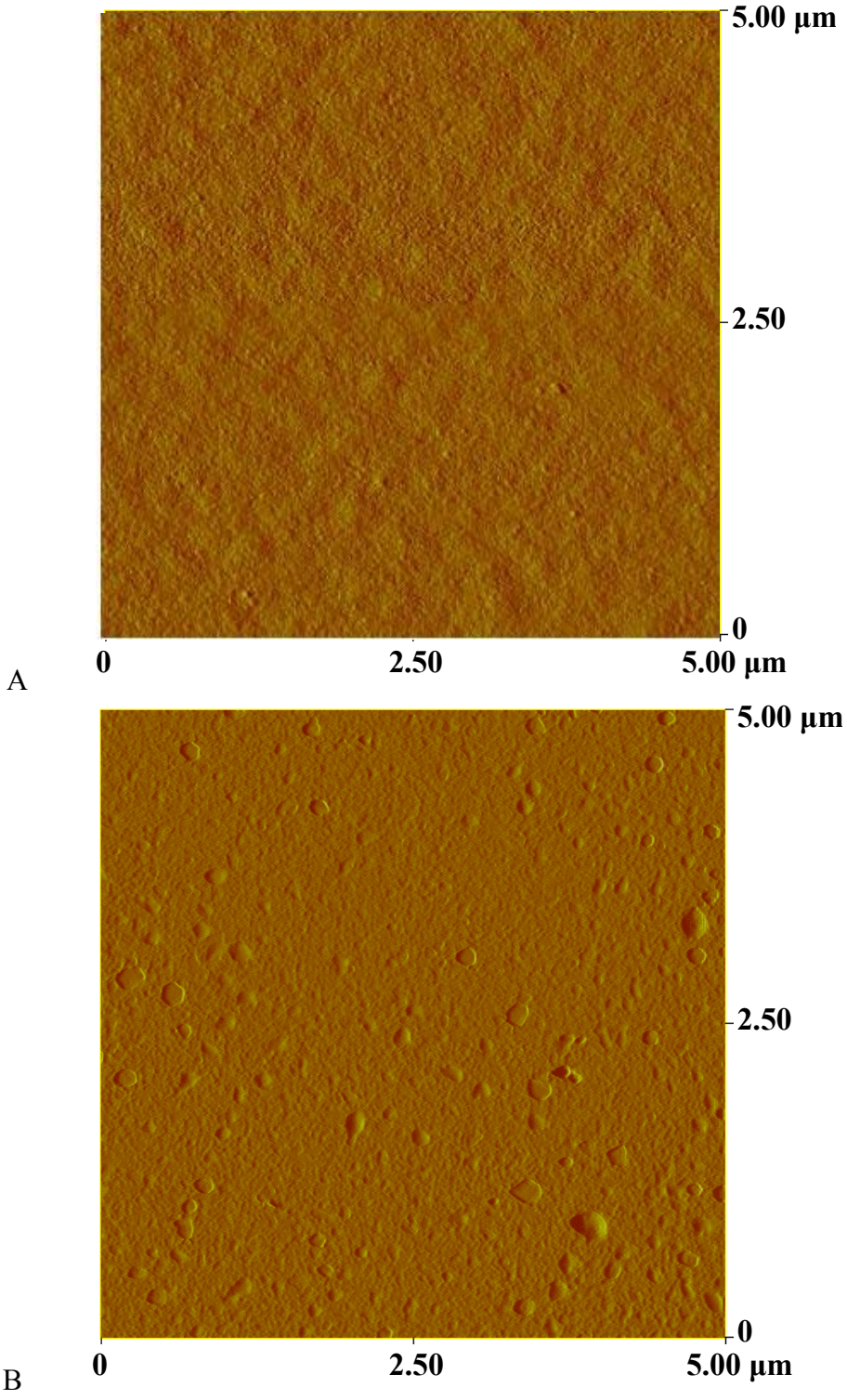

Figure 6-9. AFM scans of the etched surface. A) After being etched. B) After being annealed under the optimized conditions.

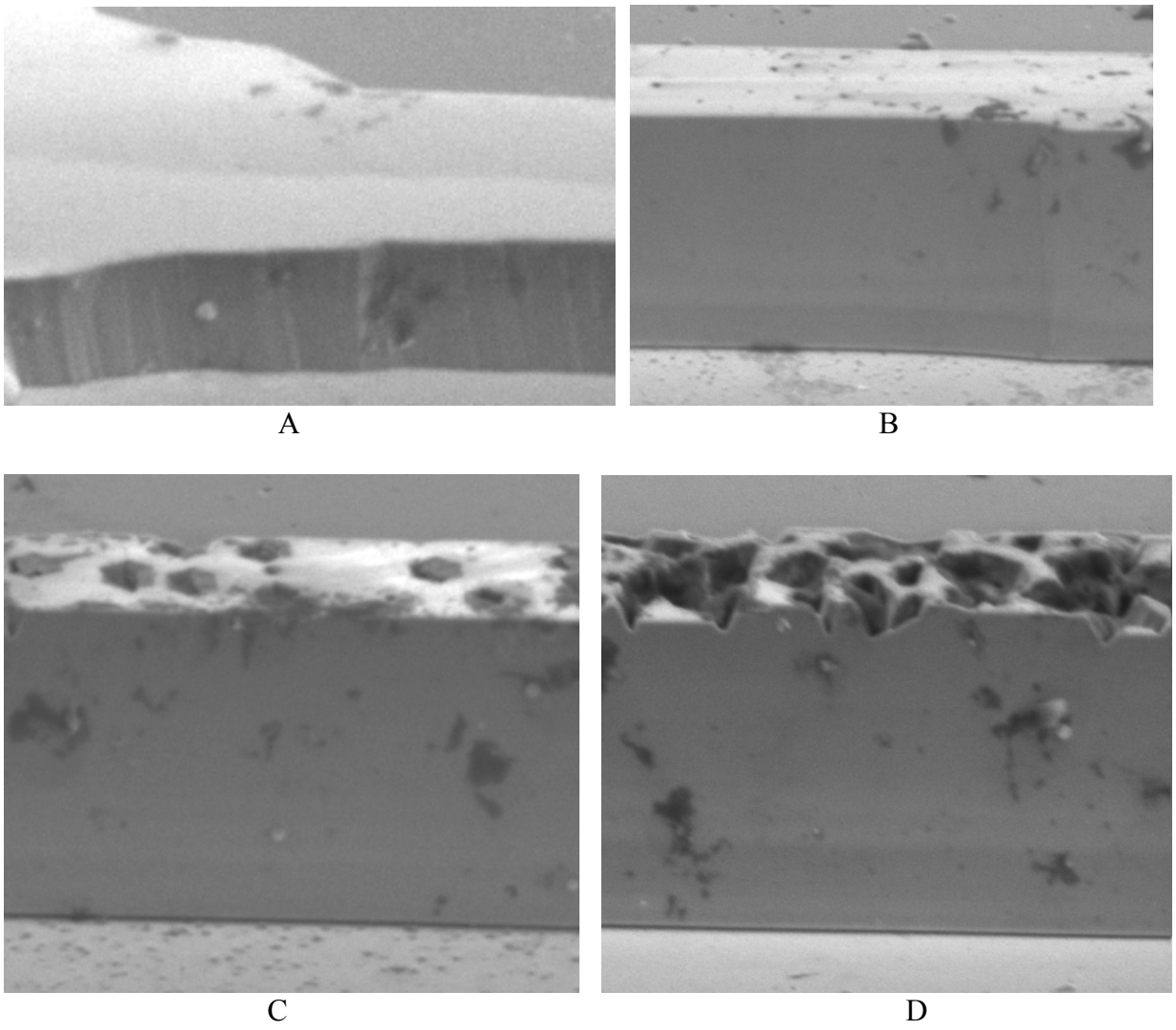

Figure 6-10. SEM images of regrowth at increasing ditances from the exposed GaN area. A) Adjacent to the exposed area. B) 250 μm away from the exposed area. C) 500 μm away from the exposed area. D) 1000 μm away from the exposed area.

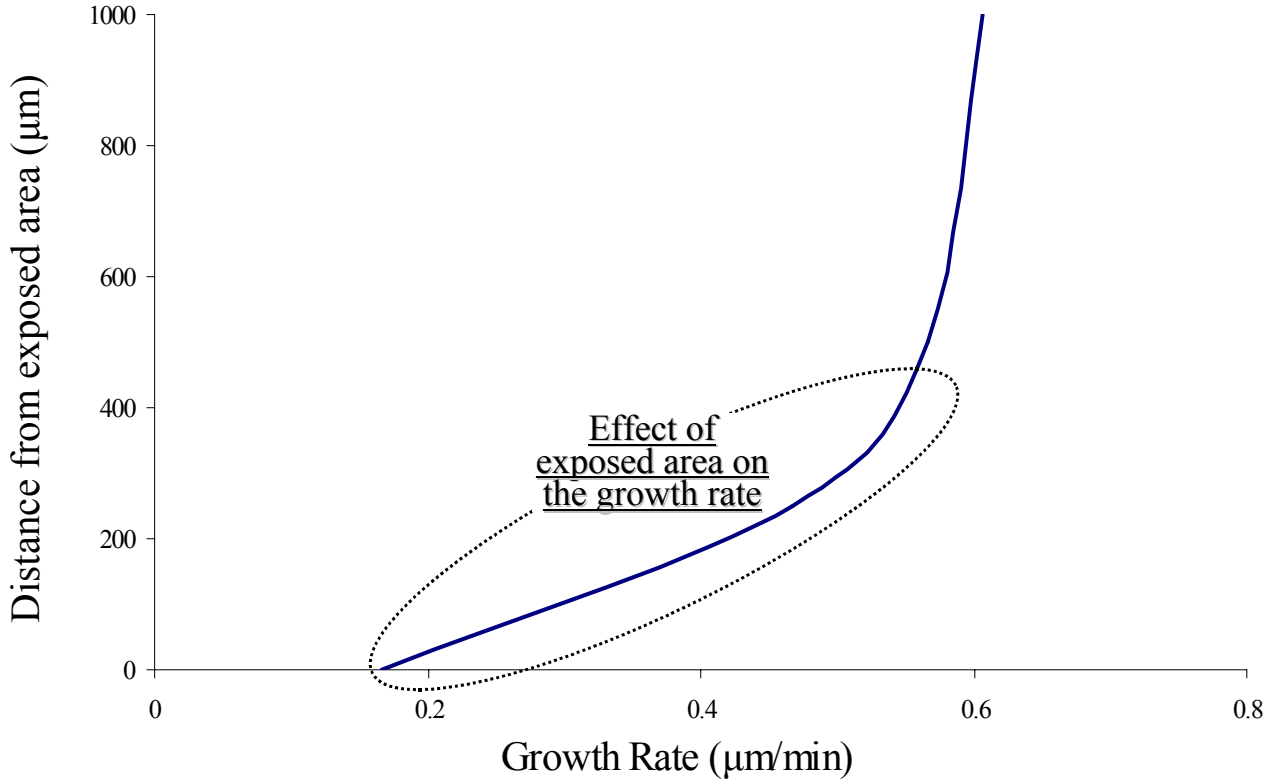

Figure 6-11. Effect of the exposed GaN surface on the growth rate

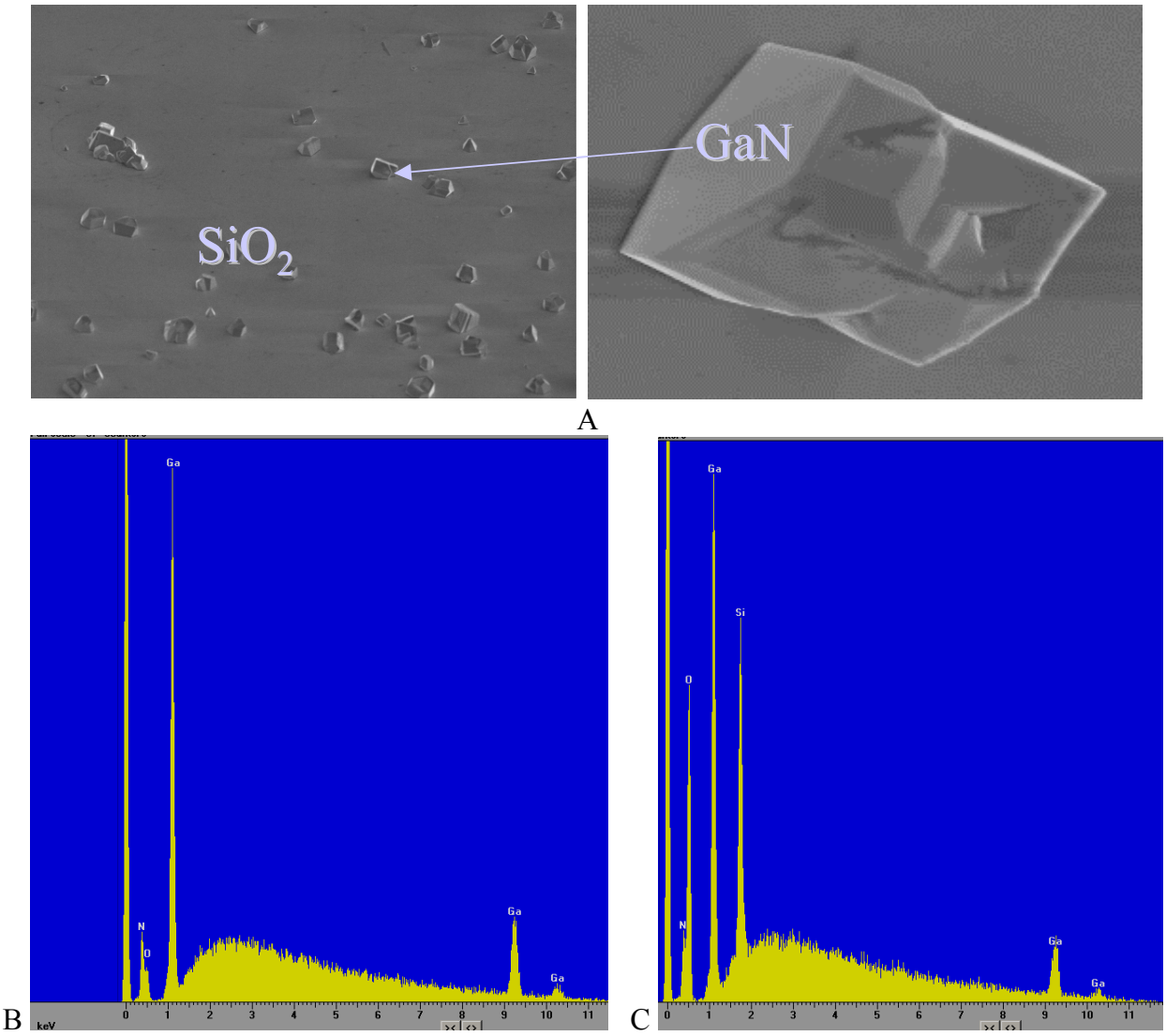

Figure 6-12. SEM and EDX of GaN nucleation on the SiO_2 mask. A) SEM images of the GaN islands on the SiO_2. B) EDX of an island. C) EDX of the SiO_2 field.

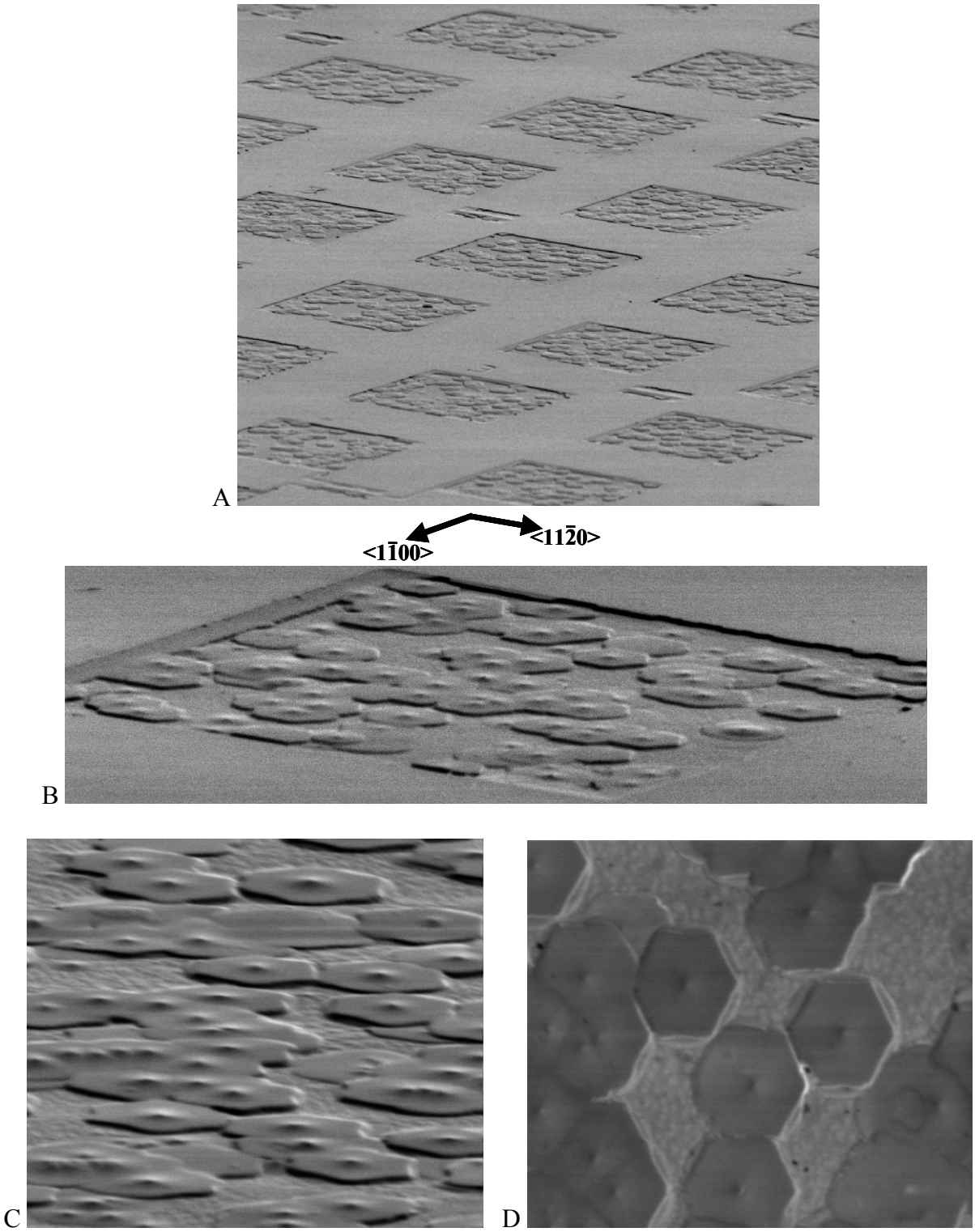

Figure 6-13. SEM images of a regrown sample after 10 minutes. A) Large area view showing several features. B) Closer view at an individual feature. C) Magnified view of the nucleated islands within the feature. D) Plan view of the nucleated islands.

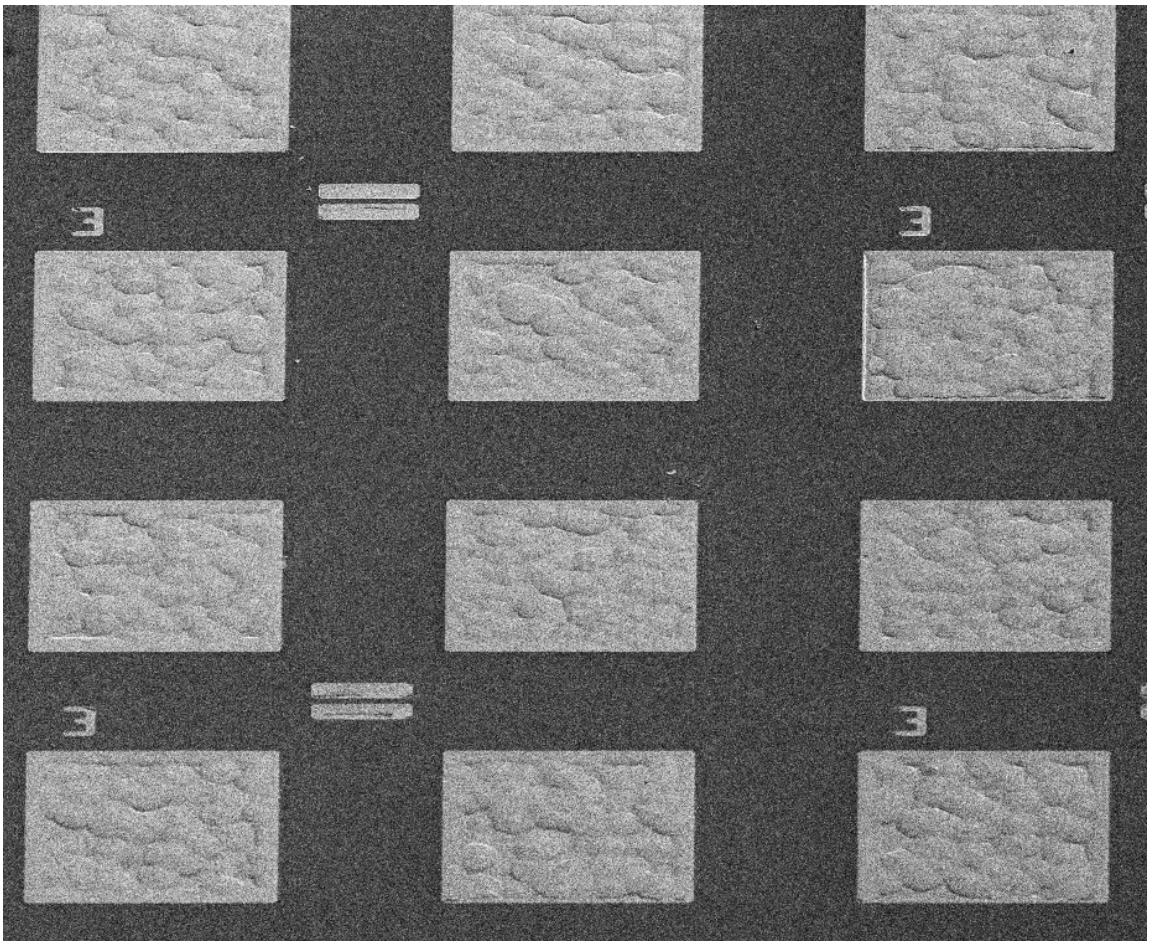

A

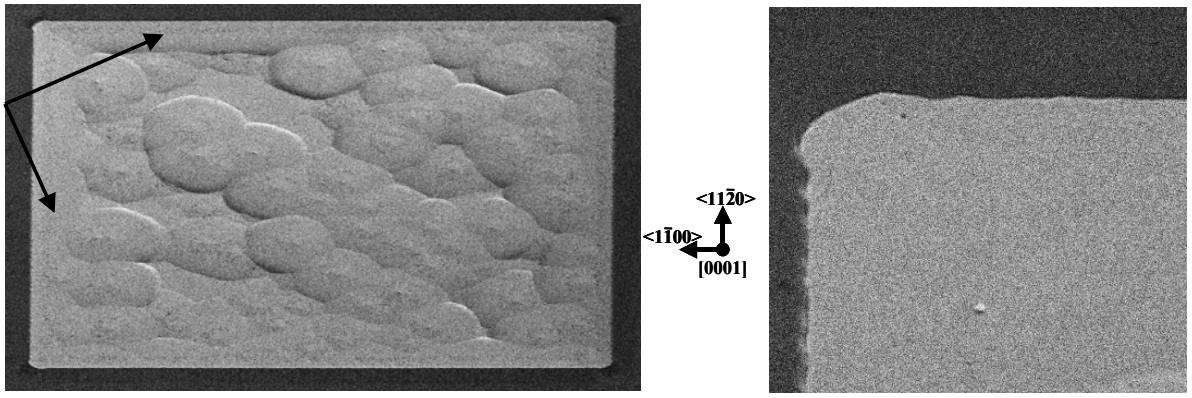

B C

Figure 6-14. SEM images of a regrown sample after 20 minutes. A) Large area view showing several features. B) Closer view at an individual feature. C) Magnified view of the corner.

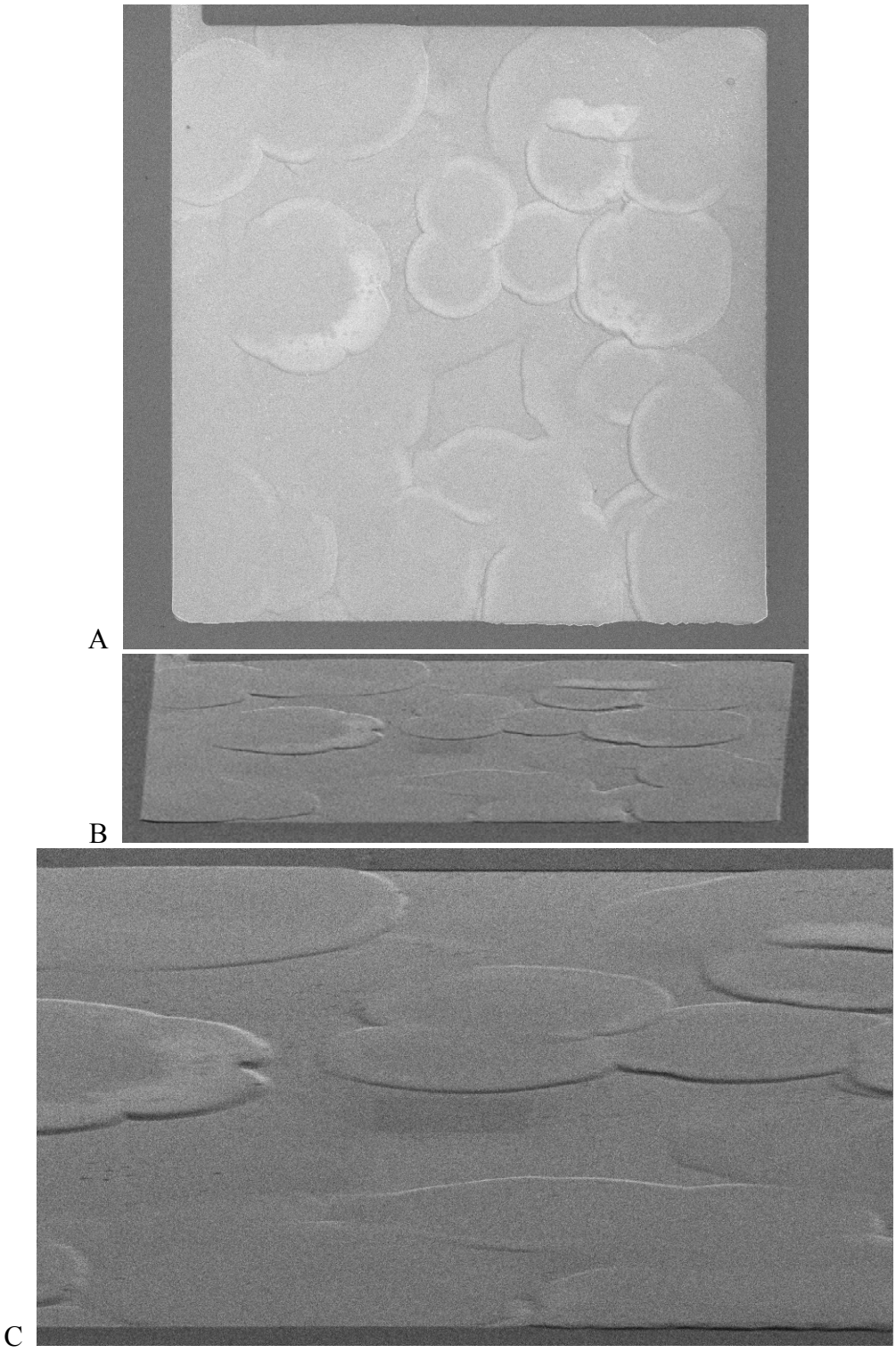

Figure 6-15. SEM images of a regrown sample after 30 minutes. A) Plan view showing of an individual feature. B) Angled view of the same feature. C) Magnified view of the feature at an angle.

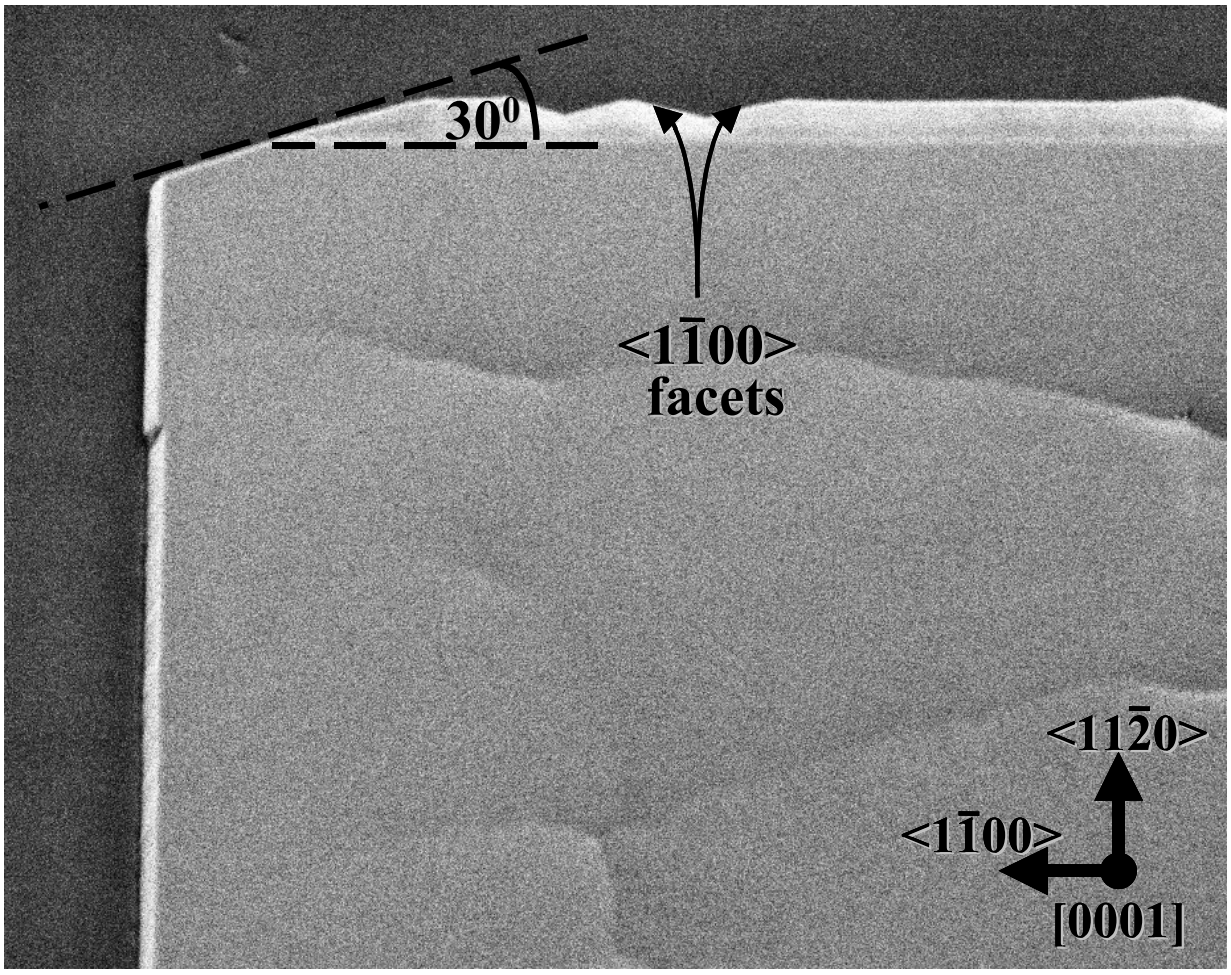

Figure 6-16. SEM image showing the relative orientations of the regrown material.

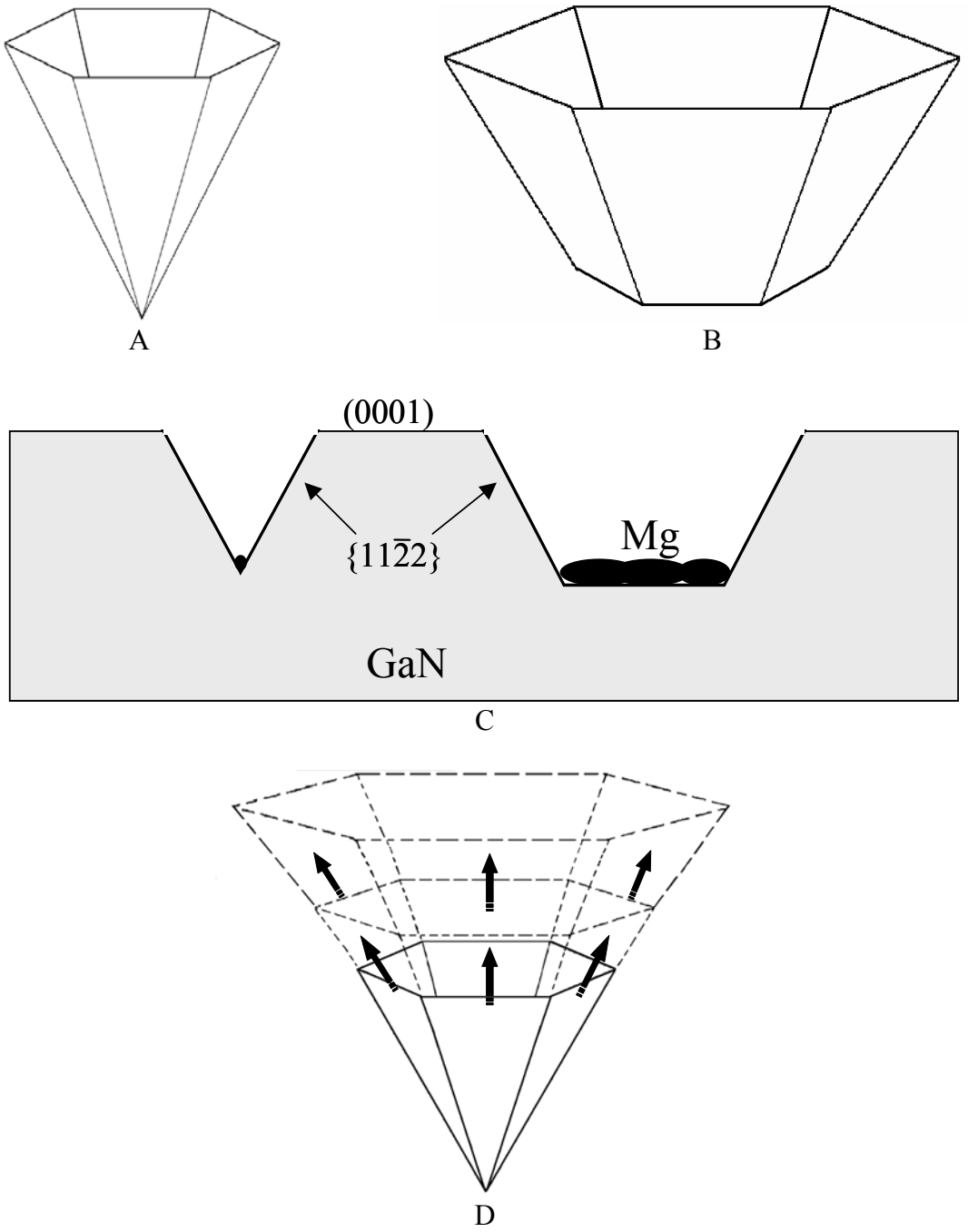

Figure 6-17. Mg-induced defects. A) Structure resulting from small Mg clusters. B) Structure resulting from large Mg clusters. C) Cross section View. D) Illustration of the growth of Mg-induced defects.

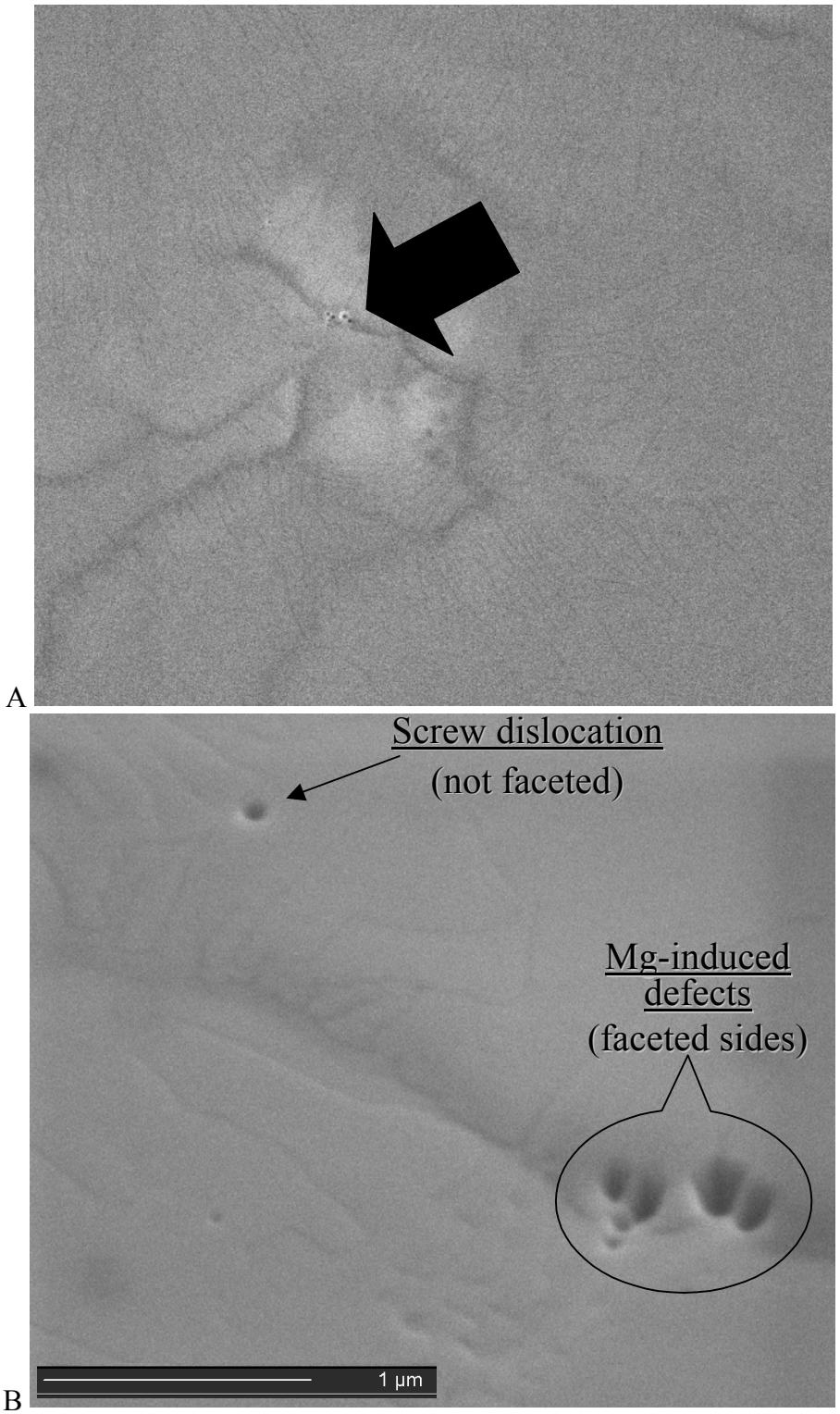

Figure 6-18. SEM images of a Mg-induced defect. A) Large overhead view showing the defect in context. B) High magnification image of the defect.

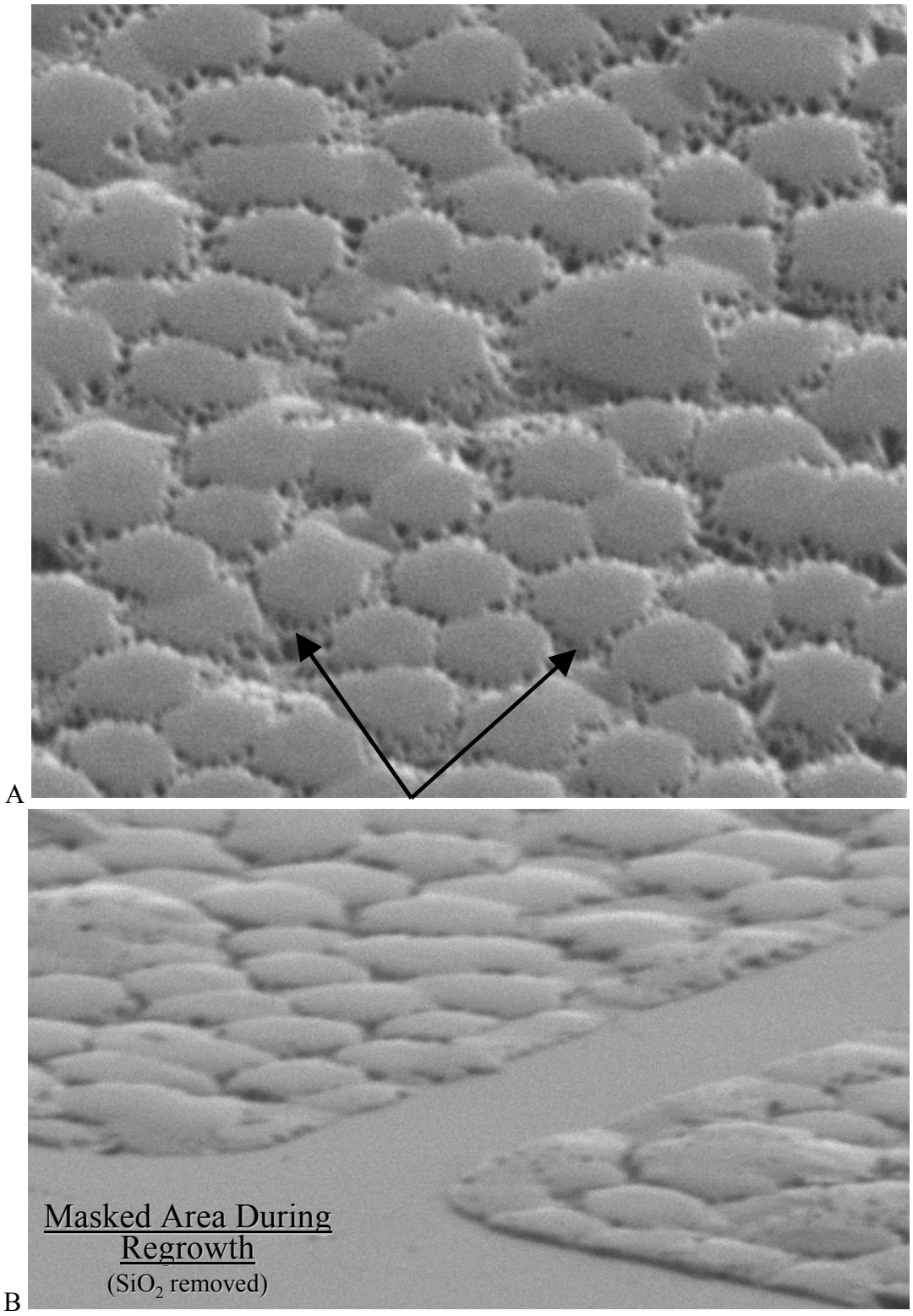

Figure 6-19. SEM images of regrowth with an excessive (Mg/Ga) after 10 minutes.

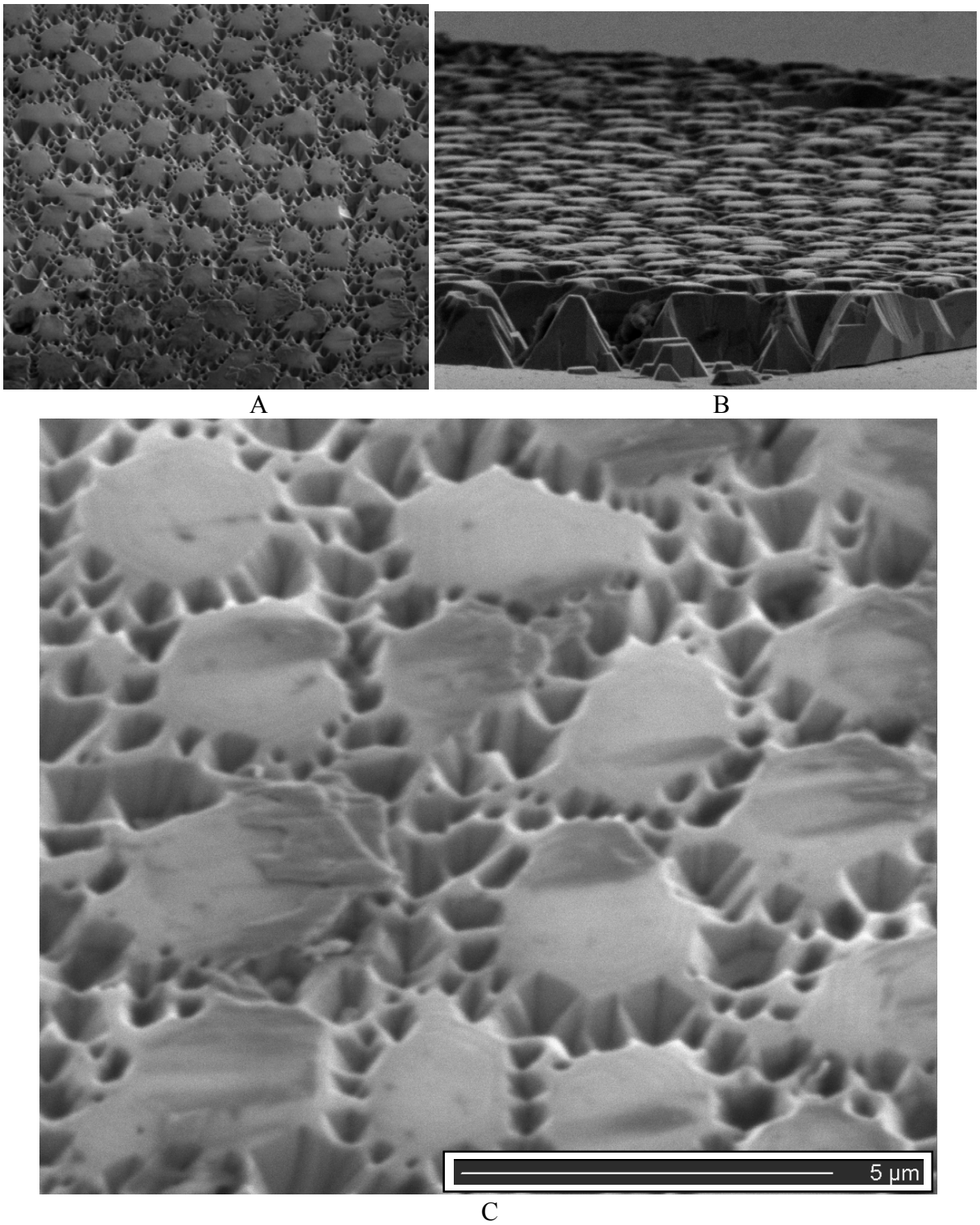

A B C

Figure 6-20. SEM images of regrowth with an excessive (Mg/Ga) after 60 minutes.

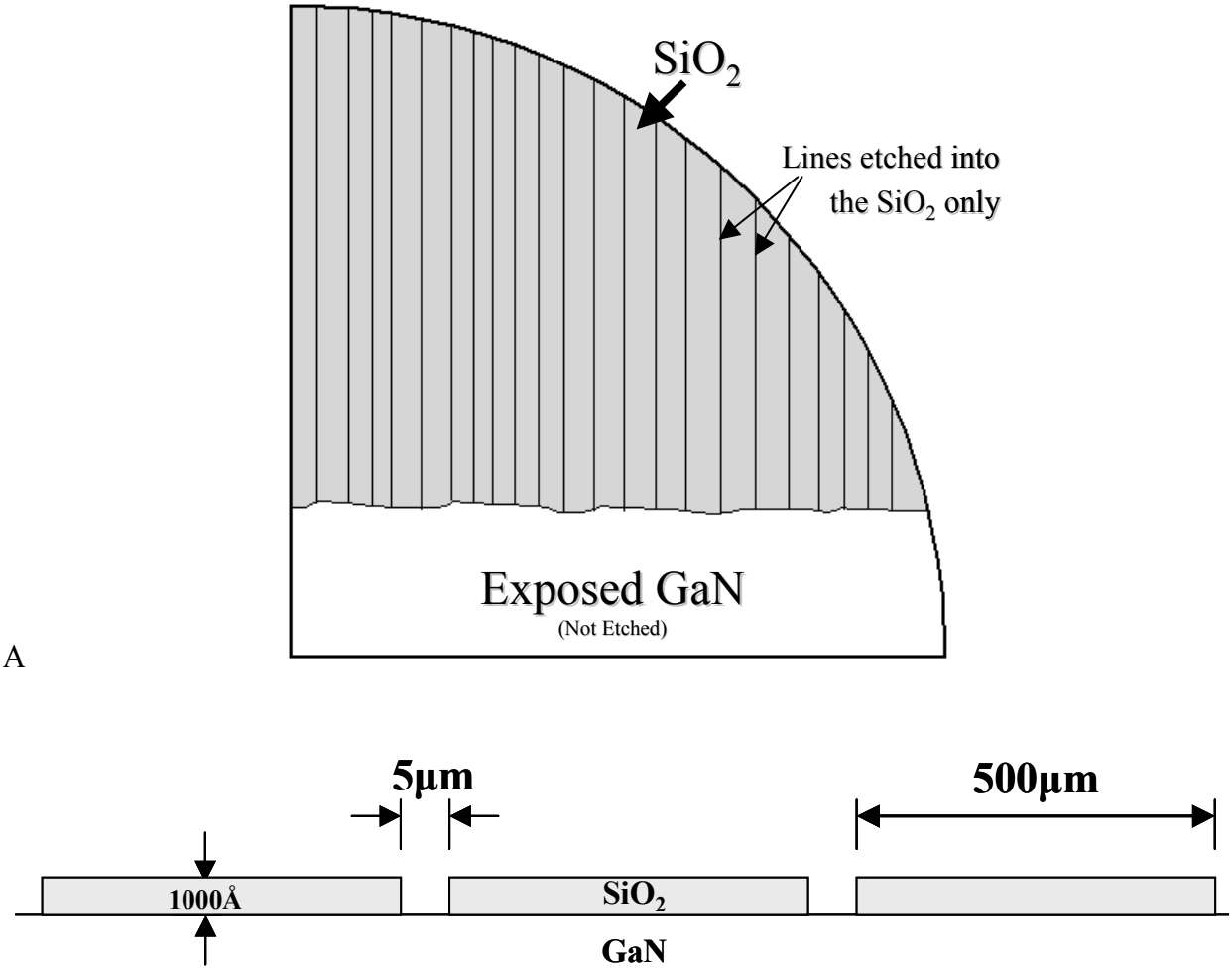

Figure 6-21. Substrate used for doping experiment. A) Plan view. B) Cross section. C) SEM image of the patterned and non-patterned areas after regrowth.

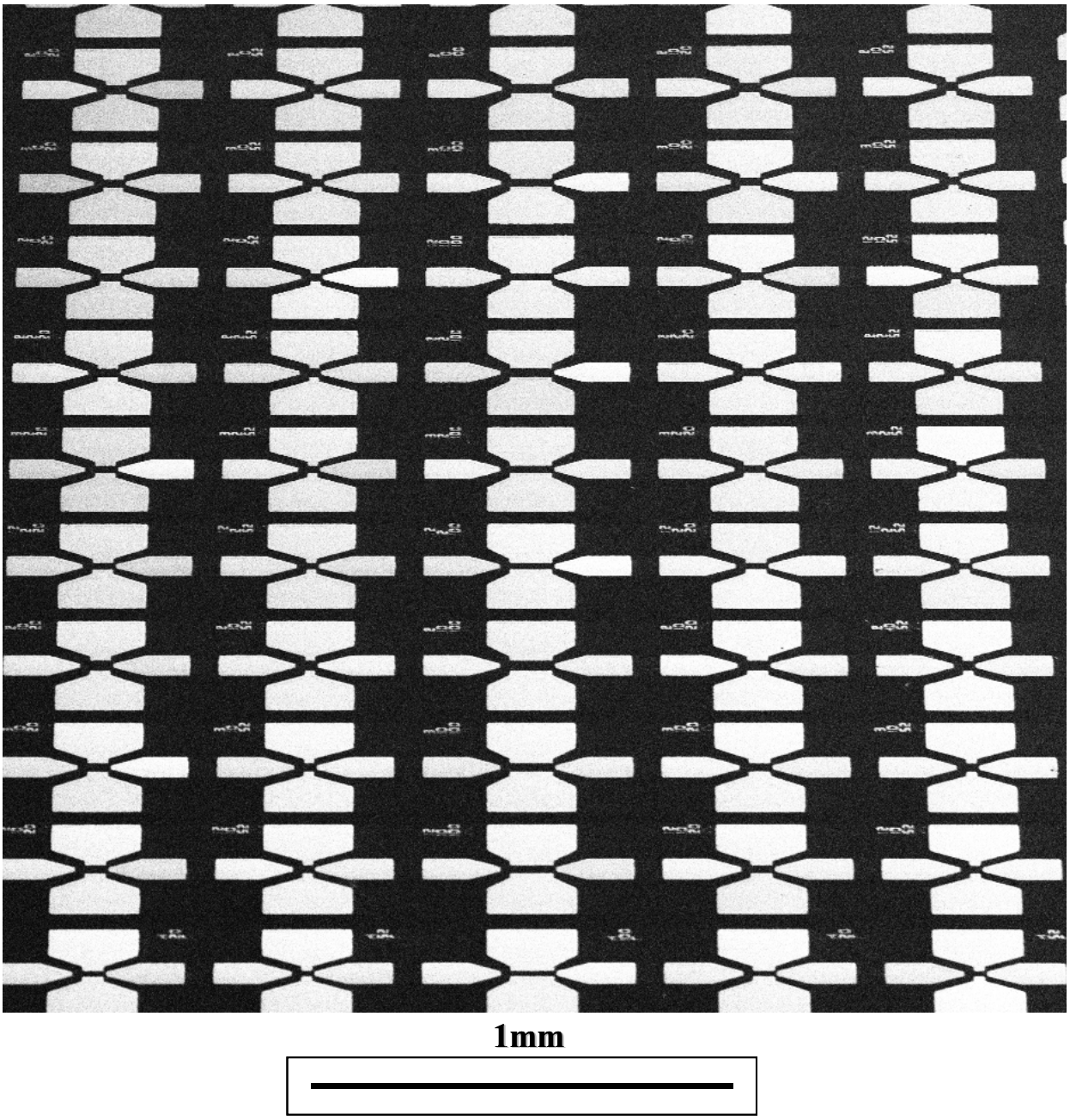

Figure 6-22. Overview of regrowth using Sc_2O_3 as a mask.

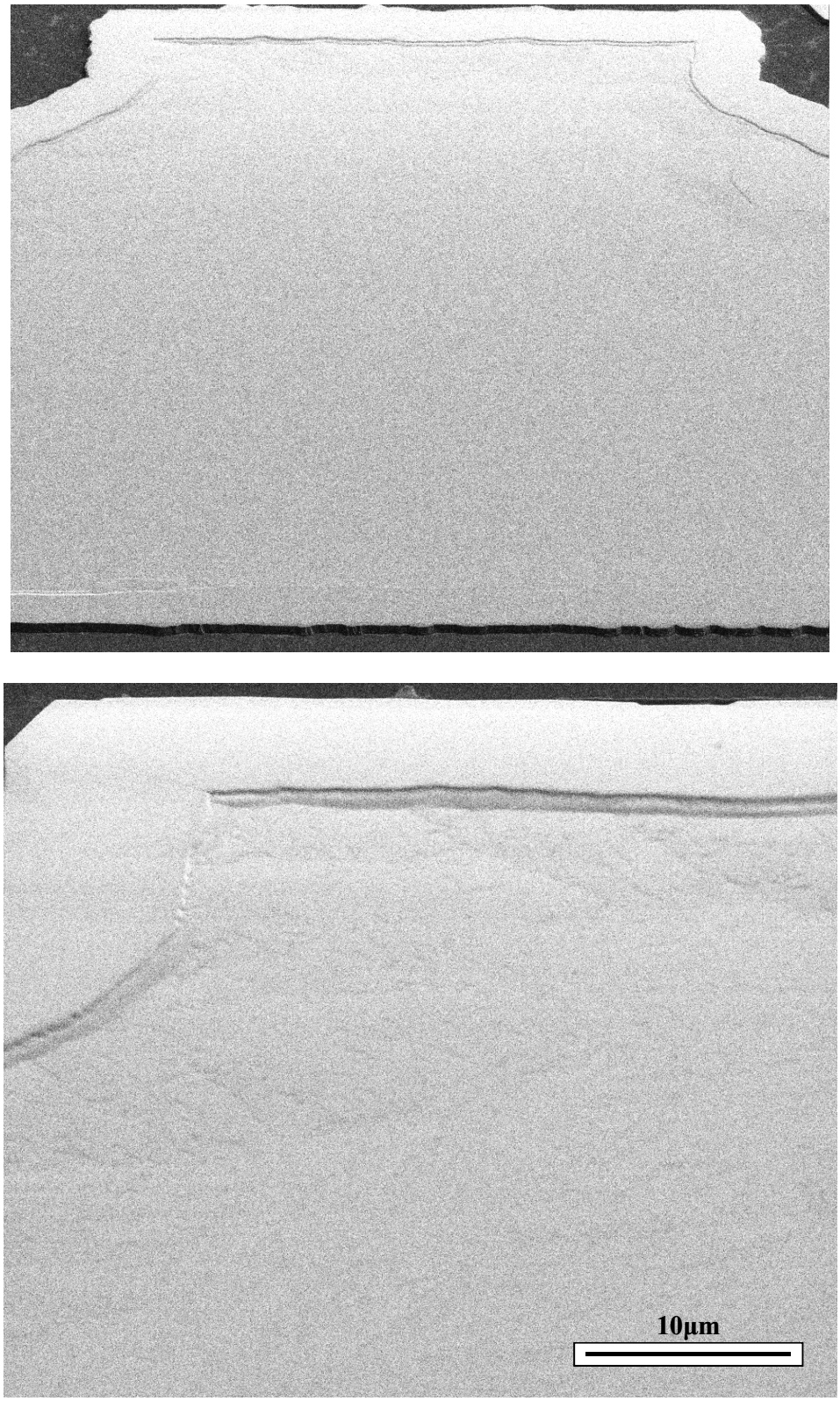

Figure 6-23. SEM images of a feature that has been regrown in using Sc_2O_3 as a mask.

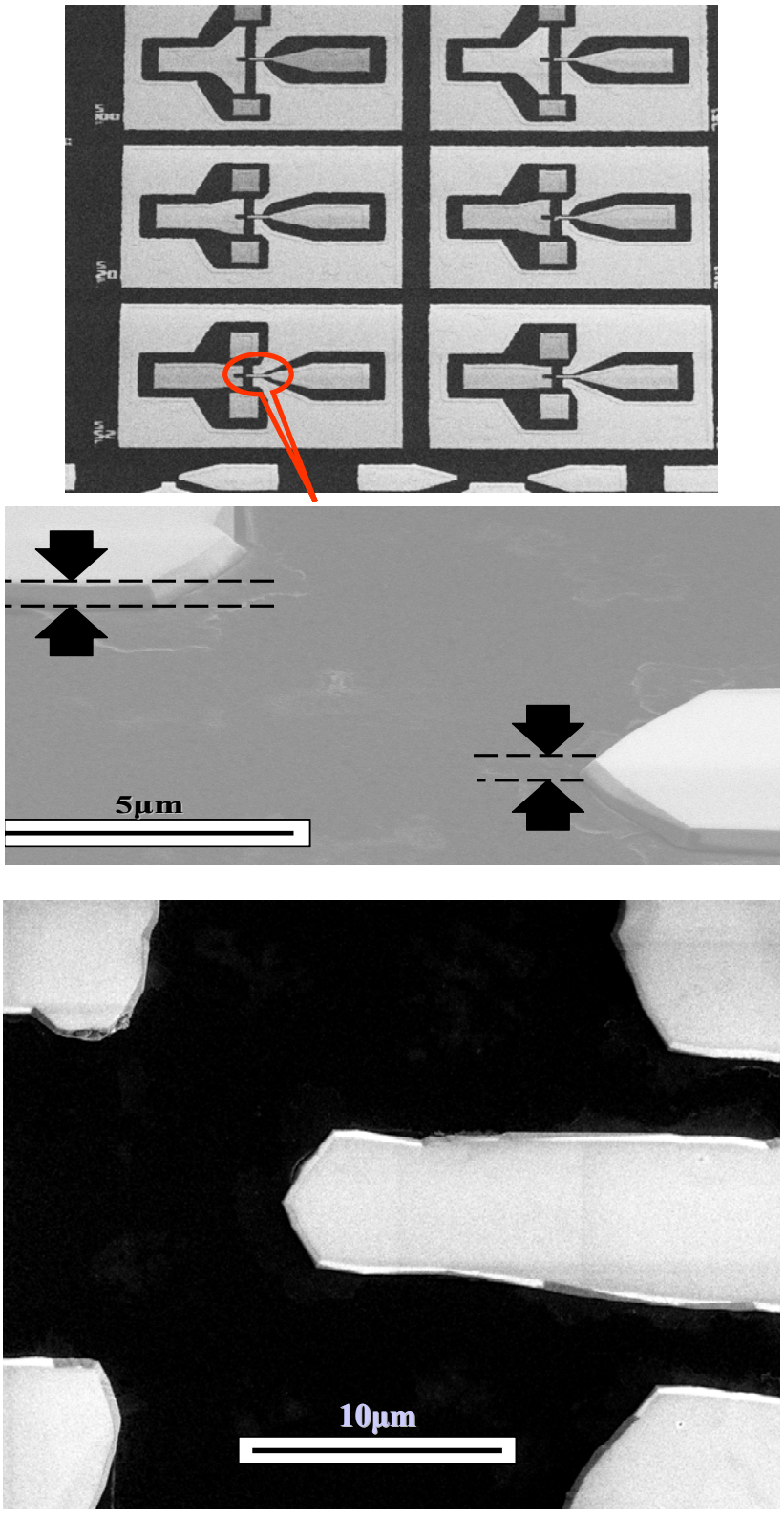

Figure 6-24. SEM images of well controlled growth at small dimensions when using Sc_2O_3 as a regrowth mask.

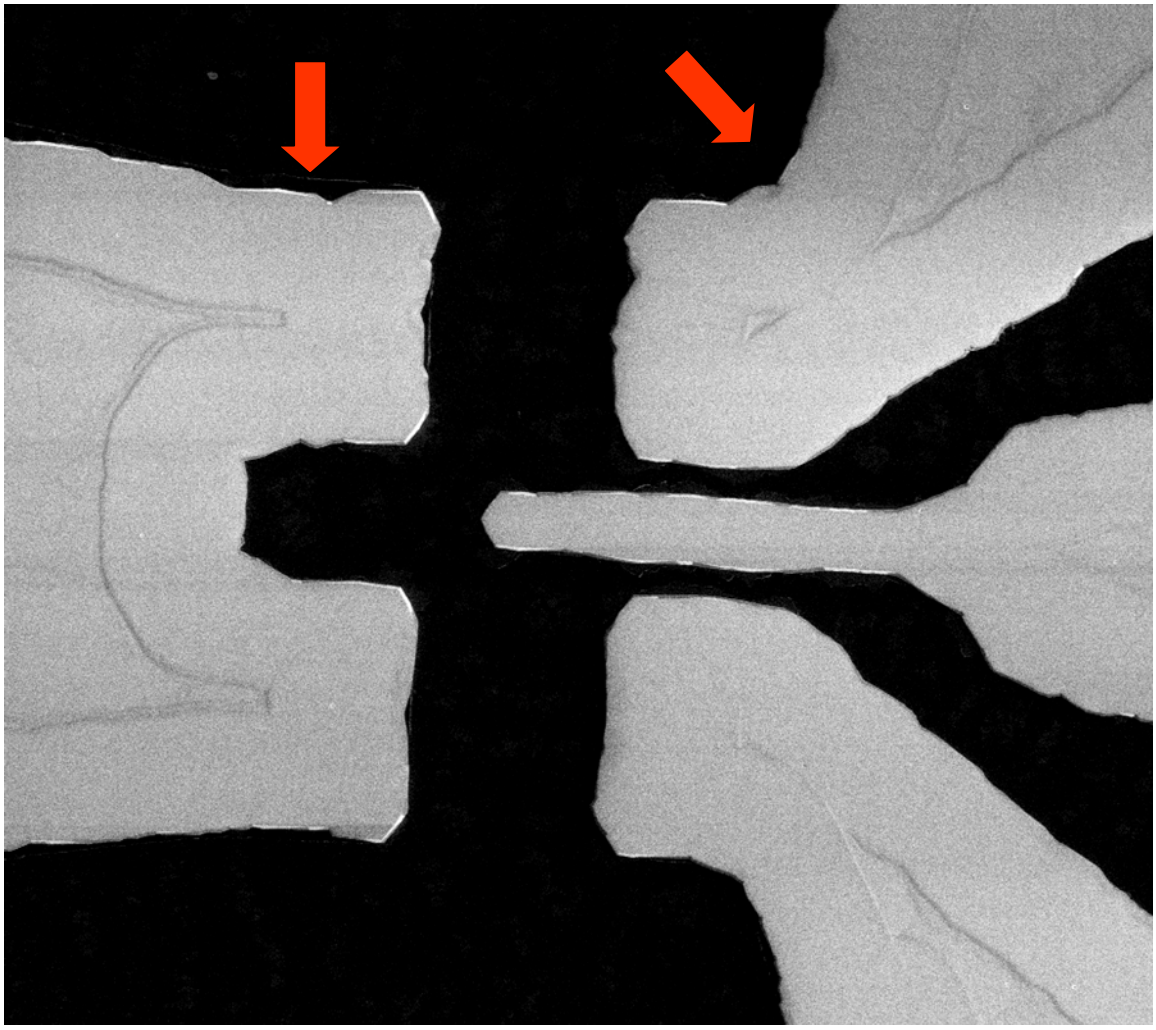

Figure 6-25. SEM of distorted growth profile.

A

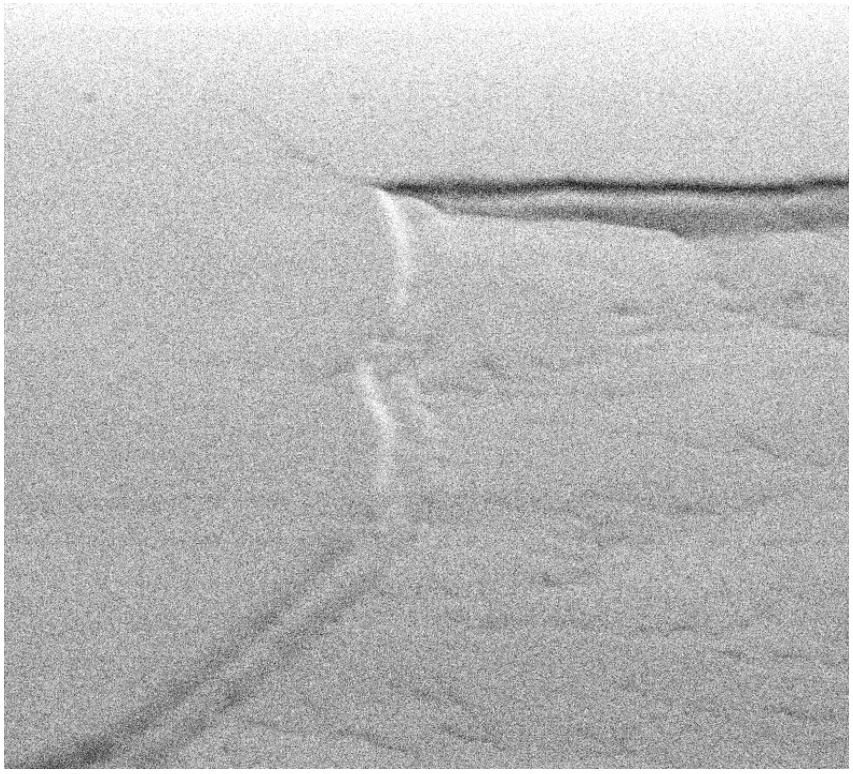

B

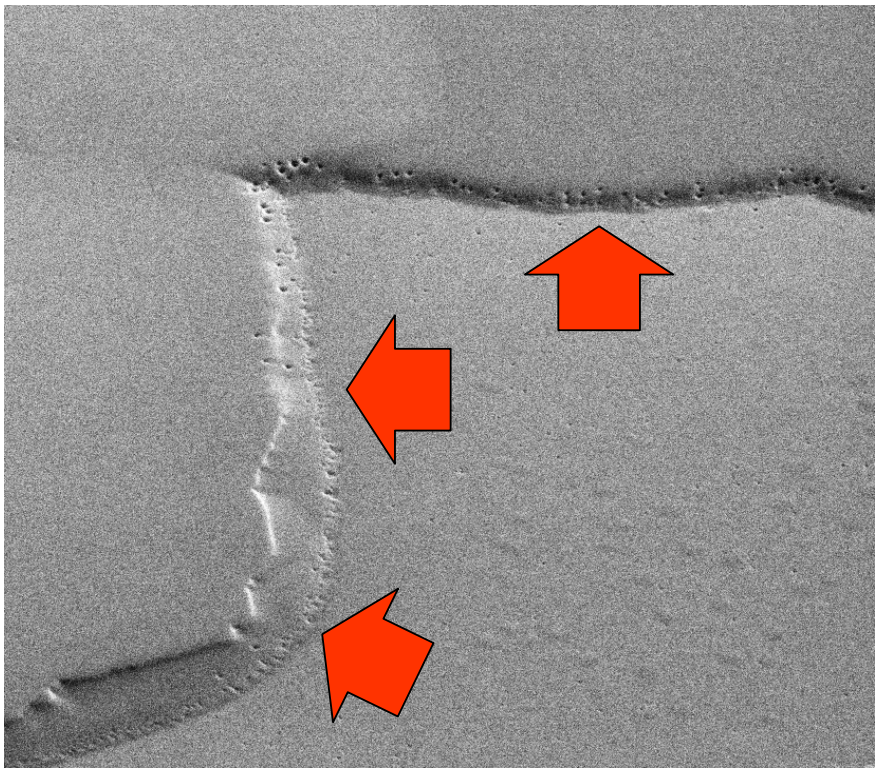

Figure 6-26. Comparison of regrown material using different masks. A) SiO_2. B) Sc_2O_3.

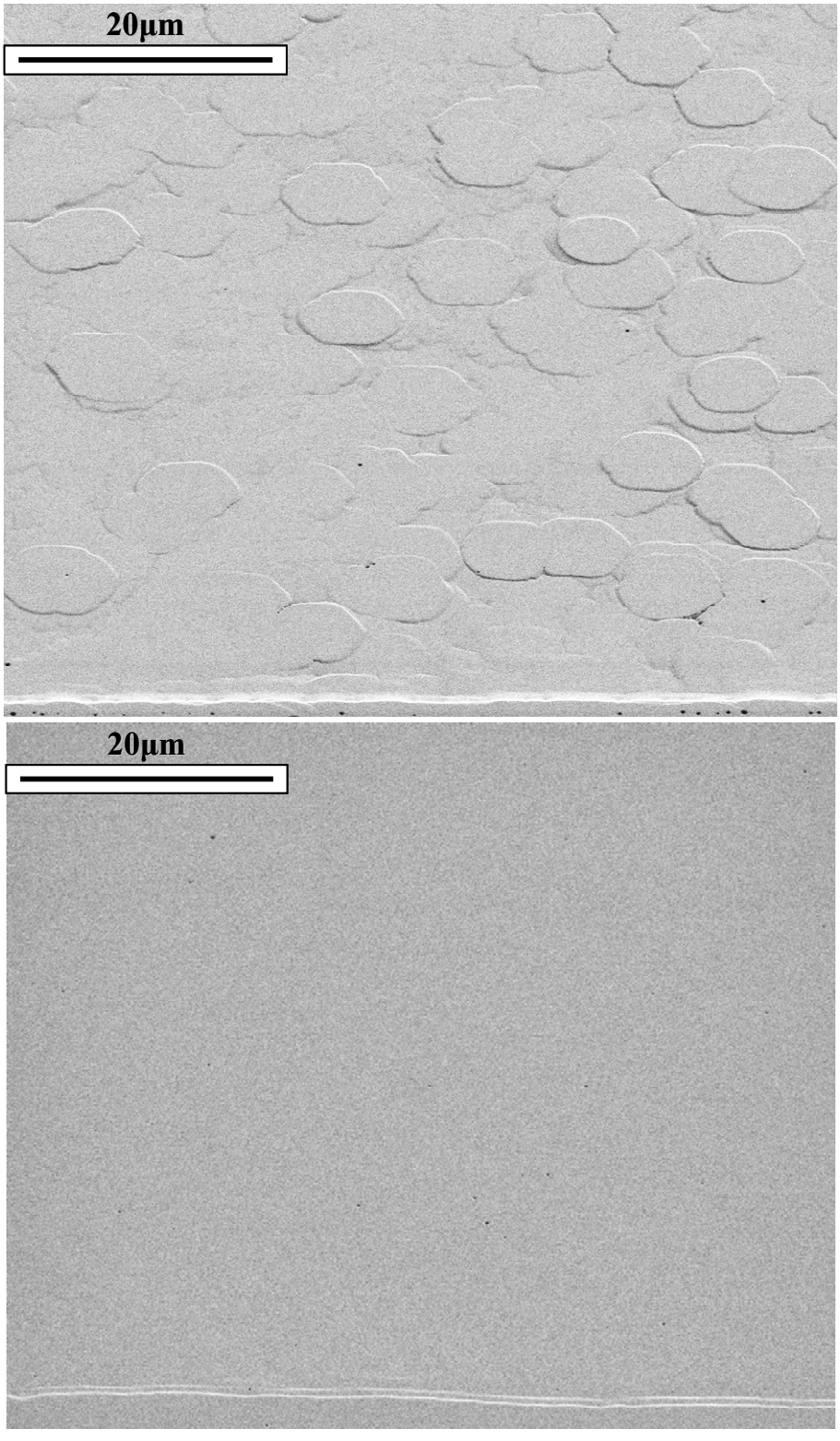

Figure 6-27. Comparison of growth morphology for an increasein Mg flow. A) Standard Mg flow of 11 sccm. B) Increased Mg flow to 22 sccm with all other conditions constant.

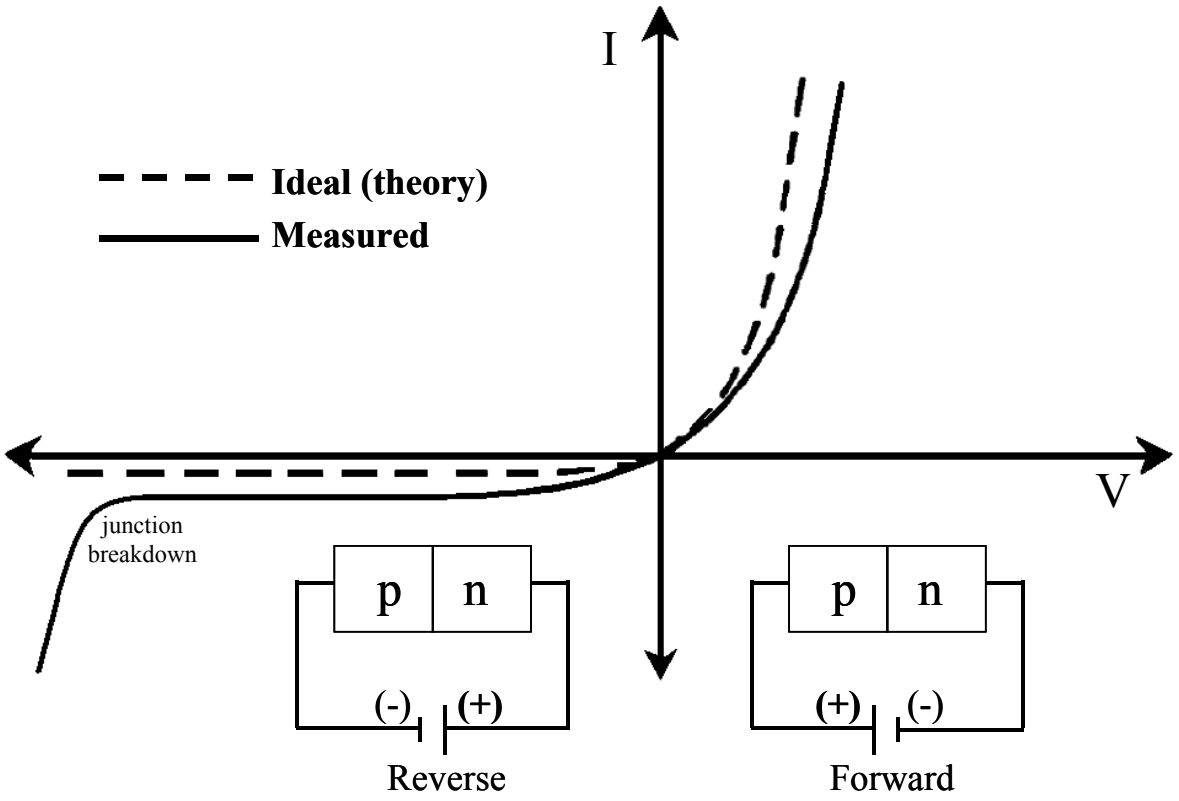

Figure 6-28. Examples of an ideal and measured I-V curve with the p-n junction configurations for forward and reverse bias.

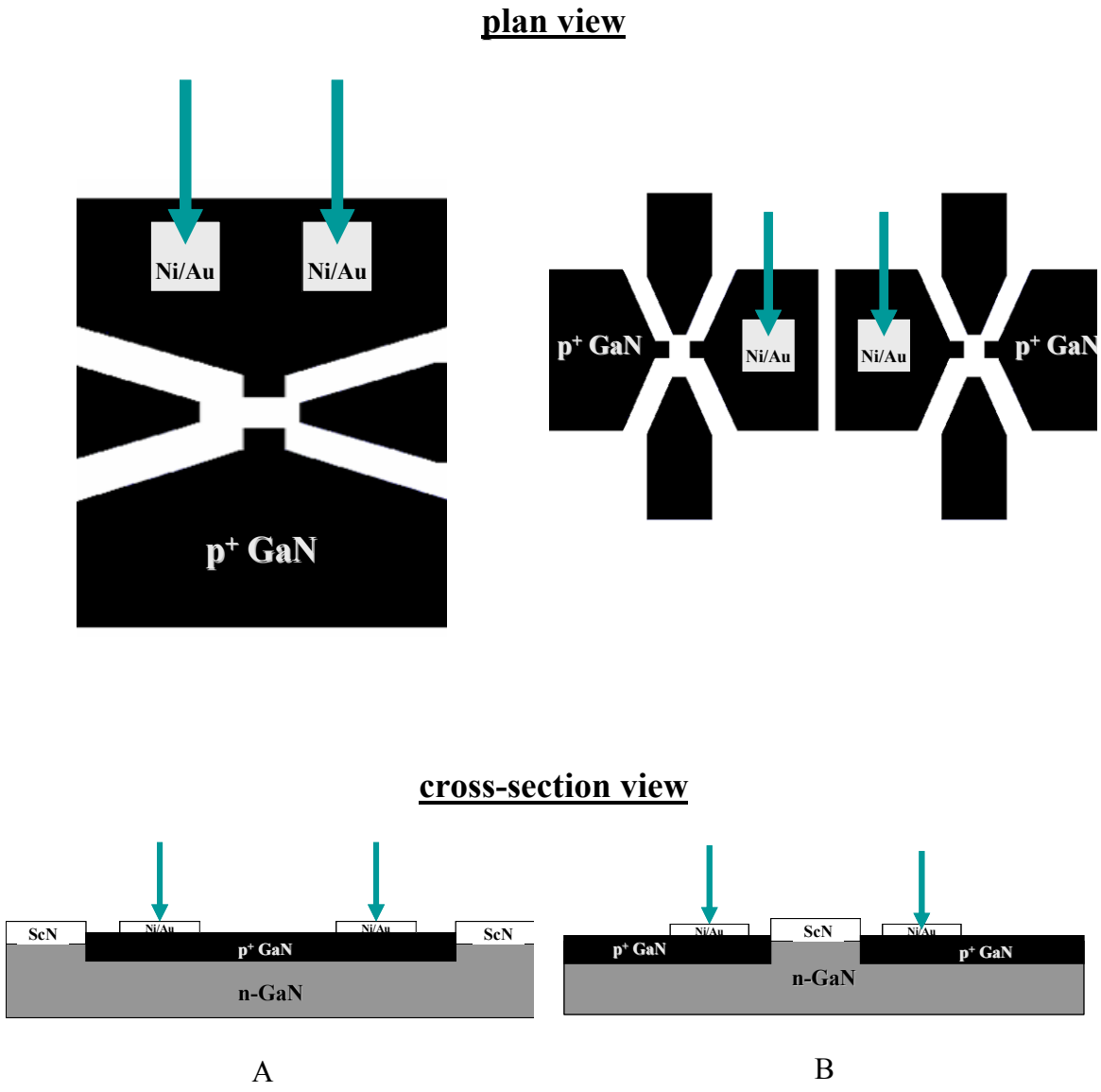

Figure 6-29. Configurations for the I-V measurements. A) Measuring two contacts on the same regrown feature. B) Measuring two contacts on different regrown features.

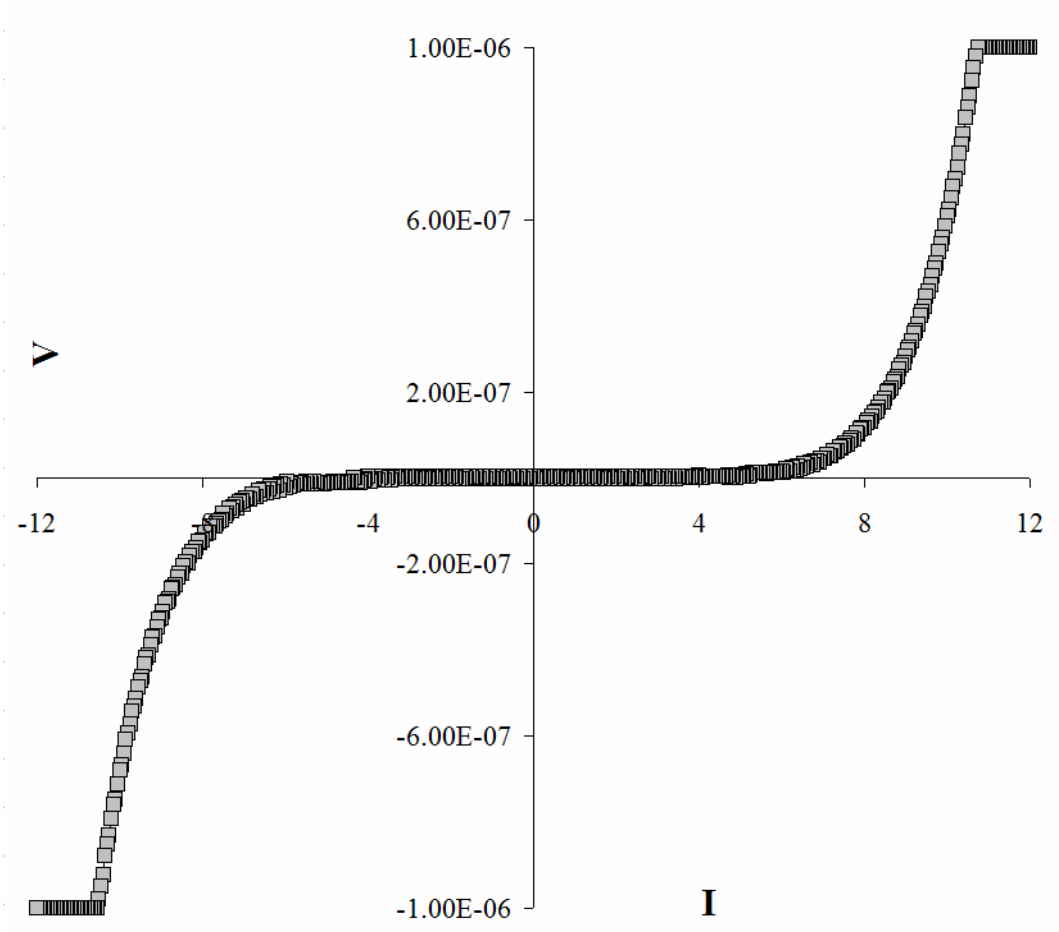

Figure 6-30. I-V measurement for the regrown pnp structure using the Sc_2O_3 mask.

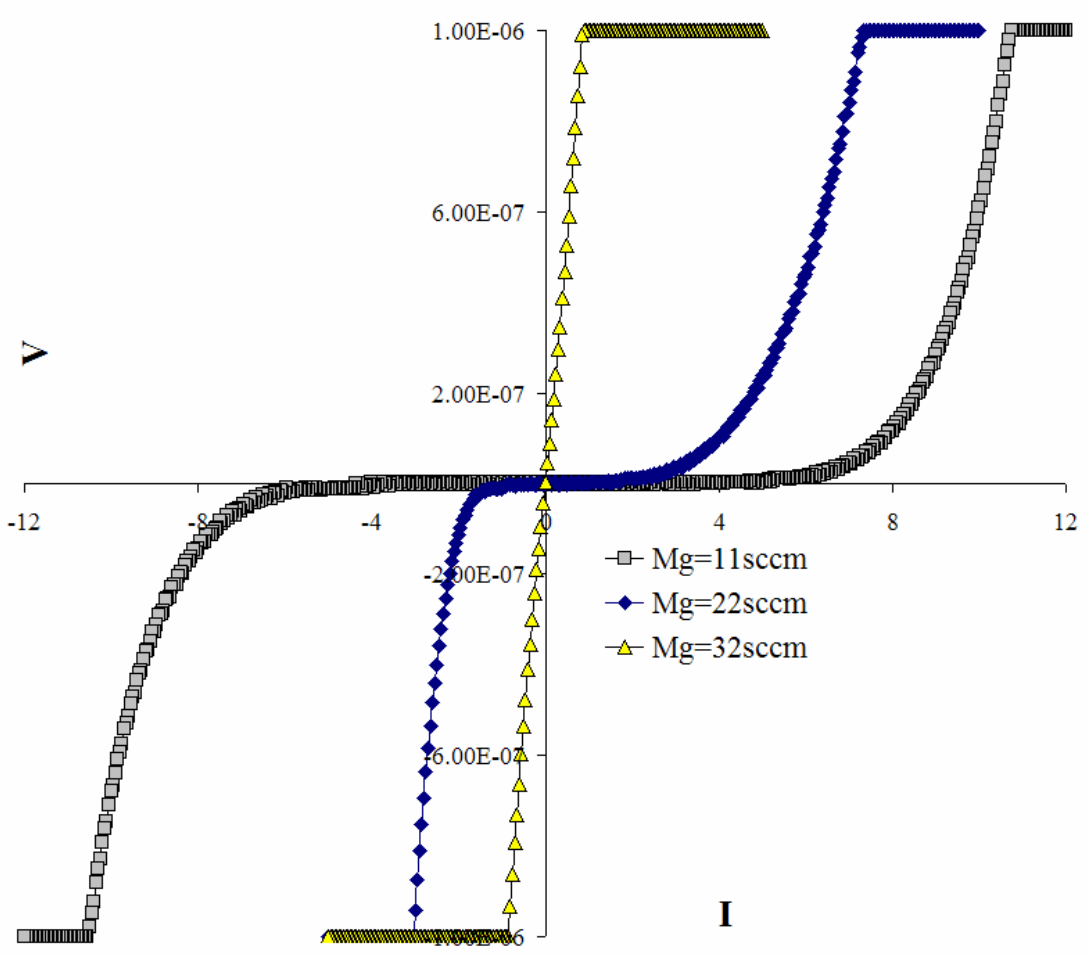

Figure 6-31. I-V measurements for pnp structures regrown with varying Mg flows.

CHAPTER 7
PROCESS OPTIMIZATION OF GAN MOS DEVICE FABRICATION: RESULTS AND DISCUSSION

The first step in choosing a good dielectric is to test its electrical properties. Excellent electrical properties are meaningless though, if the material cannot withstand the chemical and thermal treatments required for the fabrication of a device. The fabrication of electronic devices requires numerous steps with very specific parameters. The processing parameters can have a significant impact on the device characteristics and performance. In general, the fabrication of a MOSFET device consists of the basic processes listed in Table 7-1. These processes all require either chemical or thermal treatments, which could potentially damage the oxide. It is essential that the integrity of the dielectric oxide be maintained during device fabrication. The stability of the dielectric oxide or its lack of can put limits on processing steps, which can make the fabrication process quite difficult or even impossible.

In addition to the general steps required for MOSFET device processing there are several challenges specific to the fabrication of GaN MOSFETs. The fabrication of a GaN MOSFET device is particularly severe due to GaN's excellent chemical and thermal stability, which requires that harsh chemical treatments and extreme temperatures be employed. Thus, it is especially important that any candidate dielectric for GaN-based MOS devices be distinctively robust and be able to maintain its stability during the device processing steps. The focus of this chapter is on the ability of potential dielectric oxides to endure the most fundamental processing steps employed for the fabrication of a GaN MOSFET. The stability of the oxide during substrate processing and within the MOCVD growth environment will also be examined for the use in MOCVD regrowth applications. The issues involved in the design of a processing sequence will also be discussed and based on the oxides' limitations, some general processing sequences will be proposed for the fabrication of GaN-based p-MOSFETs and CMOSFETs. Then the issues

involved in the design of a processing sequence based on the MOCVD regrowth work that was done will be discussed and a specific processing sequence is developed for the fabrication of a p-MOSFET.

Processing of GaN MOS Heterostructures for Device and Regrowth Applications

The main focus of this chapter is on the effect of the thermal and chemical treatments used during the processing of GaN MOS heterostructures for device and regrowth applications. Particular attention is given to the effects that processing has on the oxide's electrical properties and their consequence for device performance. As was mentioned earlier, the oxide/GaN interface quality is a critical issue for GaN-based MOS devices and increasing the smoothness of the Oxide/GaN interface will prevent localized high breakdown fields and provide a high carrier mobility. Defects such as fixed and mobile charge states in the oxide and interface traps at the oxide/GaN interface can be introduced into the oxide during processing and would be detrimental to device performance. The oxides will mainly be judged on how they would perform as a gate dielectric in GaN-based MOS devices. The importance of MOCVD GaN regrowth applications was mentioned earlier. In order to successfully develop this technique, a suitable regrowth mask is needed. The regrowth mask needs to have several attributes in order to function properly. Many requisites for a regrowth mask are the same as those needed for potential dielectrics during device processing. This is because the regrowth is essentially just another step in the overall fabrication of a GaN-based device and therefore many of the same issues that would be faced during processing are also pertinent in regrowth applications.

Whenever possible, imaging was performed using SEM over an optical microscope due to its greater imaging capabilities. The use of an optical microscope instead of imaging using SEM was necessary in many situations during processing due to having the photoresist (PR) still in place. The lower pressures needed for SEM are much harder to achieve due to the outgassing

of the PR. The SEM imaging of a sample with photoresist is limited and very difficult to obtain good resolution due to the interactions of the PR with the electron beam.

General Issues for MOCVD Regrowth Applications

Deposition of the mask film needs to be uniform and free of pinholes. If many small areas are left exposed, then regrowth will occur through them and further processing steps can be made difficult. Regrowth from exposed areas as small as 5 μm^2 could be very detrimental. Figure 7-1A shows how significant the regrowth could be through a very small area in the SiO_2 mask that was exposed during growth. A feature this size could disturb the spin process for any photoresist applied to the film for a subsequent processing step. Regrowth through the mask can also occur if the mask is too thin. Even if the mask material has proven to be stable under these growth conditions, if it is too thin, decomposition of the film can be catalyzed through the diffusion of species from both interfaces. Figure 7-1B shows an example where the mask was too thin and significant regrowth occurred uniformly over the whole film.

The selective removal of oxides from within the patterned areas for the application of a mask for MOCVD regrowth using a wet chemical etching process has some problems associated with it. Although these difficulties apply to all oxides being used as a regrowth mask, some oxides are more problematic than others. It is commonly known that due to the isotropic nature of wet etching, an undercut of the oxide under the patterned mask can occur. The undercut can expose the substrate around the etched feature. This can result in regrowth taking place on the surface edge of the etched trenches and the formation of poorly defined edges around the regrown features. This can make it difficult to align future masks for the subsequent processing steps. It also creates is the potential of having a negative impact on device performance. All the mask layers are precisely aligned with each other allowing little to no tolerance for misalignment. Features in close proximity to each other can form a regrown connection, making

it impossible to perform tests. At the very least the nonuniform regrowth around the edges would result in erratic trends in data for a variation in device distances. As shown in Figure 7-2, using a wet etch can produce optimal processed features but not necessarily over the whole wafer. The potential for successful patterning using a wet etch is greater when SiO_2 is used as the mask, due to the controllability of the etchant. Other oxides and materials do not have an established etchant that can be used which will result in reproducible and uniform patterning. For regrowth applications, there needs to be an anisotropic etch profile of the regrowth mask. In most instances, this can be efficiently obtained through the dry etching of the mask material. Dry etching also has issues that need to be addressed when optimizing the processing sequence for the regrowth substrates.

The harsh dry etch plasma environment can produce elevated temperatures during the dry etch which causes the PR to bond strongly to the oxide and the substrate. When this occurs, the PR can be very difficult to remove and sometimes will leave a residue behind. In order to clean off any residual PR that may be on the SiO_2/GaN substrates, a 30 sec. O_2 plasma exposure and a following 1 minute bath in an (1:10) HCL solution has been found to be very effective in removing most of the PR residue. Optical images of a substrate before and after an O_2/HCl treatment are shown in Figure 7-3. The images clearly show that all of the residual PR has been removed from the etched GaN feature and most of it from the SiO_2 mask.

In addition to the PR bonding to the mask film or substrate, the elevated temperatures and plasma chemistry produced by the dry etch environment, can facilitate the decomposition of the PR. The formation and deposition of PR-based etch byproducts onto areas that are being actively etched can lead to a rough surface morphology or a highly defective surface with many pillars and large features due to being masked. The baking of the PR and minimizing the etch time are

common methods to deal with this problem. Another factor that should be considered is substrate selection. The use of Ti/W backside coated sapphire substrates brought up an unexpected problem during dry etching. The Ti/W coating caused the temperature to rise during the dry etch and produced the problems associated with the photoresist that were just discussed. Thus, the type of substrate should be factored in when planning the dry etch process.

These issues with the PR are particularly important for the processing of regrowth substrates due to the effect of the PR residue on the regrowth behavior. Due to the negative effect that hydrocarbon impurities would have on the regrown film's properties, every attempt is made to remove all residual PR before the regrowth. It was expected that if any PR was to remain it would either be baked off during the heat up, be grown over or even act as a preferential site for nucleation. As can be seen in Figure 7-4, this was not the case. The PR residue actually inhibited regrowth from occurring. In Figure 7-4C, it is evident that there is nearly a complete absence of nucleation where the PR residue was located. The major problem that this creates is not the impurity contamination from the PR but the effect on performing the electrical characterization. For any feature that has an area where no regrowth has taken place, deposition of the metal contact on it would act as a shorting path. This would make testing the properties of the regrown material impossible.

Processing of SiO_2/GaN MOS

SiO_2 is the industry standard for Si-based devices and has proven to be thermally and environmentally stable during many different GaN processing steps. It is even used sometimes as an etch mask for the dry etching of GaN. The well established etch chemistry and recipes makes the processing of SiO_2 easy to obtain reproducible results of high quality. The robust nature of SiO_2 is a great advantage for use as a regrowth mask. It is this stability and its highly developed knowledge base, which is why it is exclusively used in ELO applications. However, there are

some issues that can be problematic for SiO_2 or any potential dielectric during processing. The majority of the regrowth work was done using SiO_2 as the regrowth mask and thus its performance under a large number of different processing and regrowth variables was well studied.

The wet chemical etching of SiO_2 is easily accomplished using a buffered oxide etch (BOE), which is a dilute solution of hydrofluoric acid. It is extremely aggressive and can etch hundreds of angstroms of SiO_2 in less than a minute. This can make it difficult to control. For applications where only selective removal of the SiO_2 is desired from within exposed features of a patterned mask, it is necessary to dilute the BOE to 50% to 25% strength. The dilution of the etchant can be very problematic and several issues can become a factor. Since wet chemical etching is an isotropic process that will remove material equally in all directions, the undercutting of the film is a common problem. In Figure 7-2, a processed patterned substrate using optimized conditions is shown. The SiO_2 film had been wet etched using dilute BOE and the GaN was subsequently dry etched providing very smooth surface and sidewalls. It can be seen in Figure 7-2B, that even under the most optimized of conditions, there will always be some degree of undercut of the SiO_2 film when wet etching is used. Figure 7-5 shows a substrate that was poorly processed and illustrates some of the problems encountered in the wet etch process. The degree of undercut seen in the image is much closer to what usually occurs than the image images in Figure 7-2. Another problem shown in the figure is from micromasking. This occurs when some residue from a processing step is left on a surface to be dry etched. The residue etches at a different rate than the substrate and therefore a pitted surface can occur. The micromasking in this figure occurred from oxide residue left on the GaN surface from an incomplete and non uniform wet etch of the SiO_2. This can be seen in Figure 7-6, where the use

of dilute BOE resulted in the non-uniform etching of the oxide from within the patterned features.

Due to the problems encountered in wet etching, dry etching is most commonly used for the selective removal of SiO_2, when an anisotropic etch profile is needed. Optimization of the dry etch process for SiO_2 was minimal since it has been extensively researched and well developed due to its use in Si MOS devices. There are issues however, that can arise from the dry etching of SiO_2 on GaN. The dry etching of SiO_2 is mainly performed using F-based plasma chemistries (SF_6, CF_4, CHF_3). This is an additional benefit of using SiO_2, since fluorine-based plasma chemistries are known to not damage the GaN surface. Fluorine atoms do not act as an active etching species on the GaN surface due to the especially high sublimation temperature of Ga fluoride, which is up to 800^{o}C [101]. The main problem encountered was caused by the excessive dry etching of the SiO_2, using CHF_3 as the process gas. As shown in Figure 7-7, if the SiO_2 dry etch time is too long, the GaN surface can be damaged. The damage is caused by the hydrogen in the CHF_3 plasma, which is an active etching species on the GaN surface due to the high volatility of gallium hydride (GaH_x). Normally, the use of CHF_3 would not produce any damage to the GaN surface, because there would be too little active H produced to make any impact. But if the GaN surface was exposed to CHF_3 plasma for an extended period of time, enough H could be produced to cause damage to the surface.

Processing Issues Specific to Sc_2O_3 and MgO Thin Films on GaN

The processing of Sc_2O_3 and MgO thin films on GaN for the use as a regrowth mask is much more complicated than that for SiO_2/GaN substrates. Issues with the PR are especially problematic during the processing of substrates for regrowth applications. This is due to the large amount of dry etching needed for both the oxide mask and the GaN substrate. The use of Cl_2-based chemistries for the dry etching of the Sc_2O_3 and MgO films in addition to the GaN

substrate is particularly challenging. The longer the exposure time to the harsh plasma environments, the more the PR will decompose. Optimization of the etching conditions and parameters such as the PR type and baking conditions can help minimize the amount of decomposition but for any polymer-based photoresist exposed to a Cl_2-based plasma environment, decomposition is unavoidable. An alternative mask is often used when dry etching GaN. Usually, a metal film is sputtered on the substrate to be used as a mask. The use of FeN as an etch mask for GaN has proven to work well because no volatile iron halides exist and thus the FeN film is very resistive to Cl_2-based plasmas [101]. The use of an alternative etch mask was avoided in this study because of the addition of extra processing steps. Using an alternative mask would not replace any steps because PR deposition and development would still be required in order to transfer the regrowth pattern into the etch mask. Thus, the use of an alternative mask would add in several more steps in the processing sequence as well as many more parameters that need to be optimized. Photoresist is the industry standard for use as a mask. Being able to successfully process the regrowth substrates using PR would be a definite advantage for the use of this technology.

As was previously mentioned, the bonding of the PR to the oxide or substrate can occur during dry etching. The treatment used for the removal of residual PR from SiO_2/GaN substrates can not be used on thin films of Sc_2O_3 and MgO due to the potential damage that could occur. There is no effective method of removing strongly bonded photoresist residue from Sc_2O_3 and MgO without damaging them. Sometimes if the PR becomes too strongly bonded, it can remove some of the oxide with it when it is removed after all the etching has been done. Thus, the best thing to do is to avoid forming such a strong bond between them.

Since the dry etching of Sc_2O_3, MgO and GaN all require the use of Cl_2 plasma chemistry, additional problems of selectivity are created when etching the oxide/GaN material system. The etch rate of GaN is significantly greater than either Sc_2O_3 or MgO under the same etch conditions. If the oxide film is not completely uniform in thickness or it doesn't etch uniformly, the effect of the differing etch rates can be large and result in very rough GaN surfaces or even the formation of large mesas within the exposed area being etched. An example of this is seen in Figure 7-8, where large mounds formed within the etched feature due to the non-uniform etching of the Sc_2O_3. The formation of the mounds was caused by areas that still had Sc_2O_3 when the GaN surface began to be exposed and rapidly etch. This can be avoided through the proper optimization of the dry etch conditions.

For the processing of thin films of Sc_2O_3 and MgO, there is a very narrow window of suitable conditions and several factors in determining the optimal conditions need to be considered. The difficulty lies with the conflicting demands, which require that certain parameters be carefully balanced so as to satisfy both restrictions. Due to these issues, the processing parameters must precisely optimized. A key parameter in the photolithography procedure is the baking time of the PR. In order to avoid excessive bonding of the PR to the oxide film or substrate, the baking time of the PR both before exposure and development and after, must not be too great. This must be balanced out with the need to avoid decomposition of the PR during etching. In Figure 9, the effects of using too small of an amount of time for the post development bake, also called a hard bake. Figure 9A is an optical image of a MgO/GaN substrate after dry etching both the MgO film and GaN substrate. The white spots in the PR are areas where the PR has been etched through down to the GaN substrate. Figure 9B is an SEM image of an area between two etched features after the PR has been removed. The extent of

damage that was conferred to the MgO film and GaN substrate from the decomposition of the PR is easily observed. In order to strengthen the photoresist and make it more durable during the dry etch exposure, the time of the bake can be increased. Figure 9C shows an optical image of a processed substrate where the hard bake time was increased. The edges of the PR have degraded and roughened up but the rest of the PR has not exposed any of the oxide film or GaN substrate. Figure 9D is an SEM image of the substrate in Figure 9C after removing the PR. It shows how the degradation of the edges of the PR led to warping of the feature outline and the formation of strongly bonded PR residue along the edges. The image also shows how the integrity of the oxide was not harmed and the etched GaN surface is very smooth. The hard bake time needs to be increased further to avoid the decomposition along the edges but not too much such that the PR becomes bonded to the oxide.

Processing MgO / GaN MOS Structures

As previously mentioned, MgO has a major limitation in its lack of environmental stability. Its reactivity with water and hydroxylation in air adds a large restriction on its processing exposure. Despite the environmental difficulties with MgO, it should still be possible to process a device using standard lithographic techniques by limiting the amount of water that is used on the MgO surface and keeping the sample under vacuum between processing steps. However, the processing of MgO for GaN MOS devices is extremely difficult to perform without degrading the oxide surface. Figure 10 shows an example of the degradation that occurs on the MgO surface from processing using standard photolithographic techniques. The optical image is of a patterned feature in photoresist on a thin film of MgO and was taken minutes after processing.

Initially, MgO degradation problems were attributed to excess exposure and air. Next, the growth rate of the material was looked at and optimized. This situation was thoroughly

investigated and consisted of performing numerous experiments where several variations in the processing parameters were used in an attempt to find an optimal set of processing conditions. After being unsuccessful in optimizing the parameters used for the growth and processing of MgO, the process chemistry was studied in order to gain some insight into the problem. It was discovered that the difficulties encountered were not due to any unoptimized set of conditions used for growth or processing but were inherent in the material system.

All photolithographic processes are based on acid-base chemistry. The typical positive photoresist consists of three main components. The first is a phenol-based resin polymer, usually novolac that serves as the base of the photoresist. The second is a photoactive compound (PAC), based on the chemical diazonaphthaquinone (DQ). The third is a solvent, which governs the viscosity that determines the film's thickness. The novolac resin contains hydroxyl groups (OH) that make it hydrophilic and easily dissolves in an alkaline or basic solution. The DQ is nonionizable and hydrophobic and when added to the novolac, it makes the novolac hydrophobic and strongly inhibits the dissolution of the both of them. Upon exposure to UV light of the proper wavelength, the DQ undergoes a chemical reaction that converts it into indene carboxylic acid (ICA). ICA is hydrophilic and very ionizable, making the novolac easily dissolve in the developer, which is a basic solution. The photoresist components and main chemical reactions involved in this process are shown in shown in Figure 7-11. The nucleation and growth of MgO on GaN(0001) surfaces occurs in the {111} orientation. Unlike the (100) and (110) surfaces, the MgO(111) surface is polar and very reactive [102]. Its been shown that the reactivity of the MgO surface is dependent on the specific sites of different planes involved, but that for all cases the MgO surface was basic [103]. Thus, the direct contact of the ICA with the basic MgO surface could lead to an acid-base reaction between them. Figure 7-12 shows several of the possible

reactions that could occur between the PR and MgO surface during the exposure and development steps.

Very little literature exists on the potential reactions between the polymeric photoresist and oxide surfaces in photolithographic processing of electronic devices. This mainly due to the lack of need based on SiO_2 being the dominant insulator for MOS devices for decades. The current drive for alternative high κ dielectrics for use in Si-based devices as well as for III-V materials makes the issue of chemical stability with photoresists much more important. The significance of acid-base interactions between polymers and ceramic surfaces has been well established [103-108]. Buchwalter has studied the adhesion of polyimides on different substrates and surfaces that are important in the microelectronics industry [104-107]. Polyimides are the basic building blocks of many conventional photoresists used in the microelectronic industry. In one study, he was determining the peel strength of polyimides on an MgO substrate as a measure of the degree of adhesion [106]. Compared to the other substrates examined, MgO showed the weakest adhesion to the polyimide film. After peeling the polyimide films form the substrates, XPS of the polyimide side that was in contact with the MgO substrate revealed the presence of Mg. It was reasoned that an acid-base reaction had occurred at the interface that led to either corrosion of the MgO or the production of a carboxylate salt with Mg^{2+} ions and an acidic carboxyl group in the polyimide. Work performed by a different group investigated the surface of MgO substrates after being lithographically processed [76]. Using XPS, they observed heavy carbon contamination, which they attributed to chemical reaction by-products that were produced during the lithography process. After annealing the MgO substrate in argon at 760^0C for 40 minutes, they saw a large reduction in the C1s peak but it was still present. They identified the carbon peak as a carbonate species and determined that the reduction in the C1s peak was due to

the desorption of the physisorbed contaminants such as CO_2 and bicarbonate ($Mg(HCO_3)_2$) but that the remaining contaminant after annealing was chemisorbed $MgCO_3$.

To gain a more quantitative prediction of possible acid-base interactions between photoresist, an alternative approach is needed that is based on the specific material properties of all the relevant species in the system. Bolger devised an approach to determine the relative strength of acid-base reactions between organic polymers and oxide surfaces [108]. He defined a parameter (Δ), which can determine the strength of acid-base interactions from the isoelectric point (IEPS) of the oxide surface and the organic polymer's acid ionization constant (pK_a). The IEPS is a measure of the acid-base nature of a material's surface and is essentially equivalent to a pH value for solutions. The parameter (Δ) is defined in Equation 7-1.

$$\Delta = \text{IEPS} - pK_a \tag{7-1}$$

The magnitude and the sign of Δ gives the degree to which acid-base interactions will occur. Three different regimes were identified based on the magnitude and the sign of Δ and are given in Table 7-3. The IEPS for several oxides have been determined and so their value can be easily found [109]. There is a general trend for the IEPS value of oxides based on the cation charge and is listed in Table 7-4. The lower the cation charge is, the more basic the oxide will be. The pK_a values for most of the reactive acidic groups in polymer chemistry can be found in any chemistry textbook. The IEPS value for MgO is 12 [109] and the pK_a of the carboxylic acid group in ICA is 4.5 [110], thus the value of Δ would be 7.5. This value indicates that a strong reaction would occur between ICA and the MgO surface. The IEPS values of two other commonly used oxides in the electronics industry, sapphire (Al_2O_3) and silicon dioxode (SiO_2) are listed in Table 7-5 along with MgO [109]. Also listed is the value of Δ for their interaction with ICA. Comparing the value of Δ for MgO (7.5) and SiO_2 (-2.5), the compatibility of SiO_2 with lithographical

processes is understandable. The availability of the material parameters and the simple calculations required make this approach extremely useful. The degree of the possible acid-base interactions between any candidate dielectric oxide and the photoresist required for device lithography can easily be predicted by using the parameter Δ.

An additional problem exists under the unexposed areas of the PR. After exposure, development and post baking, a loss of adhesion of the PR to the MgO film was seen to occur. This is believed to be caused by the hydrolysis of the PR during the baking step. Adsorption and diffusion of water on polyimide films has been seen by some groups who investigated the metal/polyimide interface [111-113]. Oxidation of the metal at the metal/polyimide interface led to loss of adhesion between the two films. The reaction of MgO to form $Mg(OH)_2$ (Equation 7-2) is reversible and its equilibrium is dependent on the availability of H_2O and the temperature.

$$Mg(OH)_2 \leftrightarrow MgO + H_2O \qquad (7\text{-}2)$$

In the rocksalt structure of MgO, the octahedral coordination of Mg and O differs from that in (Mg(OH)2), which consists of layers MgO_6 octahedra and close-packed protons [114]. The orientation relationship between the two structures and the difference in their bonding arrangements is shown in Figure 7-13. The reconstructive reaction of MgO into $Mg(OH)_2$ involves the rearrangement of the Mg and O sublattices, which produces a 55% increase in the lattice volume [114]. This large change in volume can produce delamination between the $Mg(OH)_2$ film on the surface and the rest of the bulk MgO film. The mechanism for PR hydrolysis and subsequent delamination of the $Mg(OH)_2$ film is illustrated in Figure 14. The adhesion of the $Mg(OH)_2$ surface to the PR will then be much greater than its adhesion to the MgO film. During the baking step the polymer chains in the PR are being cross-linked into rigid structures causing stresses on the PR and allowing the areas with poor adhesion to relieve the

stress through deformation and pop off the surface. Images of the PR popping off the surface of MgO films after processing is shown in Figure 7-15. Nomarski optics was used to enhance the contrast in the topography difference. The height difference is shown through the change in focus of the two areas.

MgO / GaN MOS diodes

It was possible to fabricate GaN MOS diodes using MgO as the gate dielectric. The processing of MgO required very limited exposure of the thin film to heat and water. The general fabrication of the MOS diodes was described earlier. This section will discuss the specific steps and parameters that were crucial to successfully processing the MgO. The processing of MgO into a diode requires no etching of the oxide/GaN system and essentially consists of the deposition of the metal contacts on the MgO surface. This does require that a patterned mask of PR be deposited on the MgO. For the deposition of metal contacts, the lift-off process is commonly used. The lift-off process uses a bilayer stack for a mask that is made of a layer of LOR (lift-off release) with a layer of standard PR on top. The role of the LOR is to create an undercut from the PR on top. This acts to facilitate easy separation of the bulk metal film from the specific contact areas so that the contacts are all uniform. The key for success in this process is the use of an LOR layer with minimal softbake times and temperatures.

After the LOR is spun on, it receives a softbake for approximately 1 min. at a temperature of 105^0C. The PR used is 1818, which is spun after the LOR softbake. The PR also receives a 1 min. softbake at 105^0C. It is essential that the times and temperatures remain low. This minimizes the possibility of any reactions occurring with the oxide surface. After exposure and development, no hard bake is given. The standard softbake for LOR is at 150^0C for 5 min. Thus, baking at a lower temperature for a shorter time keeps a much higher amount of solvent in the LOR and PR. The excess solvent prevents a strong bond from occurring at the MgO/LOR

interface. Normally, if the softbake time is too small and the temperature is too low, the resolution of the pattern is diminished. The resolution is not critical for the diode contacts. The excess solvent makes the PR less sensitive to UV light and so it will be less soluble in the developer. This can occur if the wrong baking conditions are used or if there is too much time between steps. Figure 7-16 shows an example of incomplete removal of the LOR/1818 bilayer within the contact area. Typically this does not occur due to the LOR layer. LOR is not photosensitive and no reaction occurs upon UV illumination. The amount of LOR removed and the degree of undercut is controlled by its exposure to the developer solution. The exposure and development times for the LOR/1818 bilayer is the same as for 1818 alone. The LOR etch rate is extremely fast and only takes seconds to etch out the undercut for the top PR layer. Therefore, removal of the 1818 PR is facilitated by the dissolution of the LOR layer underneath. This procedure for MgO/GaN diode fabrication has proven to be quite successful and is regularly used.

Processing Sc_2O_3 /GaN MOS Structures

Based on the general rules for the basicity of oxides that were given earlier, M_2O_3 oxides would be in the neutral to slightly basic range. No reactions or surface degradation was seen during the lithographical processing of the Sc_2O_3 thin films. The problem of selectivity during the dry etching of the Sc_2O_3 /GaN material system can be avoided through the optimization of the etching sequence. Figure 7-17A shows a feature after 1 minute of dry etching. Residual Sc_2O_3 can be seen remaining within the feature. An additional dry etch for 30 sec. was performed in order to remove this remaining Sc_2O_3 and can be seen in Figure 7-17B. The optical image seen in Figure 7-17B shows the outline of the residue spots seen in Figure 7-18A. After putting the substrate under the profilimeter it was discovered that all the Sc_2O_3 had been etched away and the contrast difference seen in Figure 7-17B was due to the height difference of the GaN surface

morphology. This was one of the major difficulties in the dry etching of Sc_2O_3/GaN heterostructures. The etch rate for GaN using the Sc_2O_3 dry etch conditions was significantly larger than the etch rate for Sc_2O_3. Thus, as soon as an area of the GaN surface was exposed it started etching away at an accelerated rate causing an extremely rough morphology within the etched feature. Through further experimentation of different etching time sequences, it was discovered that if the etch times were reversed, and the 30 sec. etch was done first and then the 1 min. etch was done, the non-uniform etching of the GaN surface would not occur. Looking at Figure 7-18A, after 30 seconds it appears that the Sc_2O_3 has been uniformly etched up to this point. Figure 7-18B shows the same feature after an additional 1min. etch where the Sc_2O_3 continued to etch uniformly until reaching the GaN interface. The etching carried on in a uniform manner after reaching the GaN surface and produced a smooth uniform etch profile in the GaN.

The increase in etch time was believed to cause an increase in temperature. The increased temperature led to an increase in PR decomposition and etch by-products, which then would deposit on the etching surface causing a localized difference in the etch rate. After recording the temp for different RF/ICP powers and etch times, there was no significant fluctuation in the temperature as a function of time. Between each etch step, the chamber was purged in order to cool the sample. Variation in the length of the purge step also did not alter the temperature very much. Thus, the variation in etch morphology with etch time appears not to be temperature dependent. The actual mechanism is believed to be a function of the rate of PR decomposition and etch by-product reactions. By increasing the time, the amount of by-product reactions as well as the probability of more complicated reactions is also increased. The production of etch resistant species forming and collecting on the surface increases with time. Over time, the

agglomeration of these species on the actively etching surface acts as a micromask producing a very rough and non-uniform etched surface.

Issues in the Design of GaN MOSFET Fabrication

Design of Device Pattern for Regrowth Applications

The choice for which regrowth pattern to use was not straightforward. There are many factors that need to be considered when choosing a regrowth pattern. The first is obviously the device to be fabricated. In addition to the mask layer, which contains the regrowth pattern, all the corresponding mask layers for subsequent patterning must be designed and available. There are 2 main areas of focus in designing a device pattern for regrowth applications. The first deals with issues that affect the material regrowth quality and the second concerns issues involved in device testing and characterization. Table 7-5 lists some general issues involved in the design of a mask for MOCVD regrowth.

Within a range of the above mask characteristics, the growth conditions can be adjusted so as to realize the growth of high quality material. When considering which mask to use or design, the behavior of the regrowing material needs to be accounted for. The choice in feature shape should be relatively straightforward.

The feature size is perhaps the most important. When designing the device regrowth pattern, the choice on the feature size must involve looking beyond the two-dimensional plane of the mask and focusing more on the three-dimensional size of the feature. The first step is determining the approximate depth of regrowth that will be required. Once this parameter is set, then the range of possible length and width dimensions will also be determined. Figure 7-19 illustrates the relationship between the feature dimensions and the growth behavior. For features whose length and/or width are not balanced with the depth of the feature, poor quality growth will result.

The size of the regrowth features and their spacing are intimately linked on the effect of the growth rate. When examining them together locally within a uniform pattern they could be viewed as the local pattern fill factor (θ). It is possible that if the feature is too small and the spacing between the features is too large, no amount of optimization of the growth conditions can be done in order to achieve good quality material. In Figure 7-20, the growth rate of features of different sizes for the same growth is plotted. From the plot, it can be seen that when the area to be regrown becomes too small and their spacing is too large, the growth rate increases at an extremely large rate. In order to decrease the growth rate, the flow of TMG would be decreased until the desired rate of growth is achieved. The problem is that when the TMG is reduced beyond a certain point, growth is severely diminished and for TMG flow rates above this point, the growth rate is excessively large. There is no range of TMG flow rates in between the two growth extremes that will produce material of good quality. Growth conditions could be altered to produce a reasonable growth rate but it would be at the expense of material quality. By adjusting the other growth conditions, the system would change from the optimal growth regime for selective area growth (SAG) and thus the growth behavior would be altered, producing undesirable results.

The pattern fill factor might seem that it is a combination of the two previous mask traits, but this not necessarily the case. The pattern fill factor is a measure of the pattern as a whole. If a new mask is being designed explicitly for this purpose and the regrowth feature is the only one on the mask, then the determination of the feature size and spacing is equivalent to choosing a fill factor. When the regrowth feature is not the only one on the mask, then the pattern fill factor will have to be considered as well. Particularly, if there are very large areas of the mask that are

either completely open or completely covered. Any features adjacent to these areas will grow significantly different from the others

After the material has been regrown, its needs to be characterized. The material's electrical properties could be determined by performing all the processing steps to fabricate the end device and then test it. This is not practical at the research or industry level. Also, testing the performance of the complete device won't necessarily characterize the properties of the regrown material if poor results are obtained. It will be too difficult too determine which step in the fabrication process is the source of the poor performance. Thus, in addition to the processing required for the main device, the processing of a simpler test structure must be also factored in and designed. An example of a mask attribute that could become an issue is that of the feature size. Even if the feature size is not an issue for the testing of the final device, it may become a problem when the electrical properties of the regrown material are to be tested. The feature that will serve as the device must also be the one tested, even if they are part of the same regrowth mask. A different size or shape of the feature could change the growth quality and dopant incorporation. Thus, when determining the feature size for the device, the ability to produce a test structure for measuring the electrical properties of the regrown material should be considered. Within the size range required by the physics of the device, there are a few issues related to the feature size. If the feature size is too small, it may be too difficult to test manually with probes. At a minimum, the creation of a test structure will require the deposition of metal contacts. A contact layer of the mask set could be used for this, depending on its alignment with the regrowth layer. Essentially, it is the size of the contact that determines the feasibility to test the device, and so the feature size needs to be at least the same size as the contact. If the feature size is too large, there may be issues with processing, especially if dry etching is required. The

larger the area that is needed to be dry etched, the more likely defects will occur or particulate matter will deposit on it.

Several different regrowth patterns were investigated for regrowth. Three typical patterns that were used are shown in Table 7-6 along with their fill factors and pitch dimensions. The first pattern was the mask layer for the deposition of ohmic contacts for the source and drain of a MOSFET. This mask seemed ideal for device fabrication but the θ was too small and made the growth rate much too fast to control. Also, the feature size was too small to correctly deposit contacts without misalignment as well as test using probes. The second pattern shown was good for regrowth due to the larger feature size, but there wasn't a corresponding mask layer for making a device test structure. The third pattern was chosen because of the large feature size which was favorable for regrowth and allowed for testing. The main reason why the third pattern was chosen because the mask set was for fabricating a MOSFET and had several additional layers within it that allowed for flexibility in design of the processing sequences for the test structure and final device.

Design of a Processing Scheme for the Fabrication of p-GaN MOSFETs

A processing sequence has been developed around using the optimized regrowth conditions to regrow p^+ GaN into the areas that will serve as the source and drain for the p-MOSFET. As was mentioned earlier, the regrowth mask intended for use a final metal deposition layer of a MOSFET device. The complete set of masks contains all the necessary layers for the complete fabrication of a MOSFET device. The specific processing sequence designed uses these layers for the critical fabrication steps ensuring the perfect alignment of the key areas to be processed. Thus, the complete procedure for the fabrication of the p-MOSFET device is not a general theoretical approach but is instead the blueprint for the actual production of a functioning device. The critical area of interest on the device has been illustrated during each of the steps in

the processing sequence. The exact location with respect to the complete pattern unit used for regrowth is shown in Figure 7-21. The general steps of the complete processing sequence are illustrated in Figure 7-22.

The starting point is with a lightly n-type doped GaN substrate grown by MOCVD with at least 500 Å to 1000 Å of Sc_2O_3 grown at a temperature of approximately 600^0C. An alternative oxide could easily be substituted for Sc_2O_3 for the regrowth mask as long as it has proven to be environmentally stable during the growth and processing steps. Next is the deposition of the regrowth pattern using standard photolithographic techniques using a thick photoresist with a sufficiently long hard bake time to be able to withstand the large amount of dry etching needed. The areas that are chosen to be the p-MOS source and drain will be selectively dry etched using Cl_2 plasma chemistry. The etching was broken up into 30 sec. steps to avoid non-uniformity of the etched surface. After dry etching, removal of the PR etch mask must be performed well. Even after a hot acetone bath with sonication, the presence of PR residue was unavoidable. High temperature sonication in Microposit Remover 1165© for extended periods of time has proven to be successful. However, under certain dry etch conditions, no amount of surface treatment could remove the PR residue. The use of a particularly dry etch resistant PR could prove more successful but it may be necessary to use a different material, such as Ni, for an etch mask.

The process that was optimized for the p^+ regrowth by MOCVD will then be used to make the p-MOS source and drain. After an activation anneal in an RTA at 750^0C for 5 minutes under N_2, a device test structure should be fabricated. The test structure is then measured to confirm the desired properties of the regrown material. The patterning of the metal deposition mask for the source and drain ohmic contacts and metal deposition would be the same standard

method used for contact deposition on ion implanted regions. For the use of Sc_2O_3, it may be necessary to remove the surface of the regrowth mask before deposition of the gate oxide. If a conductive layer of ScN has formed during the regrowth step this could be detrimental to the device's performance. The remaining steps in the fabrication sequence would use standardized techniques used in industry for processing.

Integration of p-MOSFET Device Processing into the Fabrication of a CMOSFET Device

After the successful development of GaN n and p-MOS technology, the next step will be to apply this technology towards developing a GaN CMOSFET device. The general steps of two proposed processing sequences for a GaN CMOSFET device are illustrated in Figure 7-23. The first step will be to grow a p-GaN/semi-insulating GaN structure by MOCVD that will serve as the substrate. The second step involves producing the n^+ source and drain regions for n-MOSFET portion of the device. After depositing and patterning a mask on the substrate that exposes the desired regions, the n^+ regions will be produced by ion implantation of $^{29}Si^+$ at large enough doses to compensate the acceptors in the p-GaN substrate and make the regions heavily n-type. A high temperature anneal would normally be performed after the implantation in order to activate the implanted species. In this processing sequence the activation of the n-type carriers will be performed in a later step. The next step will be producing n^- regions that will serve as the channel for the p-MOSFET portion of the device as well as isolate it from the substrate. This process will be similar to the previous step except that the doses of $^{29}Si^+$ will be smaller since the regions need only be weakly n-type.

The novel step in this processing sequence is producing the p^+ regions for the p-MOSFET source and drain through MOCVD regrowth. The same general procedure that was previously described for the fabrication of a p-MOSFET using MOCVD regrowth can be applied here. An added benefit is that the regrowth step will serve as the activation step of the n-type carriers as

well. Also, by performing the activation anneal in the MOCVD growth environment, decomposition of the surface is less likely. If a relatively unstable gate oxide is used, another benefit would be that this step precedes the deposition of the oxide and thus avoids any possible environmental stability issues with the oxide.

The alternative processing sequence that was also illustrated in Figure 7-23 would be used if the dielectric oxide was shown to be thermally stable. This sequence is primarily the same as the other except that the oxide would be deposited earlier in order to protect the surface of the channel regions from degradation. Maintaining a good quality interface between the oxide and GaN for the gate regions is essential for minimizing the D_{it}, which is critical to device performance. The optimal sequence chosen should be based on the dielectric's ability to withstand the thermal and chemical environment of the complete fabrication process.

Table 7-1. General processes involved in MOSFET device fabrication.

- Epitaxial growth of device layer onto substrate
- Oxide deposition
- Deposition and patterning of masks (photolithography)
- Ion implantation of source and drain regions
- Implant activation anneal
- Metal contact deposition
- Ohmic contact anneal
- Isolation (Dry etch)

Table 7-2. Index of the acid-base reaction strength based on the parameter Δ.

(Δ) Magnitude	(Δ) Sign	Strength of Acid-Base Interactions
Large	(-)	Weak, negligible acid-base forces
Large	(+)	Strong, possibly resulting complete reaction between polymer and oxide surface
Small	(-) or (+)	Acid-base forces are comparable to the dispersion force component between the two phases

Table 7-3. General trend of IEPS values for oxides.

Oxide	Cation charge	IEPS range
M_2O	+1	11.5 < IEPS
MO	+2	8.5 < IEPS < 12.5
M_2O_3	+3	6.5 < IEPS < 10.4
MO_2	+4	0.5 < IEPS < 7.5
M_2O_5	+5	IEPS < 0.5
MO_3	+6	IEPS < 0.5

Table 7-4. Acid-base reaction parameters of commonly used oxides in the electronics industry.

Oxide	IEPS	Acidity/Basicity	Δ (pK_a =4.5)
MgO	12	Basic	7.5
Al_2O_3	8	Neutral	3.5
SiO_2	2	Acidic	-2.5

Table 7-5. Factors involved in the design of a mask for MOCVD regrowth.

Mask attributes	Regrowth issues	Device Issues
Feature shape	No rounded edges	Device performance
Feature size	Effect on growth rate and morphology	Device performance Ability to test the regrown structure's electrical properties
Feature spacing	Effect on growth rate and unintentional growth between features	Device performance Ability for subsequent unproblematic processing steps
Pattern fill factor (θ)	Effect on growth rate within the feature of interest	Device performance

Table 7-6. The different masks used for selective regrowth of GaN.

Mask Pattern	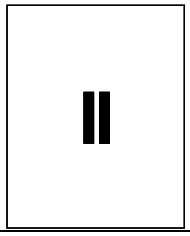	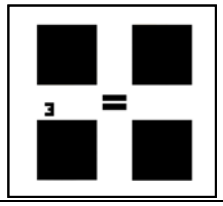	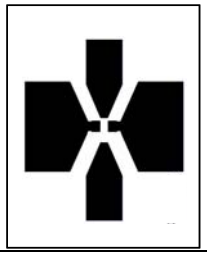
θ	.018	.337	.351
Pitch Dimensions	405 x 550μm	260 x 260μm	400 x 520μm
Type of Mask	MOSFET n^+ ohmic metal layer	Ohmic metal layer	MOSFET final metal layer

A

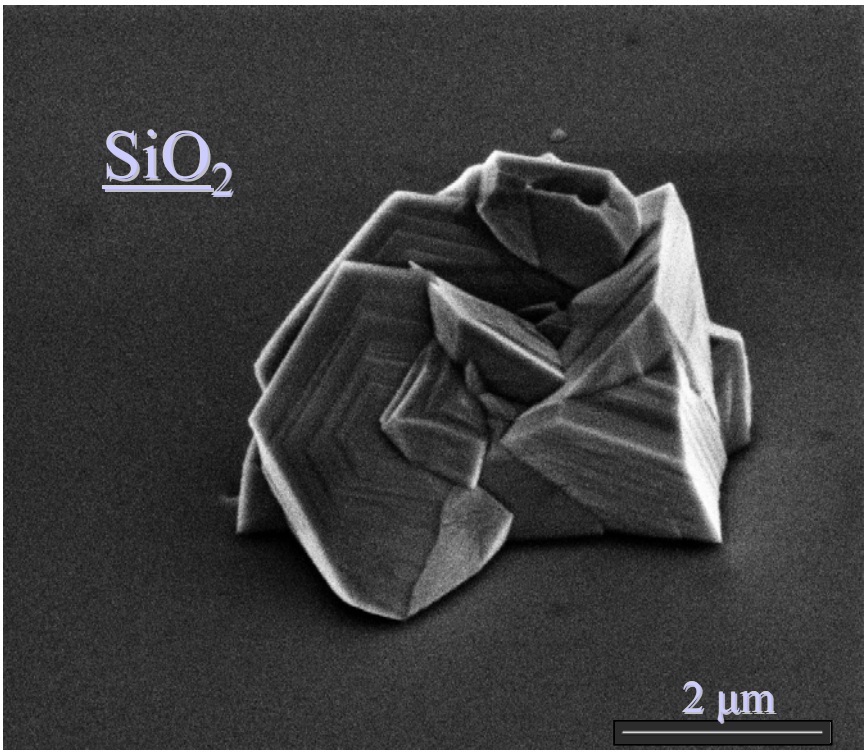

B

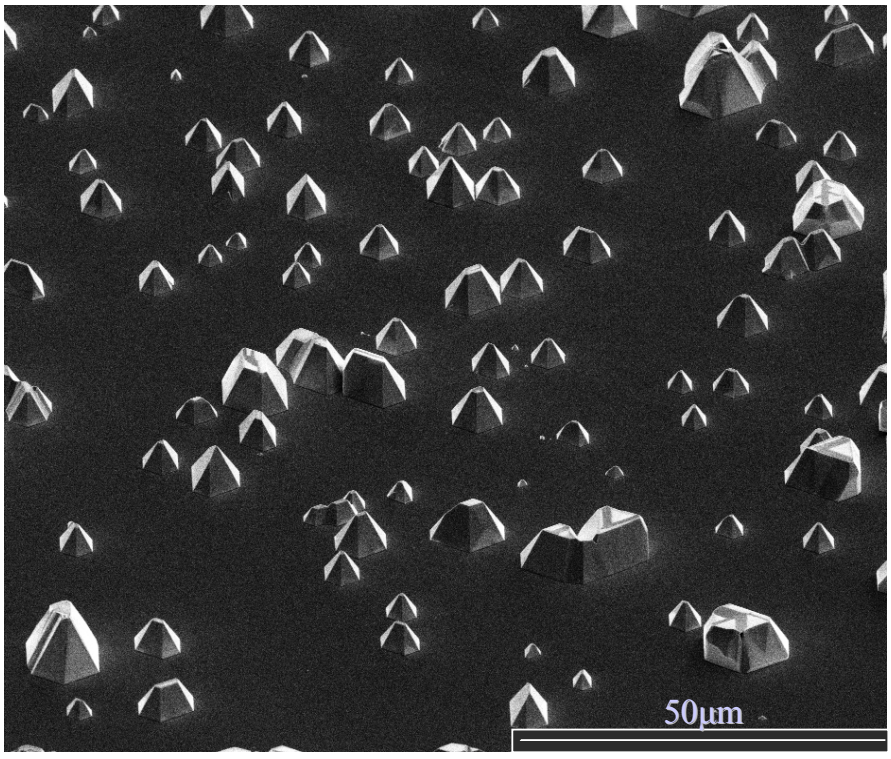

Figure 7-1. Example of regrowth occurring through the mask. A) Non-uniform deposition produced a small exposed area in the mask. B) Decomposition of a mask that was too thin.

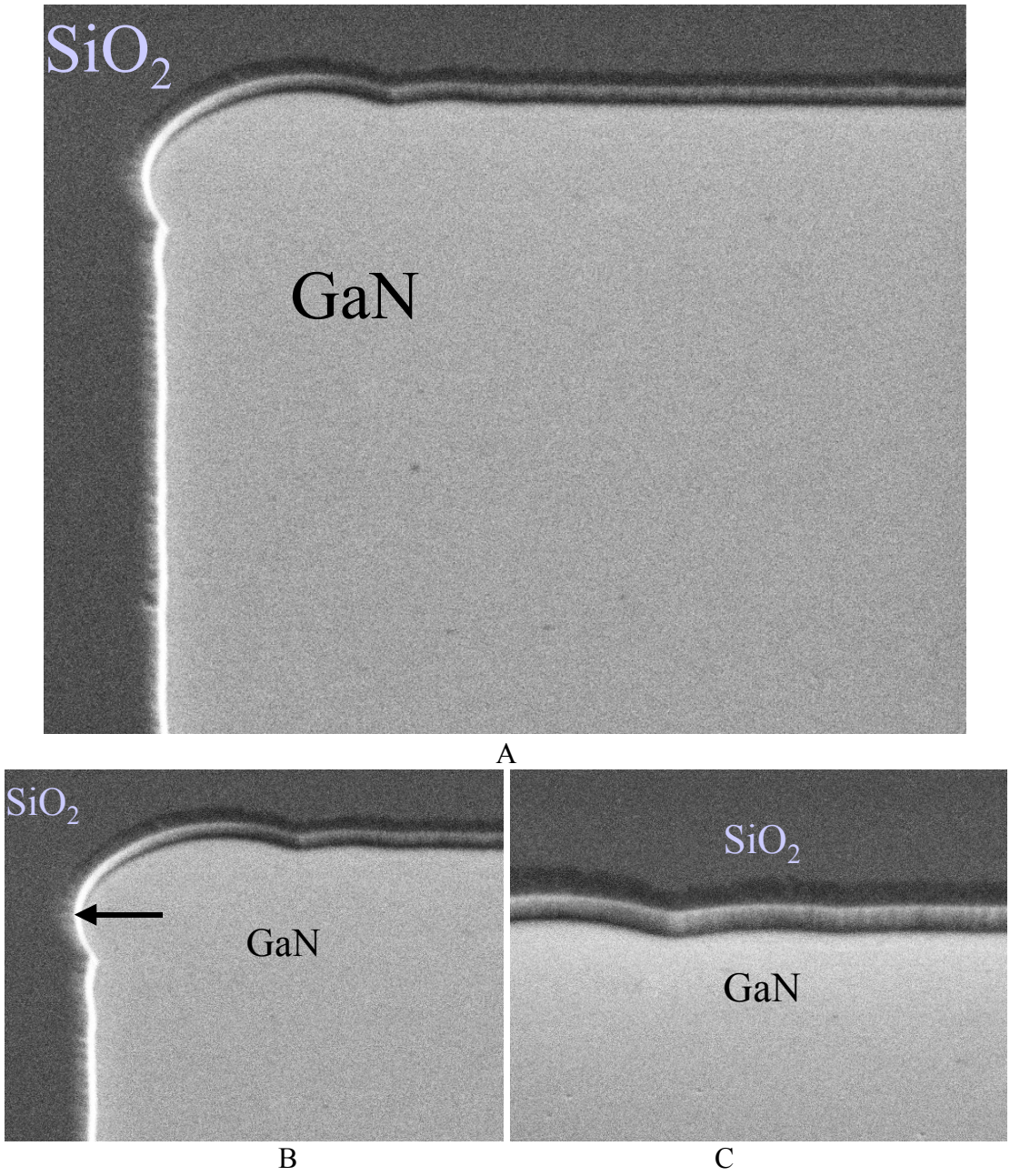

Figure 7-2. SEM images of a processed SiO_2/GaN substrate for regrowth. A) Substrate was processed using the optimized SiO_2 wet etch conditions. B) Image shows that the SiO_2 has a very minor undercut resulting from the wet etch. C) Higher magnification image showing the well-defined edges and smoothness of the etched feature.

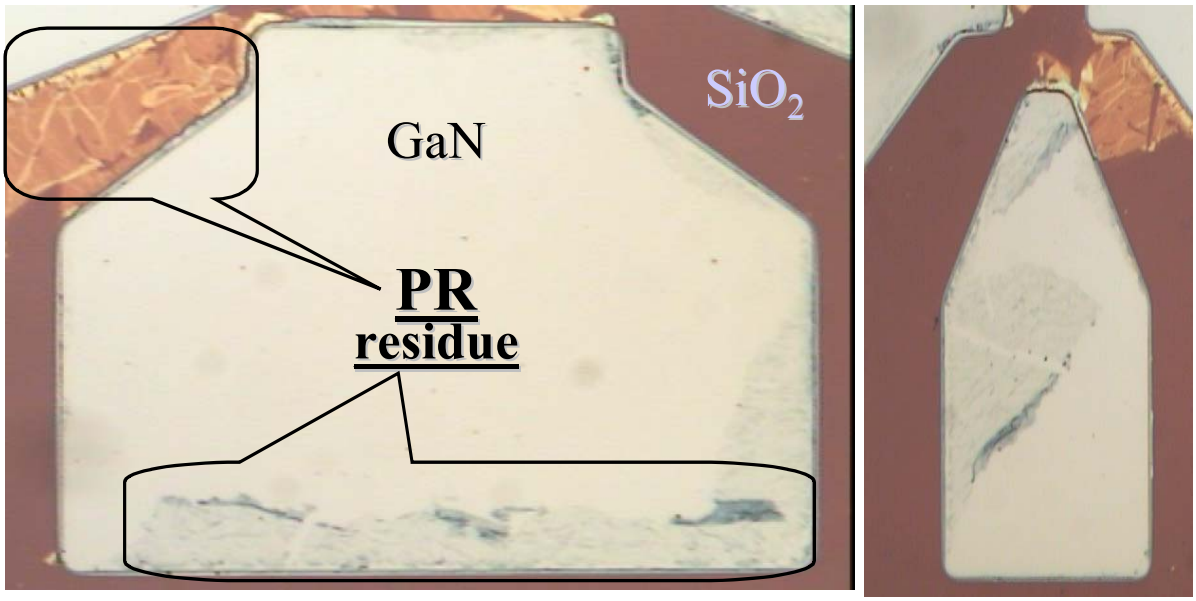

A

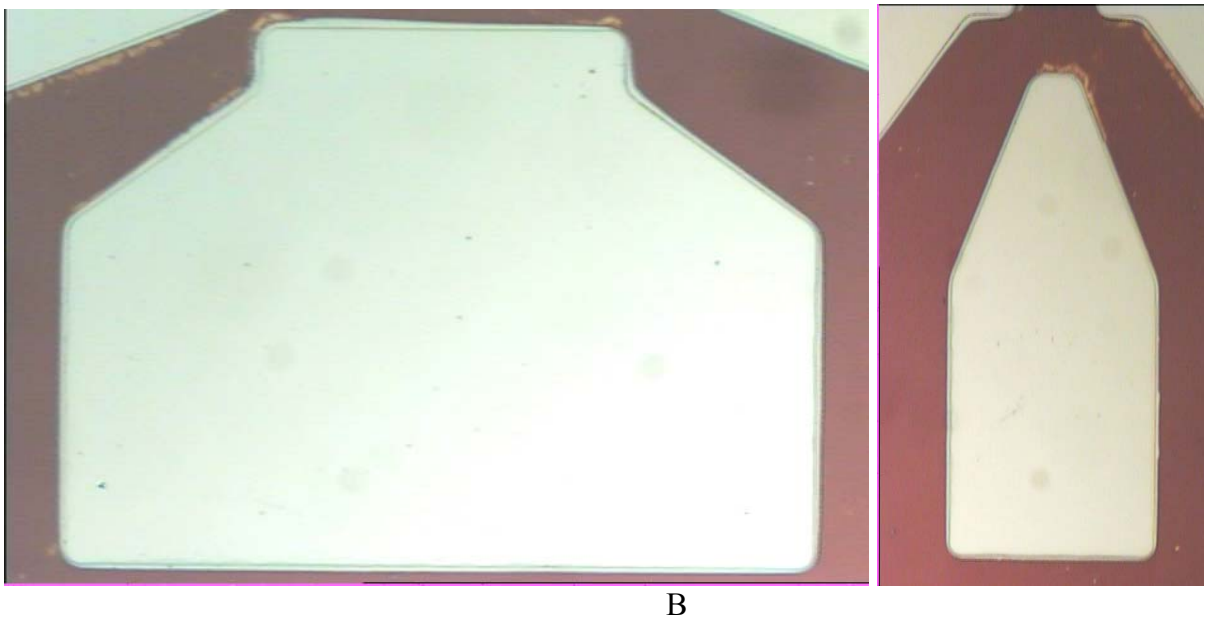

B

Figure 7-3. Effects of O_2 plasma cleaning. A) Before O_2 plasma cleaning. B) After O_2 plasma cleaning.

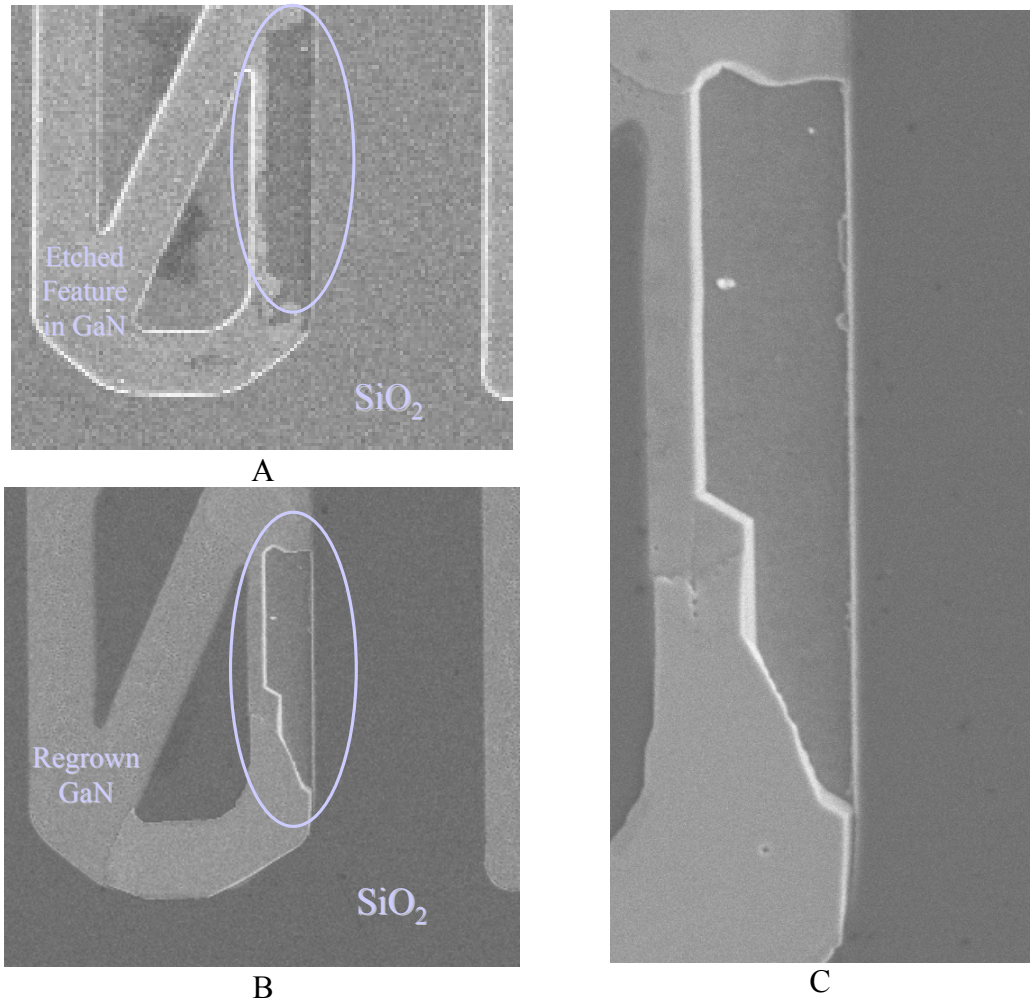

Figure 7-4. Effect of residual photoresist on regrowth behavior. A) Etched substrate before regrowth. B) Same location in (A) after regrowth. C) Magnified view of location in (B).

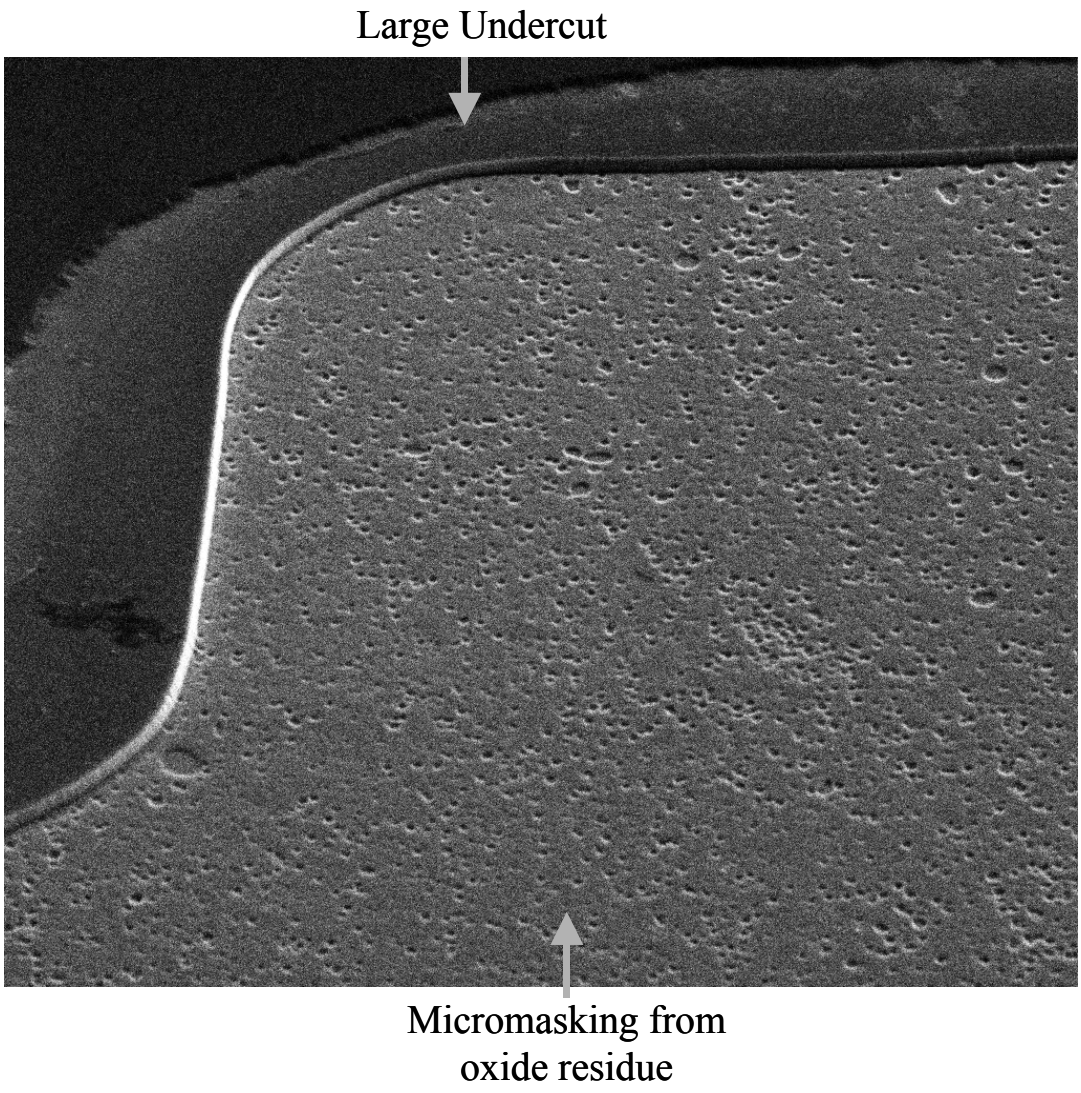

Figure 7-5. Problems encountered in oxide/GaN heterostructure processing using a wet etch to remove the oxide.

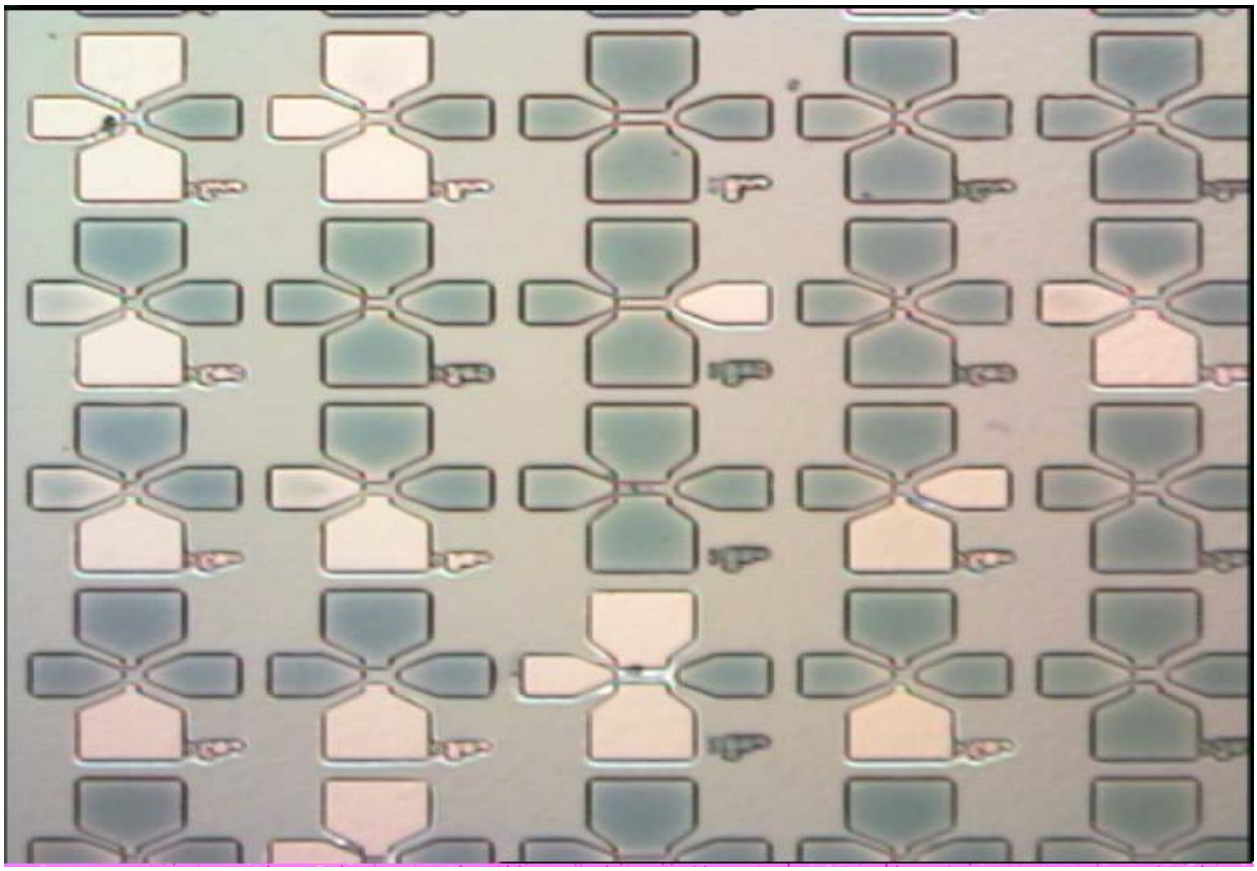

Figure 7-6. Optical image showing the non-uniform removal of SiO_2 from within the patterned features.

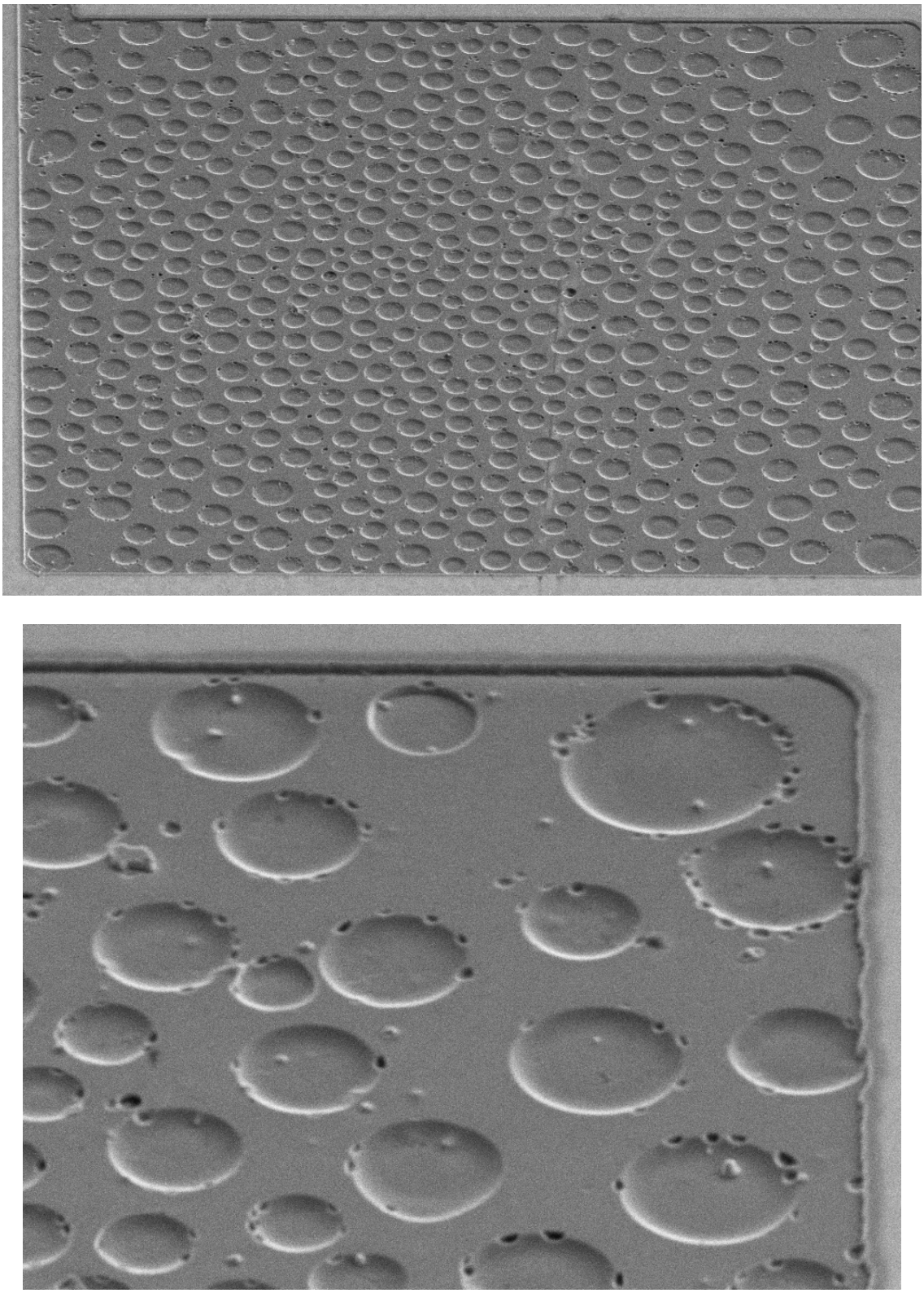

Figure 7-7. GaN surface damage from excessive SiO_2 etching.

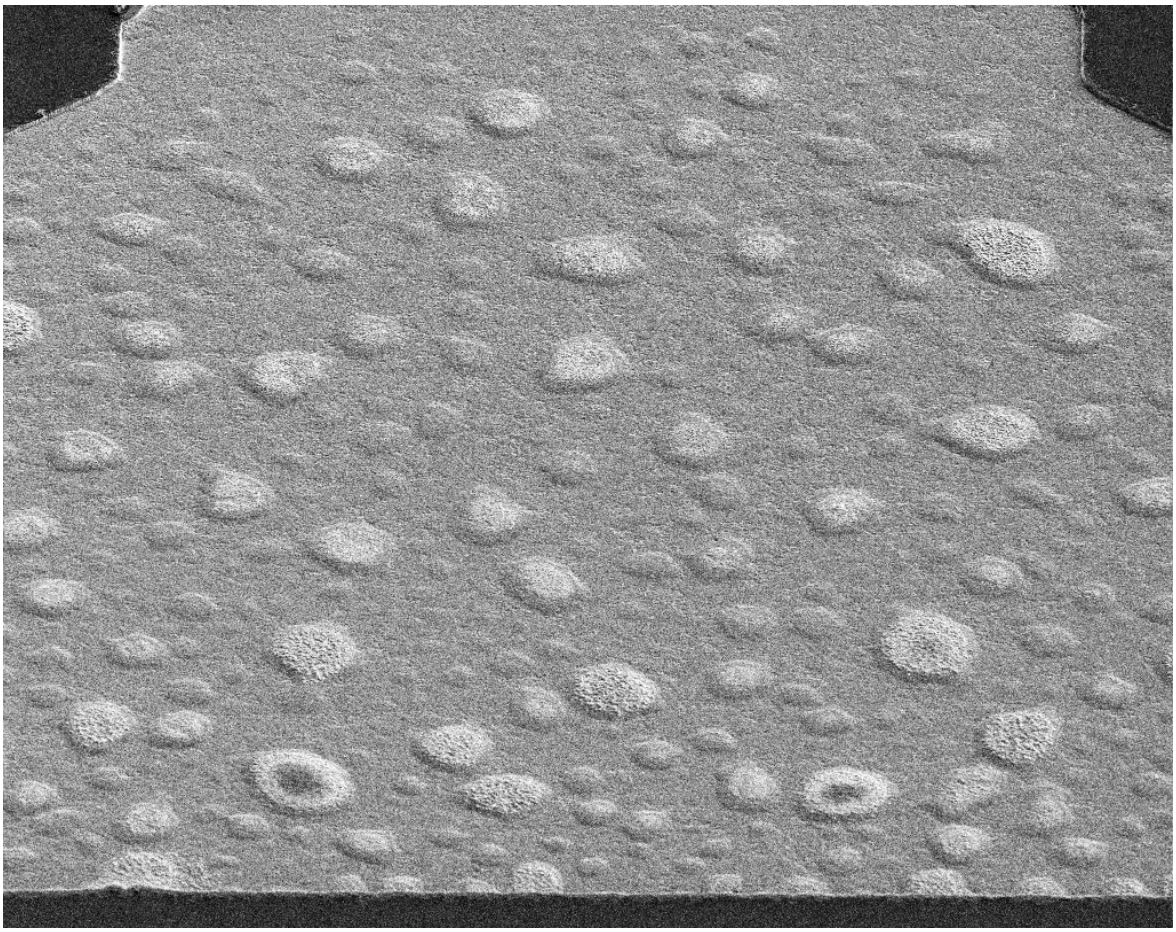

Figure 7-8. SEM image of a very rough etched GaN feature due to the non-uniform etch of Sc_2O_3.

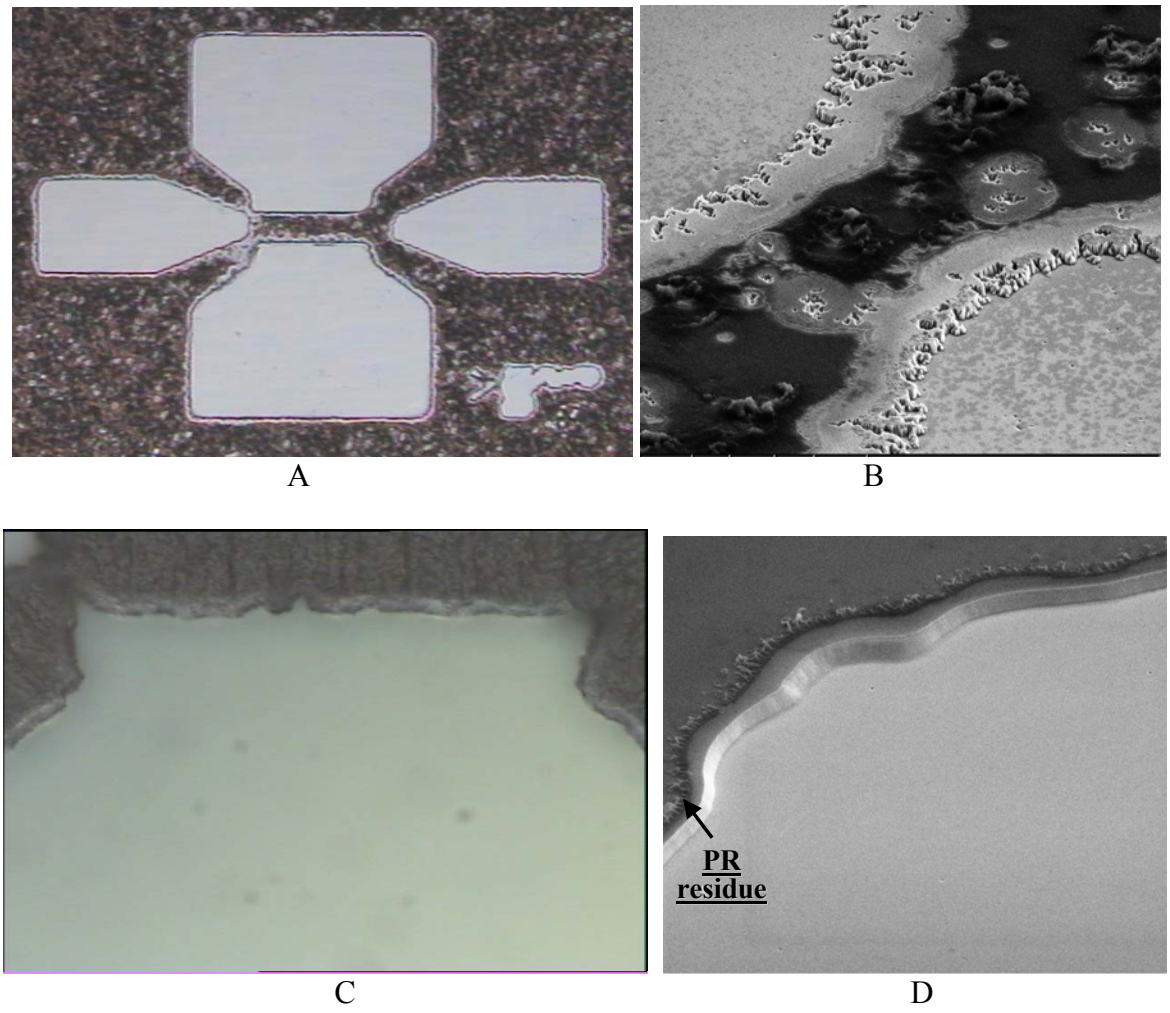

Figure 7-9. Images of PR decomposition and its detrimental effects during the dry etching of MgO/GaN. A) Optical image of patterned MgO after all dry etching has been performed. B) SEM image of the surface of sample in (A). C) Optical close up showing PR decomposition. D) SEM image of sample in (C) after removing the PR.

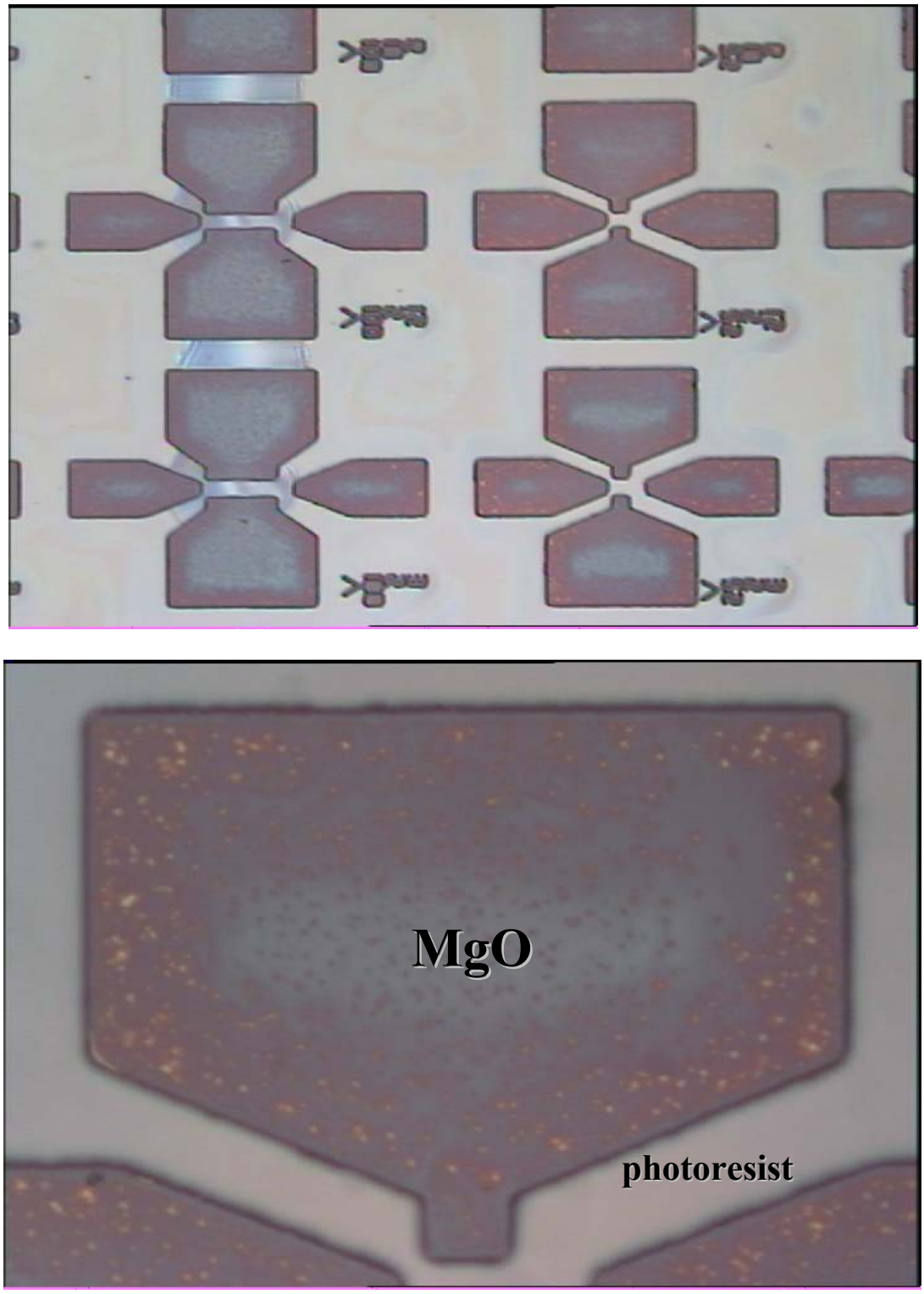

Figure 7-10. Optical image of a patterned feature in photoresist on a thin film of MgO that was processed using standard photolithographic techniques.

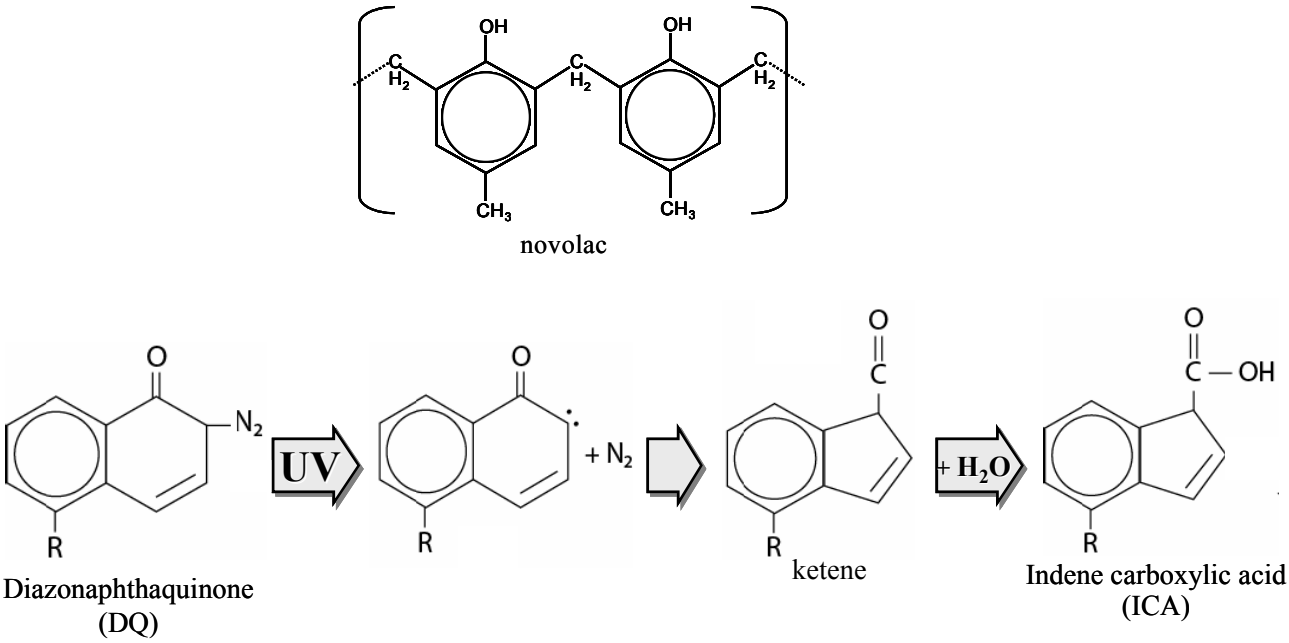

Figure 7-11. Main components of a positive photoresist and the main chemical reactions involved in photoresist exposure.

Possible reactions upon exposure

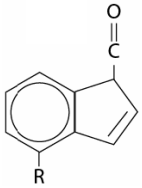

+ H_2O →

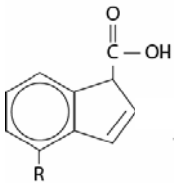

+ H^+ (1)

$MgO + H^+ \rightarrow MgO{\bullet}H^+ \rightarrow Mg^{2+} + OH^-$ (2)

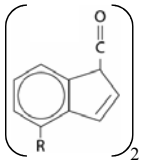

+ $Mg(OH)_2$ →

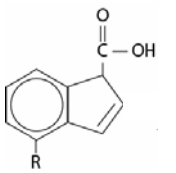

+ Mg^{2+} (3)

In Developer Solution

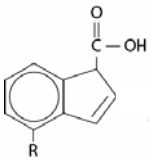

+ OH^- →

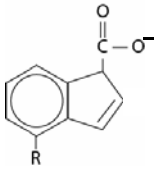

+ H_2O (4)

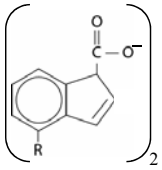

+ Mg^{2+} →

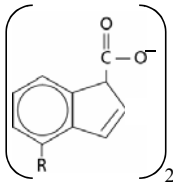

Mg^{2+} (5)

carboxylic acid salt

Figure 7-12. Possible reactions between the photoresist and MgO surface during the exposure and development steps using standard lithographic techniques.

$$(111)_{MgO} \parallel (0001)_{Mg(OH)_2}$$

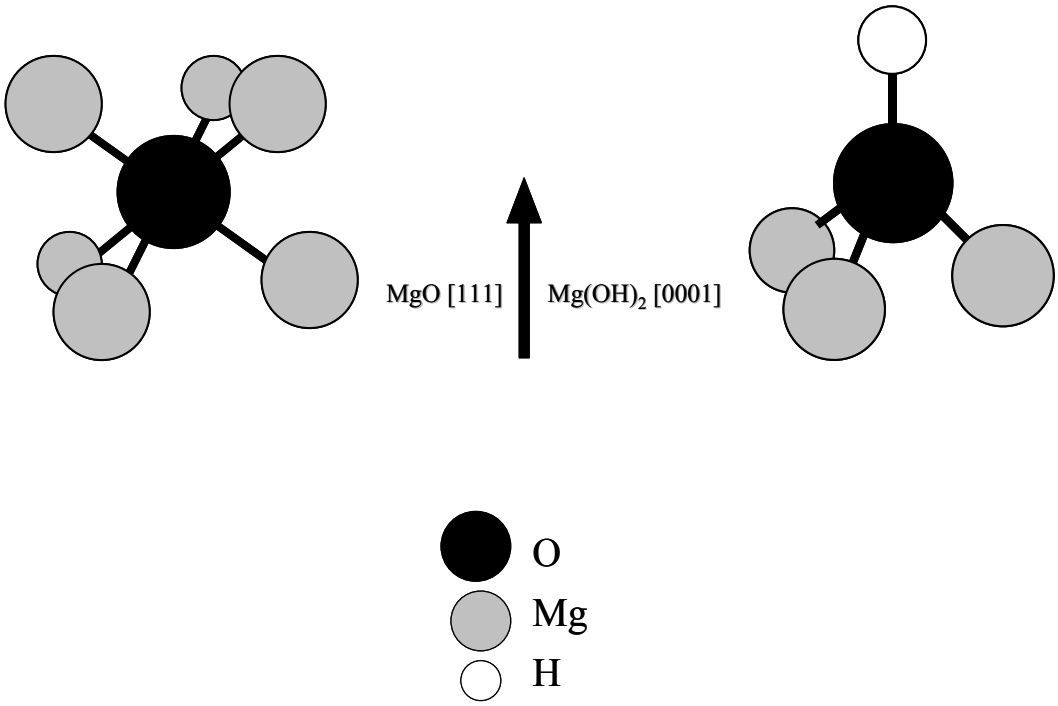

Figure 7-13. Orientation relationship between MgO and $Mg(OH)_2$ and their bonding arrangement.

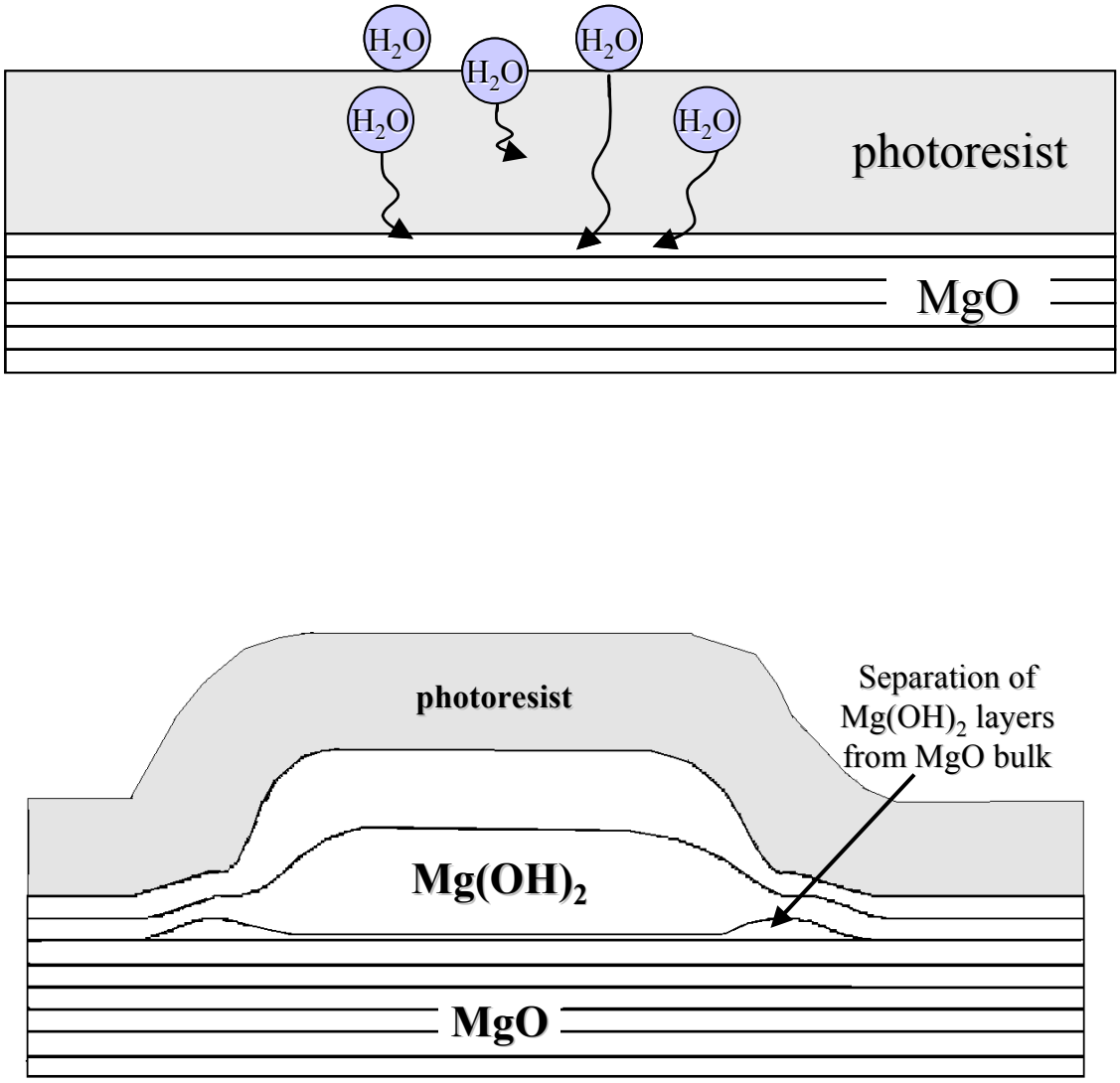

Figure 7-14. Hydrolsis of photoresist and $Mg(OH)_2$ formation, causing the separation of the photoresist from the MgO film.

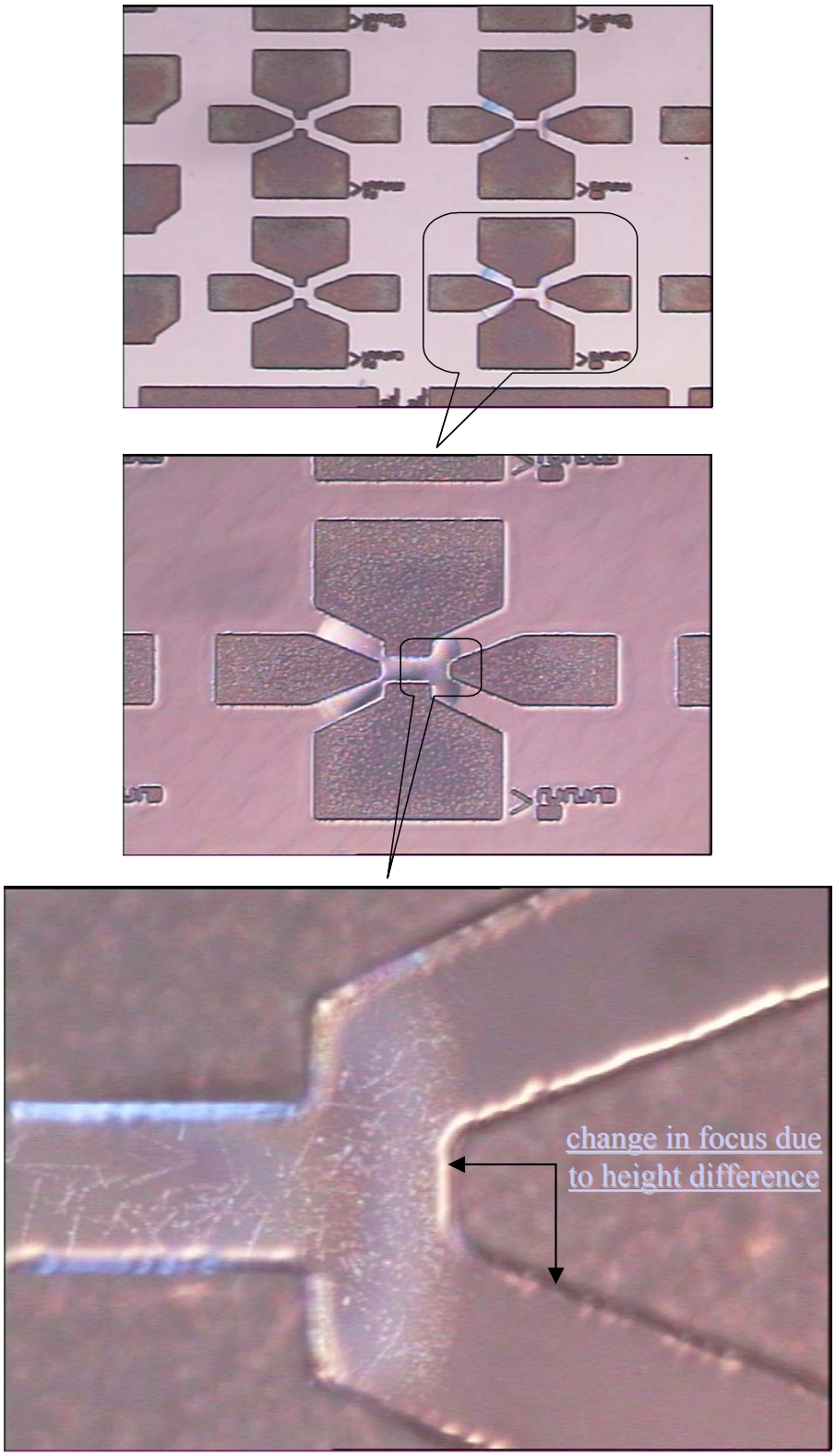

Figure 7-15. Optical images of patterned photoresist on MgO immediately after processing.

A

B

Figure 7-16. Metal contacts on MgO. A) Example of a well processed and uniformly deposited contact. B) Example of incomplete removal of the LOR/1818 bilayer within the contact area.

A

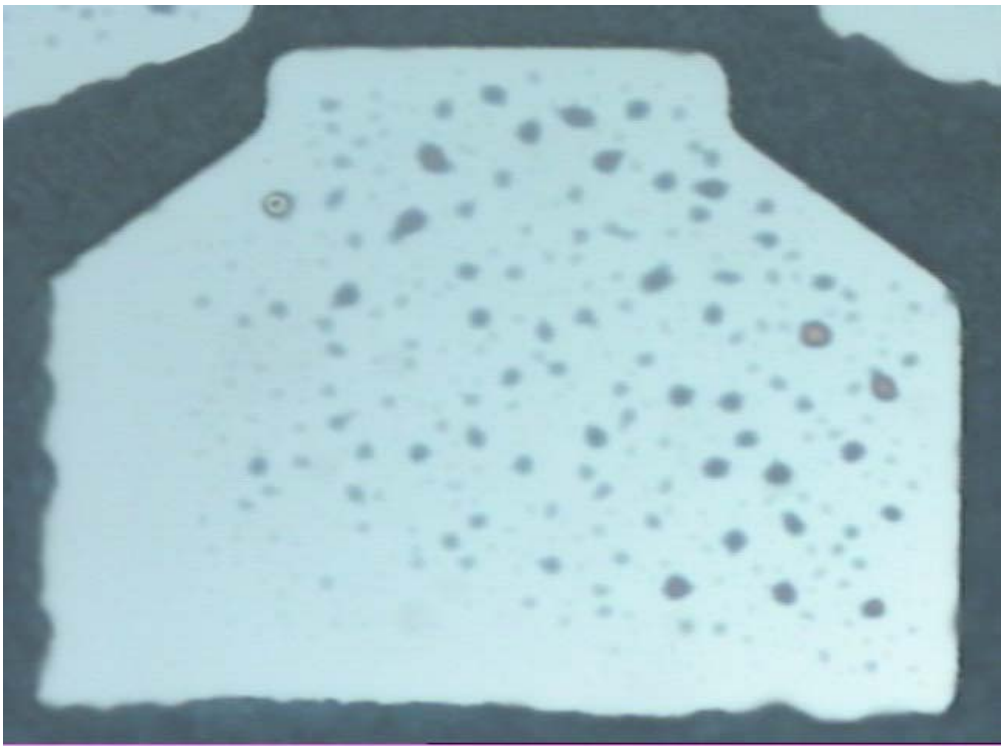

B

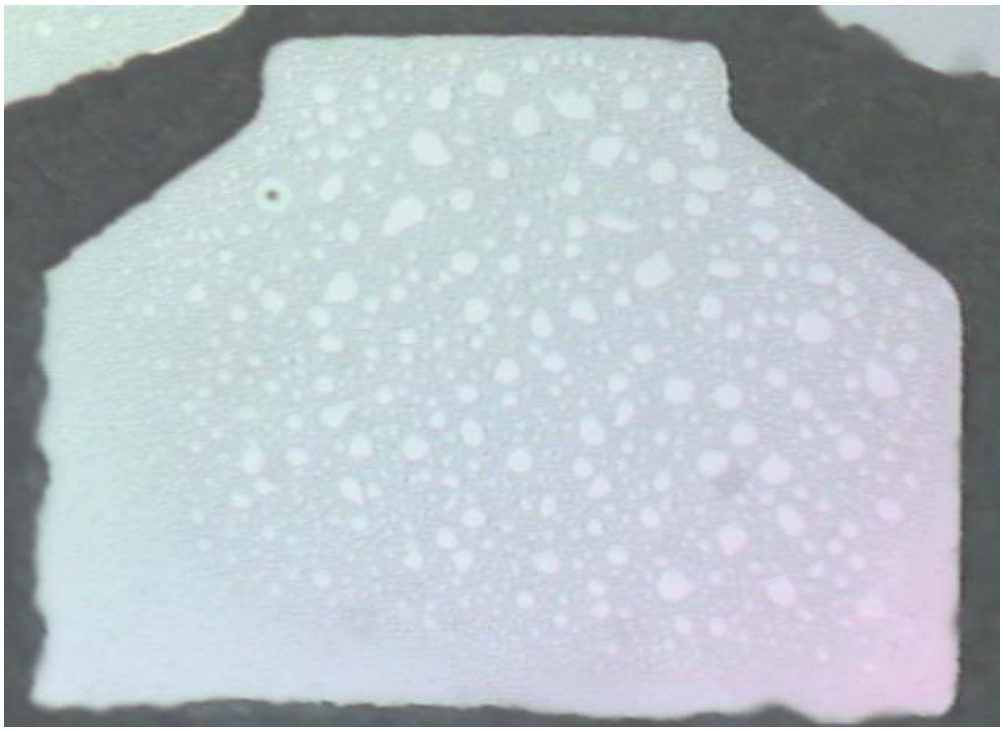

Figure 7-17. Optical images of a specific feature during Sc_2O_3 dry etching. A) After a 1 min. dry etch. B) After an additional 30 sec. dry etch.

A

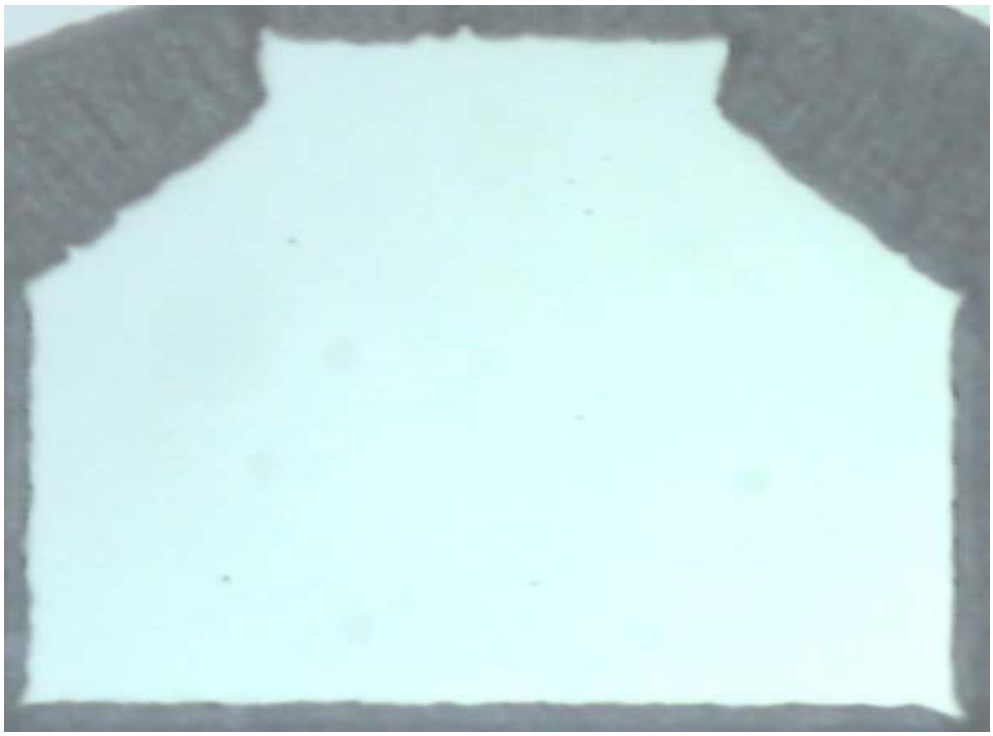

B

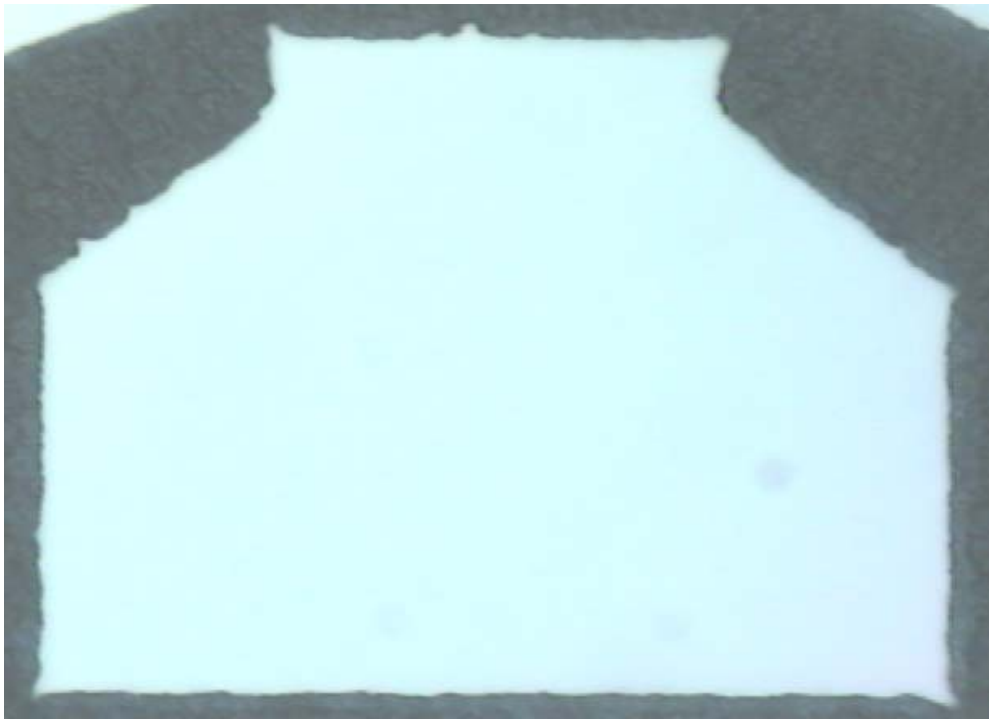

Figure 7-18. Optical images of a specific feature during Sc_2O_3 dry etching. A) After a 30 sec. dry etch. B) After an additional 1 min. dry etch.

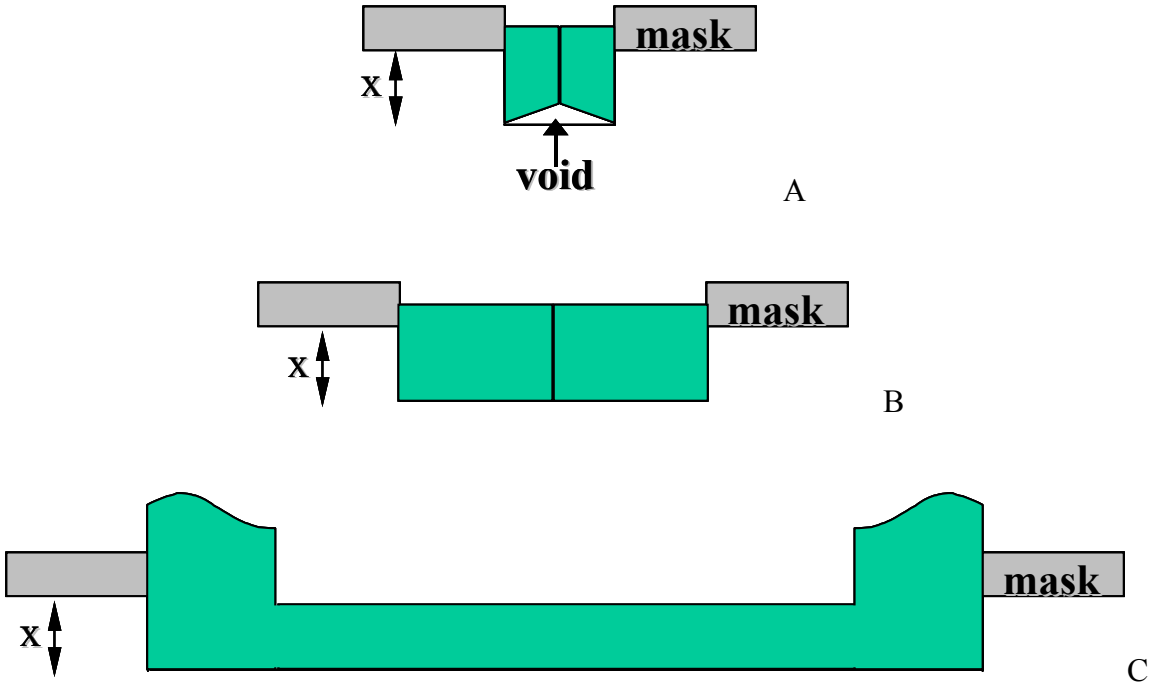

Figure 7-19. Relationship between feature dimensions and regrowth quality for a set depth of x. A) Feature width is too small. B) Feature width is optimal. C) Feature width is too large.

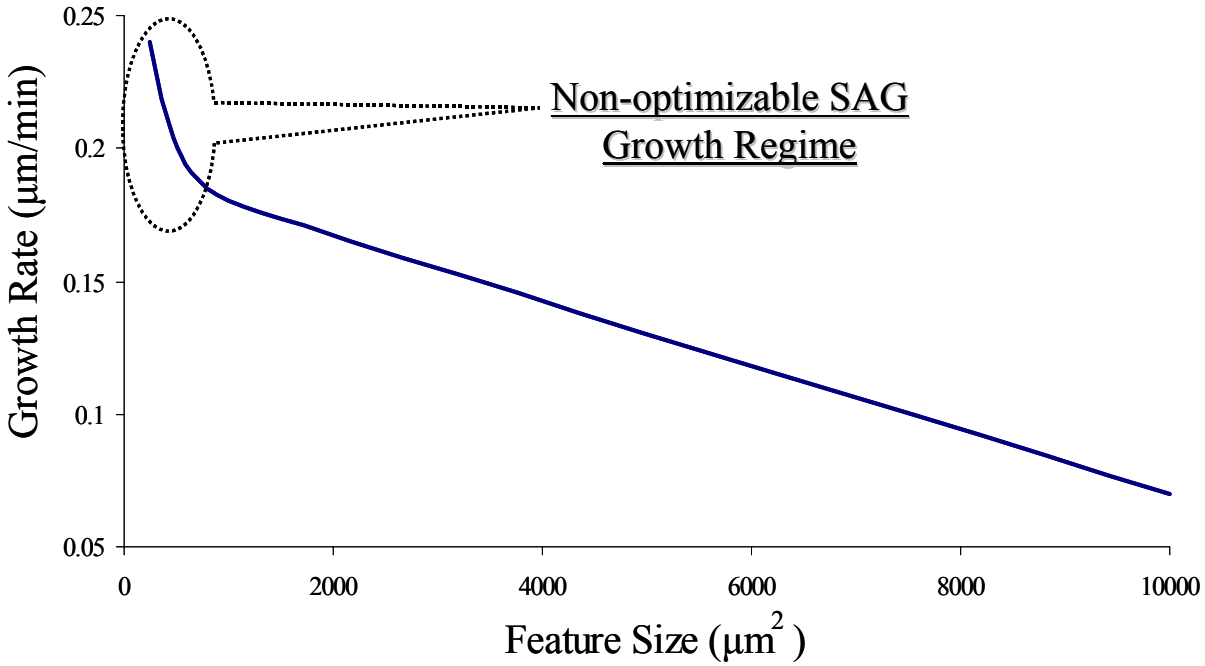

Figure 7-20. Relationship of the growth rate to the feature size for a given θ.

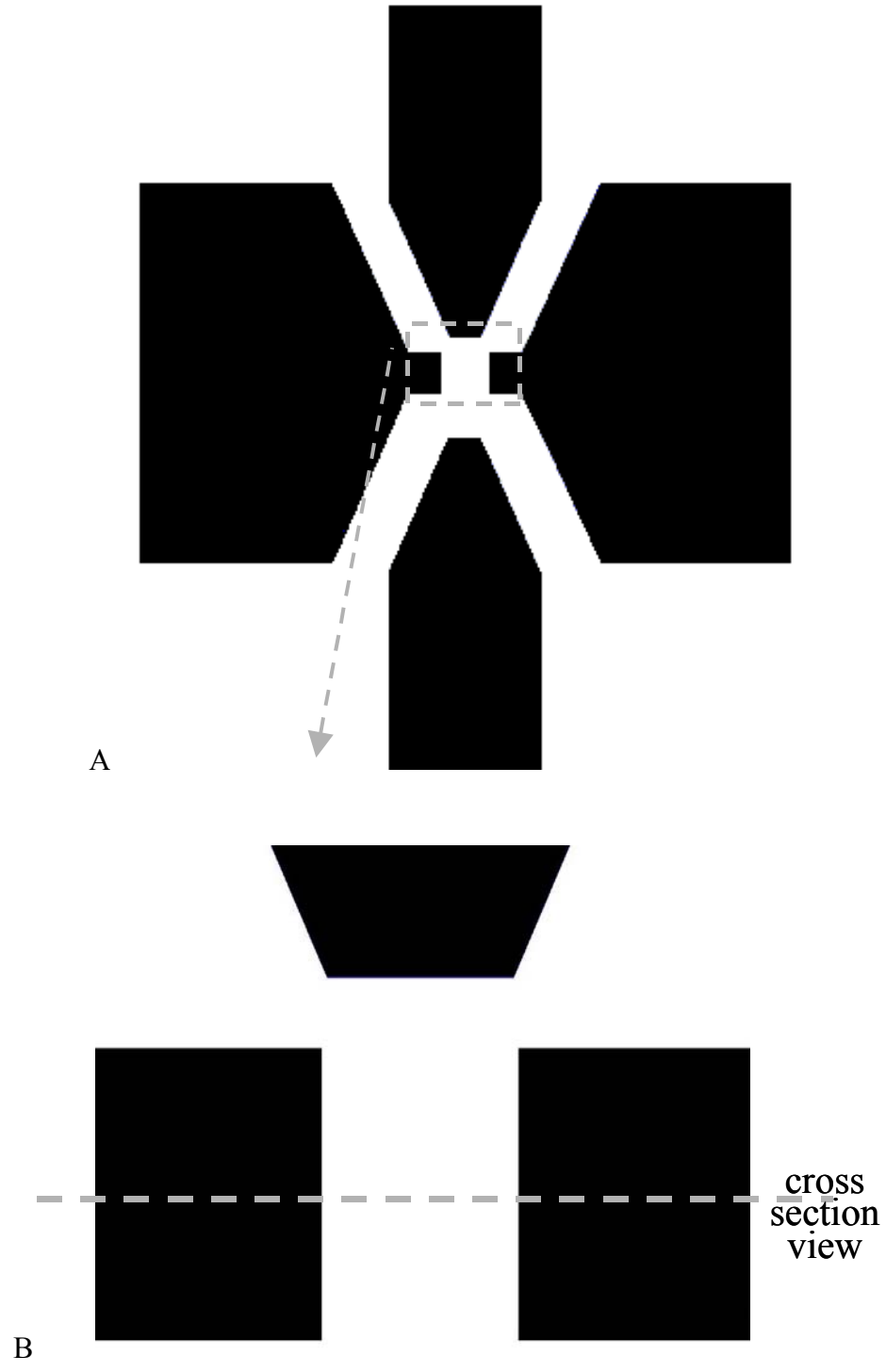

Figure 7-21. Description of area shown in the processing sequence figures. A) Section of total regrowth feature being shown in the p-MOSFET processing sequence. B) Origin of the cross section view.

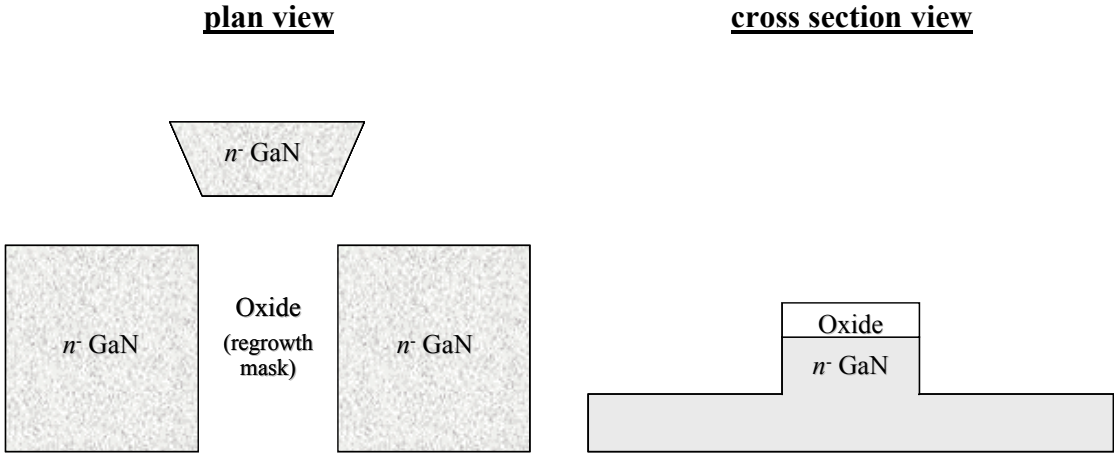

Step 1. Etch the source and drain regions into the oxide and GaN substrate

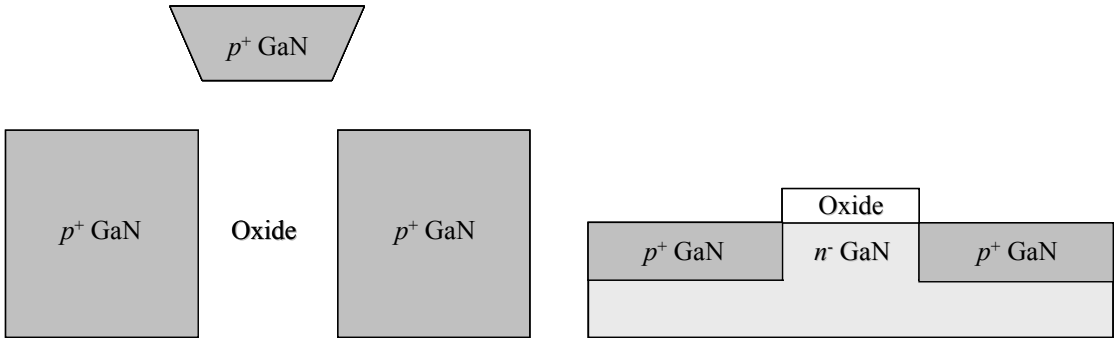

Step 2. Regrowth of the p^+GaN source and drain

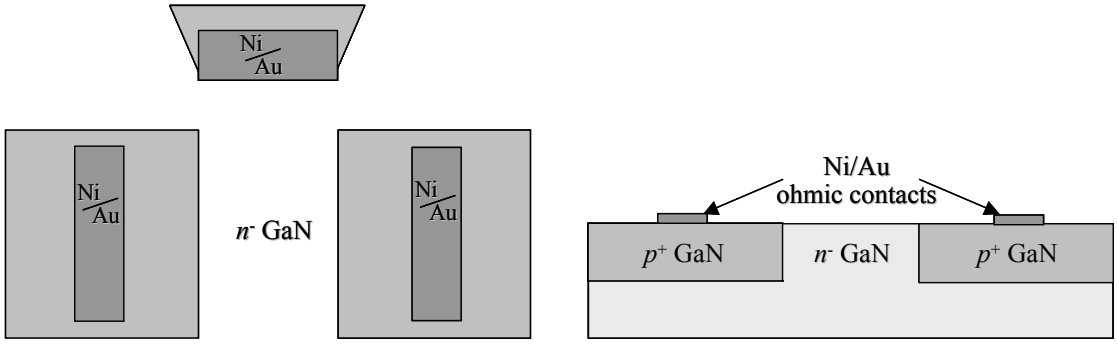

Step 3. Deposition of the source and drain ohmic contacts

Figure 7-22. Processing sequence for a GaN p-MOSFET.

plan view **cross section view**

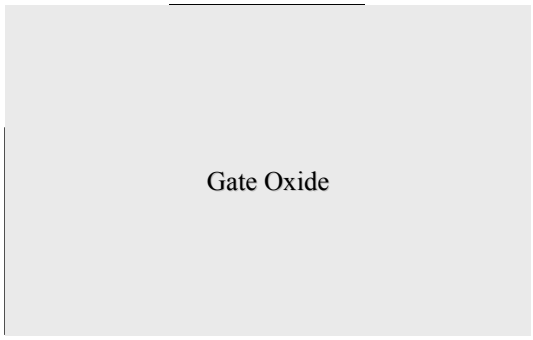

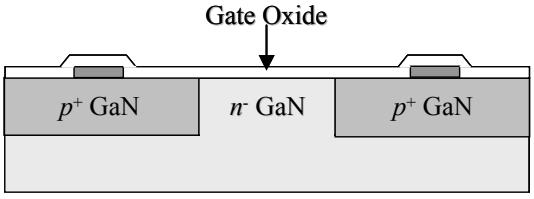

Step 4. Deposition of the gate oxide

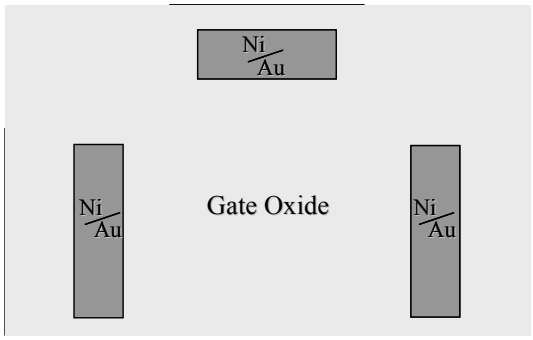

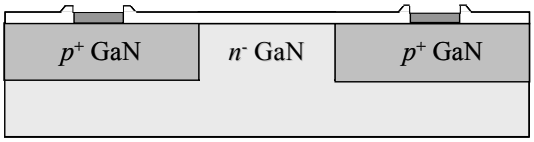

Step 5. Etch windows into the oxide

Figure 7-22. Continued.

plan view **cross section view**

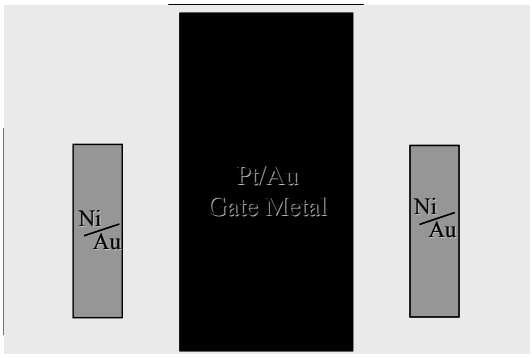

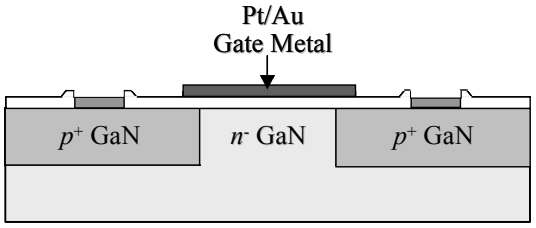

Step 6. Deposition of the gate metal contacts

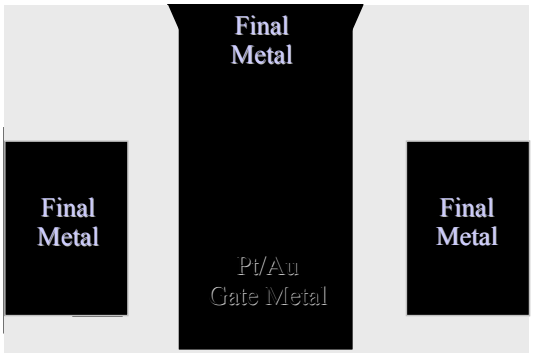

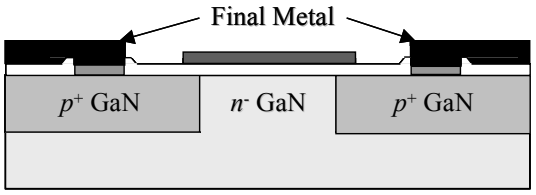

Step 7. Deposition of the final metal contacts

Figure 7-22. Continued.

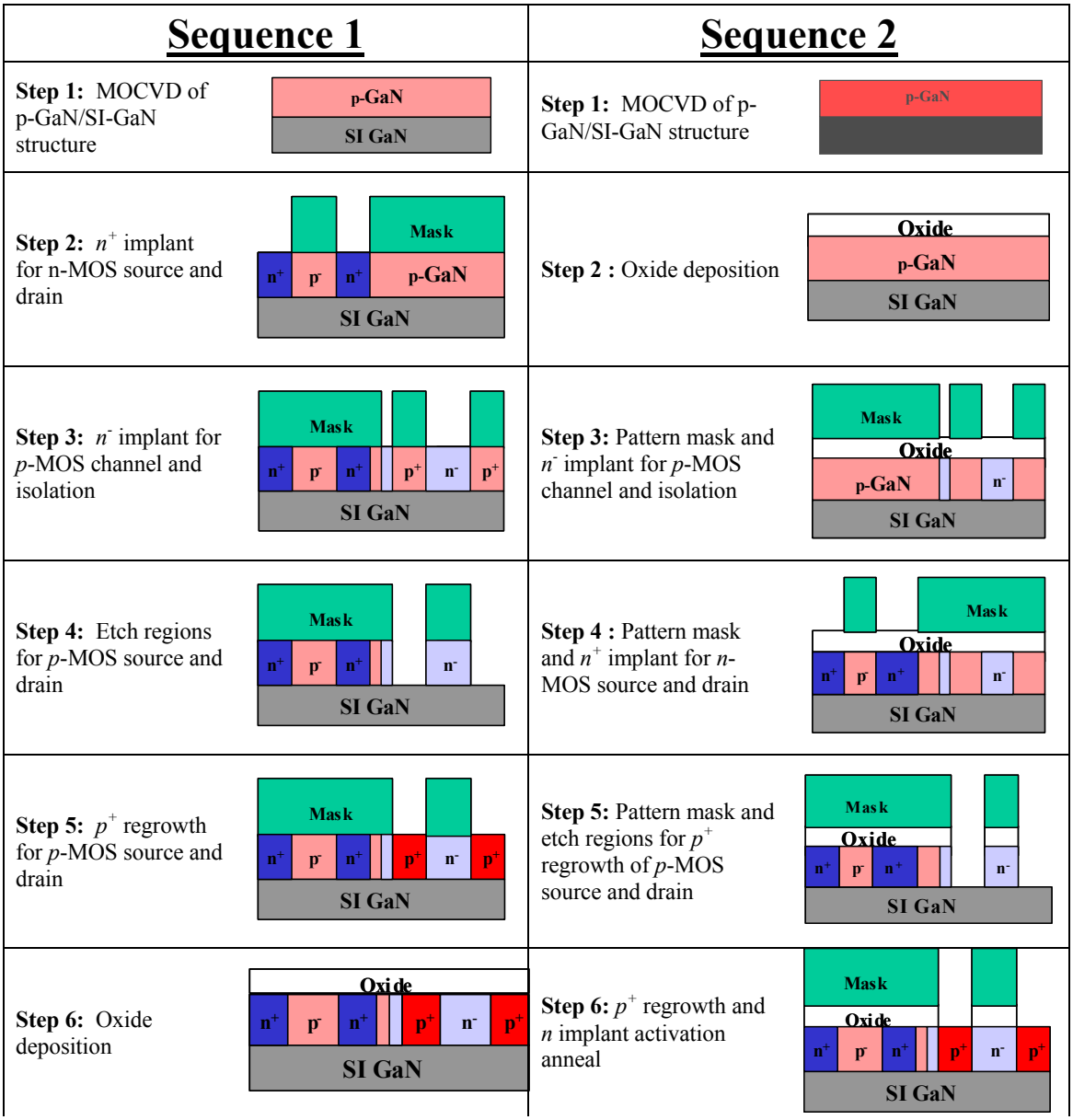

Figure 7-23. Proposed sequences for the processing of a GaN CMOSFET device.

CHAPTER 8
SUMMARY AND CONCLUSIONS

Summary of Epitaxial Growth of Sc_2O_3 Films on GaN

The epitaxial growth of thin films of scandium oxide (Sc_2O_3) on GaN was investigated. The effects on the Sc_2O_3 films after high temperature annealing in an oxygen deficient environment were examined. The Sc_2O_3 films showed little to no degradation after annealing. Extensive structural characterization was performed on the epitaxial grown Sc_2O_3 before and after annealing and detailed analysis of the results was described. The potential dielectrics being evaluated for GaN-based devices are nearly all fcc-based cubic oxides. Thus, this investigation can be used as a general outline for the examination of the epitaxial growth and structure of other potential oxide dielectrics for GaN-based devices. The exact orientation relationship between Sc_2O_3 on GaN was defined and it was shown that cubic Sc_2O_3 epitaxial grows in twin variant orientations on hexagonal GaN. The twinning of cubic oxides can produce excessive defects, which would reduce its performance as a gate dielectric for GaN MOS devices. The thermodynamic and kinetic factors that influence the twinning growth on GaN was discussed and approaches towards minimizing the twinning growth mode were proposed.

Summary of Dielectric Stability for GaN-based MOS Devices

The thermal and environmental stability in the GaN MOCVD environment of potential dielectric oxides for use in GaN-based MOS devices was examined. The oxide films that were studied were MgO, Sc_2O_3 and Sc_2O_3/MgO stacked structures. Two types of Sc_2O_3 films were looked at, those that were grown at a high temperature (HT) and those grown at a low temperature (LT). The effect of the thickness of the Sc_2O_3 cap on MgO was also examined. The structural, electrical and chemical effects of the MOCVD anneal on the oxides was evaluated with respect to their application and performance as a gate dielectric for GaN MOS devices. The

annealing conditions used are the growth conditions used for the MOCVD regrowth of GaN. Thus, the suitability of the oxides for use as a regrowth mask was also judged. All the oxides investigated showed signs of degradation after being annealed. Both Sc_2O_3 films remained structurally stable after annealing, but formed a conductive layer of ScN on the surface. This makes them unsuitable for use as a gate dielectric, but their thermal stability showed that they had potential use as a regrowth mask. MgO had particularly severe roughening and its electrical properties degraded significantly. These results show MgO might be useful as a regrowth mask but would perform well as a gate dielectric if it were to be exposed to the GaN MOCVD environment. The Sc_2O_3/MgO showed the best results for use as a gate dielectric. Particularly, the thinner 50 Å Sc_2O_3 cap shown only a very small decrease in the breakdown voltage after the MOCVD anneal. It was shown that the Sc_2O_3 cap dissolved into the MgO, but this appears to have prevented the formation of a ScN layer on the surface. One problem seen with 50 Å Sc_2O_3 capped MgO sample was that after annealing it had decomposed upon exposure to air. The Sc_2O_3 cap had previously protected the MgO film from environmental degradation and so this issue needs to be addressed for future work. MOCVD of GaN is the dominant growth technique and its environment is particularly harsh with respect to temperature and chemical reactivity. Little to no research has been done to assess the effects of the GaN MOCVD environment on potential dielectric oxides. It was not surprising that some amount of degradation was seen on all the films. However, the key discoveries made were very beneficial in progressing the understanding of the environmental effects on these oxides, which is essential for the development GaN MOS and Oxide/GaN device applications.

Summary of Selective Area Regrowth of p-type GaN

The use of selective area regrowth for the fabrication of GaN-based devices was examined. The regrowth of GaN into the etched features of a GaN substrate is extremely

complex and very little work has been done in this area. The general mechanisms involved in the selective area regrowth of GaN were examined. The environmental effects on the processed regrowth substrate prior to growth was studied and optimal conditions to avoid excessive decomposition were established. The evolution of growth from etched features and the conditions that influence the regrowth are considered.

A novel application of MOCVD regrowth was investigated. It consisted of regrowing the p^+ GaN source and drain regions of a p-MOSFET device. This alternative approach to creating the p^+ regions would avoid the problems associated with *p*-type doping via ion implantation by doping the material during the MOCVD regrowth. The regions for the p^+ source and drain were etched out of the substrate and then GaN, heavily doped with Mg was selectively regrown into the etched trenches. The extent of autodoping from the use of SiO_2 as the regrowth mask was significant and completely prevented the regrowth of p-type GaN. Alternative oxides were examined for use a regrowth mask. The use of MgO and Sc_2O_3 as a regrowth mask was explored. The use of MgO as a regrowth mask was shown to be unsuccessful and the probable mechanism of failure is discussed. The use of Sc_2O_3 as a regrowth mask was demonstrated. Successful regrowth was accomplished using the Sc_2O_3, where all etched features were completely regrown without any nucleation occurring on the Sc_2O_3 mask or any significant degradation of the Sc_2O_3. Very uniform and smooth regrowth was achieved using the Sc_2O_3 mask and further investigation of the effects on the electrical properties are under way.

Summary of Process Optimization of GaN MOS Device Fabrication

The ability of potential dielectric oxides to endure the most fundamental processing steps employed for the fabrication of a GaN MOSFET was examined. The effect of the thermal and chemical treatments used during the processing of GaN MOS heterostructures for device and regrowth applications was determined. Specific issues concerning the limitations that exist with

the use of the candidate dielectrics were addressed. A general approach for the evaluation of any potential dielectric material's compatibility with the acid-base chemistry of photolithography was given.

The specific issues involved in designing a processing sequence that implements selective area regrowth were discussed. Based on the MOCVD regrowth work that was performed a specific processing sequence is developed for the fabrication of a p-MOSFET. General processing sequences for the fabrication of GaN-based p-MOSFETs and CMOSFETs were also proposed that employ the selective area regrowth technique.

LIST OF REFERENCES

[1] P. M. Asbeck, E. T. Yu, S. S. Lau, G. J. Sullivav, J. Van Hove, and J. M. Redwing, Electron. Lett. **33**, 1230 (1997).

[2] M. S. Shur, MRS Symp. Proc. **483**, 15 (1998).

[3] Y. F. Wu, B. P. Keller, P. Fini, S. Keller, T. J. Jenkins, L. T. Kenias, S. P. DenBaars, and U. K. Mishra, IEEE Electron. Device Lett. **19**, 50 (1998).

[4] A. T. Ping, Q. Chen, J. W. Yang, M. A. Khan, and I. Adesida, IEEE Electron. Device Lett. **19**, 54 (1998).

[5] B. P. Gila, J. W. Johnson, R. Mehandru, B. Luo, A. H. Onstine, and V. Krishnamoorthy, phys. stat. sol. (a) **188**, 239 (2001).

[6] K. J. Bacmann, The Materials Science of Microelectronics, VCH, New York, N. Y. (1995).

[7] W. A. Doolittle, G. Namkoong, A. G. Carver, and A. S. Brown, Solid State Electron. **47**, 2143 (2003).

[8] J. W. Johnson, B. Luo, F. Ren, B. P. Gila, V. Krishnamoorthy, C. R. Abernathy, S. J. Pearton, J. I. Chyi, T. E. Nee, C. M. Lee, and C. C. Chuo, Appl. Phys. Lett. **77**, 3230 (2000).

[9] A. Tarakji, X. Hu, A. Koudymov, G. Simin, J. Yang, M. A. Khan, M. S. Shur, and R. Gaska, Solid State Electron. **46**, 1211 (2002).

[10] G. Simin, A. Koudymov, H. Fatima, J. P. Zhang, J. Yang, M. A. Khan, X. Hu, A. Tarakji, R. Gaska, and M. S. Shur, IEEE Electron Device Lett. **23**, 458 (2002).

[11] F. Ren, M. Hong, S. N. G. Chu, M. A. Marcus, M. J. Schurman, A. Baca, S. J. Pearton and C. R. Abernathy, Appl. Phys. Lett. **73**, 3893 (1998).

[12] R. C. Jaeger, Introduction to Microelectronic Fabrication, Addison-Wesley, Reading, Mass. (1998).

[13] J. W. Johnson, B. Luo, F. Ren, B. P. Gila, W. Krishnamoorthy, C. R. Abernathy, S.J. Pearton, J. I. Chyi, T. E. Nee, C. M. Lee, and C. C. Chuo, Appl. Phys. Lett. **77**, 3230 (2000).

[14] F. Ren, C. R. Abernathy, J. D. MacKenzie, B. P. Gila, S. J. Pearton, M. Hong, M. A. Marcus, M. J. Schurman, A. G. Baca, and R. J. Shul, Solid State Electron. **42**, 2177 (1998).

[15] E. Alekseev, A. Eisenbach, and D. Pavlidis, Electron. Lett. **35**, 24 (1999).

[16] F. Ren, M. Hong, S. N. G. Chu, M. A. Marcus, M. J. Schurman, A. Baca, S. J. Pearton, and C. R. Abernathy, Appl. Phys. Lett. **73**, 3893 (1998).

[17] M. Hong, H.M. Ng, J. Kwo, A.R. Kortan, J.N. Baillargeon, S.N.G. Chu, J.P.Mannaerts, A.Y. Cho, F. Ren, C.R. Abernathy, and S.J. Pearton, Electrochem. Soc. Proc. **11**, 369 (2000).

[18] H. C. Casey, Jr., G. G. Fountain, R. G. Alley, B. P. Keller, and S. P. Denbaars, Appl. Phys. Lett. **68**, 1850 (1996).

[19] S. Aurlkumaran, T. Egawa, H. Ishikawa, T. Jimbo, and M. Umeno, Appl. Phys. Lett. **73**, 809 (1998).

[20] S. C. Binari, K. Doverspike, G. Kelner, H. B. Dietrich, and A. E. Wickenden, Solid State Electron. **41**, 177 (1997).

[21] J. W. Johnson, B. Luo, F. Ren, B. P. Gila, V. Krishnamoorthy, C. R. Abernathy, S. J. Pearton, J. I. Chyi, T. E. Nee, C. M. Lee, and C. C. Chuo, Appl. Phys. Lett. **77**, 3230 (2000).

[22] P. B. Klein, S. C. Binari, K. Ikossi, A. E. Wickenden, D. D. Koleske, and R. L. Henry, Appl. Phys. Lett. **79**, 3527 (2001).

[23] J. W. Johnson, B. P. Gila, B. Luo, F. Ren, K. P. Lee, C. R. Abernathy, and S. J. Pearton, J. Electrochem. Soc. **148**, G303 (2001).

[24] J. Kim, R. Mehandru, B. Luo, F. Ren, B. P. Gila, and A. H. Onstine, Appl. Phys. Lett. **80**, 4555 (2002).

[25] J. Kim, R. Mehandru, B. Luo, F. Ren, B. P. Gila, and A. H. Onstine, Appl. Phys. Lett. **81**, 373 (2002).

[26] B. Luo, J. W. Johnson, J. Kim, R. Mehandru, B. Luo, F. Ren, and B. P. Gila, Appl. Phys. Lett. **80**, 1661 (2002).

[27] B. Luo, R. Mehandru, J. Kim, F. Ren, B. P. Gila, and A. H. Onstine, J. Electrochem. Soc. **149**, G613 (2002).

[28] R. Mehandru, Luo B, J. Kim, F. Ren, B. P. Gila, and A. H. Onstine, Appl. Phys. Lett. **82**, 2530 (2003).

[29] A. H. Onstine, B. P. Gila, J.Kim, A. M. Herrero, R. Mehandru, C. R. Abernathy, F. Ren, and S. J. Pearton, Electrochem. Soc. Proc. **11**, 344 (2003).

[30] H. Morkoc¸, A. D. Carlo, and R. Cingolani, Solid State Electron. **46**, 157 (2002).

[31] R. Therrin, G. Lucovsky, and R. F. Davis, phys. stat. sol. (a) **176**, 793 (1999).

[32] B. P. Gila, J. Kim, B. Luo, A. Onstine, W. Johnson, F. Ren, C. R. Abernathy and S. J. Pearton, Solid State Electron. **47**, 2139 (2003).

[33] M. Hong, A. R. Kortan, H. M. Ng, J. Kwo, S. N. G. Chu, J. P. Mannaerts, A. Y. Cho, C. M. Lee, J. I. Chyi, and K. A. Anselm, J. Vac. Sci. Technol. B, **20**, 1274 (2002).

[34] J. Sun, J. M. Redwing, and T. F. Kuech, phys. stat. sol. (a), **176**, 693 (1999).

[35] H. T. Lam, and J. M. Vohs, Surface Science, **426**, 199 (1999)

[36] S. A. Safvi, J. M. Redwing, M. A. Tischler, and T. F. Kuech, J. Electrochem. Soc. **144**, 1789 (1997).

[37] S. A. Safvi, J. M. Redwing, A. Thon, M. A. Tischler, and T. F. Kuech, MRS Symp. Proc. 449, 101 (1997).

[38] D. Mazzarese, A. Tripathi, W. C. Conner, K. A. Jones, L. Calderon, and D. W. Eckart, J. Electron. Mater. **18**, 369 (1989).

[39] S. H. Kim, H. S. Kim, J. S. Hwang, J. G. Choi, and P. J. Chong, Chem. Mat. **6**, 278 (1994).

[40] S. Haffouz, B. Beaumont, M. Leroux, M. Laugt, P. Lorenzini, P. Gibart, and L. G. Hubert-Pfalzgraf, MRS Internet J. Nitride Semicond. Res. **2**, 37 (1997).

[41] Z. Liliental-Weber, M. Benamara, W. Swider, J. Washburn, I. Grzegory, S. Porowski, R. D. Dupuis, and C. J. Eiting, MRS Internet J. Nitride Semicond. Res. **5S1**, W9.7 (2001).

[42] K. Hiramatsu, J. Phys: Condens. Matter. **13**, 6961 (2001).

[43] B. Beaumont, P. Vennegues, and P. Gibart, phys. stat. sol. (b) **227**, 1 (2001).

[44] O. H. Nam, T. S. Zheleva, M. D. Bremser, and R. F. Davis, J. Elec. Mat. **27**, 233 (1998).

[45] H. Marchand, J. P. Ibbetson, P. T. Fini, S. Keller, S. P. DenBaars, J. S. Speck, and U. K. Mishra, Submitted to J. Crystal Growth, (1998).

[46] A. Kimura, C. Sasaoka, A. Sakai, and A. Usui, MRS Symp. Proc. **482**, 119 (1998).

[47] B. Beaumont, M. Vaille, G. Nataf, A. Bouille, J. C. Guillaume, P. Vennegues, S. Haffouz, and P. Gibart, MRS Internet J. Nitride Semicond. Res. **3**, 20 (1998).

[48] A. M. Roskowski, P. Q. Miragli, E. A. Preble, S. Einfeldt, and R. F. Davis, J. Cryst. Growth, **241**, 141 (2002).

[49] T. Zheleva, S. Smith, D. Thomson, and K. Linthicum, J. Electron. Mater. **28**, L5 (1999).

[50] K. Linthicum, T. Ghrke, D. Thomson, E. Carlson, P. Rajagopal, T. Smith, D. Batchelor, and R. F. Davis, Appl. Phys. Lett. **75**, 196 (1999).

[51] T. Akasaka, S. Ando, T. Nishida, H. Saito, and N. Kobayashi, Appl. Phys. Lett. **79**, 1414 (2001).

[52] T. Akasaka, S. Ando, T. Nishida, T. Saitoh, and N. Kobayashi, J. Cryst. Growth **248**, 537 (2003).

[53] S. Haffouz, B. Beaumont, and P. Gibart, MRS Internet J. Nitride Semicond. Res. **3**, 8 (1998).

[54] P. de Mierry, B. Beaumont, E. Feltin, H. P. D. Schenk, P. Gibart, F. Jomard, S. Rushworth, L. Smith, and R. Odedra, MRS Internet J. Nitride Semicond. Res. **5**, 8 (2000).

[55] H. Morkoc, Nitride Semiconductors and Devices, Springer-Verlag, Berlin (1999).

[56] S. Nakamura S. Pearton, and G. Fasol, The Blue Laser Diode, Springer-Verlag, Berlin (2000).

[57] S. J. Pearton, F. Ren, A. P. Zhang, and K. P. Lee, Mat. Sci. and Eng. R **30**, 55 (2000).

[58] H. Ishikawa, S. Kobayashi, Y. Koide, S. Yamasaki, S. Nagai, J. Umezaki, M. Koike, and M. Murakami, J. Appl. Phys. **81**, 1315 (1997).

[59] M. E. Coltrin, and C. C. Mitchell, J. Cryst. Growth, **254**, 35 (2003).

[60] F. Ren, M. Hong, S. N. G. Chu, M. A. Marcus, M. J. Schurman, A. Baca, S. J. Pearton, and C. R. Abernathy, Appl. Phys. Lett. **73**, 3893 (1998).

[61] P. Hirsch, Electron Microscopy of Thin Crystals, R. E. Krieger Pub. Huntington, N. Y. (1977).

[62] S. Guha, E. Cartier, M. A. Gribelyuk, N. A. Bojarczuk, and J. Karasinski, Appl. Phys. Lett. **77**, 130 (2000).

[63] J. Kwo, M. Hong, A. R. Kortan, K. L. Quenney, Y. J. Chabal, R. L. Opila, Jr., D. A. Muller, S. N. G. Chu, B. J. Sapjeta, T. S. Lay, J. P. Mannaerts, T. Boone, H. W. Krautter, J. J. Krajewskui, A. M. Sergnt, and J. M. Rosamilia, J. Appl. Phys. **89**, 3920 (2001).

[64] G. Apostolopoulos, G. Vellianitis, A. Dimoulas, M. Alexe, R. Scholz, M. Fanciulli, D. T. Dekadjevi, and C. Wiemer, Appl. Phys. Lett. **81**, 3549 (2002).

[65] A. Fissel, H. J. Osten, and E. Bugiel, J. Vac. Sci. Technol. B, **12**, 1765 (2003).

[66] M. Malvestuto, R. Carboni, F. Boscherini, F. D'Acapito, S. Spiga, M. Fanciulli, A. Dimoulas, G. Vellianitis, and G. Mavrou, Phys. Rev. B, **71**, 075318 (2005).

[67] A. Dimoulas, A. Travlos, G. Vellianitis, N. Boukos, and K. Argyropoulos, J. Appl. Phys. **90**, 4224 (2001).

[68] A. Dimoulas, G. Vellianitis, A. Travlos, V. Ioannou-Sougleridis, and A. G. Nassiopoulou, J. Appl. Phys. **92**, 426 (2002).

[69] B. P. Gila, G. T. Thaler, A. H. Onstine, M. Hlad, A. Gerger, A. Herrero, K. K. Allums, D. Stodilka, S. Jang, B. Kang, T. Anderson, C. R. Abernathy, and F. Ren, S.J. Pearton, Solid-State Electron. **50**, 1016 (2006).

[70] P. B. Klein, S. C. Binari, K. Ikossi, A. E. Wickenden, D. D. Koleske, and R. L. Henry, Appl. Phys. Lett. **79**, 3527 (2001).

[71] B. P. Gila, A. H. Onstine, J. Kim, K. K. Allums, F. Ren, C. R. Abernathy, and S. J. Pearton, J. Vac. Sci. Technol. B **21**, 2368 (2003).

[72] Y. Irokawa, Y. Nakano, M. Ishiko, T. Kachi, J. Kim, F. Ren, B. P. Gila, A. H. Onstine, C. R. Abernathy, S. J. Pearton, C. C. Pan, G. T. Chen, and J. I. Chyi, Appl. Phys. Lett. **84**, 2919 (2004).

[73] H. Cho, K. P. Lee, B. P. Gila, C. R. Abernathy, S. J. Pearton, and F. Ren, Electrochem. Sol. St. Lett. **6**, G119 (2003).

[74] Y. Kuroda, E. Yasugi, H. Aoi, K. Miura, and T. Morimoto, J. Chem. Soc. Faraday Trans. **84**, 2421 (1988).

[75] J. Refson, M. Wogelius, H. Fraser, J. T. Payne, B. Lee, and D. Milman, Phys. Rev. B, **52**, 4590 (1995).

[76] J. Du, S. Gnanarajan, and A. Bendavid, Supercond. Sci. Technol. **18**, 1035 (2005).

[77] H. Onishi, C. Egawa, T. Aruga, and Y. Iwasawa, Surf. Sci. **191**, 479 (1987).

[78] D. Abriou, F. Creuzet, and J. Jupille, Surf. Sci. **352**, 499 (1996).

[79] D. Abriou, and J. Jupille, Surf. Sci. Lett. **430**, L527 (1999).

[80] Y. Yamashita, A. Endoh, K. Shinohara, M. Higashiwaki, K. Hikosaka, T. Mimura, S. Hiyamizu, and T. Matsui, IEEE Electron Dev. Lett. **22**, 367, (2001).

[81] K. Shinohara, Y. Yamashita, A. Endoh, K. Hikosaka, T. Matsui, T. Mimura, and S. Hiyamizu, IEEE Electron Dev. Lett. **22**, 507 (2001).

[82] K. Hikosaka, S. Sasa, N. Harada, and S. Kuroda, IEEE Electron Dev. Lett. **9**, 241 (1988).

[83] C. Chen, S. Keller, G. Parish, R. Vetury, P. Kozodoy, E. L. Hu, S. P. Denbaars, U. K. Mishra, and Y. Wu, Appl. Phys. Lett. **73**, 3147 (1998).

[84] R. F. Davis, T. Gehrke, K. J. Linthicum, P. Rajagopal, A. M. Roskowski, T. Zheleva, E. A. Preble, C. A. Zorman, M. Mehregany, U. Schwarz, J. Schuck, and R. Grober, MRS Internet J. Nitride Semicond. Res. **6**, 14 (2001).

[85] D. D. Koleske, A. E. Wickenden, and R. L. Henry, MRS Internet J. Nitride Semicond. Res. **5S1**, W3.64 (2000).

[86] N. Grandjean, J. Massies, F. Semond, S. Y. Karpov, and R. A. Talalaev, Appl. Phys. Lett. **74**, 1854 (1999).

[87] D. D. Koleske, A. E. Wickenden, R. L. Henry, M. E. Twigg, J. C. Culbertson, and R. J. Gorman, Appl. Phys. Lett. **73**, 2018 (1998).

[88] D. D. Koleske, A. E. Wickenden, R. L. Henry, M. E. Twigg, J. C. Culbertson, and R. J. Gorman, MRS Internet J. Nitride Semicond. Res. **4S1**, G3.70 (1999).

[89] D. D. Koleske, A. E. Wickenden, R. L. Henry, W. J. DeSisto, and R. J. Gorman, J. Appl. Phys. **84**, 1998 (1998).

[90] A. Rebey, T. Boufaden, and B. El Jani , J. Cryst. Growth **203**, 12 (1999).

[91] C. D. Thurmond, and R. A. Logan, J. Electrochem. Soc. **119**, 622 (1972).

[92] R. A. Logan, and C. D. Thurmond, J. Electrochem. Soc. **119**, 1727 (1972).

[93] S. Heikman, S. Keller, S. P. Denbaars, U. K. Mishra, F. Bertram, and J. Christen, Jpn. J. Appl. Phys. **42**, 6276 (2003).

[94] Z. Liliental-Weber, T. Tomaszewicz, D. Zakharov, M. O'Keefe, S. Hautakangas, K. Saarinen, J. A. Freitas, and R. L. Henry, phys. stat. sol. (a), **203**, 1636 (2006).

[95] Z. Liliental-Weber, M. Benamara, W. Swider, J. Washburn, I. Grzegory, and Z. S.Porowski, D. J. H. Lambert, R. D. Dupuis, and C. J. Eiting, Physica B, **273**, 124 (1999).

[96] V. Ramachandran, R. M. Feenstra, W. L. Sarney, L. Salamanca-Riba, J. E. Northrup, L. T. Romano, and D. W. Greve, Appl. Phys. Lett. **75**, 2740 (1999).

[97] S. Heikman, Doctoral Dissertation, University of California, Santa Barbara (2002).

[98] M. G. Norton, S. R. Summertelt, and C. B. Carter, Appl. Phys. Lett. **56** 2246 (1990).

[99] B. H. Moeckly, S. E. Russek, D. K. Lathrop, R. A. Buhrman, J. Li, and J. W. Mayer, Appl. Phys. Lett. **57** 1687 (1990).

[100] S. Coluccia, S. Lavagnino, and L. Marchese, J. Chem. Soc. Faraday Trans. I, **83**, 477 (1987).

[102] P. W. Tasker, J. Phys. C: Solid State Phys. **12**, 4977 (1979).

[103] S. Russo, and C. Noguera, Surf. Sci. **262**, 245 (1992).

[104] L. P. Buchwalter, J. Adhes. Sci. Tech. **1**, 341 (1987).

[105] L. P. Buchwalter, J. Adhes. Sci. Tech. **4**, 697 (1990).

[106] T. S. Oh, L. P. Buchwalter, and J. Kim, J. Adhes. Sci. Tech. **4**, 303 (1990).

[107] F. M. Fowkes, D. O. Tischler, J. A. Wolfe, L. A. Lannigan, C. M. Ademu-John, and M. J. Halliwell, J. Polymer Science: Polymer Chemistry Ed. **22**, 547 (1984).

[108] J. C. Bolger, Adhesion Aspects of Polymeric Coatings, K. L. Mittal (Ed.), Plenum Press, New York (1983).

[109] G. A. Parks, Chem. Rev. **65**, 177 (1965).

[110] G. Wade, Organic Chemistry, Prentice Hall, Upper Saddle River, N. J. (1999).

[111] H. Jiang, B. Chou, and S. Beilin, Int. Conf. on Multichip Modules and High Density Packaging, p.7 (1998).

[112] D. G. Kim, S. E. Molis, T. S. Oh, S. P. Kowalczyk, and J. Kim, J. Adhesion Sci. Tech. **5**, 509 (1991).

[113] B. K. Furman, H. Clearfield, and S. Purushothaman, J. Vac. Sci. Tech. A, **10**, 2913, (1992).

[114] R. Sharmay, M. J. McKelvy, H. Bearat, A. V. G. Chizmeshya, and R.W. Carpenter, Philos. Mag. **84**, 2711 (2004).

BIOGRAPHICAL SKETCH

I began my academic career in the summer of 1995 at the University of Florida (UF) and received my bachelor's degree in business in 2000. I immediately began my post baccalaureate work at UF in the Chemical Engineering Department. After about a year of undergraduate work, I became a graduate student in the department under Dr. Tim Anderson, who was the chair of the department at the time. I received a master's degree in chemical engineering in fall 2002 and then began work on my Ph.D. in the Materials Science and Engineering Department in spring 2003.